

# **NOVEL ALIGNMENT MATERIALS FOR USE IN LIQUID CRYSTAL DISPLAYS**

**Joette Russell Tanner**

A dissertation submitted to the faculty of the University of North Carolina at Chapel Hill in  
partial fulfillment of the requirements for the degree of Doctor of Philosophy in the  
Department of Chemistry

Chapel Hill  
2006

Approved by

Advisor: Edward T. Samulski

Reader: Joseph M. DeSimone

Reader: John M. Papanikolas

Gary L. Glish

J. Michael Ramsey

## **ABSTRACT**

Joette Russell Tanner: Novel Alignment Materials for Use in Liquid Crystal Displays

(Under the direction of Edward T. Samulski)

Obtaining stable and uniform alignment of liquid crystals on a macroscopic scale is essential for the fabrication and operation of high-quality liquid crystal displays. The alignment layer imposes the proper orientation of the liquid crystals in the initial state. Currently, the preferred modification technique is rather primitive: the conductive substrate is coated with a polyimide layer that after thermal curing is mechanically rubbed. This technique generates dust particles that interfere with display operation and often results in irreversible electrostatic damage to the electronic components of the display. Also, the details of the alignment mechanisms associated with unidirectional rubbing are not well understood. Thus, there is a demand for non-contact alignment techniques that are easily reproduced and quantified.

The work presented in this dissertation focuses on the development of novel alignment layers for use in liquid crystal displays, alignment layers that eliminate the need for a mechanical rubbing step in the fabrication process. The goal of this research was to find a material that could induce spontaneous, uniform alignment by means of easily quantified mechanisms. Several types of alignment layers, including surfactant monolayers, carbon nanotube and metal-oxide nanorod films and polymer films were examined for possible use in liquid crystal displays. Perfluoropolyether films embossed by soft-

lithography methods with a pattern of parallel grooves induced uniform homeotropic alignment of nematic liquid crystals on a macroscopic scale, offering the most promising alternative to traditional polyimide alignment layers.

## **ACKNOWLEDGEMENTS**

I would like to thank Ed Samulski for his support and prodding throughout this process and for having faith in my potential when my own faith was lost. I am grateful for the opportunity to hold my head high once more. I would also like to thank our collaborator Akihiko Sugimura for allowing me to study in his laboratory in Osaka, Japan. I could never have imagined such an incredible experience and I truly appreciate his graciousness and generosity. My view of the world is forever changed. I also want to thank all the members of the Samulski group that have made my time in lab so enjoyable and intellectually rewarding.

I would like to thank my parents Anthony Russell and Teresa Graves for loving me, for reading to me as a child and valuing education, for helping me to see my potential in academics and otherwise, for making me work as a waitress and cashier and allowing me to “build character,” and for encouraging me to obtain a formal education even though circumstances did not permit them to do so themselves. I truly appreciate the sacrifices that were made of their time and personal pursuits and desires that I might have all the opportunities possible for a good life. I will never be able to repay that debt. I would also like to thank my sister Jenny Baird for telling me at a young age that I didn’t have to “be one thing” for the rest of my life. This advice helped me to open my mind to all the possibilities out there waiting for me (and also caused me to change my major four times in college ☺). It helped me to explore other talents and interests while working on this research. This degree



will be only a part of the long road of learning that I hope will include guitar lessons, pottery classes, maybe even an interior design or literature degree. I would also like to thank my grandmothers, uncles and aunts and in-laws for supporting me and for being good examples of what it means to work hard.

I would like to thank my husband Mike for his love and support. Sometimes I think that he is more proud than even I am of this accomplishment. I also want to thank him for being my best friend and for helping me to find my calm side. I am grateful for his attentiveness and concern despite his hectic schedule. I do not know what the future holds for us with science, medicine or family, but I know that we can endure and enjoy the journey as we face it together. I would also like to thank my many friends from college and church who have supported me emotionally and spiritually as I have pushed through this experience. Their love, faith, and kind words have helped me to stand again and again, dust myself off and prepare for the next battle.

Finally, I would like to thank my Heavenly Father for this opportunity. As a young girl in Alabama I never imagined that I could accomplish so much and I definitely could not have done so without inspiration from the Spirit. I am grateful that my experience here was not an easy or typical one. Through the adversity, I have learned ten-fold more about life than science.

## TABLE OF CONTENTS

	Page
LIST OF FIGURES.....	vi
LIST OF ABBREVIATIONS.....	xii
 Chapter	
I INTRODUCTION.....	1
1.1 Background and Significance.....	1
1.2 Liquid Crystal Display Pixel.....	2
1.3 Liquid Crystals.....	4
1.3.1 Liquid Crystal Structure and Shape.....	5
1.3.2 Liquid Crystalline Phases.....	7
1.4 Characterization of Liquid Crystals.....	7
1.4.1 Transmitted Polarized Light Microscopy.....	9
1.4.2 Birefringence.....	11
1.5 Liquid Crystal Alignment.....	12
1.5.1 Modes of Liquid Crystal Alignment.....	13
1.5.2 Mechanisms of Liquid Crystal Alignment.....	15
1.6 Research Objectives.....	18
1.7 References.....	20

II	ALIGNMENT OF NEMATIC LIQUID CRYSTALS USING ORGANIZED MOLECULAR FILMS.....	22
2.1	Organized Molecular Films.....	22
2.2	Experimental Details.....	24
2.2.1	Materials.....	24
2.2.2	Instrumentation.....	25
2.2.3	Preparation of Polyimide Films.....	25
2.2.4	Deposition of Self-Assembled Monolayers.....	25
2.2.5	Deposition of Hybrid Molecular Films.....	27
2.2.6	Deposition of Gradient Molecular Films.....	28
2.2.7	Fabrication of Liquid Crystal Optical Cells.....	28
2.3	Results and Discussion.....	29
2.3.1	Birefringent Textures of Polyimide Films as Control.....	29
2.3.2	Birefringent Textures of DMOAP Self-Assembled Monolayers.....	30
2.3.3	Concentration Dependence of Liquid Crystal Alignment Using CTAB Self-Assembled Monolayers.....	32
2.3.4	Birefringent Textures of DMOAP/Polyimide Hybrid Films.....	37
2.3.5	Birefringent Textures of Low Concentration/High Concentration CTAB Hybrid Films.....	39
2.3.6	Birefringent Textures of Gradient Molecular Films.....	40
2.4	Conclusions.....	44
2.5	References.....	46

III	ALIGNMENT OF NEMATIC LIQUID CRYSTALS USING CARBON NANOTUBES AND METAL-OXIDE NANORODS.....	47
3.1	Carbon Nanotube Films.....	47
3.2	Experimental Details.....	48
3.2.1	Materials.....	48
3.2.2	Instrumentation.....	48
3.2.3	Carbon Nanotube Synthesis.....	49
3.2.4	Carbon Nanotube Film Deposition.....	49
3.2.5	Fabrication of Liquid Crystal Optical Cells.....	52
3.3	Results and Discussion.....	52
3.3.1	Birefringent Textures of Carbon Nanotube Films Prepared by Gradual Evaporation.....	52
3.3.2	Deposition of Carbon Nanotubes by Controlled Dipping.....	55
3.3.3	Atomic Force Microscopy Analysis of Carbon Nanotube Orientation.....	55
3.3.4	Birefringent Textures of Patterned Carbon Nanotube Films.....	58
3.3.5	Liquid Crystal Display Pixel Prototypes.....	60
3.4	Conclusions.....	60
3.5	Metal-Oxide Nanorod Films.....	61
3.6	Experimental Details.....	62
3.6.1	Materials.....	62
3.6.2	Instrumentation.....	63
3.6.3	Synthesis of Zinc Oxide and Tin Oxide Nanorods.....	63
3.6.4	Dispersion of Zinc Oxide and Tin Oxide in	

	Chloroform.....	64
3.6.5	Dispersion of Zinc Oxide and Tin Oxide in Water....	68
3.6.6	Metal-Oxide Film Deposition.....	69
3.6.7	Fabrication of Liquid Crystal Optical Cells.....	70
3.7	Results and Discussion.....	70
3.7.1	Birefringent Textures of Zinc Oxide Nanorod Films..	70
3.7.2	Effects of Zinc Oxide Nanorod Aggregation on Liquid Crystal Alignment.....	72
3.7.3	Birefringent Textures of Tin Oxide Nanorod Films...	75
3.7.4	Effects of Surfactant Used for Dispersion on Liquid Crystal Alignment.....	75
3.8	Conclusions.....	77
3.9	References.....	79
IV	ALIGNMENT OF NEMATIC LIQUID CRYSTALS USING PERFLUORO POLYETHERS.....	81
4.1	Perfluoropolyethers.....	81
4.2	Experimental Details.....	83
4.2.1	Materials.....	83
4.2.2	Instrumentation.....	84
4.2.3	Perfluoropolyether Synthesis.....	85
4.2.4	Deposition of Thin Perfluoropolyether Films.....	86
4.2.5	Preparation of Embossed Perfluoropolyether Films...	86
4.2.6	Fabrication of Liquid Crystal Optical Cells.....	87
4.3	Results and Discussions.....	87
4.3.1	Birefringent Textures of Thin Perfluoropolyether	

	Films.....	87
4.3.2	Comparison of Alignment of Positive and Negative Dielectric Liquid Crystals on Fluorinated Alignment Layers.....	91
4.3.3	Time-Dependent Stability of Liquid Crystal Alignment on Thin Perfluoropolyether Films.....	97
4.3.4	Surface Energy Measurements on Thin Perfluoropolyether Films.....	97
4.3.5	Surface Anchoring Energy Measurements on Thin Perfluoropolyether Films.....	100
4.3.6	Birefringent Textures of Rubbed Perfluoropolyether Films.....	103
4.3.7	Birefringent Textures of Pretreated Thin Perfluoropolyether Films.....	105
4.3.8	Time-Dependent Stability of Liquid Crystal Alignment on Pretreated Thin Perfluoropolyether Films.....	112
4.3.9	Surface Energy Measurements on Pretreated Thin Perfluoropolyether Films.....	115
4.3.10	Birefringent Textures of Embossed Perfluoropolyether Films.....	117
4.3.11	Mechanisms of Liquid Crystal Alignment on Perfluoropolyether Films.....	123
4.4	Conclusions.....	125
4.5	References.....	127
V	ALIGNMENT OF NEMATIC LIQUID CRYSTALS USING PERFLUOROPOLYETHER LANGMUIR-BLODGETT FILMS.....	129
5.1	Langmuir-Blodgett Films.....	129
5.2	Experimental Details.....	132
5.2.1	Materials.....	132

5.2.2	Instrumentation.....	133
5.2.3	Perfluoropolyether Synthesis.....	133
5.2.4	Preparation of Perfluoropolyether Langmuir- Blodgett Films.....	133
5.2.5	Fabrication of Liquid Crystal Optical Cells.....	135
5.3	Results and Discussion.....	136
5.3.1	Birefringent Textures of Perfluoropolyether Langmuir- Blodgett Films.....	136
5.3.2	Atomic Force Microscopy of Perfluoropolyether Langmuir-Blodgett Films.....	140
5.3.3	Surface Energy Measurements on Perfluoropolyether Langmuir-Blodgett Films.....	143
5.3.4	Surface Anchoring Energy Measurements on Perfluoro- polyether Langmuir-Blodgett Films.....	144
5.3.5	Birefringent Textures of Pretreated Perfluoropolyether Langmuir-Blodgett Films.....	149
5.3.6	Time-Dependent Stability of Liquid Crystal Alignment on Pretreated Perfluoropolyether Langmuir-Blodgett Films.....	154
5.3.7	Mechanisms of Liquid Crystal Alignment on Perfluoro- polyether Langmuir-Blodgett Films.....	159
5.4	Conclusions.....	162
5.5	References.....	163

## LIST OF FIGURES

Figure	Page
1.1 Schematic representation of a liquid crystal pixel in both the bright (off) and dark (on) states.....	3
1.2 A schematic representation of the crystalline solid, liquid and liquid crystalline phases of matter.....	4
1.3 Chemical structure of a typical organic molecule (4-cyano-4'-pentyl-1,1'-biphenyl, more commonly called K-15) that exhibits liquid crystalline behavior.....	5
1.4 Schematic representation of the orientational and positional order found in the three most common liquid crystalline phases.....	8
1.5 Schematic representation of polarizing microscope.....	10
1.6 Plot of sample rotation angle (with respect to crossed polarizers) versus normalized intensity of transmitted light.....	13
1.7 Schematic representation of liquid crystal alignment modes.....	14
1.8 Chemical structure of polyimide, a polymer commonly used for alignment layer preparation.....	16
1.9 Schematic representation of the mechanisms of liquid crystal alignment. The elastic energy costs of orienting the liquid crystal director (denoted by black arrows) perpendicular and parallel to the grooved substrate are compared.....	17
2.1 Chemical structures of the surfactants used to prepare self-assembled monolayers.....	24
2.2 Photograph of the dipping apparatus built in-house.....	26
2.3 Photograph of the mechanical rubbing apparatus built in-house.....	26
2.4 Schematic representation of the deposition of a gradient molecular film by evaporation.....	29
2.5 Birefringent texture images for alignment of a positive dielectric liquid crystal by polyimide.....	30
2.6 Birefringent texture images for alignment of both (A) positive and (B) negative dielectric liquid crystal by SAMs of DMOAP.....	31



2.7 Schematic representation of the liquid crystal alignment mechanism associated with homeotropic alignment of liquid crystal by DMOAP SAMs.....	32
2.8 Birefringent texture images for alignment of liquid crystal by SAMs of CTAB prepared at (A) high concentration ( $6 \times 10^{-5}$ M ) and (B) low concentration ( $5 \times 10^{-7}$ M) by agitation method.....	33
2.9 Birefringent texture images for alignment of both (A) positive and (B) negative dielectric liquid crystal by SAMs of CTAB prepared at $6 \times 10^{-5}$ M by agitation method.....	34
2.10 Birefringent texture images for alignment of liquid crystal on SAMs of CTAB prepared at various concentrations by the dip-coating method.....	36
2.11 Schematic representation of two modes of LC alignment observed for SAMs of CTAB prepared at varying concentration by the dip-coating method.....	37
2.12 Birefringent textures images of liquid crystal alignment by DMOAP/polyimide hybrid film.....	38
2.13 Birefringent textures images of liquid crystal alignment by high concentration CTAB/low concentration CTAB hybrid film.....	40
2.14 Plot of the measurements of the contact angles of water, ethylene glycol and diiodomethane with respect to the one-dimensional position along the substrate, the zero position marking the portion of the substrate closest to the trough during deposition by evaporation (substrate is 50 mm from trough at zero position).....	41
2.15 Plot of the surface energy of the gradient (calculated based on the water and ethylene glycol contact angle data) with respect to the one-dimensional position along the substrate.....	42
2.16 Birefringent texture images of LC alignment on a gradient molecular film.....	43
2.17 Plot of calculated surface energy and light intensity with respect to the one-dimensional position along the substrate.....	44
3.1 Transmission electron micrographs of (A) purified SWNTs and (B) etched SWNTs with average bundle lengths of 2.0 $\mu\text{m}$ .....	50
3.2 Schematic representations of CNT deposition methods.....	50
3.3 Schematic representation of CNT deposition on substrate patterned with alternating hydrophilic and hydrophobic regions.....	51
3.4 Birefringent texture images for the three regions of alignment obtained from the self-assembly of CNTs (2.0 $\mu\text{m}$ bundles).....	54

3.5 Birefringent texture images for the alignment of nematic LC by self-assembled CNTs (0.5 $\mu\text{m}$ bundles).....	55
3.6 Representative AFM images of dense CNT films (region (ii)).....	56
3.7 Representative AFM images of sparse CNT films.....	57
3.8 Graph of the distribution of SWNT bundles on substrates dipped at 143.0 $\mu\text{m}/\text{sec}$ with respect to their deviation from the dipping direction (designated as 0 degrees).....	58
3.9 (A) Bright field and (B) birefringent texture images of liquid crystal alignment by patterned CNT films.....	59
3.10 Transmission electron micrographs of (A) ZnO (scale bar 100 nm) and (B) SnO <sub>2</sub> (scale bar 100 nm) dispersions in chloroform.....	66
3.11 Transmission electron micrographs of (A) ZnO (scale bar 0.5 $\mu\text{m}$ ) and (B) SnO <sub>2</sub> (scale bar 100 nm) dispersions in chloroform.....	66
3.12 Chemical structures of surfactants used to successfully disperse ZnO and SnO <sub>2</sub> in chloroform.....	67
3.13 Transmission electron micrographs of ZnO dispersed in water by DMOAP ((A) scale bar 200 nm and (B) scale bar 100 nm).....	69
3.14 Scanning electron micrographs of ZnO dispersed in water by PAA (scale bars 1.0 $\mu\text{m}$ ).....	70
3.15 Birefringent texture images for the alignment of liquid crystal K-15 by ZnO nanorod films.....	71
3.16 Phase contrast images of substrates dipped in ZnO/chloroform dispersions of varying age.....	73
3.17 Atomic force microscopy images of three substrates dipped in ZnO/chloroform solutions of varying age.....	74
3.18 Birefringent texture images for the alignment of liquid crystal K-15 by SnO <sub>2</sub> nanorod films.....	76
3.19 Phase contrast images of substrates dipped in SnO <sub>2</sub> /chloroform dispersions of varying age.....	77
4.1 Chemical structures of Krytox and Fomblin Z. These basic structures were the first used in the synthesis of PFPEs.....	82

4.2 Chemical structures of perfluoropolyether precursor polymers used in this research.....	85
4.3 Birefringent textures observed for alignment of K-15 on thin PFPE films of variable thickness.....	88
4.4 Birefringent textures observed for alignment of (A) K-15 and (B) MLC-6608 on thin films of S-PFPE.....	89
4.5 Birefringent textures observed for alignment of (A) K-15 and (B) MLC-6608 on thin films of PFPE deposited on bare float glass.....	90
4.6 Birefringent textures observed for alignment of (A) K-15 and (B) MLC-6608 on thin films of PFPE.....	92
4.7 Birefringent textures observed for alignment of (A) K-15 and (B) MLC-6608 on thin films of Teflon-AF.....	93
4.8 Birefringent textures observed for alignment of (A) K-15 and (B) MLC-6608 on thin films of trichloro(1H,1H,2H,2H-perfluoro-octyl) silane.....	93
4.9 Birefringent textures observed for the alignment of K-15 and MLC-6608 on DMOAP and CTAB.....	94
4.10 Birefringent textures for the alignment of (A) K-15, (B) ZLI-2293, (C) ZLI-4792, (D) MLC-6608, (E) MLC-6609, and (F) MLC-6610 on thin films of PFPE.....	96
4.11 Time-dependent stability of alignment of K-15 on PFPE.....	98
4.12 Time-dependent stability of alignment of MLC-6608 on PFPE.....	99
4.13 Comparison of surface energies of fluorinated materials and traditional alignment materials.....	100
4.14 Plot of the optical retardation versus inverse voltage for the alignment of ZLI-2293 on thin PFPE film.....	102
4.15 Birefringent textures observed for alignment of K-15 on (A) thin PFPE film and (B) rubbed PFPE film.....	104
4.16 Birefringent textures observed for the alignment of K-15 on pretreated thin PFPE films.....	107
4.17 Birefringent textures observed for the alignment of MLC-6608 on pretreated thin PFPE films.....	108

4.18	Birefringent textures observed for the alignment of K-15 on pretreated thin PFPE films.....	110
4.19	Birefringent textures observed for the alignment of K-15 on pretreated thin PFPE films.....	111
4.20	Birefringent textures observed for the alignment of K-15 on pretreated thin S-PFPE films.....	112
4.21	Time-dependent stability of alignment of K-15 on PFPE treated with toluene.....	113
4.22	Time-dependent stability of alignment of MLC-6608 on PFPE treated with toluene..	114
4.23	Time-dependent stability of alignment of K-15 on PFPE treated with water.....	115
4.24	Comparison of surface energies of pretreated thin PFPE films with other fluorinated materials and traditional alignment layers.....	116
4.25	AFM images of embossed PFPE films.....	118
4.26	Surface energies of embossed PFPE films.....	119
4.27	Birefringent textures observed for the alignment of (A) K-15 and (B) MLC-6608 on embossed PFPE films.....	121
4.28	Birefringent textures observed for the alignment of (A) K-15 and (B) MLC-6608 on embossed PFPE films.....	122
4.29	Birefringent textures observed for the alignment of (A) K-15 and (B) MLC-6608 on embossed PFPE films.....	122
4.30	Birefringent textures observed for the alignment of (A) K-15 and (B) MLC-6608 on embossed PFPE films.....	123
4.31	Summary of alignment mechanisms associated with experimental results.....	124
4.32	Schematic representation of a multi-domain embossed PFPE film.....	126
5.1	Schematic representation of a Langmuir-Blodgett trough.....	132
5.2	Photograph of KSV 500 Langmuir-Blodgett trough.....	134
5.3	Schematic representation of the deposition of a Langmuir-Blodgett film.....	135
5.4	Birefringent textures for alignment of K-15 on multilayer LB films of PFPE.....	137
5.5	Comparison of alignment of positive and negative dielectric LCs on PFPE LB films of 1	

monolayer thickness.....	138
5.6 Comparison of alignment of positive and negative dielectric LCs on PFPE LB films of 5 monolayer thickness.....	139
5.7 Comparison of alignment of positive and negative dielectric LCs on PFPE LB films of 10 monolayer thickness.....	140
5.8 Atomic force microscopy images of multilayer PFPE LB films.....	141
5.9 AFM images of the formation of polymer islands in PFPE LB films.....	142
5.10 Comparison of the surface energies of PFPE LB films with other fluorinated alignment materials.....	144
5.11 Plot of the optical retardation versus inverse voltage for PFPE LB film of 1 monolayer thickness.....	146
5.12 Plot of the optical retardation versus inverse voltage for PFPE LB film of 5 monolayer thickness.....	146
5.13 Plot of the optical retardation versus inverse voltage for PFPE LB film of 10 monolayer Thickness.....	147
5.14 Plot of surface anchoring energy versus thickness (number of monolayers).....	147
5.15 Birefringent textures of alignment of K-15 on pretreated PFPE LB films of 1 monolayer thickness.....	151
5.16 Birefringent textures of alignment of K-15 on pretreated PFPE LB films of 5 monolayer thickness.....	152
5.17 Birefringent textures of alignment of K-15 on pretreated PFPE LB films of 10 monolayer thickness.....	153
5.18 Time-dependent alignment stability of PFPE LB films pretreated with toluene.....	155
5.19 Time-dependent alignment stability of PFPE LB films pretreated with water.....	156
5.20 Time-dependent alignment stability of PFPE LB films pretreated with toluene.....	157
5.21 Time-dependent alignment stability of PFPE LB films pretreated with water.....	158
5.22 Summary of alignment mechanisms associated with experimental results.....	161

## LIST OF ABBREVIATIONS

AC	alternating current
AFM	atomic force microscopy
CNT	carbon nanotube
CTAB	cetyltrimethylammonium bromide
DBTDA	dibutyltin diacetate
DD	dipole dipole
DMOAP	<i>N,N</i> -dimethyl- <i>n</i> -octadecyl-3-aminopropyltrimethoxysilyl chloride
DMPA	2,2-dimethoxy-2-phenyl acetophenone
DSC	differential scanning calorimetry
EIM	2-isocyanatoethyl methacrylate
ITO	indium tin oxide
LB	Langmuir-Blodgett
LC	liquid crystal or liquid crystalline
LCD	liquid crystal display
MWNT	multi-walled nanotubes
N	nematic
NMR	nuclear magnetic resonance
PAA	poly(acrylic acid, sodium salt)
PCM	phase contrast microscopy
PFPE	perfluoropolyether
PLM	polarized light microscopy

S <sub>A</sub>	smectic A
S <sub>C</sub>	smectic C
SAM	self-assembled monolayer
SEM	scanning electron microscopy
SWNT	single-walled nanotubes
TEM	transmission electron microscopy
TMAH	tertramethylammonium hydroxide
ZDOL	poly(tetrafluoroethylene oxide- <i>co</i> -difluoromethylene oxide) $\alpha,\omega$ diol

# **CHAPTER 1**

## **INTRODUCTION**

### **1.1 Background and Significance**

The earliest observations of liquid crystalline behavior were noted in the late 1800s by Friederich Reinitzer and Otto Lehmann,<sup>1,2</sup> but it was not until the late 1960s that the fabrication of a rudimentary liquid crystal display (LCD) was proposed by RCA scientist G. H. Heilmeier.<sup>3</sup> Since that time much research has been dedicated to the improvement of these displays, resulting in their ubiquitous presence in daily life. Liquid crystal displays, initially used only in small devices such as wristwatches and pocket calculators, have become more sophisticated and now include applications in personal digital assistants, cellular telephones, desktop computer monitors, notebook PCs and even large-screen televisions. The world market for LCDs has seen extensive growth in the last thirty years with revenues of approximately 33.5 billion USD in 2003.<sup>4,5</sup> The increasing demand for larger displays requires improvement of both the materials and techniques used in the fabrication process, with the desired end result being an increase in product yield and performance and a reduction in cost to the consumer.

In LCDs, the liquid crystals are sandwiched between two glass plates coated with both a conducting layer and an alignment layer. Additional components of the display include various optical layers such as a polarizer, analyzer, and color filter and a backlight.



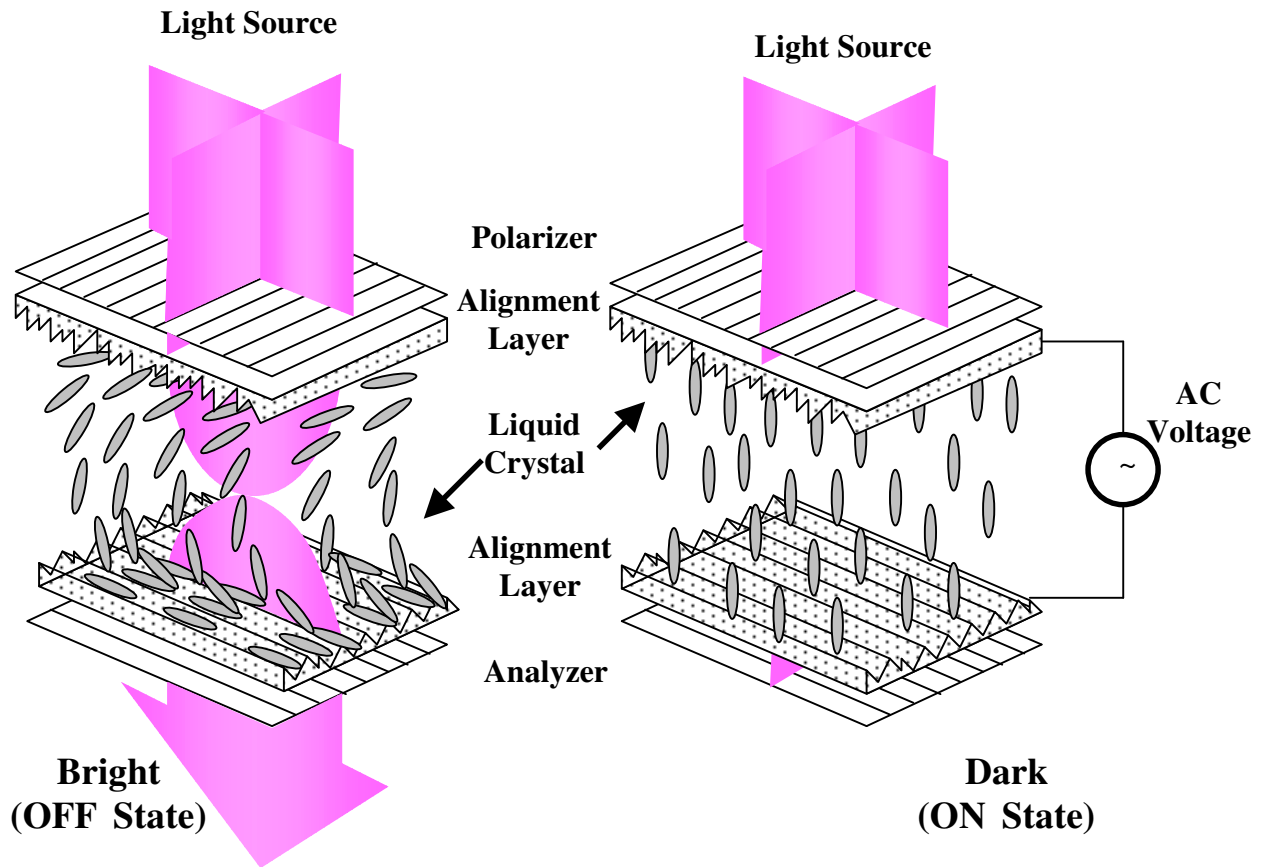
Obtaining stable and uniform alignment of liquid crystals on a macroscopic scale is essential to the high-quality operation of LCDs. Liquid crystal alignment determines the electro-optical switching mode and speed of the display and good alignment prevents the formation of random multidomains caused by mismatches in liquid crystal director (symmetry axis) orientation that deteriorate the displayed image.<sup>4</sup> The alignment layer imposes the proper orientation on the liquid crystals. Conventionally, this orienting effect is achieved by mechanically rubbing the alignment layer with either synthetic or natural fabric, a rather primitive technique that generates dust and often results in irreversible electrostatic damage to the electronic components of the display.<sup>6,7</sup> Thus, there is a demand for non-contact alignment techniques.

The work presented in this dissertation focuses on the development of novel alignment layers for use in LCDs, alignment layers that eliminate the need for a mechanical rubbing step in the fabrication process. The goal of this research was to find a material that could induce spontaneous, uniform liquid crystal alignment by means of easily quantified mechanisms. Several types of alignment layers, including surfactant monolayers, carbon nanotube films and polymer films were examined for possible use in LCDs.

## **1.2 Liquid Crystal Display Pixel**

The fundamental unit of the LCD is the liquid crystal (LC) pixel which may be operated in either a bright or dark state. As seen in Figure 1.1, a typical pixel consists of a light source, two polarizers rotated  $90^\circ$  with respect to one another, two conductive and transparent substrates coated with an alignment layer which are also rotated  $90^\circ$  with respect to one another, and the LC layer. In the bright state, the alignment layer determines the orientation of the LC molecules. Plane polarized light is generated as light passes through

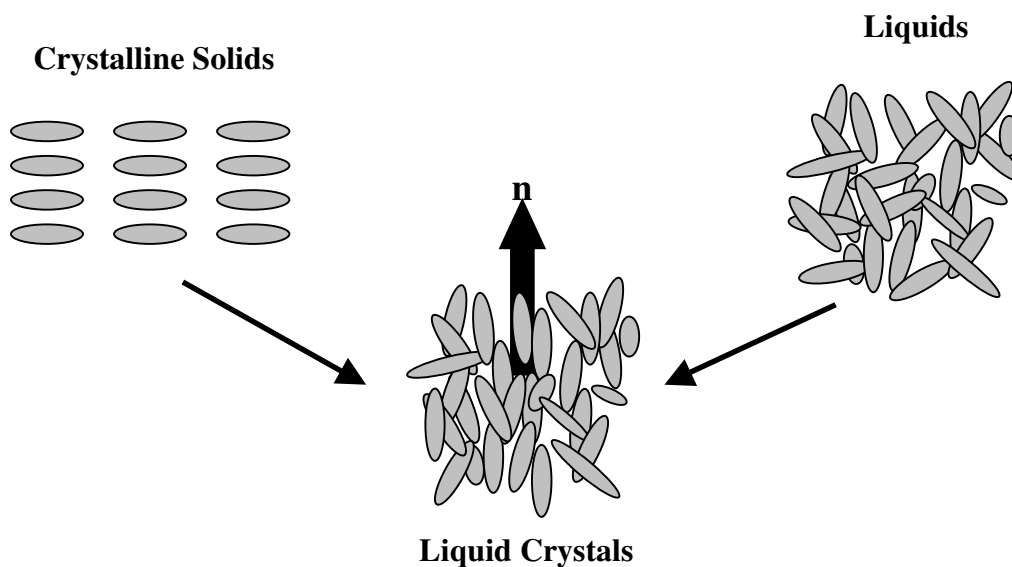
the first polarizer. This plane of light is rotated as a function of the LC director orientation and thus, is able to pass through the second polarizer (also called the analyzer) and emit from the other side of the pixel. In the dark state, an electric field is applied across the pixel, orienting the LC molecules perpendicular to the substrates. The plane polarized light passes through the LC layer parallel to the optic axis of the molecules and is not rotated and thus cannot pass through the analyzer and be emitted. The bright and dark states are also called the off and on states, respectively, in reference to the use of the electric field to reorient the LC director.<sup>4,8</sup>



**Figure 1.1** Schematic representation of a liquid crystal pixel in both the bright (off) and dark (on) states.

### 1.3 Liquid Crystals

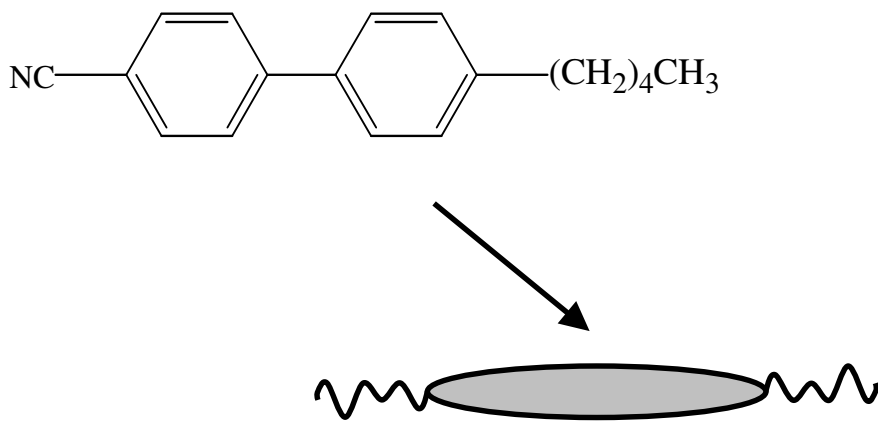
The two most common condensed matter phases, solids and liquids, are both characterized by close packing of molecules, but differ in the ordering and mobility of those individual molecules. In a crystalline solid, the molecules have a three-dimensional periodic arrangement that requires the molecular axis of each molecule to point in a particular direction with respect to the lattice, that arrangement also prevents the diffusion of any individual molecule. The molecules in liquids, however, have a random arrangement and may diffuse about readily. The term mesomorphism describes an intermediate phase of matter that arises when the molecules in fluids spontaneously order. This mesomorphic or LC phase exhibits properties of both liquids and crystalline solids (Figure 1.2). The molecules in the LC phase diffuse about randomly much like those of an isotropic liquid, but they maintain some orientational (and sometimes positional) order as they do so.<sup>9,10</sup>



**Figure 1.2** A schematic representation of the crystalline solid, liquid and liquid crystalline phases of matter. In the case of crystalline solids, the molecules have both orientational and positional order in three dimensions. Isotropic liquids have neither orientational, nor positional order. Liquid crystalline fluids have orientational and sometimes positional order in one or two dimensions.

### 1.3.1 Liquid Crystal Structure and Shape

Mesomorphic phases come about because of molecular shape restrictions or excluded volume interactions. The structural component responsible for inducing liquid crystallinity is the mesogenic core, usually comprised of aromatic rings linked either directly or by some quasi-rigid linking group. This core provides the rigidity necessary for excluded volume interactions and is terminated by flexible chains, commonly known as tails. These hydrocarbon chains facilitate the transformation from the solid to the LC phase. Figure 1.3 shows the structure of an organic molecule that exhibits liquid crystalline behavior as well as a schematic of the geometrical shape of such a molecule. Many types of molecules may form LC phases, but all of these molecules must exhibit some form of anisotropy. Either the shape of the molecule must be such that one molecular axis is very different from the other two (length to diameter ratio of the molecule must be greater than three, but is typically eight or higher) or the core and tail components of the molecule must have very different solubility properties. Interactions between these anisotropic molecules promote organization of the fluid.<sup>11</sup>



**Figure 1.3** Chemical structure of a typical organic molecule (4-cyano-4'-pentyl 1,1'-biphenyl, more commonly called K-15) that exhibits liquid crystalline behavior. Below the chemical structure is a simplified geometrical representation of the shape of the molecule.

Depending on the detailed molecular structure, a liquid crystal may pass through several LC phases before reaching the isotropic phase. These transitions may be dependent upon changes in either temperature (thermotropic mesomorphism) or concentration (lyotropic mesomorphism). The most common type of molecule that forms LC phases is the rod-shaped or calamitic molecule. In packing, the long axes of the molecules are generally parallel. These molecules spontaneously orient within a given temperature or concentration range. Molecules that have a discotic or bent shape may also exhibit liquid crystalline behavior. However, this research focuses on the use of calamitic, thermotropic liquid crystals.<sup>9-12</sup>

The molecular structure of the LC also determines the dielectric anisotropy of the LC phase, a property that dictates the behavior of LC molecules in an electric field and thus, is important for display applications. The dielectric anisotropy of the LC molecules is determined by two factors: (1) the polarizability anisotropy ( $\alpha_a$ ) and (2) the dipole orientation effect. The polarizability anisotropy always makes a positive contribution for rod-like molecules, meaning that there is a larger contribution when measuring the field parallel to the long molecular axis. The dipole orientation effect makes a positive contribution when the net permanent dipole moment of the molecule makes a small angle with the long axis and a negative contribution when the angle is large. Thus the placement of electronegative functionalities such as CN and F in the LC structure is a significant factor in determining the net dielectric anisotropy. The sign of the net dielectric anisotropy depends on the relative magnitude of the two contributions and is denoted by  $\Delta\epsilon = \epsilon_{||} - \epsilon_{\perp}$ . This net dielectric anisotropy varies widely for different LC materials and leads to a method of LC alignment by electric fields, as shown in the dark state of the LCD pixel (Figure 1.1).<sup>10,12</sup>

### 1.3.2 Liquid Crystalline Phases

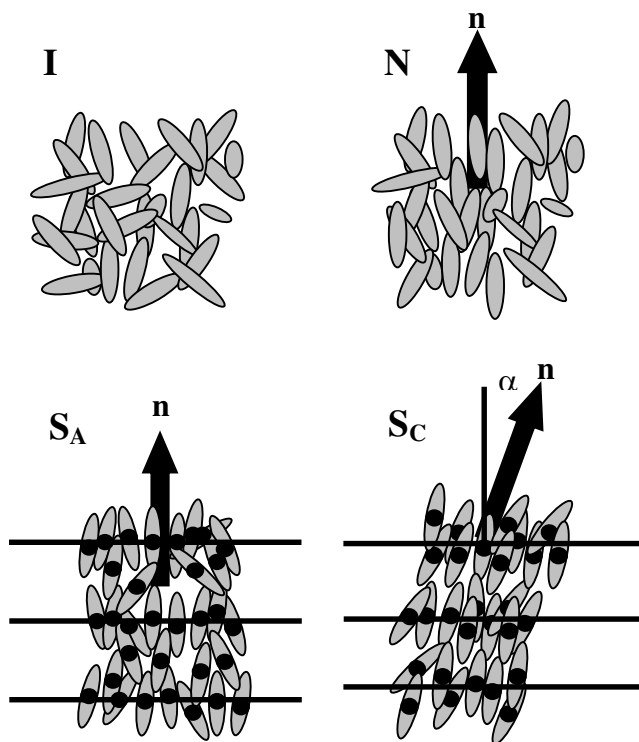
Calamitic molecules may organize into several LC phases that may be characterized by the appearance of orientational and/or positional order. The nematic (N) phase is the simplest and most common. In this phase the molecules maintain a preferred orientational direction as they diffuse throughout the sample, aligning with the long axes of the molecules parallel to one another on average (Figure 1.4). The direction of orientation is identified by the director  $\mathbf{n}$ . No positional order is exhibited by the nematic phase.

Two other common liquid crystal phases are the Smectic A and C phases (Figure 1.4). These phases exhibit orientational order like that found in nematics, but there is also positional order since the centers of mass of the molecules are arranged in layers. If the director is perpendicular to the layers, the phase is called Smectic A ( $S_A$ ). If the director is tilted at some angle  $\alpha$  between 0 and  $90^\circ$ , the phase is called Smectic C ( $S_C$ ). Other LC phases have been discovered that exhibit various types of positional ordering, but these phases will not be discussed in this text.<sup>9-12</sup>

## 1.4 Characterization of Liquid Crystals

There are numerous techniques that may be used in the identification and characterization of LC phases with the two most commonly used techniques being transmitted polarized light microscopy (PLM) and differential scanning calorimetry (DSC). DSC reveals the presence of LC phases in a given material by detecting enthalpy changes associated with thermodynamic phase transitions. PLM allows for an examination of the textures of these phases and for a qualitative and quantitative look at the alignment of the LC molecules. More sophisticated techniques used in LC characterization are X-ray analysis and nuclear magnetic resonance (NMR) spectroscopy. X-ray analysis maps the location of the

LC molecules within the phase, explicitly providing the phase structure and therefore, classification of the phase. NMR is also used to obtain more detailed information about the structure of LC phases.<sup>9</sup> The discussion in this text is limited to the more commonly used technique PLM.

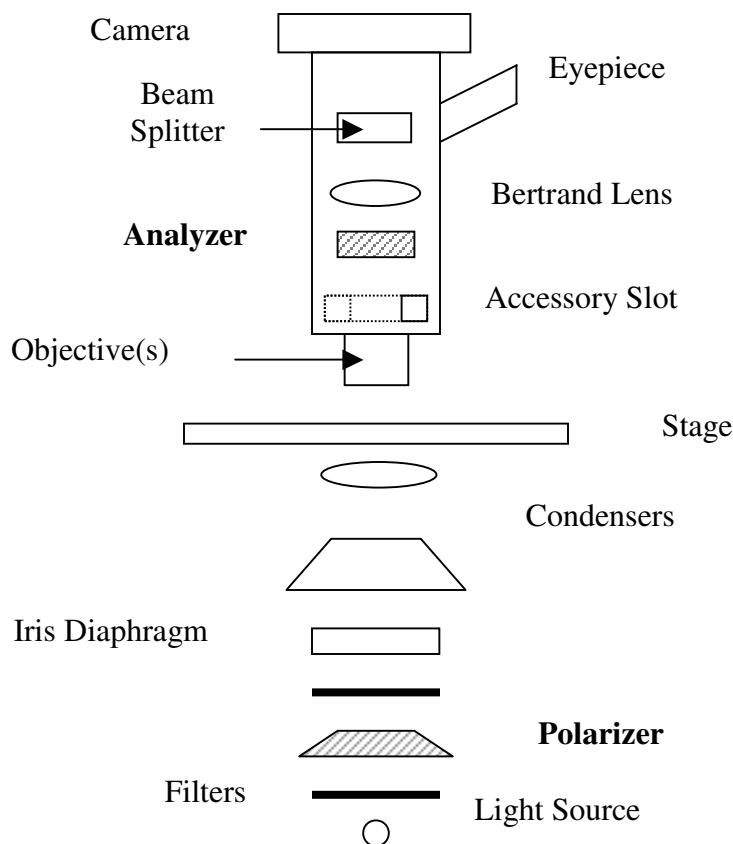


**Figure 1.4** Schematic representation of the orientational and positional order found in the three most common liquid crystalline phases. An isotropic liquid is represented by a random arrangement of rod-like molecules and denoted by I. The nematic (N), Smectic A (S<sub>A</sub>) and Smectic C (S<sub>C</sub>) phases are also shown. The liquid crystal director ( $\mathbf{n}$ ) denotes the average direction of orientation of the molecules and is represented by the black arrow.

### 1.4.1 Transmitted Polarized Light Microscopy

The production of polarized light and the examination of polarization state and amplitude changes upon passing through optically transparent samples allow for the study of anisotropic optical properties. These properties, such as birefringence, are a measure of the molecular and supramolecular structural anisotropy and may be studied nondestructively using a sensitive polarizing microscope. Figure 1.5 is a schematic representation of the components of such a microscope with the most important components being the two polarizing elements called the polarizer and analyzer. The polarizer is placed below the sample stage such that light can be polarized linearly before passing through the sample. This light, with a known polarization state, subsequently passes through the sample where its state is subject to alteration. The second polarizing element, the analyzer, is placed above the sample stage to observe the polarization state and amplitude of the light as it exits the sample. The polarizer and analyzer are generally rotated  $90^\circ$  with respect to one another so that no light is detected when there is either no sample present or an isotropic sample is placed on the sample stage. Accessory plates with a pre-defined effect on the polarization state may be placed in the accessory slot above the sample and below the analyzer. These accessory plates, which produce a reference state, as well as the Bertrand lens are useful in quantifying the changes in polarization induced by the sample.<sup>9, 13-15</sup>





**Figure 1.5** Schematic representation of polarizing microscope. The polarizer and analyzer are shaded for emphasis. Transmitted polarizing microscopes, like compound microscopes are equipped with a set of objectives and matching eyepieces to provide a variety of resolving powers and magnifications. The light source and first condenser (which focuses light on the sample) are both set at a fixed distance from the objectives. The second condenser, called the substage condenser, can be moved up or down relative to the microscope stage. Both condensers are generally optimized for Kohler illumination. The intensity of the light reaching the sample is controlled by the iris diaphragm. The sample is placed on the microscope stage, which ideally should be both freely rotatable and also rigidly lockable. One polarizer is situated below the microscope stage so that light can be linearly polarized before reaching the sample. The second polarizer, also called the analyzer, is situated above the specimen and is used to analyze the results of the light passing through the sample. A slot is included for the insertion of accessories such as a quarter-wave plate, quartz wedge or compensator. The Bertrand lens may also be added to or removed from the field as needed for conoscopic measurements. The beam splitter divides the resulting light between the eyepiece and camera so that the images may be both seen by the microscopist and detected by a CCD camera linked to a computer.

### 1.4.2 Birefringence

When light enters an optically transparent sample, its wavelength and velocity decrease by a factor called the index of refraction ( $n$ ). An isotropic material has a single index of refraction, thus light polarized in any direction travels at the same velocity through the material. If the sample is an anisotropic material such as a liquid crystalline material or solution, the index of refraction differs as a function of direction relative to the sample axes. For example, the index of refraction parallel to the LC director has one value  $n_{||}$  while the index of refraction perpendicular to the director has a second value  $n_{\perp}$ . Light polarized along different directions travels at different velocities in the LC and thus two perpendicular components of light that enter in phase grow out of phase as they propagate through the LC material. This optical phenomenon is called birefringence and is dependent upon sample thickness according to equation (1.1):

$$\Delta n = n_{||} - n_{\perp} = \Gamma/t \quad (1.1)$$

where  $\Gamma$  is the optical retardation or the phase difference between the two components of the light as they exit the sample and  $t$  is the sample thickness. When an anisotropic or birefringent material is examined under a polarizing microscope, an optical texture appears that gives information about the molecular organization within the material.<sup>12 14</sup>

Birefringence may be measured either qualitatively or quantitatively by means of transmitted polarized light microscopy. Qualitatively, birefringence is verified by examining the sample as it is placed between the polarizer and analyzer, which are rotated 90° with respect to one another. The sample stage is then rotated 360° and the amplitude or intensity of the polarized light exiting the sample is measured. The appearance of alternating dark and bright states at 45° intervals of sample rotation is evidence of birefringence. Figure 1.6

shows the sinusoidal light intensity changes associated with rotating an anisotropic or birefringent sample. This observed intensity is a function of two independent factors: the orientation of the crossed polarizers with respect to the sample director and a combination of the sample birefringence and thickness and the wavelength of light. The intensity of light relative to the sample orientation may be expressed by the following equation (1.2):

$$I_R = A^2 \sin^2 2\theta \sin^2 [(\pi t/\lambda)(\Delta n)] \quad (1.2)$$

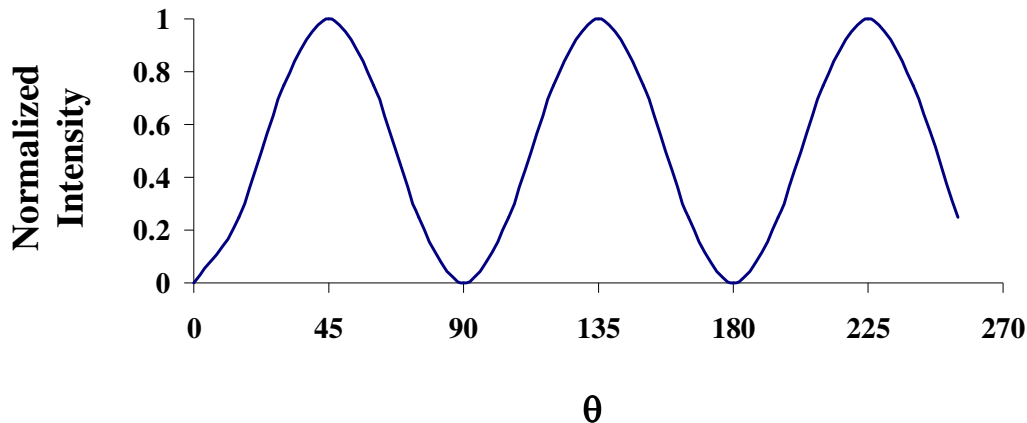
where  $A$  is the amplitude of the light wave,  $\theta$  is the sample rotation angle with respect to the crossed polarizers,  $t$  is the sample thickness,  $\lambda$  is the wavelength of the light and  $\Delta n$  is the birefringence. The birefringence may be further examined by quantitative means to determine the exact phase shift induced by the sample. The de Senarmont compensator, a quarter-wave plate, is introduced into the accessory slot. The sample is rotated  $45^\circ$  with respect to the crossed polarizers. The analyzer is then rotated to achieve a dark state, thus determining the optical retardation according to equation (1.3):

$$\Gamma = 2\varphi \quad (1.3)$$

where  $\varphi$  is the angle of rotation of the analyzer. If the sample thickness is known, the birefringence may be determined mathematically by means of equation (1.1) as previously discussed.<sup>13</sup>

## 1.5 Liquid Crystal Alignment

Many organic and inorganic materials have been used as alignment layers, utilizing such deposition methods as dip coating, sputtering, and spin coating. As previously discussed, some of these alignment layers require further treatment such as mechanical rubbing to induce unidirectional alignment. Others may spontaneously induce alignment.



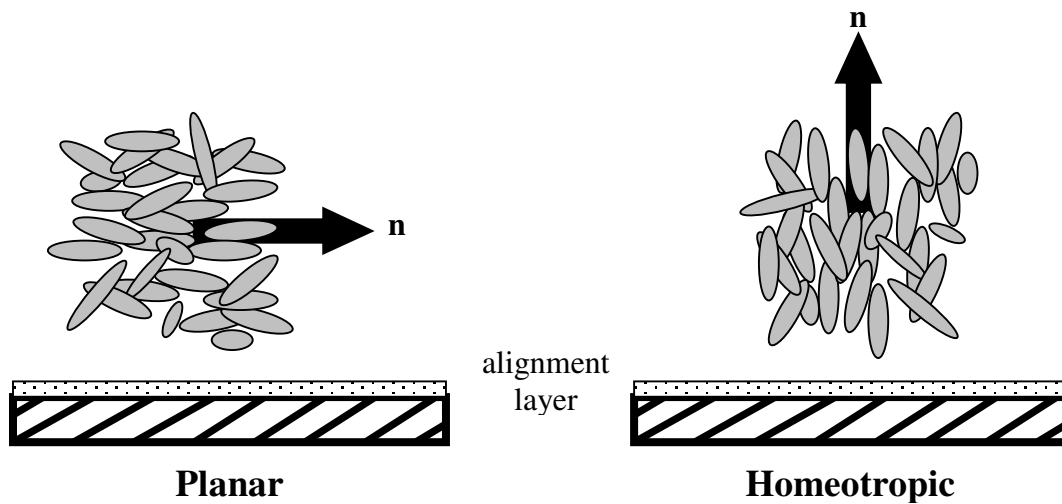
**Figure 1.6** Plot of sample rotation angle (with respect to crossed polarizers) versus normalized intensity of transmitted light. As the sample is rotated through  $360^\circ$ , the transmitted intensity of light sinusoidally varies to give dark and bright states at  $45^\circ$  intervals.

### 1.5.1 Modes of Liquid Crystal Alignment

When analyzing LC materials by transmitted polarized light microscopy, the optical texture that is observed depends not only on the molecular organization of the sample, but also on the alignment of the LC director with respect to the substrate. There are two modes of LC alignment, of which a schematic representation is given in Figure 1.7. Planar alignment occurs when the LC director orients parallel to the substrate and is confirmed by the appearance of alternating dark and bright states at  $45^\circ$  intervals of sample rotation between crossed polarizers. Homeotropic alignment involves the orientation of the director perpendicular to the substrate. With homeotropic alignment, the molecules are oriented on average with their long axes and more importantly, their optic axes perpendicular to the substrate. Thus, as the polarized light propagates through the sample it travels along the optic axis, experiencing only one index of refraction and therefore, no change in its polarization state. With the analyzer rotated  $90^\circ$  with respect to the polarizer, no light is

observed. Therefore, confirmation of homeotropic alignment requires insertion of the Bertrand lens into the light path, allowing a view of the objective back focal plane in which a diffraction pattern or conoscopic image is observed. The details of this image may then be used to determine the orientation of the sample director.<sup>9, 13</sup>

In some cases, the LC director may be orientated at an angle somewhere between the planar ( $0^\circ$  with respect to the substrate) and homeotropic ( $90^\circ$  with respect to the substrate) modes. This mode of alignment is referred to as planar alignment with a pretilt angle. If the LC director is oriented at an angle less than  $45^\circ$ , but greater than  $0^\circ$  with respect to the substrate, the sample is said to exhibit planar alignment with a low pretilt angle. Planar alignment with a high pretilt angle refers to the orientation of the LC director at an angle greater than  $45^\circ$ , but less than  $90^\circ$ . A sample that exhibits planar alignment with a pretilt angle is characterized by the appearance of dark and bright states at  $45^\circ$  intervals of sample rotation, similar to those observed for samples with planar alignment. However, the contrast between the dark and bright states decreases steadily as the pretilt angle increases.



**Figure 1.7** Schematic representation of liquid crystal alignment modes. The liquid crystal director (**n**) is represented by the black arrow.

### 1.5.2 Mechanisms of Liquid Crystal Alignment

Polyimide alignment layers are the current standard for liquid crystal displays. This material, the chemical structure of which is given in Figure 1.8, has several advantages, including simple layer preparation (i.e. polyimide is a liquid at room temperature and thus easily deposited as a thin film by spin-coating), high chemical and thermal resistance, good adhesion to glass and oxide substrates, and potential for modification of the chemical structure and thus modification of the alignment characteristics.<sup>16</sup>

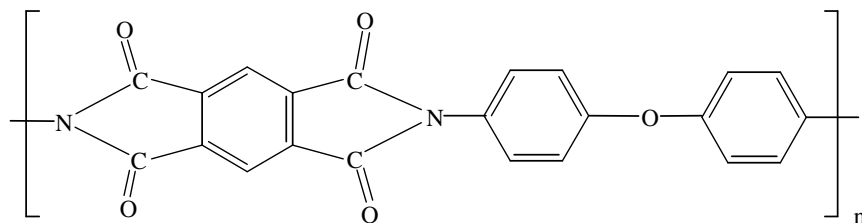
Typically, alignment involves modification of a solid substrate such that its interface with the LC has some anchoring action that results in either planar (tangential) or homeotropic (perpendicular) orientation of the LC director with respect to the interface. Such modification is carried out on a substrate having an electrically conductive layer (usually indium tin oxide or ITO-coated glass) for electric-field-induced reorientation of the director, which in turn results in a variation in the transmitted light intensity. Currently, the preferred modification technique is rather primitive: the conductive substrate is coated with a polyimide layer that after thermal curing is mechanically rubbed.<sup>6,7</sup> The alignment mechanism associated with unidirectional rubbing has contributions from both the physical grooves caused by rubbing the polyimide substrate<sup>6</sup> and the putative molecular interactions<sup>7</sup> between exposed polyimide functionalities and the LC. However, the details of LC alignment are not well understood.<sup>6, 7, 16 18</sup>

As the polyimide film is mechanically rubbed with a synthetic or natural fabric, microscopic and nanoscopic grooves are scratched into the surface. The elastic energy costs associated with aligning the director either parallel or perpendicular to the grooves determines the preferred alignment direction. As seen in the schematic representation in

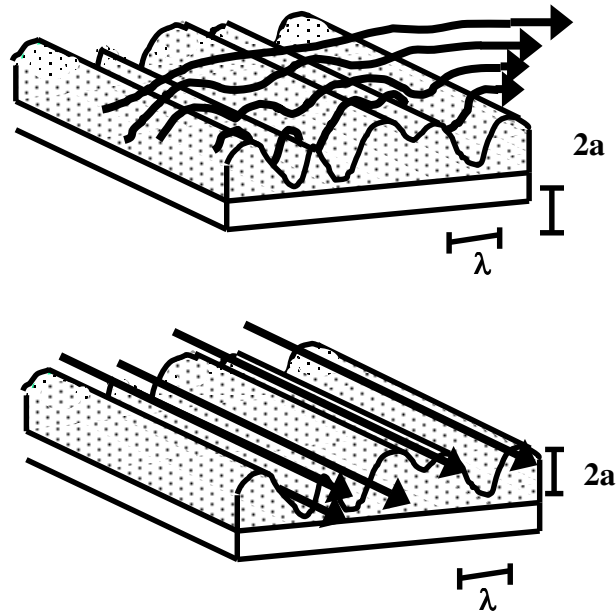
Figure 1.9, the energy costs associated with the director aligning parallel to the grooves are much lower, thus explaining planar alignment of the LC parallel to the rubbing direction.<sup>6,19-</sup>

<sup>21</sup> Additional contributions to this preferred alignment direction may come from interactions between the exposed polyimide functionalities and the LC. It is possible that the orientation of the molecular chains of the polymer is altered (elongated and aligned in the rubbing direction) in the rubbing process due to local heating and simultaneous shearing force. The exposed functionalities of these oriented polyimide chains are then free to interact with the LC, thus reinforcing the preference for planar alignment parallel to the rubbing direction.<sup>7,16-</sup>

18



**Figure 1.8** Chemical structure of polyimide, a polymer commonly used for alignment layer preparation.



Elastic free energy for a sinusoidal surface:

$$\Delta F = (\pi^3 K / 2\lambda) (2a/\lambda)^2$$

K = elastic constant

**Figure 1.9** Schematic representation of the mechanisms of liquid crystal alignment. The elastic energy costs of orienting the liquid crystal director (denoted by black arrows) perpendicular and parallel to the grooved substrate are compared. Perpendicular orientation results in severe distortion of the director.



## 1.6 Research Objectives

The objectives of this research were first, to better understand the mechanisms associated with LC alignment by developing systems that could be easily controlled and quantified and second, to develop novel alignment layers and fabrication techniques that would eliminate the need for mechanical rubbing. Chapter two discusses the use of self-assembled monolayers as alignment layers for the study of LC alignment mechanisms. Steric hindrances between the LC molecules and the alignment layer surface were shown to be the biggest contributor to the alignment of the LC molecules. Two liquid crystals having different chemical functionalities, but the similar shapes were shown to align in the same manner with a dependency on the self-assembled monolayer structure, thus minimizing the possible contributions from molecular interactions. Chapter three discusses the use of carbon nanotube and metal-oxide nanorod films as alignment layers. The use of these anisotropically conductive and self-assembling materials would eliminate the need for both a conductive and alignment layer in displays as well as the need for a mechanical rubbing step. Given that carbon nanotubes and metal-oxide nanorods have no molecular interactions with LC molecules, these films also gave insight into the alignment mechanism related to contributions from steric interactions between LC molecules and the surface. Chapter four discusses the use of thin films of perfluoropolyethers as alignment layers. These films have very low surface energy, inducing spontaneous homeotropic alignment of positive dielectric liquid crystals and possibly, producing faster switching times for display applications. This material is also compatible with soft-lithography, making it possible to fabricate grooved alignment layers similar to traditional polyimide alignment layers without mechanical rubbing. Perfluoropolyether exhibited unique alignment characteristics when compared to

more traditional materials, allowing for a thorough examination of the mechanisms associated with alignment including possible contributions from electric field effects and dipole dipole and steric interactions. Chapter five discusses the use of Langmuir-Blodgett films of perfluoropolyether as alignment layers. These alignment layers were used to better understand the alignment characteristics of perfluoropolyethers, including mechanisms of alignment, surface energy and surface anchoring energy.

## 1.7 References

- (1) Reinitzer, F. *Montash. Chem.* **1888**, 9, 421-441.
- (2) Lehmann, O. *Zeits. Phys. Chem.* **1889**, 4, 462-472.
- (3) Heilmeyer, G.H.; Zanoni, L.A.; Barton, L.A. *Proc. I.E.E.E.* **1968**, 56, 1162-1171.
- (4) Rasing, T.; Musevic, I. *Surfaces and Interfaces of Liquid Crystals*; Springer: Berlin, 2004.
- (5) Fisch, M.R. *Liquid Crystals, Laptops and Life*; World Scientific: Singapore, 2004.
- (6) Berreman, D. W. *Phys.Rev. Lett.* **1972**, 28, 1683-1686.
- (7) Geary, J. M.; Goodby, J. W.; Kmetz, A. R.; Patel, J. S. *J. Appl. Phys.* **1987**, 62, 4100-4108.
- (8) Kaneko, E. *Liquid Crystal TV Displays: Principles and Applications of Liquid Crystal Displays*; KTK Scientific Publishers: Tokyo, 1987; pp 1-32.
- (9) Collings, P.J.; Hird, M. *Introduction to Liquid Crystals Chemistry and Physics*; Taylor & Francis Ltd.: Bristol, 1997.
- (10) De Gennes, P.G. *The Physics of Liquid Crystals*; Clarendon Press: Oxford, 1974; pp1-224.
- (11) Kumar, S. *Liquid Crystals: Experimental Study of Physical Properties and Phase Transitions*; Cambridge University Press: New York, 2001; pp1-63.
- (12) Chandrasekhar, S. *Liquid Crystals*; Cambridge University Press: New York, 1992.
- (13) Viney, C. *Transmitted Polarized Light Microscopy*; McCrone Research Institute: Chicago, 1990; pp 1-171.
- (14) Inoue, S. *Video Microscopy*; Plenum Press: New York, 1989; pp 477-510.
- (15) Hartshorne, N.H. *The Microscopy of Liquid Crystals*; Microscope Publications Ltd.: London, 1974; pp 1-95.
- (16) Okulska-Bozek, M.; Prot, T.; Borycki, J.; Kedzierski, J. *Liquid Crystals* **1996**, 20, 349-359.

- (17) Kim, Y. B.; Olin, H.; Park, S. Y.; Choi, J. W.; Komitov, L.; Matuszczyk, M.; Lagerwall, S. T. *Appl. Phys. Lett.* **1995**, 66 2218-2219.
- (18) Zhu, Y. M.; Wang, L.; Lu, Z. H.; Wei, Y.; Chen, X. X.; Tang, J. H. *Appl. Phys. Lett.* **1994**, 65, 49-51.
- (19) de Jeu, W.H. *Physical Properties of Liquid Crystalline Materials*; Gordon and Breach Science Publishers: New York, 1980; pp 1-49.
- (20) Blinov, L.M.; Chigrinov, V.G. *Electrooptic Effects in Liquid Crystal Materials*; Springer: New York, 1994; pp 1-131.
- (21) Demus, D.; Goodby, J.; Gray, G.W.; Spiess, H.-W.; Vill, V. *Physical Properties of Liquid Crystals*; Wiley-VCH: Weinheim, 1999.

## **CHAPTER 2**

### **ALIGNMENT OF NEMATIC LIQUID CRYSTALS USING ORGANIZED MOLECULAR FILMS**

#### **2.1 Organized Molecular Films**

Zisman first published the preparation of a self-assembled monolayer (SAM) by adsorption of a surfactant onto a clean metal surface in 1946.<sup>1</sup> The potential for self-assembly was not recognized at that time, generating little research interest until the 1980s when the work of Nuzzo and Allara showed that SAMs of alkanethiols on gold could be prepared in dilute solutions.<sup>2</sup> This research along with that of Maoz and Sagiv (SAMs of trichlorosilanes on silicon oxide) incited greater interest in these systems.<sup>3</sup> Many self-assembly systems have been investigated since that time, aided by the development and application of surface-sensitive experimental techniques such as scanning probe microscopy and vibrational spectroscopy.<sup>4</sup>

Self-assembled monolayers are ordered molecular assemblies formed spontaneously by the adsorption of a surfactant molecule onto a solid substrate, facilitated by the specific affinity of the head group for the substrate. These systems have several attractive characteristics such as ease of preparation, tunability of surface properties by modification of molecular structure, use as building blocks in more complex structures, and possibility of lateral structuring on the nanometer scale. These features make possible applications in wetting, adhesion, corrosion prevention, wear protection, and chemical and biochemical

sensing.<sup>4-8</sup> Additionally, the high degree of molecular order and variety in head and tail groups of SAMs make them good candidates for alignment layers used in liquid crystal displays (LCDs).

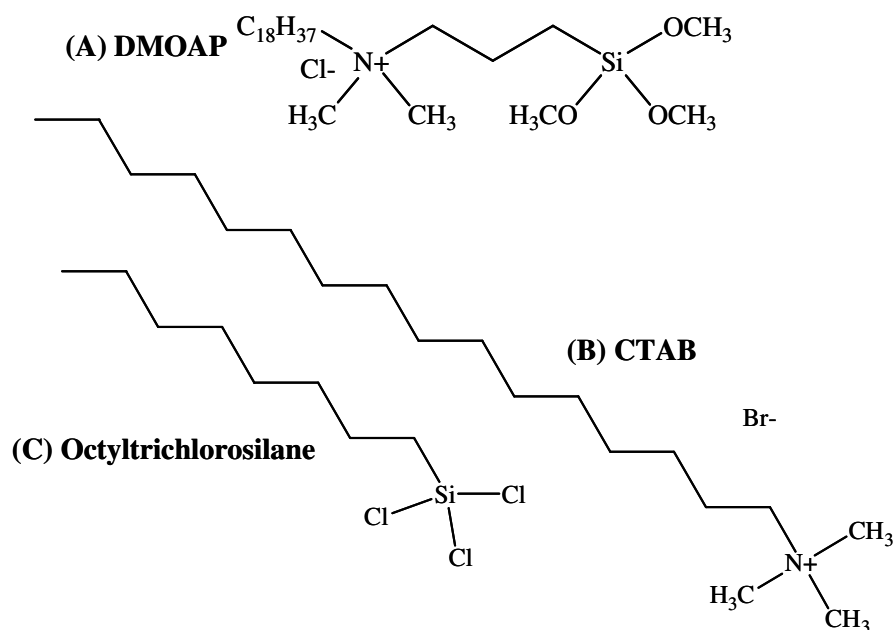
There are several advantages to using SAMs as alignment layers. First, the spontaneous, macroscopic alignment achieved using this system would eliminate the need for the mechanical rubbing step used in the current fabrication process. Second, the surfactant molecules used in SAMs are easily modified such that investigation of the mechanisms of liquid crystal (LC) alignment is made possible. Finally, both planar and homeotropic alignment can be achieved using SAMs.<sup>9</sup> Liquid crystal (LC) alignment layers have been successfully prepared using SAMs of organic molecules on a variety of conducting and insulating substrates. Two such alignment layers are SAMs of *N,N*-dimethyl-*n*-octadecyl-3-aminopropyltrimethoxysilyl chloride (DMOAP) and cetyltrimethylammonium bromide (CTAB) on both standard glass and conductive glass coated with indium tin oxide (ITO). The LC director orientation is perpendicular to the substrate in the case of DMOAP (homeotropic alignment),<sup>10</sup> while alignment layers prepared with CTAB can induce either homeotropic or planar orientation depending on the concentration of CTAB.<sup>11</sup>

In this work, LC alignment layers were prepared using SAMs of DMOAP and CTAB for comparison with standard polyimide alignment layers. Hybrid and gradient alignment layers composed of SAMs of variable concentration, in which the LC director orientation changes with respect to the 2-dimensional position on the substrate, were also prepared to examine the necessary characteristics for and the mechanisms driving good LC alignment. These alignment layers were used to fabricate optical cells in which transitions between homeotropic and planar alignment were examined by transmitted polarized light microscopy.

## 2.2 Experimental Details

### 2.2.1 Materials

Polyimide monomer (JSR, AL 1254) was used as received. Dimethyloctadecyl[3-(trimethoxysilyl)propyl] ammonium chloride (DMOAP, 60% in methanol, Acros, 33853), cetyltrimethyl ammonium bromide (CTAB, 99+%, Acros, 22716) and octyltrichlorosilane (OTS, 97%, Aldrich, 5283-66-9) were used as received. Chemical structures of the surfactants used in these experiments are shown in Figure 2.1. Ethylene glycol (Fisher Scientific, S-80005) was used as is for contact angle measurements. Nematic liquid crystals 4-cyano-4'-pentyl 1,1'-biphenyl (K-15, EM Industries, IS-1143,  $\Delta\epsilon = +13.2$ ) and MLC-6608 (Merck,  $\Delta\epsilon = -4.2$ ) were used as received. Liquid crystal optical cells were fabricated using indium tin oxide (ITO)-coated glass (Delta Technologies, Ltd., CG-811N-S115).



**Figure 2.1** Chemical structures of the surfactants used to prepare self-assembled monolayers. (A) dimethyloctadecyl[3-(trimethoxysilyl)propyl] ammonium chloride, (B) cetyltrimethyl ammonium bromide, and (C) octyltrichlorosilane.

### **2.2.2 Instrumentation**

A dipping apparatus built in-house was used for sample preparation (Figure 2.2). A sample holder was constructed with Teflon and attached to a lever by a series of aluminum plates in a guillotine fashion. This apparatus allowed for controlled vertical dipping of substrates in a variety of solutions. An apparatus for mechanical rubbing of polymer films was built in-house (Figure 2.3). A sample mount and manipulator were fabricated with Teflon. A felt roller was attached to a hand drill and firmly suspended above the sample mount such that sliding the sample mount to the right would mechanically rub the substrate at a controlled speed. Thin polymer films were prepared using a Laurell Technologies Corporation spin caster (WS-400A-6NPP/LITE). Birefringence texture measurements were made using a Nikon Microphot FX polarizing microscope equipped with a Sony CCD-IRIS camera. Images were obtained using video generation software by Roxio. Contact angle measurements were made using a CAM200 Optical Contact Angle Meter (KSV Instruments, Ltd.) and KSV software.

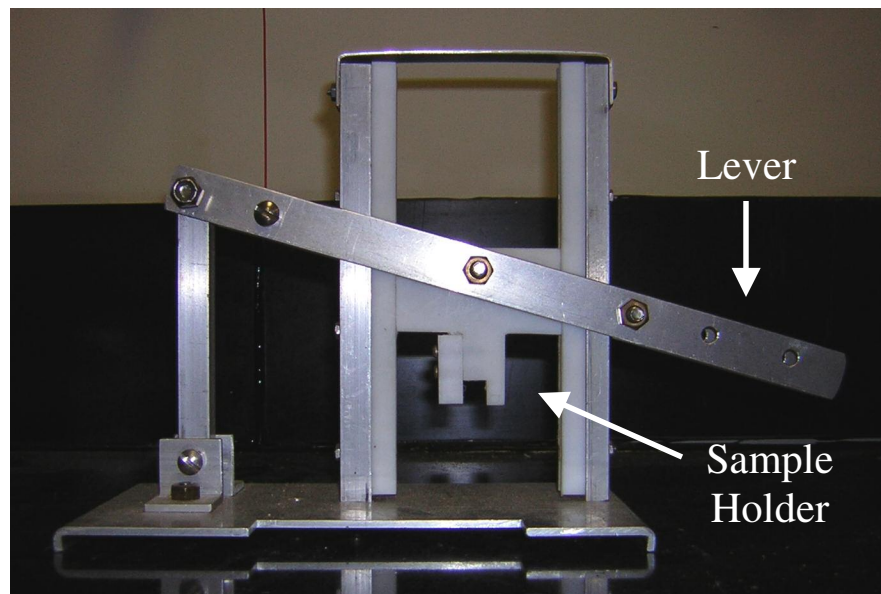
### **2.2.3 Preparation of Polyimide Films**

Thin films of polyimide on clean ITO-coated glass were prepared by spin-coating at either 1000 or 2000 RPM for 1 minute. The films were thermally cured at 180° C for 30 minutes. Upon cooling to room temperature, the films were mechanically rubbed using apparatus shown in Figure 2.3.

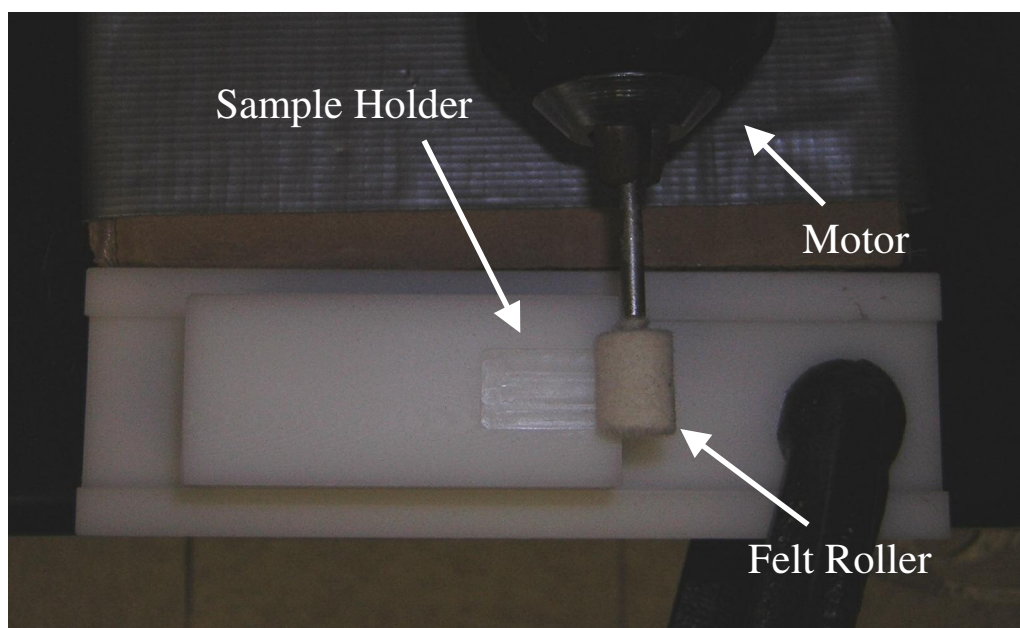
### **2.2.4 Deposition of Self-Assembled Monolayers**

SAMs of DMOAP were prepared by immersing a clean ITO-coated glass substrate into a 0.1% solution of DMOAP in deionized water. The substrate was agitated for 5 minutes and rinsed with deionized water to removed excess surfactant. The excess water was





**Figure 2.2** Photograph of the dipping apparatus built in-house.



**Figure 2.3** Photograph of the mechanical rubbing apparatus built in-house.

removed using a stream of nitrogen gas. The monolayer was thermally cured at 110° C for 1 hour. SAMs of CTAB were prepared by one of two methods: (1) Agitation method: a clean ITO-coated glass substrate was immersed in a CTAB/deionized water solution of known concentration and agitated for 5 minutes. The substrate was removed, rinsed with deionized water and dried with nitrogen. The monolayer was then thermally cured at 110° C for 1 hour. (2) Dipping method: a clean ITO-coated glass substrate was vertically dipped in a CTAB/deionized water solution of known concentration and rapidly removed. Excess water was removed by blotting with a tissue and substrates were allowed to dry at room temperature for several hours.

### **2.2.5 Deposition of Hybrid Molecular Films**

DMOAP/polyimide hybrid molecular films were prepared as follows: a clean ITO-coated glass substrate was immersed in a 0.1% solution of DMOAP in deionized water and agitated for 5 minutes. The substrate was removed, rinsed with deionized water and dried with nitrogen gas before thermally curing at 110° C for 1 hour. Upon cooling to room temperature, the substrate was dipped halfway into a polyimide solution. The excess polyimide was removed using a stream of nitrogen gas and the substrate was thermally cured at 180° C for 30 minutes. Upon cooling to room temperature, the polyimide-coated portion of the substrate was mechanically rubbed using a felt roller driven by a motor. Liquid crystal (LC) optical cells were fabricated using one substrate having a hybrid film and one substrate having a SAM of DMOAP.

Low concentration/high concentration CTAB hybrid films were prepared as follows: a clean ITO-coated substrate was vertically dipped into a low concentration CTAB/deionized water solution and rapidly removed. Water droplets were blotted with tissue. The substrate

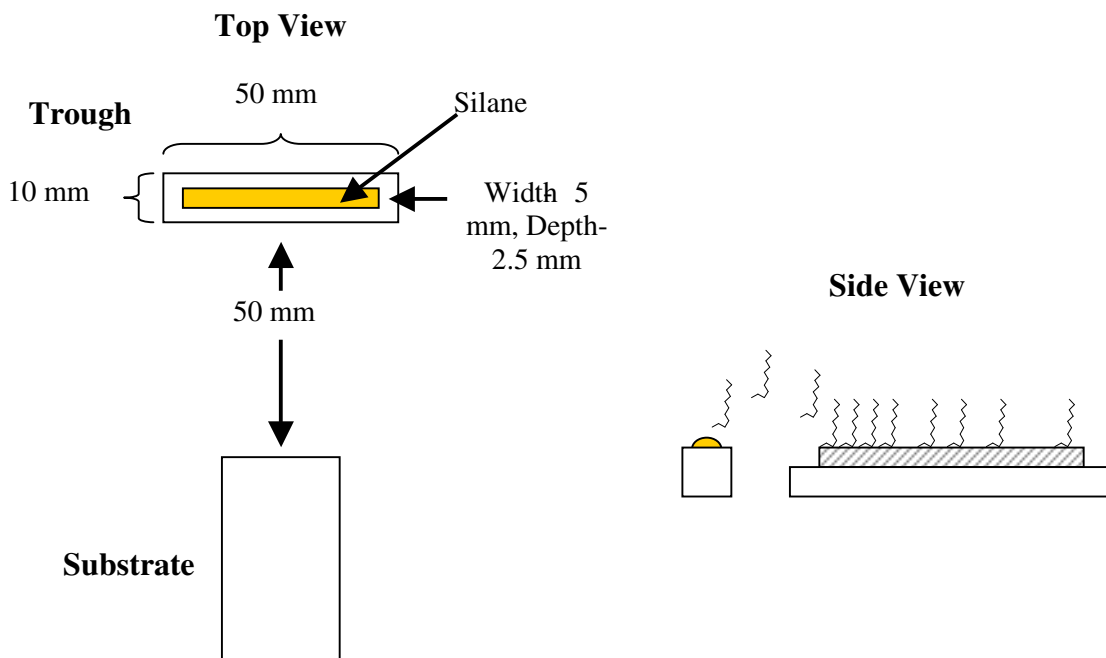
was then vertically dipped to the halfway point in a high concentration CTAB/deionized water solution and rapidly removed. Water droplets were blotted with a tissue. The substrate was allowed to dry at room temperature for several hours. LC optical cells were fabricated using one substrate having a hybrid film and one substrate having a SAM of CTAB prepared using a high concentration solution.

#### **2.2.6 Deposition of Gradient Molecular Films**

A Teflon trough having dimensions of 40 mm length, 5 mm width and 2.5 mm depth was filled with a 1:3 mixture of octyltrichlorosilane and paraffin oil. A clean glass substrate was placed in close proximity to the trough and elevated such that it was flush with the top edge of the trough. The trough and glass substrate were covered with a plastic dish and evaporation of the silane was allowed for 5 minutes. The substrate was removed and dried with nitrogen.<sup>12,13</sup> A schematic representation of the deposition of a gradient molecular film is given in Figure 2.4.

#### **2.2.7 Fabrication of Liquid Crystal Optical Cells**

Liquid crystal optical cells, used for the observation of birefringent textures, were fabricated as follows: Two substrates were sandwiched together with the alignment layers facing each other at predetermined orientations separated by a spacer (6 or 40  $\mu\text{m}$ ) and sealed together using epoxy. The optical cells were filled with either K-15 or MLC-6608 (in the isotropic or nematic state for comparison) by capillary action and examined for light intensity changes.



**Figure 2.4** Schematic representation of the deposition of a gradient molecular film by evaporation. The top view gives the trough dimensions, while the side view shows a cartoon depiction of surfactant molecules evaporating onto a substrate.

## 2.3 Results and Discussion

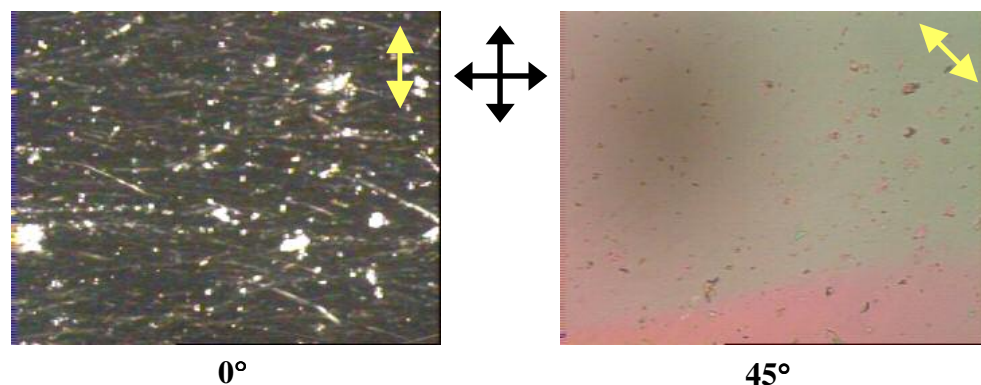
### 2.3.1 Birefringent Textures of Polyimide Films as Control

Substrates on which polyimide alignment layers were prepared by traditional methods served as controls for subsequent experiments using alignment layers prepared with self-assembled monolayers and using hybrid alignment layers. The birefringent textures seen in Figure 2.5 confirm uniform, macroscopic planar alignment of the nematic LC K-15. Alternating dark and bright states are exhibited at  $45^\circ$  intervals of sample rotation between crossed polarizers. The white spots observed in these images are a result of dust particles generated during the mechanical rubbing process. The alignment mechanism associated with this system has contributions from both the physical grooves etched in the polyimide surface

upon mechanical rubbing (the elastic energy costs are minimized when the LC director orients parallel to the grooves)<sup>14</sup> and the putative molecular interactions between exposed polyimide functionalities and the LC.<sup>15,16</sup>

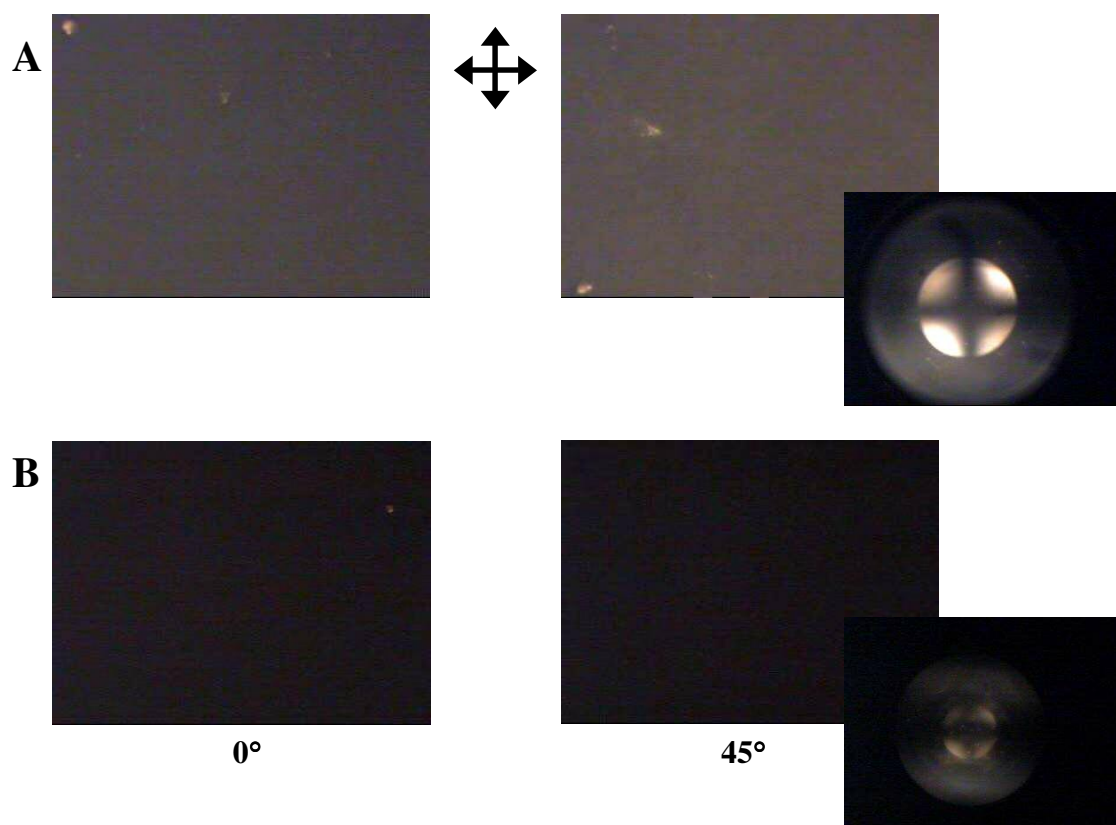
### 2.3.2 Birefringent Textures of DMOAP Self-Assembled Monolayers

Substrates having self-assembled monolayers (SAMs) of the surfactant DMOAP were prepared by the agitation method described above and thermally cured before fabrication of the LC optical cell and examination of LC alignment. These alignment layers exhibited homeotropic alignment of both positive and negative LCs as confirmed by the persistent dark state through all sample rotations (Figure 2.6). Because isotropic samples also have a persistent dark state through 360° sample rotation, it is important to confirm homeotropic alignment with a conoscopic measurement. The insets of Figure 2.6 A and B shows the conoscopic image associated with each LC optical cell. The crossed isogyres confirm that the sample is optically anisotropic with uniaxial symmetry and is being viewed along the optic axis due to homeotropic alignment of the LC director. The mechanism of alignment

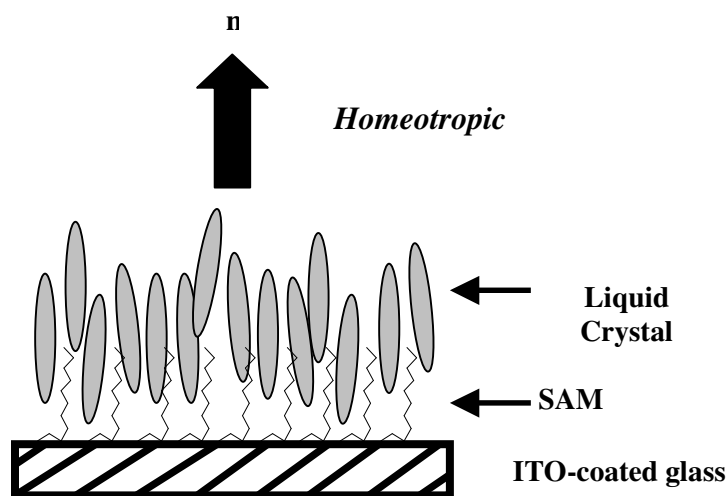


**Figure 2.5** Birefringent texture images for alignment of a positive dielectric liquid crystal by polyimide. Macroscopic, uniform planar alignment is achieved. The orientation of the crossed polars is given by the crossed black arrows while the rubbing direction is given by the double-headed yellow arrows.

associated with SAMs involves a preference for vertical close packing of LC molecules due to steric hindrances created by the long aliphatic chains of the SAMs. A schematic representation of the proposed alignment mechanism is given in Figure 2.7. Both the positive and negative dielectric LCs used in this experiment are calamitics (rod-like in shape) and would experience the proposed steric hindrances.



**Figure 2.6** Birefringent texture images for alignment of both (A) positive and (B) negative dielectric liquid crystal by SAMs of DMOAP. Macroscopic, uniform homeotropic alignment is achieved and verified by conoscopic measurements. The orientation of the crossed polars is given by the crossed black arrows.



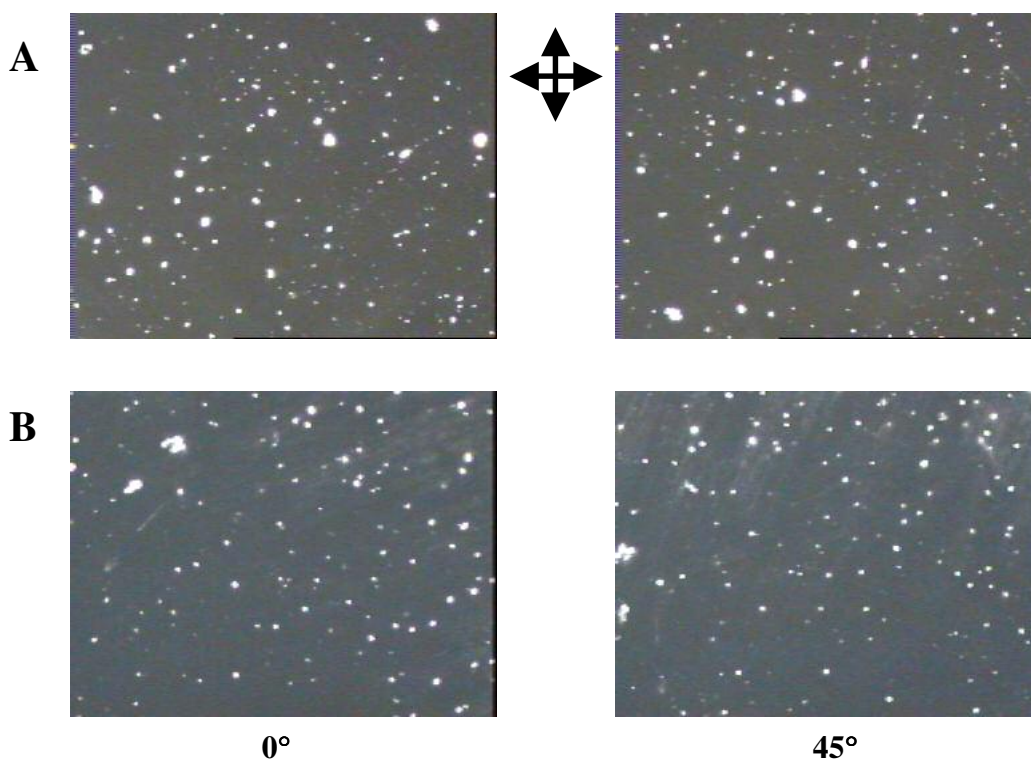
**Figure 2.7** Schematic representation of the liquid crystal alignment mechanism associated with homeotropic alignment of liquid crystal by DMOAP SAMs. The thickness of the liquid crystal film is generally on the order of many molecular lengths (tens of microns), but the alignment at the surface drives ordering throughout the film.

### 2.3.3 Concentration Dependence of Liquid Crystal Alignment Using CTAB Self-Assembled Monolayers

The birefringent textures observed for the alignment of nematic LCs by SAMs of the surfactant CTAB were dependent upon both the preparation method and the concentration of the CTAB solution. Substrates having SAMs of CTAB prepared by the agitation method showed homeotropic alignment of both positive and negative dielectric LCs at both high and low concentrations of CTAB in deionized water. Figure 2.8 A and B shows homeotropic alignment of the positive dielectric LC K-15 on substrates prepared at CTAB concentrations of  $6 \times 10^{-5}$  M and  $5 \times 10^{-7}$  M, respectively. Figure 2.9 A and B shows homeotropic alignment of positive and negative dielectric LCs, respectively on substrates prepared at a CTAB concentration of  $6 \times 10^{-5}$  M. These observations of a persistent dark state through all sample

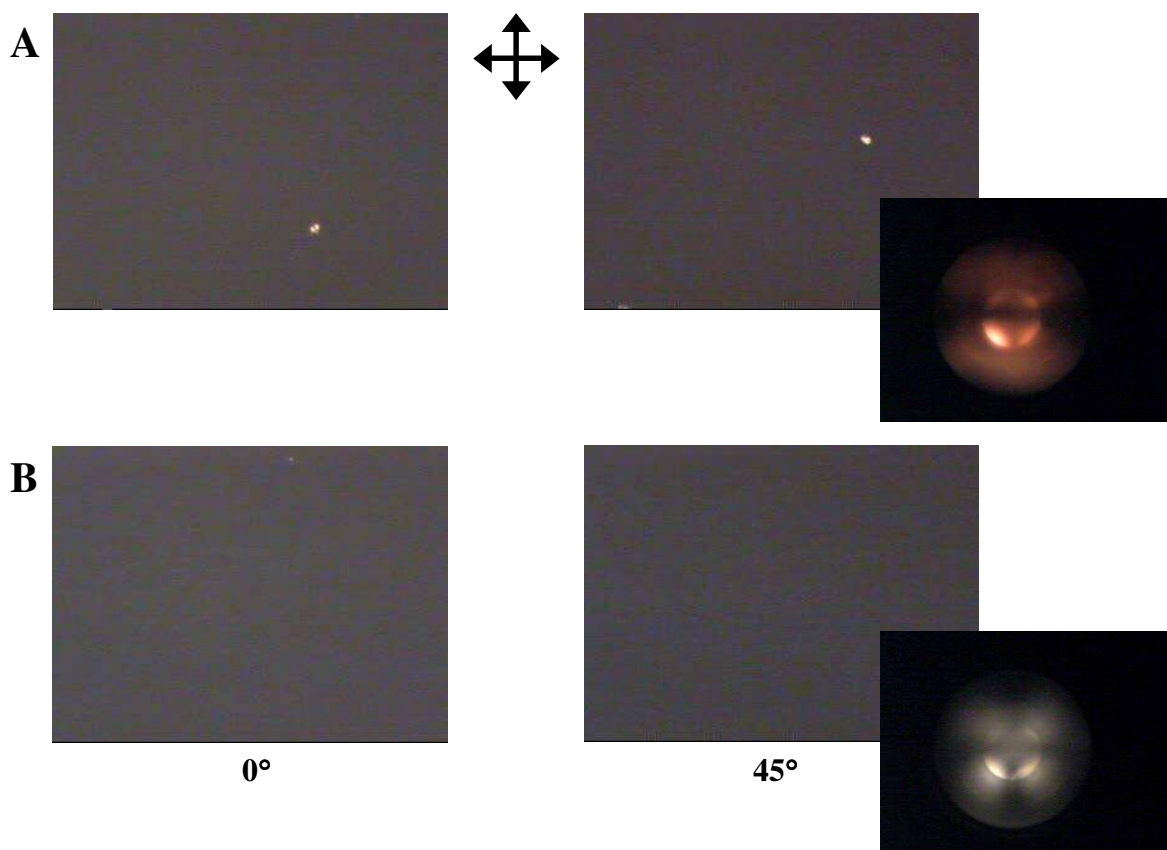
rotations were confirmed by conoscopic measurements. The proposed alignment mechanism associated with these CTAB alignment layers is identical to that of the DMOAP SAMs.

Substrates having SAMs of CTAB prepared by the dipping method showed a dependence of LC alignment on the concentration of the CTAB solution. The birefringent textures observed for the alignment of nematic LCs by SAMs of CTAB prepared at concentrations ranging from  $6 \times 10^{-5}$  to  $5 \times 10^{-7}$  M are shown in Figure 2.10. At higher concentrations such as  $6 \times 10^{-5}$  and  $3.4 \times 10^{-5}$  M, homeotropic alignment of the nematic LC was observed as confirmed by a persistent dark state and conoscopic measurements. At lower concentrations, planar alignment of the LC was observed. The uniformity of this



**Figure 2.8** Birefringent texture images for alignment of liquid crystal by SAMs of CTAB prepared at (A) high concentration ( $6 \times 10^{-5}$  M) and (B) low concentration ( $5 \times 10^{-7}$  M) by agitation method. Macroscopic, uniform homeotropic alignment is achieved and verified by conoscopic measurements. The orientation of the crossed polars is given by the crossed black arrows.



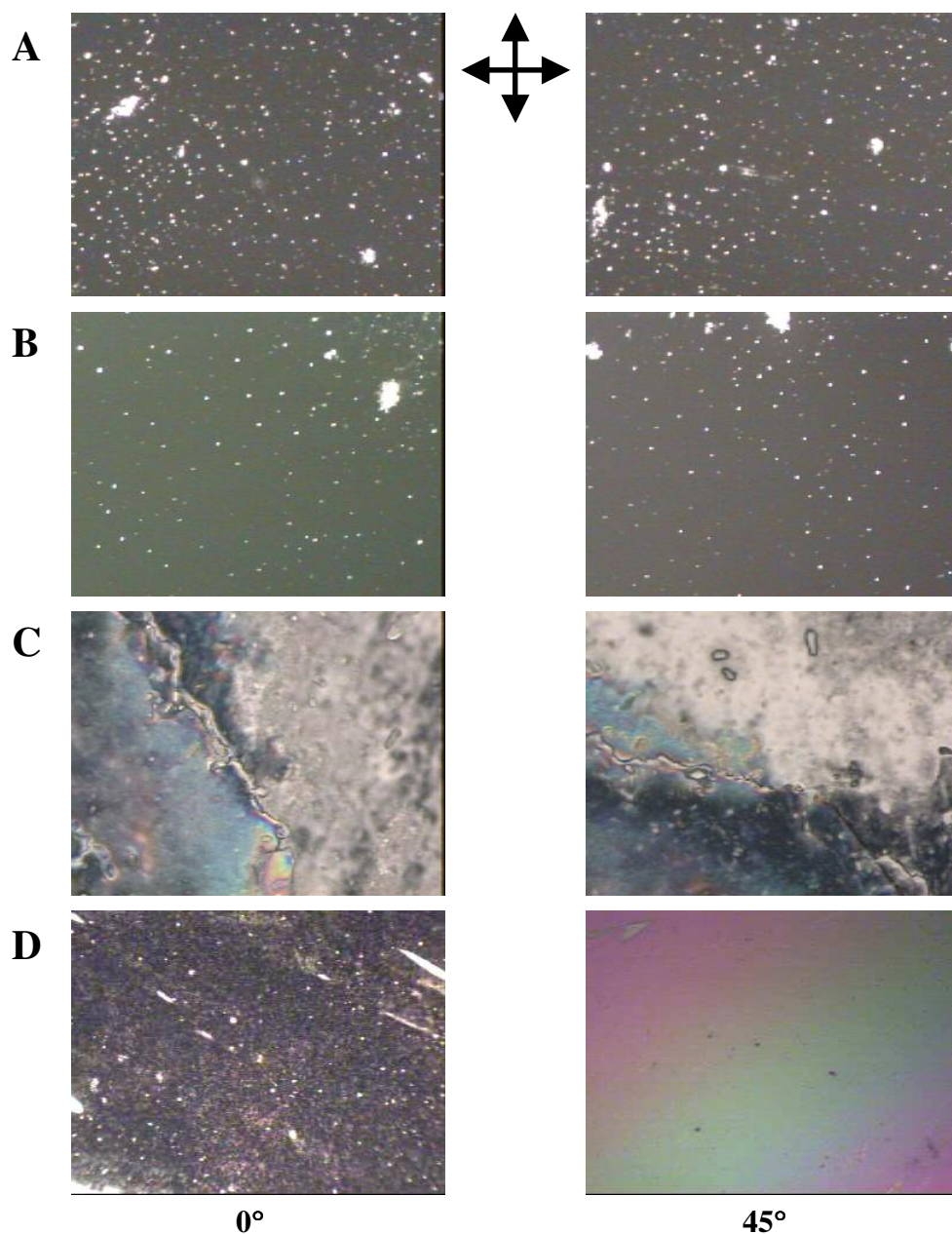


**Figure 2.9** Birefringent texture images for alignment of both (A) positive and (B) negative dielectric liquid crystal by SAMs of CTAB prepared at  $6 \times 10^{-5}$  M by agitation method. Macroscopic, uniform homeotropic alignment is achieved and verified by conoscopic measurements. The orientation of the crossed polars is given by the crossed black arrows.

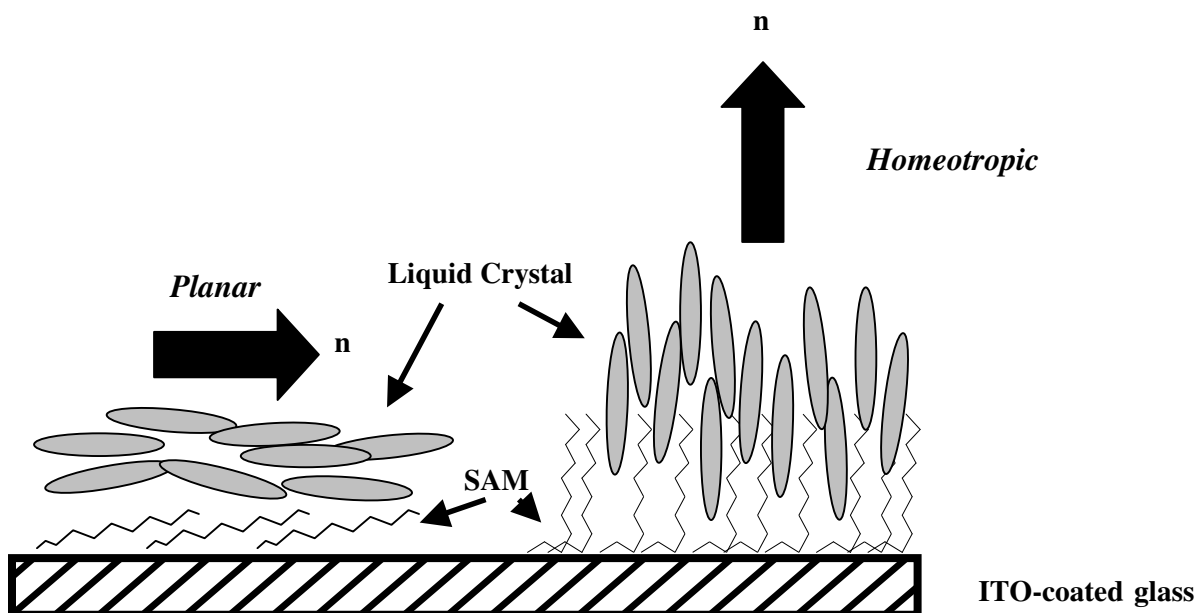
planar alignment increased as the concentration of CTAB decreased as shown in Figure 2.10

C and D. Figure 2.10 C shows random domains of planar alignment, some of which exhibit a high pretilt angle, for SAMs prepared at a CTAB concentration of  $8 \times 10^{-6}$  M, while Figure 2.10 D shows macroscopic, uniform planar alignment for SAMs prepared at a CTAB concentration of  $5 \times 10^{-7}$  M. This LC alignment dependence on concentration is related to the packing density of the CTAB surfactant molecules on the substrate surface. When a substrate is dipped into a solution, there is some degree of shear force applied as the substrate

is removed. If the surfactant molecules are tightly packed on the substrate surface, this shear force does little to disturb their preferred orientation, perpendicular to the substrate. As the packing density of the surfactant molecules decreases, the long aliphatic chains have a tendency to lie down on the substrate surface, a phenomenon reinforced and directed by shear forces. A schematic representation of this orientation of the SAMs is shown in Figure 2.11. In order to minimize free energy costs and possibly, due to small van der Waals interactions between the LC molecules and the surfactant molecules, the LC molecules prefer to maximize their contact with the substrate. With the steric hindrances of the tightly packed SAMs removed, the LC molecules orient planar to the substrate surface.



**Figure 2.10** Birefringent texture images for alignment of liquid crystal on SAMs of CTAB prepared at various concentrations by the dip-coating method. Homeotropic alignment is observed for SAMs prepared at concentrations of (A)  $6 \times 10^{-5}$  and (B)  $3.4 \times 10^{-5}$  M. Planar alignment is observed for SAMs prepared at concentrations of (C)  $8 \times 10^{-6}$  and (D)  $5 \times 10^{-7}$  M as well as  $4 \times 10^{-6}$  and  $2.25 \times 10^{-6}$  M (not pictured). The orientation of the crossed polars is given by the crossed black arrows.



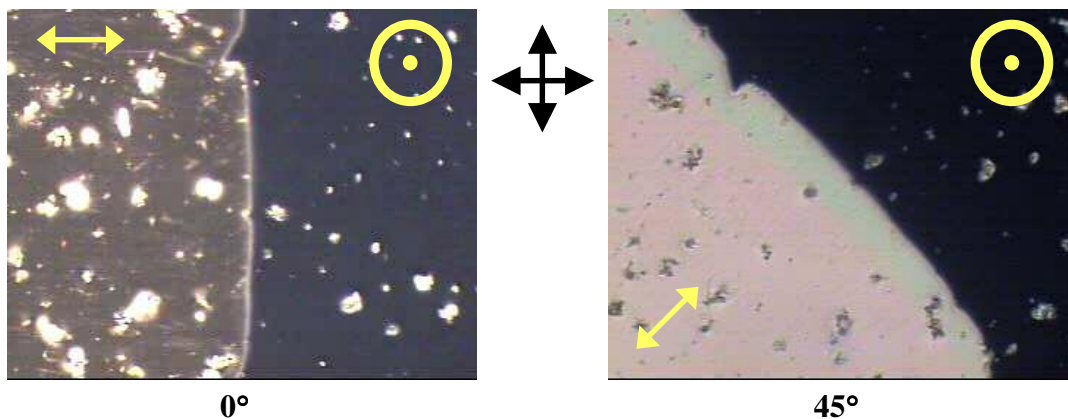
**Figure 2.11** Schematic representation of two modes of LC alignment observed for SAMs of CTAB prepared at varying concentration by the dip-coating method. The LC director orientation is dependent upon the surfactant molecule orientation and packing density.

#### 2.3.4 Birefringent Textures of DMOAP/Polyimide Hybrid Films

Understanding the LC alignment mechanisms of SAMs and quantifying the molecular packing density required for a given pretilt angle of the LC director requires an examination of the transition from homeotropic to planar alignment. Hybrid films prepared by modifying one half of the substrate with DMOAP (produces homeotropic alignment) and one half of the substrate with polyimide (produces planar alignment) were generated to determine the sensitivity of the LC director to changes in alignment mode. The LC optical cell fabricated with two substrates, one having a hybrid film and the other having a SAM of DMOAP, exhibited two regions of alignment with a small transitional region at the boundary (Figure 2.12). To the left of the boundary between the DMOAP and polyimide regions of the hybrid film, the contributions to LC alignment from the polyimide region of the hybrid film dominate over those from the SAM of DMOAP and planar alignment is exhibited. To the

right of the boundary, the DMOAP SAM and the DMOAP region of the hybrid film overlap, producing homeotropic alignment of the LC. The perceived decrease in light intensity for the homeotropic region as the LC optical cell is rotated  $45^\circ$  is due to the increased contrast between the bright state produced in the polyimide region and persistent dark state of the DMOAP region. There is a small transitional region characterized by a green stripe in Figure 2.12. This color change is due to a change in the thickness of the polyimide film rather than a change in the orientation of the LC director.

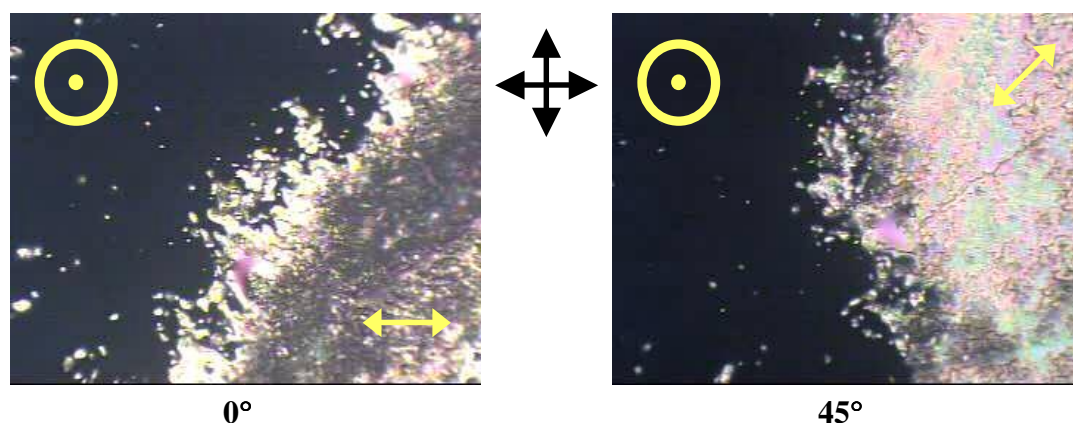
The transition from homeotropic to planar alignment observed in this hybrid system was not a gradual one. The transition at the boundary was an abrupt one due to the abrupt physical change between the two types of alignment layers, confirming the sensitivity of the LC director to changes in alignment mode. However, a more gradual transition from homeotropic to planar alignment would be desirable for a study of correlations between molecular packing density and LC director pretilt angle. A hybrid film of uniform molecular composition would allow for the most direct comparison for such a study.



**Figure 2.12** Birefringent textures images of liquid crystal alignment by DMOAP/polyimide hybrid film. Regions of planar alignment are denoted by the double-headed yellow arrows while regions of homeotropic alignment are denoted by the yellow circles (the LC director perpendicular to the plane of the page). The orientation of the crossed polars is given by the crossed black arrows.

### **2.3.5 Birefringent Textures of Low Concentration/High Concentration CTAB Hybrid Films**

Substrates having a hybrid film prepared by modifying one half of the substrate with a high concentration solution of CTAB and one half of the substrate with a low concentration solution of CTAB were used to examine the transition between homeotropic and planar modes of LC alignment. The LC optical cell fabricated with two substrates, one having a hybrid film and the other having a SAM of CTAB prepared with a high concentration solution (produces homeotropic alignment), exhibited three regions of alignment similar to that observed for DMOAP/polyimide hybrid films (Figure 2.13). To the left of the boundary between the high concentration and low concentration regions of the hybrid film, the high concentration regions of both the hybrid film and the SAM overlap, producing homeotropic alignment of the LC. To the right of the boundary, planar alignment was exhibited. The boundary consisted of a small transitional area (on the order of mm) characterized by patches of planar alignment. The orientation of the LC director in the transitional region differed from that observed in the planar region, being rotated approximately  $45^\circ$  with respect to the planar region. It was difficult to measure the physical transition between the homeotropic and planar regions of the film, therefore difficult to quantify the alignment conditions present in the transitional area. The lack of a clear boundary and the differing LC director orientations may be due to random diffusion of the surfactant molecules. While the homeotropic and planar regions are easily distinguished, a substrate having a more gradual transition between these two modes of alignment would be desirable for more detailed studies.



**Figure 2.13** Birefringent textures images of liquid crystal alignment by high concentration CTAB/low concentration CTAB hybrid film. Regions of planar alignment are denoted by the double-headed yellow arrows while regions of homeotropic alignment are denoted by the yellow circles (the LC director perpendicular to the plane of the page). The orientation of the crossed polars is given by the crossed black arrows.

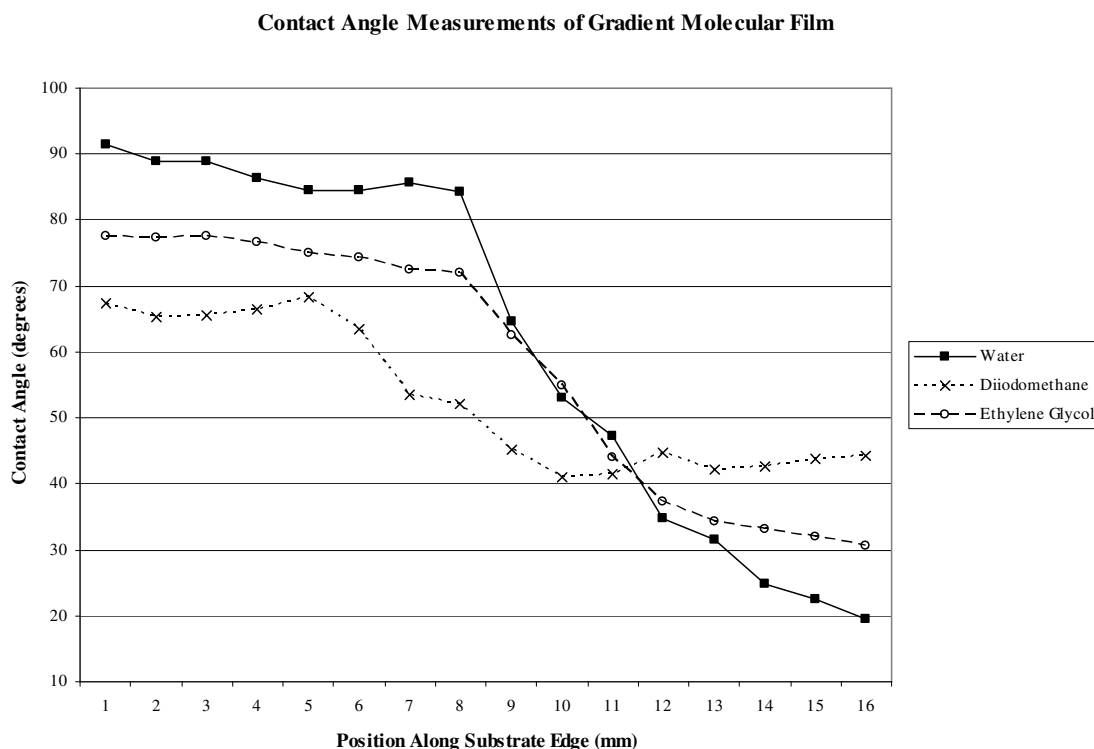
### 2.3.6 Birefringent Textures of Gradient Molecular Films

Observation of the transition between homeotropic and planar alignment and quantification of the molecular packing density necessary for either mode of alignment is best achieved using a gradient film. Gradient films of octyltrichlorosilane were deposited onto glass substrates by the evaporation method shown in Figure 2.4 and verified by contact angle measurements. Figure 2.14 is a plot of the contact angle of water, ethylene glycol and diiodomethane (three common solvents used for this measurement) with respect to the one-dimensional position along the substrate, the zero position marking the portion of the substrate closest to the trough during deposition. The presence of a molecular film influences the surface tension of the substrate. A decrease in contact angle when moving from left to right along the substrate was observed, confirming the presence of an octyltrichlorosilane gradient, in which the concentration and therefore, molecular packing density of octyltrichlorosilane decreases when moving from left to right along the substrate. Figure

2.15 is a plot of the surface energy of the gradient as calculated from the water and ethylene glycol contact angle data using the Girifalco Good-Fowkers-Young equation (2.1)<sup>17,18</sup>:

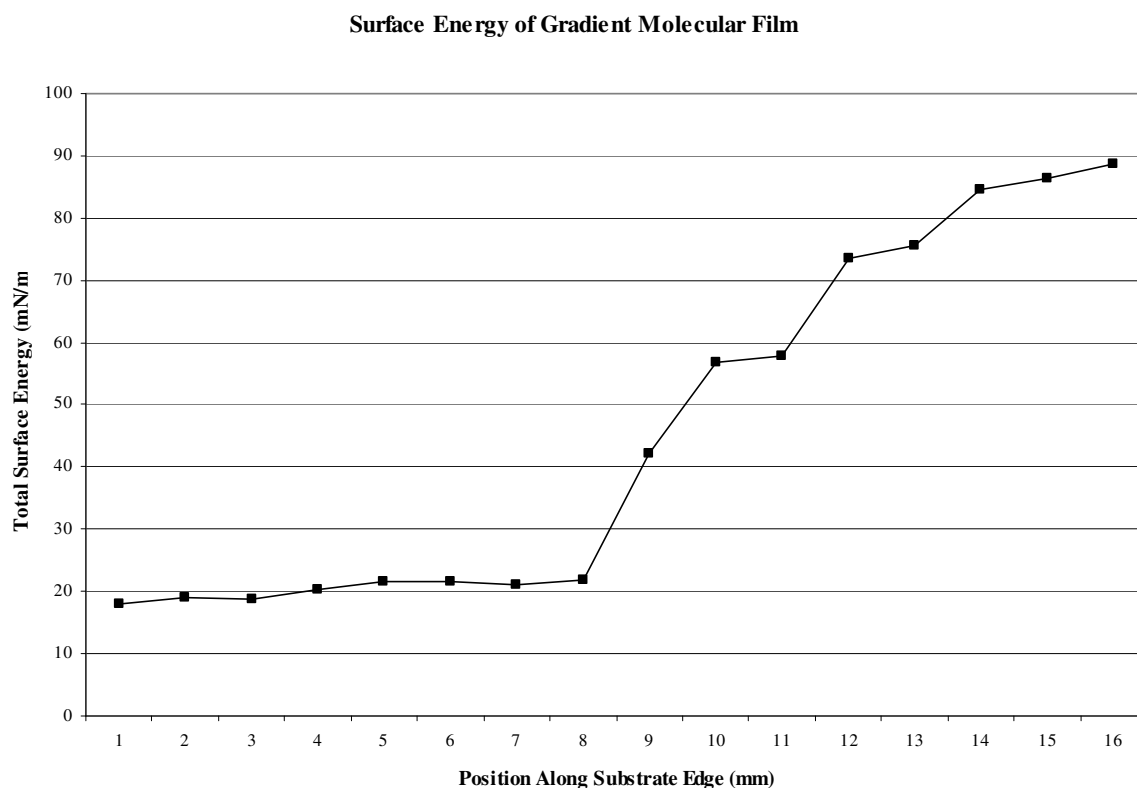
$$1 + \cos\theta = 2/\gamma_L [\gamma_L^d \gamma_s^d]^{1/2} + (\gamma_L^p \gamma_s^p)^{1/2}] \quad (2.1)$$

where  $\theta$  is the contact angle of the liquid,  $\gamma_L$  is the surface energy of the liquid,  $\gamma_s$  is the surface energy of the solid substrate,  $\gamma^d$  is the dispersive component of the surface energy and  $\gamma^p$  is the polar component of the surface energy. Surface energy is inversely related to contact angle and therefore, increases as the molecular packing density of the gradient decreases.



**Figure 2.14** Plot of the measurements of the contact angles of water, ethylene glycol and diiodomethane with respect to the one-dimensional position along the substrate, the zero position marking the portion of the substrate closest to the trough during deposition by evaporation (substrate is 50 mm from trough at zero position). As molecular packing density of the silane film decreases, the contact angle decreases.

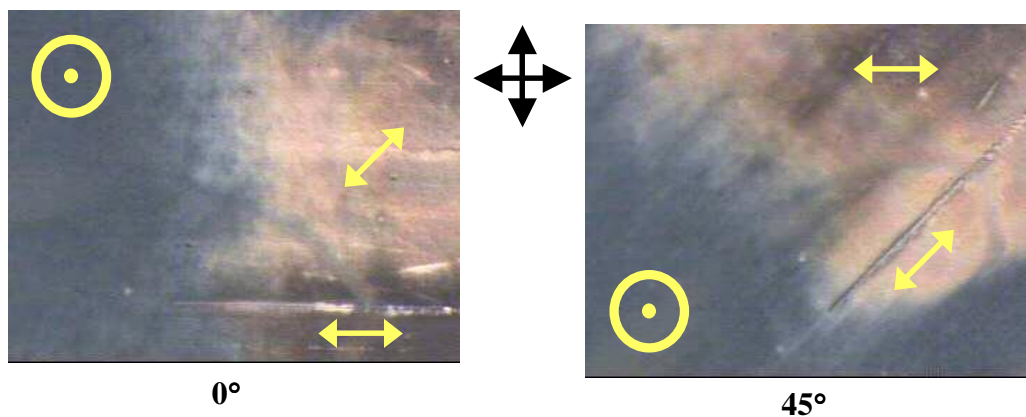




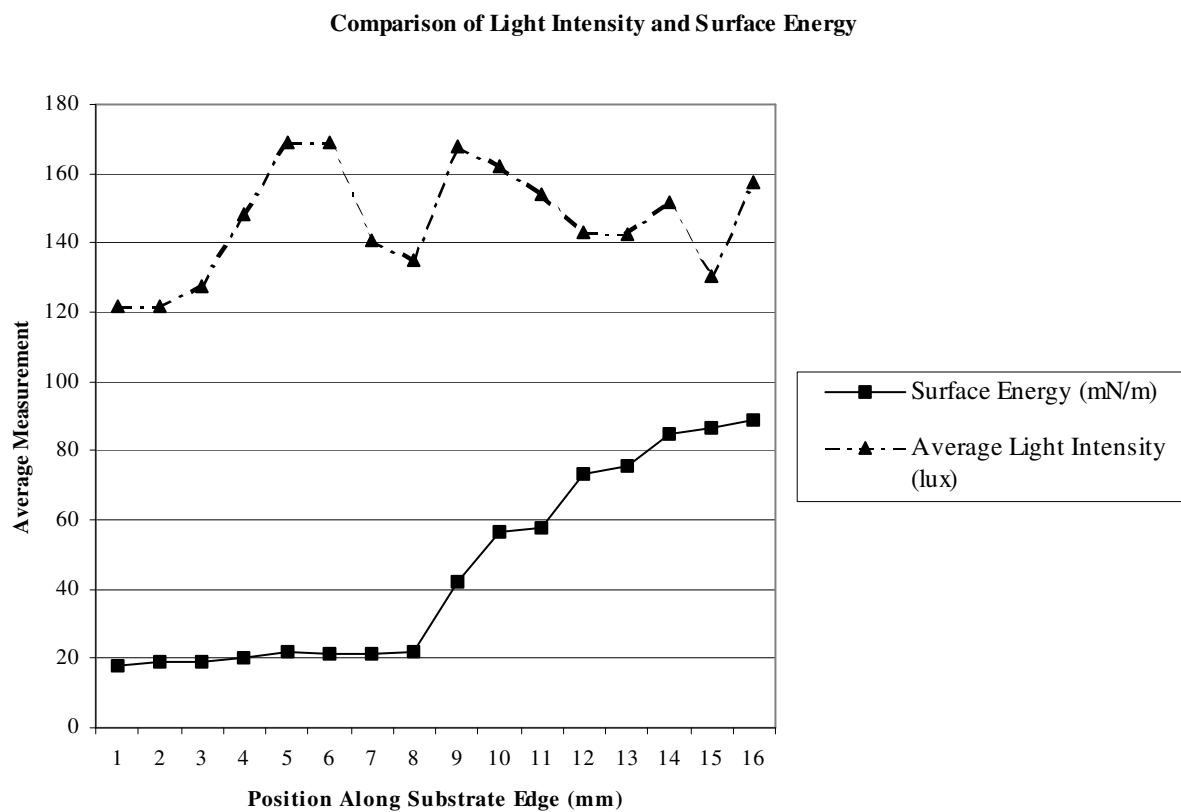
**Figure 2.15** Plot of the surface energy of the gradient (calculated based on the water and ethylene glycol contact angle data) with respect to the one-dimensional position along the substrate.

The birefringent textures observed for alignment of the nematic LC K-15 using the octyltrichlorosilane gradient film are shown in Figure 2.16. The transition from homeotropic to planar alignment is obvious with the boundary region exhibiting some planar alignment with a high pretilt angle. The high pretilt angle of the LC director is confirmed by the decrease in contrast between the dark and bright states when compared to a region of planar alignment with a low pretilt angle or no pretilt of the LC director. There appear to be at least two domains of planar alignment as noted in Figure 2.16 by the double-headed yellow arrows. These domains are attributed to differing orientations of the surfactant molecules (with respect to the substrate edge) as they bend towards the substrate.

Quantification of the boundary region was attempted by means of light intensity measurements with respect to the one-dimensional position along the substrate. These measurements were made using a transmitted light intensity function of the microscope. Figure 2.17 shows the results of these measurements. Large fluctuations in the light intensity of an almost periodic pattern were observed with the baseline intensity rising slightly from the 0 to 16 mm position on the substrate. These fluctuations are believed to result from the packing density variations possible within the large viewing area of the microscope. While the gradient molecular film confirms that orientation of the LC director is directly related to the packing density of the SAM, quantification of the packing density necessary for a given pretilt angle of the LC director was extremely difficult and so not pursued in this study. Also, the gradient molecular film was found to be unstable when in contact with the LC. Over several days, the surfactant molecules of the gradient appeared to diffuse randomly about the substrate such that uniform surfactant coverage was achieved.



**Figure 2.16** Birefringent texture images of LC alignment on a gradient molecular film. Regions of planar alignment are denoted by the double-headed yellow arrows while regions of homeotropic alignment are denoted by the yellow circles (the LC director perpendicular to the plane of the page). The orientation of the crossed polars is given by the crossed black arrows.



**Figure 2.17** Plot of calculated surface energy and light intensity with respect to the one-dimensional position along the substrate. Increases in both surface energy and light intensity are observed as the packing density of the gradient decreases.

## 2.4 Conclusions

Self-assembled monolayers of the surfactant DMOAP produced homeotropic alignment of both positive and negative dielectric nematic LCs. The mechanism of such alignment was attributed to steric hindrances generated by tight packing of the long aliphatic chains of the surfactant molecules. Homeotropic alignment was also observed for SAMs of CTAB prepared at high concentrations of the surfactant, while planar alignment was observed for SAMs of CTAB prepared at low concentrations. Hybrid films prepared with either DMOAP and polyimide or high and low concentration solutions of CTAB as well as

gradient molecular films prepared with octyltrichlorosilane provided means of examining the transition between homeotropic and planar alignment and the mechanisms associated with such LC alignment. While it is evident that there is a distinct correlation between orientation of the surfactant with respect to the substrate and orientation of the LC director, quantifying the molecular packing density necessary for either type of alignment was hindered by experimental limitations.

Alignment layers prepared using SAMs of various surfactants offer several advantages, including the elimination of the mechanical rubbing step in the fabrication process and the possibility of both homeotropic and planar alignment with very little modification of the system. These alignment layers also provide some information about the mechanisms of LC alignment. However, SAMs would not be an ideal choice for LCDs due to their insufficient stability over time.

## 2.5 References

- (1) Bigelow, W.C.; Picket, D.L.; Zisman, W.A. *J. Colloid Interface Sci.* **1946**, *1*, 513-538.
- (2) Nuzzo, R.G.; Allara, D.L. *J. Am. Chem. Soc.* **1983**, *105*, 4481-4483.
- (3) Maoz, R.; Sagiv, J. *J. Colloid Interface Sci.* **1984**, *100*, 465-496.
- (4) Schwartz, D.K. *Annu. Rev. Phys. Chem.* **2001**, *52*, 107-137.
- (5) Schreiber, F. *Progr. Surface Sci.* **2000**, *65*, 151-256.
- (6) Ulman, A. *Chem. Rev.* **1996**, *96*, 1533-1554.
- (7) Ulman, A. *An Introduction to Ultrathin Organic Films: from Langmuir Blodgett to Self-assembly*; Academic Press: Boston, 1991; pp 237-301.
- (8) Butt, H.-J.; Graf, K.; Kappl, M. *Physics and Chemistry of Interfaces*; Wiley-VCH: Weinheim, 2003.
- (9) Lu, Z.; Deng, H.; Wei, Y. *Supramol. Sci.* **1998**, *5*, 649-655.
- (10) Kahn, F.J. *Appl. Phys. Lett.* **1973**, *22*, 386-388.
- (11) Proust, J.E.; Ter-Minassian-Saraga, L.; Guyon, E. *Solid State Comm.* **1972**, *11*, 1227-1230.
- (12) Genzer, J.; Efimenko, K.; Fischer, D.A. *Langmuir* **2002**, *18*, 9307-9311.
- (13) Fischer, D.A.; Efimenko, K.; Bhat, R.R.; Sambasivan, S.; Genzer, J. *Macromol. Rapid Comm.* **2004**, *25*, 141-149.
- (14) Berreman, D. W. *Phys.Rev. Lett.* **1972**, *28*, 1683-1686.
- (15) Geary, J. M.; Goodby, J. W.; Kmetz, A. R.; Patel, J. S. *J. Appl. Phys.* **1987**, *62* 4100-4108.
- (16) Okulska-Bozek, M.; Prot, T.; Borycki, J.; Kedzierski, J. *Liquid Crystals* **1996**, *20* 349-359.
- (17) Sauer, B.B.; Dipaolo, N.V. *J. Coll. Interface Sci.* **1991**, *144*, 527-537.
- (18) Yu, T.; Peng, Z.; Ruan, S.; Xuan, L. *Thin Solid Films* **2004**, *466*, 326-330.

## **CHAPTER 3**

### **ALIGNMENT OF NEMATIC LIQUID CRYSTALS USING CARBON NANOTUBES AND METAL-OXIDE NANORODS**

#### **3.1 Carbon Nanotube Films**

Carbon nanotubes (CNTs) were first discovered by Japanese electron microscopist Sumio Iijima in 1991 when a new material was deposited on the cathode while synthesizing fullerenes by arc-discharge.<sup>1</sup> Since that time CNTs have become the focus of intense research due to their unique chemical and physical properties, namely their field emission and electron transport properties and high mechanical strength. With a tensile strength one hundred times that of steel and electrical conductivity similar to copper, this material has quickly become a core building block for nanotechnology. Potential applications for these materials include their use as field emission devices, nanoscale transistors, components of composite materials and biosensors.<sup>2</sup>

The anisotropic electrical properties and self-assembly behavior of CNTs are of particular importance in the potential application of these materials as alignment layers in liquid crystal displays (LCDs). Typically, alignment involves modification of a solid substrate such that its interface with the liquid crystal (LC) has some anchoring action that results in either planar or homeotropic orientation of the LC director with respect to the interface. Such modification is carried out on a substrate having an electrically conductive layer (e.g. ITO-coated glass) for electric-field-induced reorientation of the director, which in

turn results in a variation in the transmitted light intensity. Single-walled nanotubes (SWNTs) show high conductivity along the tube length and very low conductivity across the tube diameter.<sup>3-5</sup> SWNTs are also known to align parallel to each other in low concentration solutions while multi-walled nanotubes (MWNTs) show a propensity to spontaneously form lyotropic liquid crystalline phases above a critical CNT concentration.<sup>5-7</sup> Thus, the inherent conductivity and spontaneous self-alignment properties of CNTs make them an attractive alternative as an alignment layer that could serve dual purposes.

Deposition of CNT bundles onto solid substrates from a water solution with controlled nanotube orientation has been accomplished by a self-assembly method.<sup>6</sup> In this work CNT films were prepared by this self-assembly method as well as a dip-coating method to achieve dense and sparse deposition of CNT bundles respectively. These CNT films were used to fabricate LC optical cells in which planar alignment of nematic LC was achieved and the director orientation was manipulated with an electric field as verified by transmitted polarized light microscopy.<sup>8</sup>

## **3.2 Experimental Details**

### **3.2.1 Materials**

Graphite powder (natural, microcrystal grade, 99.9995%) used for the single-walled nanotube bundle synthesis was purchased from Alfa Aesar (cat. no. 14736). Nematic liquid crystal 4-cyano-4'-pentyl-1,1'-biphenyl (K-15, EM Industries, IS-1143) was used as received. Liquid crystal optical cells were fabricated using indium tin oxide (ITO)-coated glass (Delta Technologies, Ltd., CG-811N-S115).

### **3.2.2 Instrumentation**

Birefringence texture measurements were made using a Nikon Microphot FX polarizing microscope equipped with a Sony CCD-IRIS camera. Images were obtained using video generation software by Roxio. Atomic force microscopy (AFM) images were obtained in tapping mode using a Multimode IIIa Atomic Force Microscope (Veeco Metrology Group).

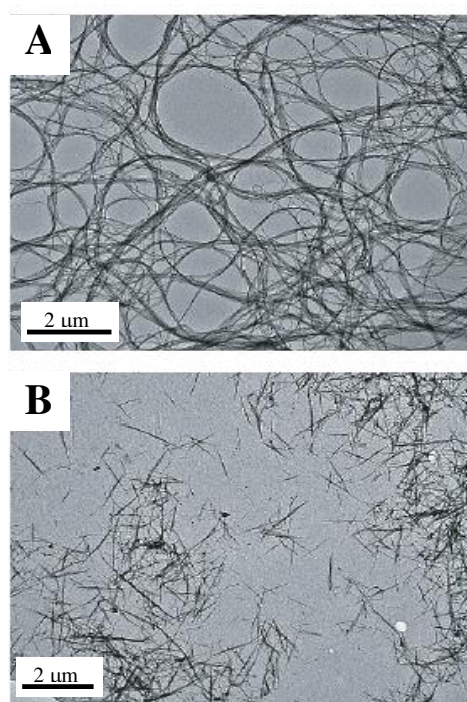
### **3.2.3 Carbon Nanotube Synthesis**

Single-walled nanotube (SWNT) bundles were synthesized by laser ablation of a graphite target containing metal catalysts (0.3% NiCo), using a Nd:YAG laser operating at a wavelength of 532 nm (400mJ/pulse) in an Ar-filled (200 standard cm<sup>3</sup>/min and 93 kPa) furnace at 1150 °C. Samples were purified first by reflux in hydrogen peroxide and further by filtration.<sup>9</sup> The purified SWNT bundles (typically > 10 μm) were shortened to lengths of approximately 2 μm and 0.5 μm by chemical etching using H<sub>2</sub>SO<sub>4</sub>/HNO<sub>3</sub>.<sup>10, 11</sup> The morphology of the bundles was changed from that of highly entangled strands to rigid rods after etching (Figure 3.1).<sup>6</sup> The processed samples were rinsed with deionized water and annealed at 200 °C in 10<sup>-6</sup> torr dynamic vacuum before suspension in deionized water (1.0 or 0.5 g/L).

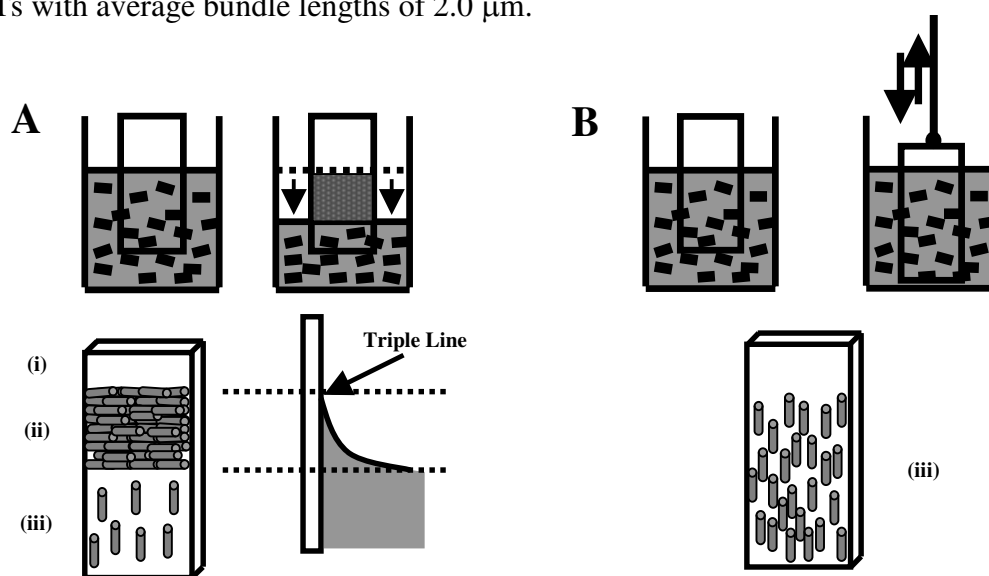
### **3.2.4 Carbon Nanotube Film Deposition**

For dense film deposition, a clean ITO-coated glass substrate was immersed vertically into the SWNT/water suspension at room temperature (Figure 3.2 A). Upon gradual evaporation of the water, the concentrated nanotubes were found to assemble and orient on the glass surface along the air/liquid/substrate triple line.<sup>6</sup> For sparse film deposition, the clean ITO-coated glass substrate was vertically dipped in the SWNT/water suspension (1.0 or 0.5 g/L) at a controlled rate using a motorized dip-coating apparatus (Figure 3.2 B).



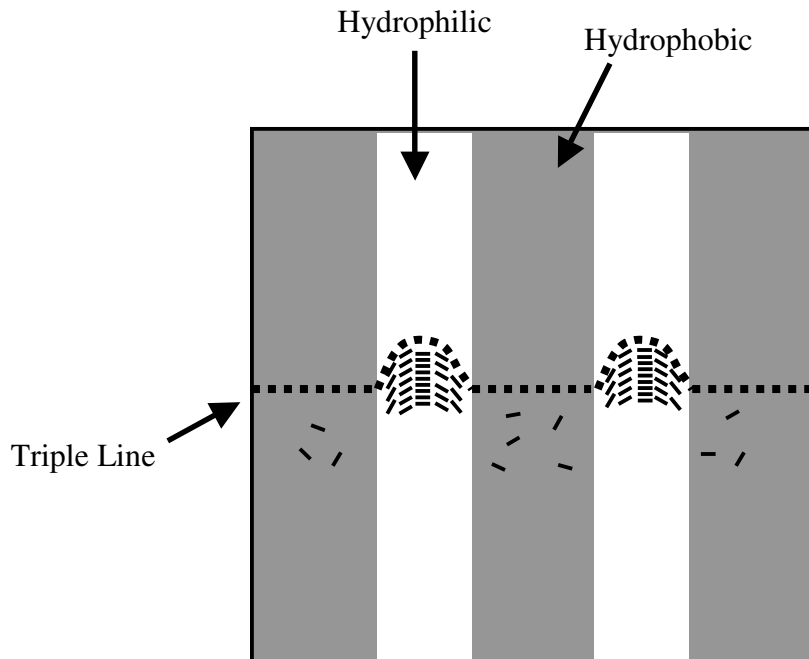


**Figure 3.1** Transmission electron micrographs of (A) purified SWNTs and (B) etched SWNTs with average bundle lengths of 2.0  $\mu\text{m}$ .



**Figure 3.2** Schematic representations of CNT deposition methods: (A) Self-assembly of CNT bundles generated by gradual evaporation of CNT/water suspension onto ITO-coated glass substrate, resulting in three distinct regions: region (i)-no CNT bundles, region (ii)-dense CNT bundle deposition and region (iii)-sparse CNT bundle deposition. (B) Sparse deposition of CNT bundles obtained by dipping of substrate into suspension at a controlled rate.

For patterned CNT film deposition, a clean ITO-coated glass substrate was first patterned with alternating hydrophobic and hydrophilic regions with the hydrophobic regions being 10  $\mu\text{m}$  in width and separated from one another by 25  $\mu\text{m}$ . The ITO-coated glass is itself hydrophilic. The hydrophobic regions were generated by standard photolithography using a photoresist and solution silanization by octadecyltrichlorosilane.<sup>12</sup> The patterned substrate was then immersed vertically into the SWNT/water suspension at room temperature. Upon gradual evaporation of the water, the concentrated nanotubes were found to assemble and orient on the glass surface along the air/liquid/substrate triple line in the hydrophilic regions (Figure 3.3). The photoresist was removed without altering the CNT adhesion.<sup>12</sup>



**Figure 3.3** Schematic representation of CNT deposition on substrate patterned with alternating hydrophilic and hydrophobic regions. The orientation of the CNT bundles in the patterned region varies slightly based on the profile of the triple line (Figure 3.2 A).

### **3.2.5 Fabrication of Liquid Crystal Optical Cells**

Liquid crystal optical cells, used for the observation of birefringent textures, were fabricated as follows: Two CNT-coated substrates were sandwiched together with the CNT films facing each other at predetermined orientations separated by a spacer (6 or 40  $\mu\text{m}$ ) and sealed together using epoxy. The optical cells were filled with K-15 (in the isotropic or nematic state for comparison) by capillary action and examined for light intensity changes. For voltage switching experiments, electrodes were attached to both substrates by solder, allowing for the application of an alternating current (AC) electric field across the LC optical cell by means of a function generator.

## **3.3 Results and Discussion**

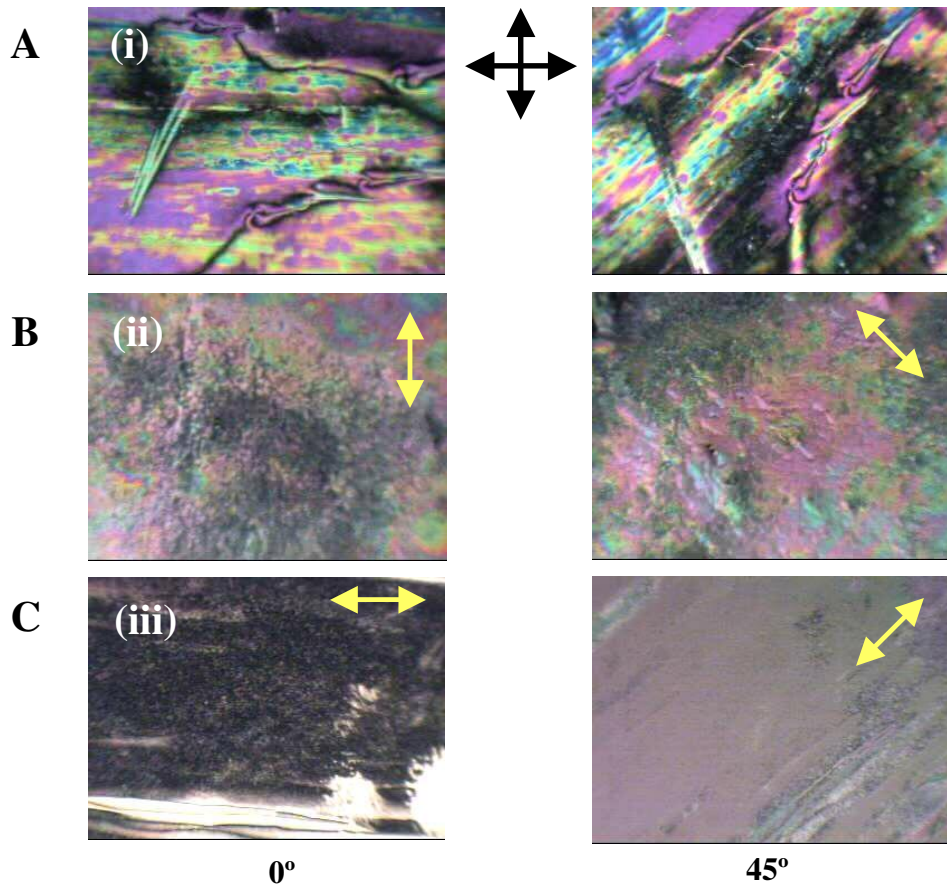
### **3.3.1 Birefringent Textures of Carbon Nanotube Films Prepared by Gradual Evaporation**

The substrates on which the self-assembled CNT films were deposited by gradual evaporation had three distinct regions (see Figure 3.2 A). Region (i) had no nanotube bundles; this portion of the glass substrate was not immersed in the SWNT/water suspension and served as a control surface. Regions (ii) and (iii) resulted from immersion of the substrate, but differed in CNT deposition. Region (ii) consisted of SWNT bundles self-assembled by gradual solvent evaporation (region (ii) in Figure 3.2 A) with the nanotubes parallel to the short axis of the substrate (parallel to the triple line). Region (iii), a sparse deposition of CNT bundles, resulted from the rapid removal of the glass substrate from the suspension. These three distinct regions of varying nanotube densities showed different alignment properties in LC optical cells.

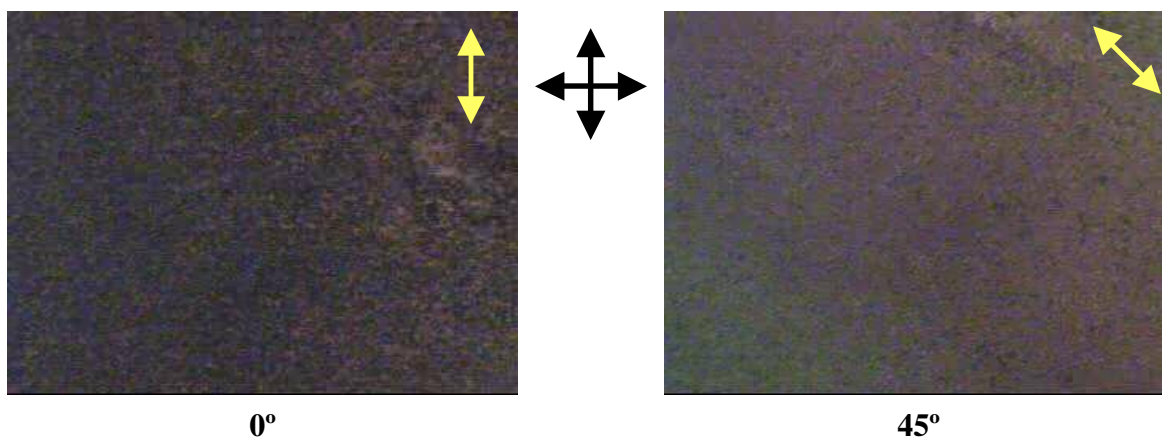
The birefringent textures of the nematic LC obtained from the macroscopic, long-range uniform alignment of K-15 were observed for substrates prepared by gradual evaporation using CNT suspensions of either 2.0 or 0.5  $\mu\text{m}$  bundles in water. The textures observed with the substrate by gradual evaporation of CNT bundles from a suspension of 2.0  $\mu\text{m}$  bundles in water are given in Figure 3.4. No LC alignment occurred in region (i) as expected for an untreated (control) substrate. However, uniform LC alignment was not evident in region (ii) (dense CNT coverage) either. Region (ii) exhibited domains of planar LC alignment. Only the very sparse deposition of CNT bundles found in region (iii) exhibited macroscopic uniform planar alignment of the LC. Figure 3.4 A through C shows the birefringent textures observed in each region of the substrate at  $0^\circ$  and  $45^\circ$  rotation of the sample director (with respect to crossed polars). Figure 3.4 C shows uniform planar alignment of K-15, giving dark states at  $0^\circ$  and  $90^\circ$  rotation of the sample director (with respect to crossed polars) and bright states at  $45^\circ$  and  $135^\circ$  director orientations. The direction of this LC alignment reflects the mean nanotube orientation direction: parallel to the long axis of the substrate and to the dipping direction and perpendicular to the triple line.

Similar birefringent textures were observed for the substrate prepared by gradual evaporation of CNTs from a suspension of 0.5  $\mu\text{m}$  bundles in water with one exception. As with films of 2.0  $\mu\text{m}$  CNT bundles, region (i) exhibited no LC alignment while region (iii) exhibited macroscopic uniform planar alignment of K-15. However, unlike the films composed of 2.0  $\mu\text{m}$  CNT bundles, region (ii) of the films composed of 0.5  $\mu\text{m}$  CNT bundles with densely packed CNT bundles, also exhibited macroscopic uniform planar alignment of the LC (Figure 3.5). It is evident from Figure 3.5 that a dark state is achieved at  $0^\circ$  orientation of the sample director (with respect to crossed polars) while a bright state is seen

at a rotation angle of  $45^\circ$ . It is also apparent that the transmittance of light in this region is fairly low. This observation is not surprising given that the CNT bundles are densely packed, forming an almost opaque alignment layer. The associated reduction in transmitted light for the dense alignment layer suggests that sparse CNT films, such as those found in region (iii), are a more viable option for LCD applications. For this reason, the sparse deposition of CNT bundles achieved by dipping the substrate into a SWNT/water suspension was further studied using a motor driven dipping apparatus and varying the dipping rate.



**Figure 3.4** Birefringent texture images for the three regions of alignment obtained from the self-assembly of CNTs ( $2.0\ \mu\text{m}$  bundles). (A) Region (i): no CNT deposition. (B) Region (ii): dense CNT deposition. (C) Region (iii): sparse CNT deposition. The orientation of the crossed polars is indicated by the crossed black arrows while the nanotube orientation is given by the double-headed yellow arrows.



**Figure 3.5** Birefringent texture images for the alignment of nematic LC by self-assembled CNTs (0.5  $\mu\text{m}$  bundles). The CNT bundles are densely packed and uniform planar orientation of the LC is accomplished. The orientation of the crossed polars is given by the crossed black arrows while the nanotube orientation is given by the double headed yellow arrows.

### 3.3.2 Deposition of Carbon Nanotubes by Controlled Dipping

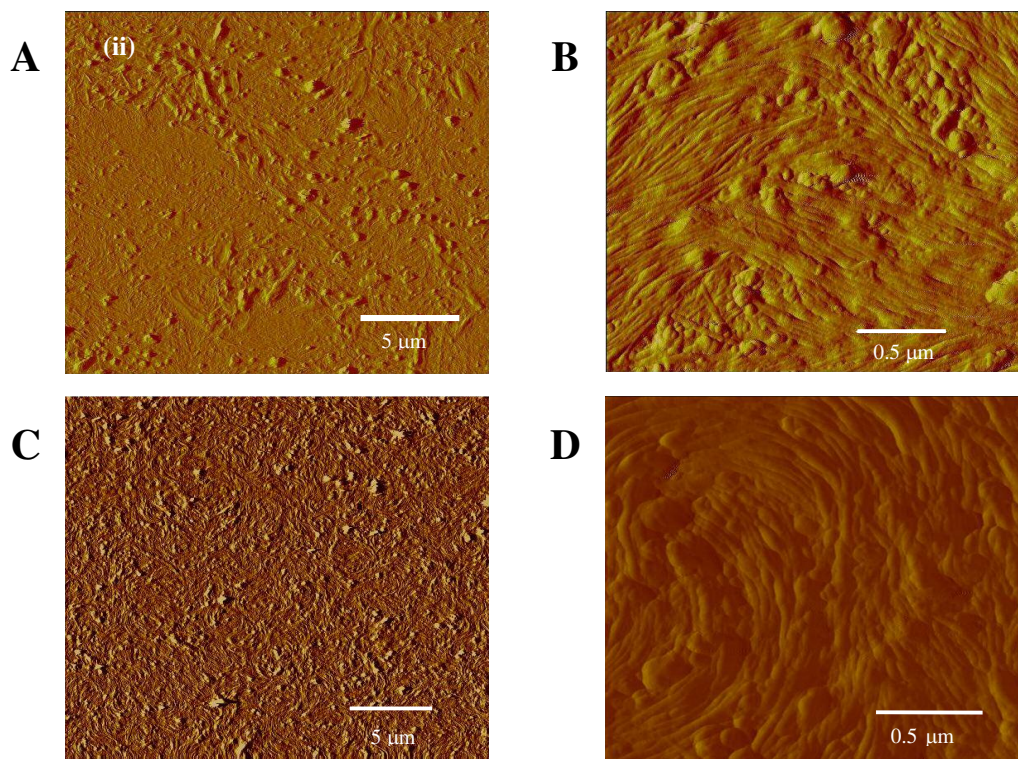
CNT films with sparse bundle deposition were prepared by vertically dipping ITO-coated glass substrates into a SWNT/water suspension at controlled rates ranging from 20 to 264  $\mu\text{m}/\text{sec}$ . Macroscopic uniform planar alignment was achieved at rates of 80  $\mu\text{m}/\text{sec}$  and higher. The optimal dipping rate (based on maximum distinction between bright and dark states) was  $\sim 143$   $\mu\text{m}/\text{sec}$ .

### 3.3.3 Atomic Force Microscopy Analysis of Carbon Nanotube Orientation

The orientation of the individual SWNT bundles for both the dense and sparse CNT films was probed by AFM (in tapping mode) and it was found that the roughness of the surface is increased upon CNT bundle deposition in all cases as can be seen in Figures 3.6 and 3.7. Figure 3.6 A and B shows the dense packing of 2.0  $\mu\text{m}$  SWNT bundles obtained by the evaporation method. It is obvious from the topology that multiple bundles are stacked on top of one another and that these bundles have domains of orientation that are randomly

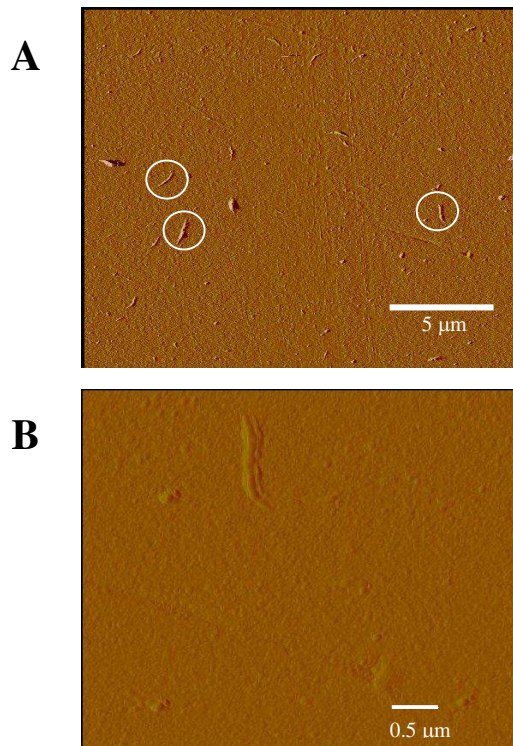


arranged on the substrate. Figure 3.6 C and D shows the dense packing of 0.5  $\mu\text{m}$  SWNT bundles obtained by the evaporation method. Again, multiple bundles appear to be stacked on top of one another as in Figure 3.6 A and B, however there appears to be an average orientation of the bundles in one direction. These results may account for the domains of planar alignment observed in the dense 2.0  $\mu\text{m}$  CNT films and the uniform planar alignment observed in the dense 0.5  $\mu\text{m}$  CNT films. In contrast to the topologies of the dense CNT films, Figure 3.7 shows that the SWNT bundles (2.0  $\mu\text{m}$ ) in the sparse films prepared by



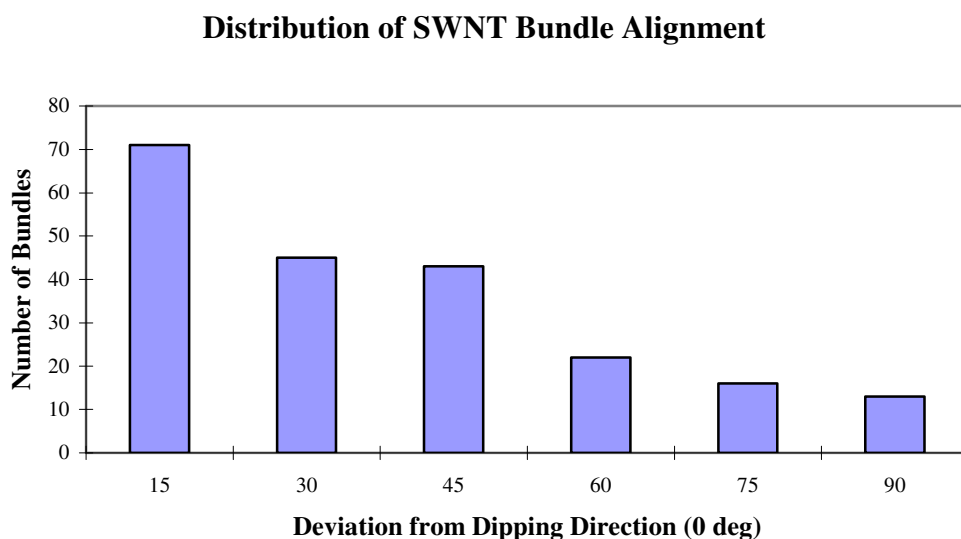
**Figure 3.6** Representative AFM images of dense CNT films (region (ii)). Images (B) and (D) are higher magnifications of a small area of images (A) and (C) respectively. Dense films composed of 2.0  $\mu\text{m}$  bundles ((A) and (B)) are characterized by thick layers of bundles stacked on one another and random domains of orientation. Dense films composed of 0.5  $\mu\text{m}$  bundles ((C) and (D)) have the rough topography seen in (A) and (B), but the tightly packed bundles have the same orientation on average.

controlled dipping sparsely cover the substrate with an irregular spacing between bundles. Smaller SWNT bundles and possibly individual CNTs also appear to have been deposited on the substrate. However, on average the individual SWNT bundles are aligned parallel to the long axis of the glass substrate and dipping direction as confirmed by analysis of the distribution of SWNT bundles with respect to their deviation from the dipping direction (Figure 3.8).



**Figure 3.7** Representative AFM images of sparse CNT films. Sparse CNT films composed of 2.0 μm bundles are characterized by sparse deposition of bundles aligned parallel (on average) with the dipping direction. (B) shows a high magnification image of a single CNT bundle.



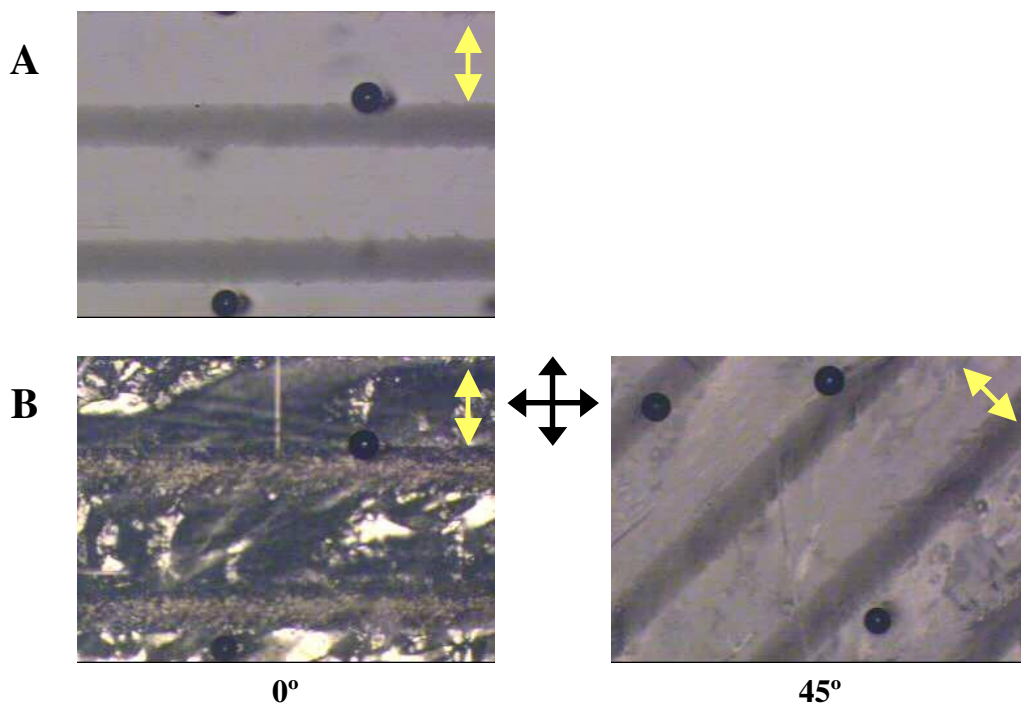


**Figure 3.8** Graph of the distribution of SWNT bundles on substrates dipped at 143.0  $\mu\text{m}/\text{sec}$  with respect to their deviation from the dipping direction (designated as 0 degrees).

### 3.3.4 Birefringent Textures of Patterned Carbon Nanotube Films

A second approach to increasing the transmittance of light through CNT films while maintaining good conductivity and good liquid crystal alignment was the deposition of a pattern of CNT bundles on the substrate. Clean ITO-coated substrates were patterned with CNT bundles by the combined photolithography and gradual evaporation methods<sup>12</sup>, each patterned line consisting of densely packed nanotube bundles oriented on average parallel to the short axis of the substrate (parallel to the triple line) and being 10  $\mu\text{m}$  in width and separated from the next line by 25  $\mu\text{m}$ . The birefringent textures of the nematic LC obtained from the planar alignment of K-15 were observed for the patterned substrates. The textures observed from the patterned CNT films as well as a bright field image of the substrate are given in Figure 3.9. Uniform planar alignment (with the exception of some defects) was exhibited as evidenced by the dark and bright states achieved at 0° and 45° rotation of the

sample, respectively (Figure 3.9 B). It is apparent that the overall transmittance of light is increased in this sample. However, the patterned lines are pronounced, even in the bright state, and may interfere with the function of the LCD pixel. Thus, of the CNT alignment layers studied, the sparse CNT films offer the best model for use in the fabrication of LCDs.



**Figure 3.9** (A) Bright field and (B) birefringent texture images of liquid crystal alignment by patterned CNT films. The CNT bundles are densely packed within each line and oriented parallel to the short axis of the substrate (parallel to the triple line). Somewhat uniform planar orientation of the LC is accomplished. The orientation of the crossed polars is given by the crossed black arrows while the nanotube orientation is given by the double-headed yellow arrows.

### **3.3.5 Liquid Crystal Display Pixel Prototypes**

Liquid crystal optical cells were fabricated with ITO-coated glass substrates deposited with CNT films prepared by either gradual evaporation of 0.5  $\mu\text{m}$  CNT bundles or controlled dipping of 2.0  $\mu\text{m}$  bundles. Macroscopic uniform planar alignment was generated with both CNT films. Application of an electric field perpendicular to the substrate for both cells resulted in homeotropic alignment with the director perpendicular to the substrate. Turning off the electric field brought about the restoration of macroscopic uniform planar alignment. Thus LC alignment by the CNT coated substrate produces the essential characteristics of a light-valve optical cell, the critical component of LCDs.

## **3.4 Conclusions**

Dense CNT films composed of SWNT bundles deposited by gradual evaporation onto ITO-coated glass substrates show bundle-length dependent LC alignment. Longer CNT bundles produce domains of planar alignment for nematic LCs while shorter bundles induce uniform planar alignment on a macroscopic scale. However, the light transmittance of LC optical cells fabricated using dense CNT films is very low. Patterning the substrate with alternating lines of densely packed CNT bundles and untreated substrate increased light transmittance, but the areas with CNT deposition were pronounced, even in the bright state, interfering with the device function.

Sparse CNT films composed of SWNT bundles deposited with controlled orientation onto ITO-coated glass substrates using a motorized dipping method are shown to induce uniform planar alignment of nematic LCs on a macroscopic scale. This alignment has the LC director oriented along the dipping direction and is not dependent on bundle length. The light transmittance of LC optical cells fabricated using sparse CNT films is significantly

increased. LC optical cells fabricated using CNT alignment layers exhibit LC director switching on application of an electric field.

It has been shown that the phenomena of self-organization in liquid crystals orients CNTs and that SWNTs dispersed in LC polymers can act as seeds for oriented domain growth.<sup>13-15</sup> Herein, it is shown that the anisotropic nature of controlled nanotube orientation deposition can align nematic LCs. Sparse CNT films give uniform planar alignment on the scale of centimeters. It is proposed that unidirectional roughness of the substrate induced by CNT deposition also contributes to alignment in a manner similar to that of a rubbed surface whereby microgrooves generate a preferred alignment direction.<sup>16</sup>

CNT films constitute a novel alignment material that possesses intrinsic anisotropic conductivity, which in time may facilitate the fabrication of liquid crystal displays, however further work is needed to fully characterize these alignment layers. The dip-coating experiments should be repeated with variations of the CNT concentration in the suspension and the dipping rate to determine the ideal topography for good LC alignment.

### **3.5 Metal-Oxide Nanorod Films**

The macroscopic planar alignment of liquid crystals achieved using substrates coated with conductive carbon nanotubes, while advantageous to the LCD industry, brings with it limitations such as the opaque nature of CNT bundles and thus CNT films, resulting in a reduction in the transmittance of light. Ideally, a material would be used that possesses both the anisotropic conductivity inherent in CNTs and the alignment capabilities of CNT films, but that also exhibits increased transmittance of to light. Such a material may be found in metal-oxide nanorods.

The synthesis of materials whose physical and chemical properties are sensitive to changes in temperature, pressure, electric and magnetic fields, optical wavelength, adsorption of gas molecules and pH is driven by potential applications in nanoelectronics, specifically chemical and biological sensors.<sup>17, 18</sup> Metal-oxides possess a broad range of electronic, chemical and physical properties that are often sensitive to the environmental changes mentioned above and have thus been studied for use in sensor technology.<sup>19</sup> Semiconductors exhibit conductivity between that of insulators and metals, good luminescence in the visible and UV, and large chemical diversity, making them good candidates for use in micro- and opto-electronics.<sup>20</sup> The synthesis of ZnO and SnO<sub>2</sub> nanorods of varying aspect ratio has been achieved by solution-phase growth.<sup>21, 22</sup> The rod-like shape, conductivity and most importantly, transparency of these nanostructures may improve upon the liquid crystal alignment achieved by carbon nanotubes. In this work metal-oxide films were prepared by dispersing these nanorods in solution and then dip-coating to achieve a sparse deposition of either ZnO or SnO<sub>2</sub> nanorods. These metal-oxide films were then used to fabricate optical cells in which planar alignment of nematic liquid crystal (LC) was examined by transmitted polarized light microscopy. The larger aspect ratio ZnO nanorods produced macroscopic planar alignment while the smaller aspect ratio SnO<sub>2</sub> nanorods exhibited only random domains of planar alignment.

### **3.6 Experimental Details**

#### **3.6.1 Materials**

The Sn<sup>4+</sup> precursor tin(IV)chloride pentahydrate (SnCl<sub>4</sub>·5H<sub>2</sub>O, 98+%, 244678) and Zn<sup>2+</sup> precursor zinc acetate dihydrate (Zn(Ac)<sub>2</sub>·2H<sub>2</sub>O, 98%, 22355-2) were purchased from Aldrich and used without further purification. Tetramethylammonium hydroxide (25 wt% in

methanol, T0280) and poly(acrylic acid, sodium salt) (45 wt% in water, 416029) were also purchased from Aldrich and used as received. The following surfactants were used as received: citric acid anhydrous (Fluka, 27488), thioglycolic acid (98%, Sigma, T3758), (3-mercaptopropyl)-trimethoxy silane (95%, Aldrich, 175617), cetyltrimethyl ammonium bromide (99+%, Acros, 22716), trioctylphosphine oxide (90%, Aldrich, 346187), dimethyloctadecyl[3-(trimethoxy-silyl)propyl] ammonium chloride (DMOAP, 60% in methanol, Acros, 33853), 3-amino-propyltrimethoxysilane (97%, Aldrich, 281778), [3-(diethylamino) propyl]-trimethoxy silane (96%, Aldrich, 448664), and N-[3-(trimethoxysilyl) propyl] aniline (Aldrich, 440809). The nematic liquid crystal 4-cyano-4'-pentyl-1,1'-biphenyl (K-15, EM Industries, IS-1143) was used as received. Liquid crystal optical cells were fabricated using indium tin oxide (ITO)-coated glass (Delta Technologies, Ltd., CG-811N-S115).

### **3.6.2 Instrumentation**

Birefringence texture measurements were made using a Nikon Microphot FX polarizing microscope equipped with a Sony CCD-IRIS camera. Images were obtained using video generation software by Roxio. Atomic force microscopy images were obtained in tapping mode using a Multimode IIIa Atomic Force Microscope (Veeco Metrology Group). Transmission electron microscopy (TEM) images were obtained using a Philips CM12 with an acceleration voltage of 100 kV. Scanning electron microscopy (SEM) images were obtained using a Hitachi S-4700. Phase contrast images were obtained using a Zeiss Axioskop2 (Carl Zeiss Microimaging, Inc.) equipped with a DIC filter and AxioCam HRm.

### **3.6.3 Synthesis of Zinc Oxide and Tin Oxide Nanorods**

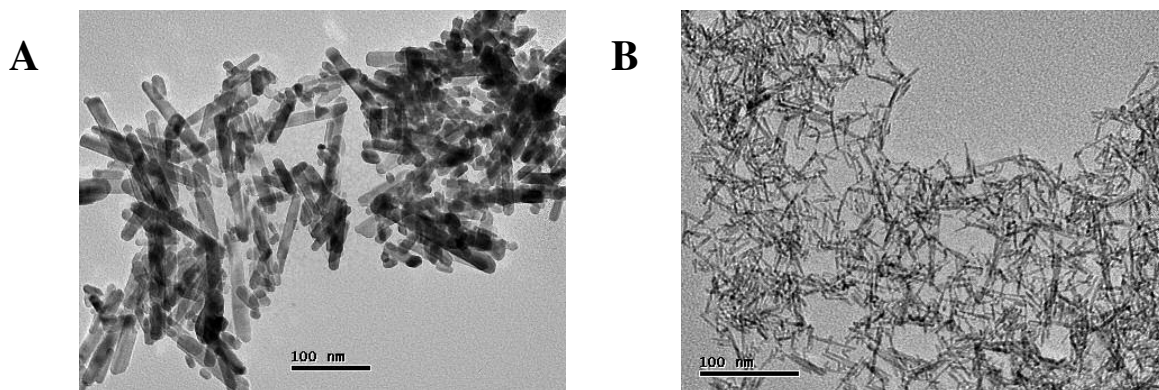
The synthesis of ZnO and SnO<sub>2</sub> nanorods was previously described in detail by B. Cheng *et al.*<sup>21, 22</sup> Briefly, the precursor material, either SnCl<sub>4</sub>·5H<sub>2</sub>O or Zn(Ac)<sub>2</sub>·2H<sub>2</sub>O, was dissolved in methanol, creating a stock solution to which fixed amounts of tetramethylammonium hydroxide (TMAH) and variable amounts of water were added. The solution was mixed in a Teflon-lined stainless steel vessel that was then sealed and heated to a predetermined temperature (usually 75° or 150° C) for a specific time period (48 hours or less). The precipitate was collected and washed by centrifugation and either dried at room temperature or stored in ethanol. The aspect ratios of the nanorods were dependent upon the water concentration and reaction temperature and time. The samples used in the following dispersion experiments were of aspect ratios 20:1 and 10:1 for ZnO and SnO<sub>2</sub>, respectively (based on average size).

#### **3.6.4 Dispersion of Zinc Oxide and Tin Oxide in Chloroform**

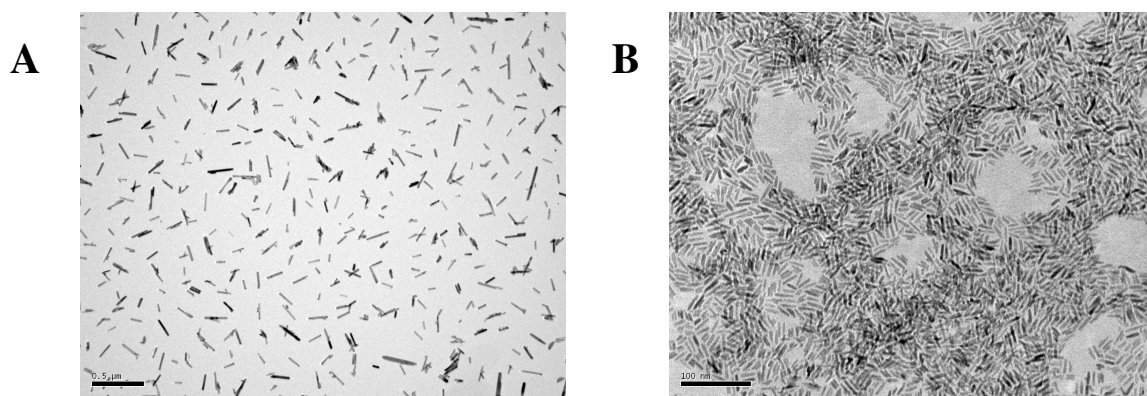
Unsuccessful attempts to disperse ZnO and SnO<sub>2</sub> in chloroform were made under a variety of conditions using the following surfactants: citric acid, thioglycolic acid, (3-mercaptopropyl)-trimethoxy silane, cetyltrimethyl ammonium bromide, and trioctylphosphine oxide.<sup>23-25</sup> TEM images of poor dispersions of ZnO and SnO<sub>2</sub> are shown in Figure 3.10. It was found that the pH of the solution after the surfactant was added was of great importance. If the pH was too low, as in the case of citric acid, the nanorods would break down into their starting materials. If the pH was too high, the surface of the nanorods would not be reactive and the surfactant would not bind. It was important to adjust the pH of the solution to be close to the isoelectric point of the metal-oxide so that the surface of the nanorods would be reactive.<sup>26</sup> TMAH was used to make the necessary adjustments in pH.

A 0.1 wt% solution of dimethyloctadecyl[3-(trimethoxysilyl)propyl] ammonium chloride (DMOAP) in water was prepared and used the same day. Approximately 5-10 mg of dry nanorods were placed in a vial, diluted with 2 mL of DMOAP solution and sonicated for 30 min. Ten microliters of TMAH were added to the suspension after which it was sonicated for 30 min. Clumps were seen to form over time and deposit on the bottom of the vial. These clumps were confirmed to be excess surfactant. After sonication approximately 2 mL of chloroform was added to the mixture and vortex stirred. The water layer became clear while the chloroform layer became cloudy. The chloroform layer was removed and washed with chloroform by centrifugation to remove excess DMOAP. In the case of SnO<sub>2</sub> nanorods, a pellet did not form during centrifugation and therefore the sample could not be washed. The dispersion was transferred to a glass vial for storage. The TEM results for the dispersion of both ZnO (~200 nm length) and SnO<sub>2</sub> (~ 10 nm length) nanorods are shown in Figure 3.11. Dispersions of ZnO and SnO<sub>2</sub> nanorods in chloroform were successfully repeated using wet nanorods, a concentrated sample of nanorods in ethanol. Also, dispersions of ZnO and SnO<sub>2</sub> nanorods in chloroform were successfully repeated using surfactants similar in structure to DMOAP, namely 3-aminopropyl-trimethoxysilane, [3-(diethylamino) propyl]-trimethoxy silane and N-[3-(trimethoxysilyl) propyl] aniline (Figure 3.12).

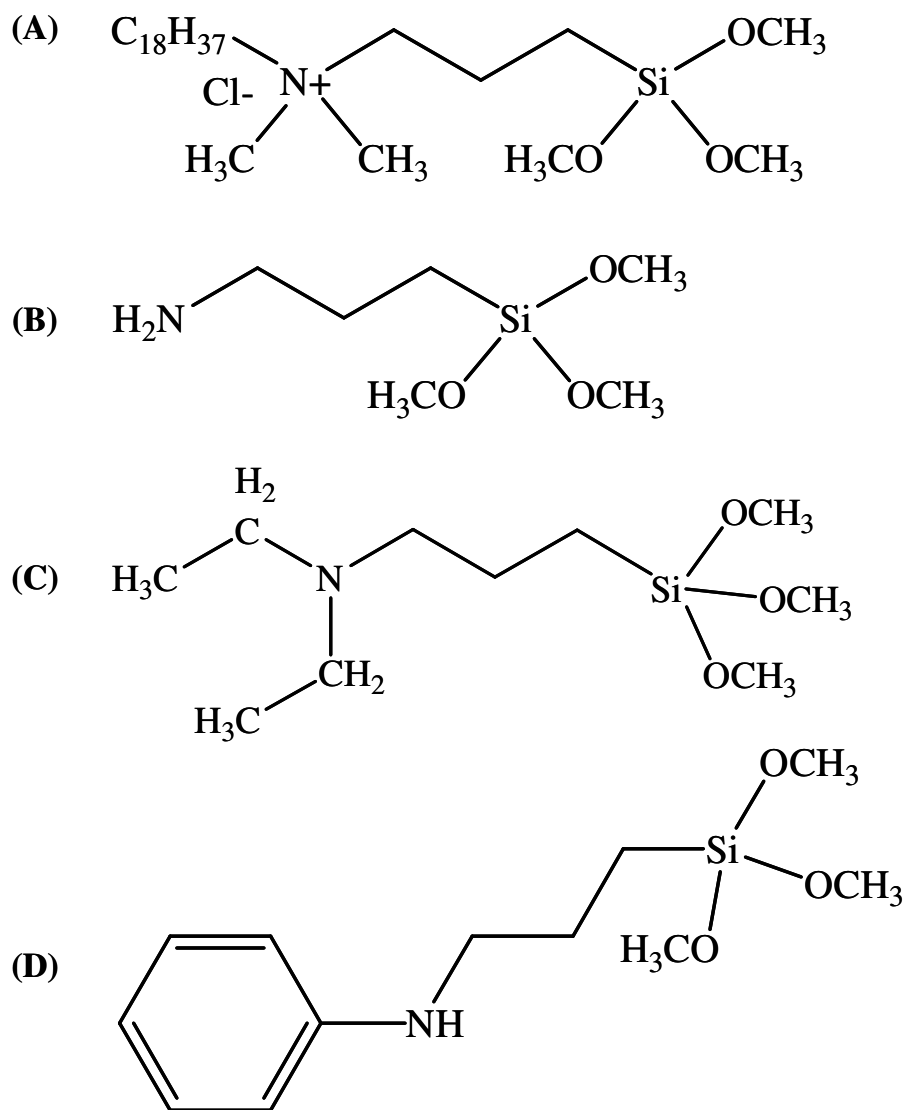




**Figure 3.10** Transmission electron micrographs of (A) ZnO (scale bar 100 nm) and (B) SnO<sub>2</sub> (scale bar 100 nm) dispersions in chloroform. Poor dispersions are characterized by the presence of aggregates of nanorods.



**Figure 3.11** Transmission electron micrographs of (A) ZnO (scale bar 0.5 μm) and (B) SnO<sub>2</sub> (scale bar 100 nm) dispersions in chloroform.



**Figure 3.12** Chemical structures of surfactants used to successfully disperse ZnO and SnO<sub>2</sub> in chloroform. (A) dimethyloctadecyl[3-(trimethoxy-silyl)propyl] ammonium chloride (DMOAP), (B) 3-aminopropyl-trimethoxysilane, (C) [3-(diethylamino) propyl]-trimethoxy silane and (D) N-[3-(trimethoxysilyl) propyl] aniline.

### 3.6.5 Dispersion of Zinc Oxide and Tin Oxide in Water

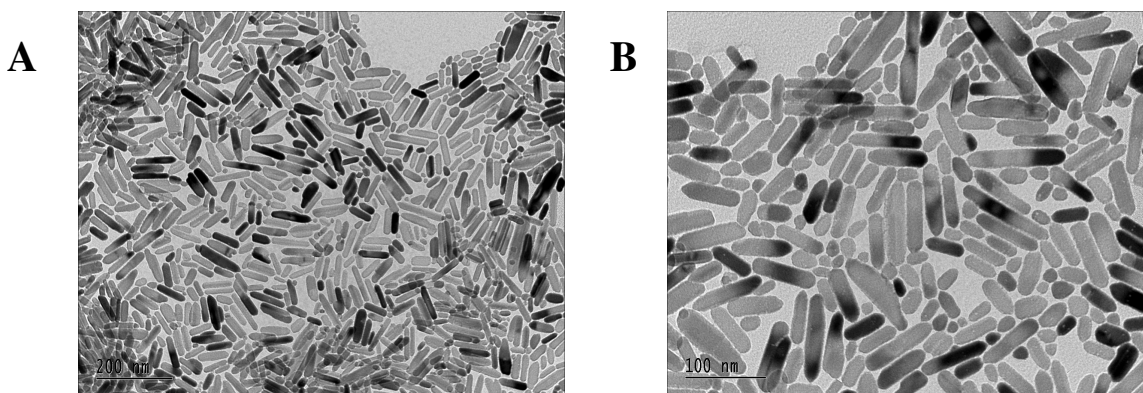
A 0.1 wt% solution of DMOAP in water was prepared and used the same day. Less than 1 mL of wet ZnO nanorods was diluted with 2 mL of the DMOAP solution and sonicated for 30 minutes. Over time the solution became semi-transparent. Ten microliters of TMAH were added to the suspension after which it was sonicated for 30 min. A precipitate was seen to form. An equal volume of chloroform was added and the solution was vortexed. Over time both layers became semi-transparent. The chloroform layer was removed and the dispersion was allowed to sit overnight before analysis by TEM (Figure 3.13). This procedure was found to be less reproducible than dispersion of ZnO in chloroform by the same surfactant and found to be ineffective at dispersing SnO<sub>2</sub> in water. Thus, another method, providing good dispersion of both ZnO and SnO<sub>2</sub> in water was sought.

A 0.1 vol% solution of poly(acrylic acid, sodium salt) (PAA) in water was prepared and used the same day.<sup>27,28</sup> Approximately 0.5 mL of wet nanorods (500-600 mg) were diluted to 5 mL with the PAA solution. The mixture was sonicated for one hour or until the solution became clear. The sample was stored in a glass vial. No settling was evident after 6 months for the ZnO dispersion and for 1 month for the SnO<sub>2</sub> dispersion. TEM images were difficult to obtain due to the hydrophobic nature of the copper grids used for imaging. Attempts were made to induce compatibility between the grid and dispersion by dipping the grid in ethanol before sample application. However, such attempts were fruitless as the nanorods seemed to flow to the edge of the grid or completely off the grid during the slow evaporation of the water at room temperature. SEM images were collected for the ZnO dispersion from a drop of the dispersion dried on a silicon wafer. These results are shown in Figure 3.14. The slow nature of the evaporation of water in the preparation of the SEM

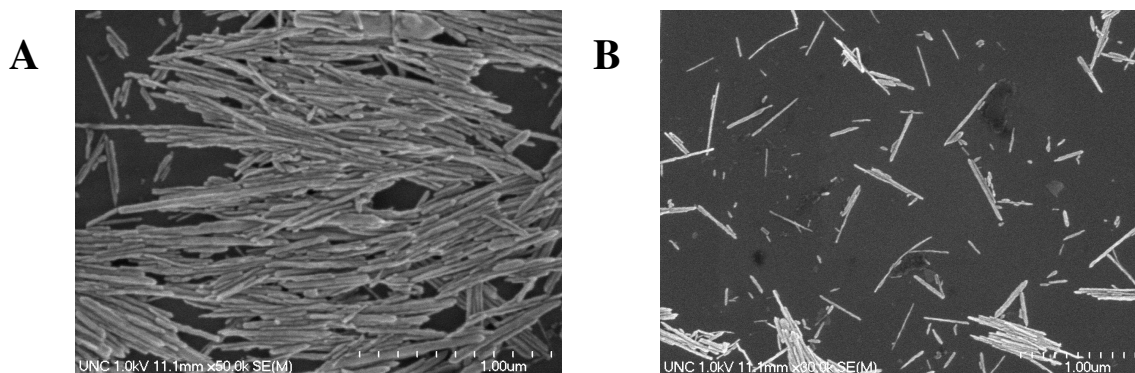
sample is evident in the unidirectional orientation of the nanorods in some parts of the viewing area. This unidirectional orientation differs greatly from the aggregation of the nanorods seen when no dispersion method is applied, thus verifying homogenous dispersion of the nanorods. The extremely small dimensions of the SnO<sub>2</sub> nanorods made it difficult to obtain clear SEM images.

### 3.6.6 Metal-Oxide Film Deposition

The gradual evaporation method for film deposition used in the carbon nanotube procedure was not applicable in the deposition of metal-oxide films due to interference from the surfactant. The surfactant coating the nanorods created a sticky residue on the film surface. Thus the dip-coating method was preferred. For sparse film deposition, a clean ITO-coated glass substrate was vertically dipped into a metal-oxide/solvent dispersion (~1.0g/L) at a controlled rate using the apparatus shown in Figure 2.2. For dense film deposition, the substrate was vertically dipped multiple times in the metal-oxide/solvent dispersion with adequate time for drying between dips.



**Figure 3.13** Transmission electron micrographs of ZnO dispersed in water by DMOAP ((A) scale bar 200 nm and (B) scale bar 100 nm).



**Figure 3.14** Scanning electron micrographs of ZnO dispersed in water by PAA (scale bars 1.0  $\mu\text{m}$ ). As the sample droplet dried, a close packing of nanorods became apparent in some regions (A) while other regions showed a more dilute arrangement (B).

### 3.6.7 Fabrication of Liquid Crystal Optical Cells

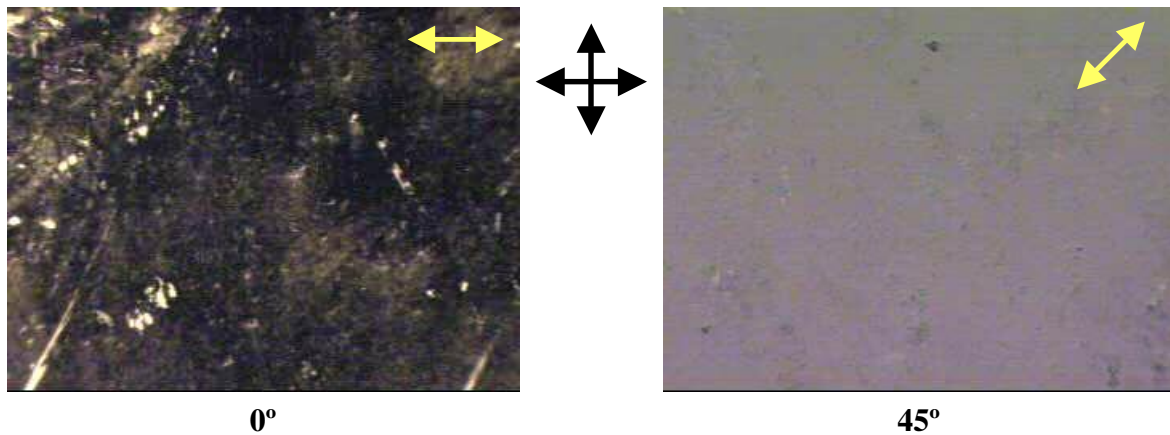
Liquid crystal optical cells, used for the observation of birefringent textures, were fabricated as follows: Two ZnO or  $\text{SnO}_2$ -coated substrates prepared by the same deposition method were sandwiched together with the nanorod films facing each other at predetermined orientations separated by a spacer (6 or 40  $\mu\text{m}$ ) and sealed together using epoxy. The optical cells were filled with either K-15 or MLC-6608 (in the isotropic or nematic state for comparison) by capillary action and examined for light intensity changes.

## 3.7 Results and Discussion

### 3.7.1 Birefringent Textures of Zinc Oxide Nanorod Films

Sparse films of ZnO nanorods were deposited by vertically dipping ITO-coated glass substrates into a ZnO/chloroform dispersion at a controlled rate and examined by transmitted polarized light microscopy. The birefringent textures of the nematic LC obtained from the macroscopic, long-range uniform alignment of K-15 were observed (Figure 3.15). The sample director was found to align parallel to the dipping direction. This result is similar to that observed with sparse CNT films prepared by the same method.

With the elimination of gradual evaporation as a deposition method, an attempt to form dense films of ZnO nanorods was carried out by vertically dipping ITO-coated glass substrates into a ZnO/chloroform dispersion multiple times, allowing adequate time for drying between dips. The birefringent textures of the nematic LC showed uniform planar alignment (with the sample director aligned along the dipping direction) in all cases. An increase in the number of ZnO layers did not appear to improve the LC alignment. Upon comparison of ZnO films deposited from new and old ZnO/chloroform dispersions, it was discovered that the age of the solution significantly impacts the quality of the LC alignment. The birefringent textures of the nematic LC showed increasing uniformity in planar alignment with increasing age of the dispersion. In some cases a substrate dipped on the day of the dispersion preparation showed only random domains of planar alignment. Substrates dipped one month or longer after dispersion preparation consistently showed macroscopic, uniform planar alignment.

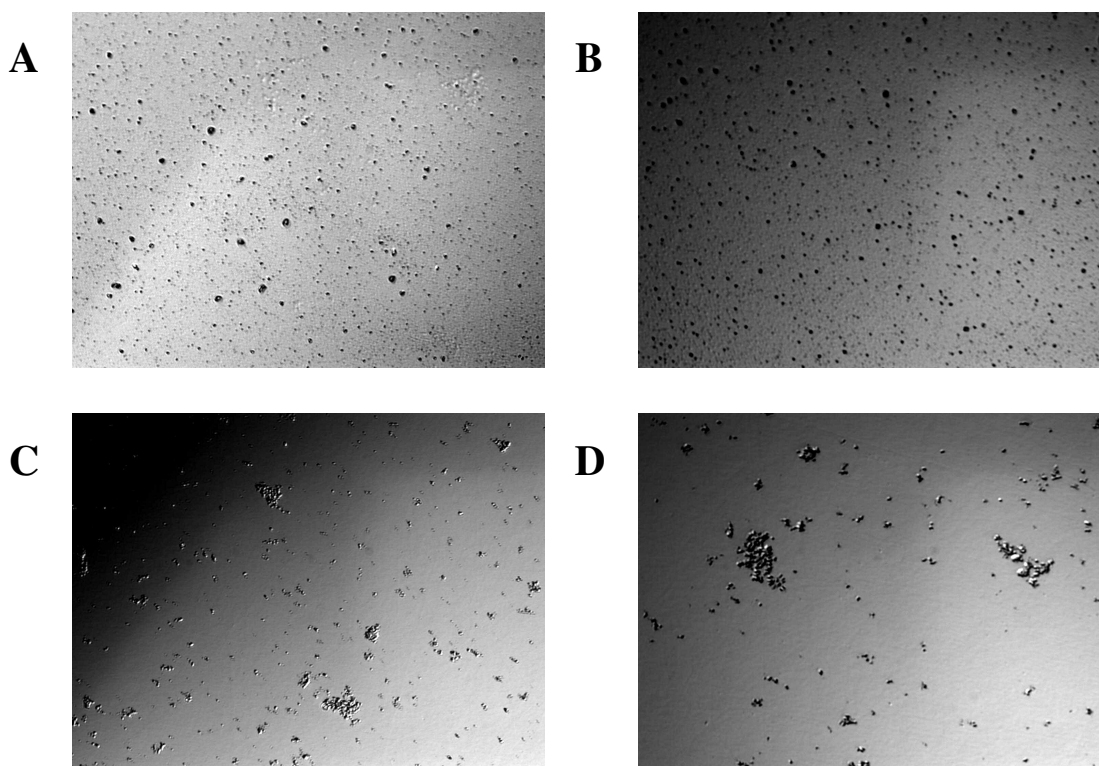


**Figure 3.15** Birefringent texture images for the alignment of liquid crystal K-15 by ZnO nanorod films. Substrates were dipped in a ZnO/chloroform dispersion to produce alignment layer. The orientation of the crossed polars is given by the crossed black arrows while the dipping direction is given by the double-headed yellow arrows. The best alignment results were obtained with dispersion solutions aged for at least one month.

### 3.7.2 Effects of Zinc Oxide Nanorod Aggregation on Liquid Crystal Alignment

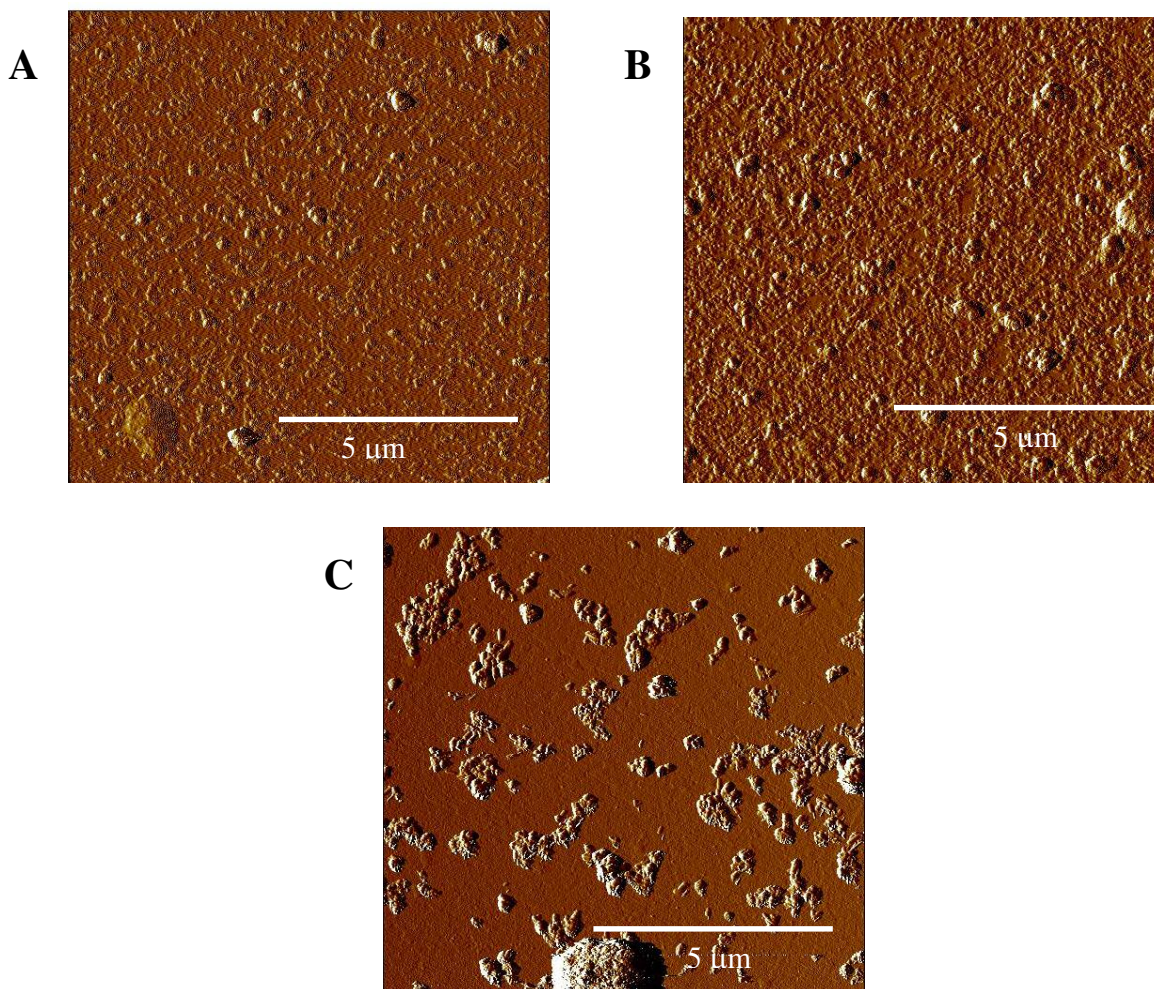
The topology of the ZnO nanorod films deposited by dip-coating was examined by both phase contrast microscopy (PCM) and AFM (in tapping mode) and it was found that the age of the dispersion had a tremendous effect on the roughness of the surface. Figure 3.16 shows the PCM images obtained for a substrate dipped in a ZnO/chloroform dispersion on the same day that the dispersion was made and for a substrate dipped in a three-month-old dispersion. It appears that despite sonication of the dispersion just before dipping, aggregates form in the dispersion over time and are deposited onto the substrate surface.

AFM images further confirm that the number of aggregates in the dispersion and therefore in the ZnO film increase as the solution ages. Figure 3.17 shows AFM images of (A) a substrate dipped on the day of dispersion preparation, (B) a substrate dipped one day after dispersion preparation and (C) a substrate dipped one month after dispersion preparation. The aggregates increase in both number and size overtime, increasing the overall roughness of the surface with the formation of hills and valleys. This topology enhances LC alignment. However, the uniformity in the alignment of the sample director is not explained by these images. It is possible that the individual ZnO nanorods within the aggregates or even the surfactant molecules attached to those nanorods are oriented in the same direction, but the very small dimensions of the ZnO nanorods and the limitations in the resolution of the AFM prevented thorough examination of this theory.



**Figure 3.16** Phase contrast images of substrates dipped in ZnO/chloroform dispersions of varying age. The first substrate ((A) 50X magnification and (B) 100X magnification) was dipped in a ZnO/chloroform dispersion on the same day that the dispersion was made. The second substrate ((C) 50X magnification and (D) 100X magnification) was dipped in a three-month old ZnO/chloroform dispersion. Note the reduction of the overall roughness, but increase in the length scale of the rough regions when using the aged dispersion.





**Figure 3.17** Atomic force microscopy images of three substrates dipped in ZnO/chloroform solutions of varying age. (A) Substrate was dipped on the same day as the dispersion preparation. (B) Substrate was dipped one day after dispersion preparation. (C) Substrate was dipped one month after dispersion preparation. It is apparent that surface roughness increase as dispersion age increases.

### 3.7.3 Birefringent Textures of Tin Oxide Nanorod Films

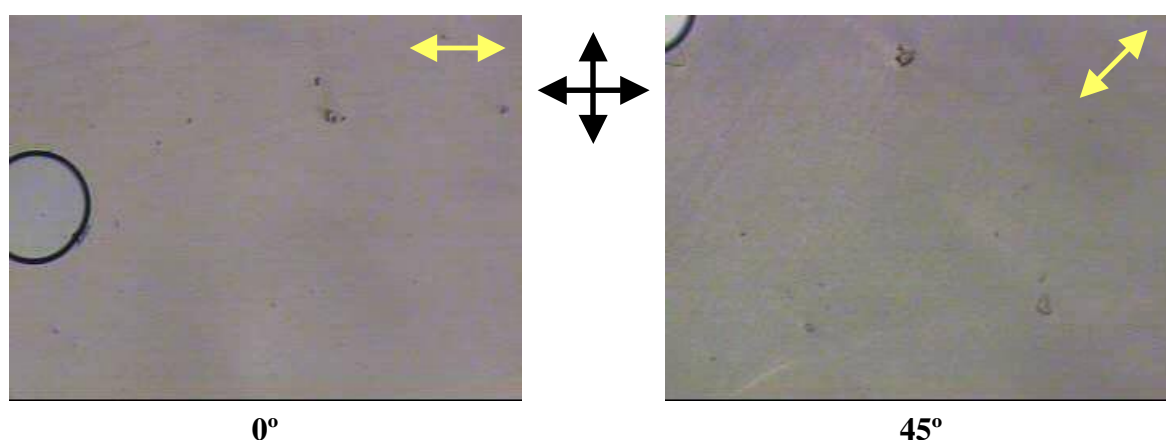
Sparse films of SnO<sub>2</sub> nanorods were deposited by vertically dipping ITO-coated glass substrates into a SnO<sub>2</sub>/chloroform dispersion at a controlled rate and examined by transmitted polarized light microscopy. The birefringent textures of the nematic LC showed only faint, random domains of planar alignment, presumably with a high pre-tilt angle of the sample director (Figure 3.18). The topology of the SnO<sub>2</sub> film was examined by phase microscopy and it was found that the surface was virtually smooth (Figure 3.19), thus accounting for the lack of a preferred alignment direction. The smaller dimensions and aspect ratio of these nanorods when compared with the ZnO nanorods may explain the decrease in surface roughness. If uniform orientation of the surfactant molecules on the nanorods contributes to LC alignment as was previously hypothesized in the ZnO/chloroform system, it is not evident in this system.

### 3.7.4 Effects of Surfactant Used for Dispersion on Liquid Crystal Alignment

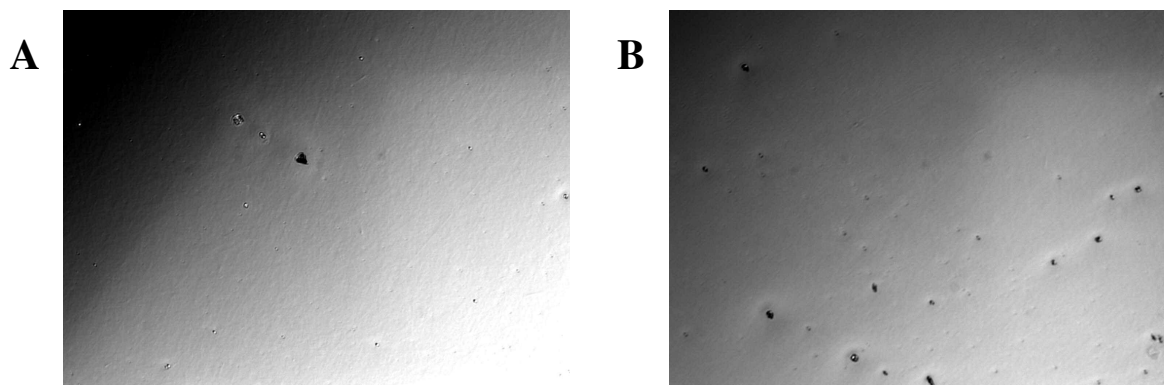
In an effort to minimize the potential contributions to LC alignment of the dispersion surfactant and to prepare dispersions that may be used for deposition of nanorods by gradual evaporation, the maximum surface coverage of the surfactant molecules was calculated using geometric calculations and computer simulations. Assuming that a ZnO nanorod is cylindrical in shape with dimensions of 20 nm by 100nm, the total surface area of one nanorod is  $6.9 \times 10^{-11} \text{ cm}^2$ . The number of nanorods in a 10 mg sample is then determined and the total surface area of the sample is calculated to be  $0.039 \text{ cm}^2$ . Computer simulations (Argus Lab) were then used to predict the shape and size of the surfactant molecule. DMOAP has an L-shape with the shorter portion of the molecule being bound to the nanorod and thus limiting the surface coverage. Having calculated the size of this portion of the

DMOAP molecule to be 8.11 Å and assuming that the surfactant molecules pack tightly, the number of DMOAP molecules needed to completely cover all the nanorods in the 10 mg sample is  $5.97 \times 10^{12}$  ( $4.9 \times 10^{-6}$  mg). These calculations confirm that the concentration of DMOAP used in the dispersion of ZnO and SnO<sub>2</sub> in chloroform is in excess by several orders of magnitude which may, despite washing of the dispersion, lead to effects on LC alignment from excess surfactant.

The concentration of surfactant in the dispersion was systematically decreased eventually resulting in poorer dispersions. However, the occurrence of poor dispersions appeared at surfactant concentrations two orders of magnitude greater than the concentration dictating maximum surface coverage. Excess surfactant in the dispersion is apparently necessary for suspension of the nanorods and cannot be eliminated as a possible producer of LC alignment.



**Figure 3.18** Birefringent texture images for the alignment of liquid crystal K-15 by SnO<sub>2</sub> nanorod films. Substrates were dipped in a SnO<sub>2</sub>/chloroform dispersion to produce alignment layer. The orientation of the crossed polars is given by the crossed black arrows while the dipping direction is given by the double-headed yellow arrows.



**Figure 3.19** Phase contrast images of substrates dipped in  $\text{SnO}_2$ /chloroform dispersions of varying age. As can be seen at (A) 50 X magnification and (B) 100X magnification, the surface is very smooth. The lack of surface roughness may explain the poor LC alignment with these films.

### 3.8 Conclusions

Sparse ZnO films composed of ZnO nanorods deposited onto ITO-coated glass substrates by dip-coating are shown to induce uniform planar alignment of nematic LCs on a macroscopic scale. This alignment however is dependent upon the age of the dispersion, with older dispersions typically generating better LC alignment. The LC director appears to be oriented along the dipping direction. The exact mechanism of this alignment is not fully understood, but an increase in surface roughness due to aggregates appears to play a significant role. Increasing the aspect ratio of these nanorods could allow for a more thorough examination of the orientation of these nanorods within their aggregates and with respect to the LC alignment direction. Also, controlled dipping rate experiments followed by AFM analysis are necessary to probe the ideal surface topology for good LC alignment.

Sparse films of  $\text{SnO}_2$  prepared by the same method showed no propensities for uniform LC alignment. The very small aspect ratio of the nanorods and thus decreased

surface roughness may account for this result. It is possible that increasing the aspect ratio of either the ZnO or SnO<sub>2</sub> nanorods to match that of the CNT bundles and depositing films of these nanorods by dip-coating may produce alignment layers having all the advantages of the CNT films such as uniform planar alignment and anisotropic conductivity, but with increased light transmittance.

### 3.9 References

- (1) Iijima, S. *Nature* **1991**, 354, 56-58.
- (2) Merkoci, A. *Microchim. Acta* **2006**, 152, 157-174.
- (3) Harris, P.J.F. *Carbon Nanotubes and Related Structures*; Cambridge University Press: Cambridge, UK, 1999.
- (4) Ebbesen, T.W. (Ed.) *Carbon Nanotubes: Preparation and Properties*; CRC Press, Inc.: Boca Raton, 1997.
- (5) Saito, R.; Dresselhaus, M.S. *Physical Properties of Carbon Nanotubes*; Imperial College Press: London, 1998.
- (6) Shimoda, H.; Oh, S.J.; Geng, H.Z.; Walker, R.J.; Zhang, X.B.; McNeil, L.E.; Zhou, O. *Adv. Mater.* **2002**, 14, 899-901.
- (7) Song, W.; Kinloch, I.A.; Windle, A.H. *Science* **2003**, 303, 1363.
- (8) Russell, J.M.; Oh, S.; LaRue, I.; Zhou, O.; Samulski, E.T. *Accepted for publication in Thin Solid Films*.
- (9) Tang, X.P.; Kleinhammes, A.; Shimoda, H.; Fleming, L.; Bower, C.; Sinha, S.; Zhou, O.; Wu, Y. *Science* **2000**, 228, 492-494.
- (10) Lui, J.; Rinzler, A.; Dai, H.; Hafner, J.; Bradley, A.R.; Boul, P.; Lu, A.; Iverson, T.; Shelimov, A.K.; Huffman, C.; Roderiguez-Macias, F.; Shon, Y.; Lee, R.; Colbert, D.; Smalley, R.E. *Science* **1998**, 280, 1253-1256.
- (11) Shimoda, H.; Gao, B.; Tang, H.P.; Kleinhammes, A.; Fleming, L.; Wu, Y.; Zhou, O. *Phys. Rev. Lett.* **2002**, 88, 0155021-0155024.
- (12) Oh, S.J.; Cheng, Y.; Zhang, J.; Shimoda, H.; Zhou, O. *Appl. Phys. Lett.* **2003**, 82, 2521-2523.
- (13) Lynch, M.D.; Patrick, D.L. *Nano Lett.* **2002**, 2, 1197-1201.
- (14) Dierking, I.; Scalia, G.; Morales, P.; LeClere, D. *Adv. Mater.* **2004**, 16, 865-869.
- (15) Mrozek, R.A.; Kim, B.-S.; Holmberg, V.C.; Taton, T.A. *Nano Lett.* **2003**, 3, 1665-1669.
- (16) Berreman, D.W. *Phys. Rev. Lett.* **1972**, 28, 1683-1686.

- (17) Wang, Z.L. and Kang, Z.C. *Functional and Smart Materials: Structural Evolution and Structure Analysis*; Plenum Press: New York, 1998; pp 1-69.
- (18) Wang, Z.L. *Adv. Mater.* **2003**, *15*, 432-436.
- (19) Kolmakov, A. and Moskovits, M. *Annu. Rev. Mater. Res.* **2004**, *34*, 151-180.
- (20) Enderlein, R. and Horing, N.J.M. *Fundamentals of Semiconductor Physics and Devices*; World Scientific: Singapore, 1997.
- (21) Cheng, B.; Russell, J.M.; Shi, W.; Zhang, L.; Samulski, E.T. *J. Am. Chem. Soc.* **2004**, *126*, 5972-5973.
- (22) Cheng, B.; Shi, W.; Russell-Tanner, J.M.; Zhang, L.; Samulski, E.T. *Inorg. Chem.* **2006**, *45*, 1208-1214.
- (23) Chan, W.C.W.; Nie, S. *Science* **1998**, *281*, 2016-2018.
- (24) Correa-Duarte, M.A.; Giersig, M.; Liz-Marzan, L.M. *Chem. Phys. Lett.* **1998**, *286*, 497-501.
- (25) Peng, X.; Schlamp, M.C.; Kadavanich, A.V.; Alivisatos, A.P. *J. Am. Chem. Soc.* **1997**, *119*, 7019-7029.
- (26) Plueddeman, E.P. *Silane Coupling Agents*; Plenum Press: New York, 1991.
- (27) Cesarano, J.; Aksay, I.A.; Bleier, A. *J. Am. Ceram. Soc.* **1988**, *71*, 250-255.
- (28) Cesarano, J.; Aksay, I.A. *J. Am. Ceram. Soc.* **1988**, *71*, 1062-1067.

## **CHAPTER 4**

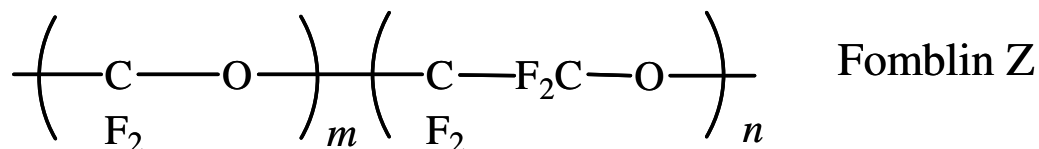
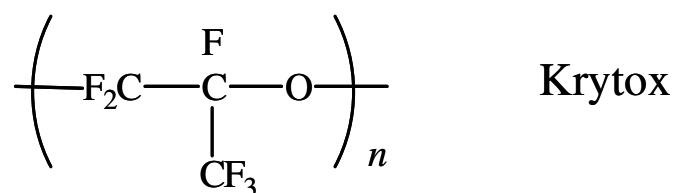
### **ALIGNMENT OF NEMATIC LIQUID CRYSTALS USING PERFLUOROPOLYETHERS**

#### **4.1 Perfluoropolyethers**

Perfluoropolyethers (PFPEs) are low molecular weight highly fluorinated oils that exhibit extraordinary properties such as high chemical resistance and excellent stability at high temperatures. The first PFPEs emerged in the 1970s as high-performance lubricants for civilian and military space applications. Since that time, they have found application in a variety of industries, including chemical, automotive, medical, cosmetics and electronics. Several families of PFPEs are now produced on an industrial scale, all sharing a common chemical structure, which consists of C-F, C-C and C-O bonds.<sup>1-6</sup>

Krytox, a homopolymer of hexafluoropropylene oxide and the first PFPE, was produced by Du Pont in the early 1970s.<sup>2</sup> Due to its high thermal performance and low vapor pressure, this material was and is used in most of the vacuum and diffusion oil pumps for the microelectronics industry. Fomblin Z, a random copolymer synthesized by photochemical polymerization of a mixture of oxygen and tetrafluoroethylene, was also developed and marketed in the early 1970s.<sup>2</sup> While Krytox and Fomblin Z were the only basic structures known for the next 15 years (Figure 4.1), recent synthetic efforts have yielded a variety of PFPEs with unique properties.





**Figure 4.1** Chemical structures of Krytox and Fomblin Z. These basic structures were the first used in the synthesis of PFPEs.

PFPEs exhibit excellent long-term thermal stability for temperatures ranging from –100 to 400 °C, explaining their extensive use as lubricants, elastomers, pump fluids and heat transfer fluids in systems that experience harsh conditions such as space shuttles and satellites.<sup>1,2</sup> PFPEs also exhibit very low surface energies (15-20 mN/m), which may account for their chemical resistance to organic solvents, acids, bases and harsh oxidants.<sup>3-6</sup> Unlike other fluoropolymers, PFPEs have very low glass transition temperatures (ranging from –120 to –70 °C) and thus, low viscosity over large temperature ranges, making them easy to spread and useful for lubrication of thin film magnetic media.<sup>5</sup> These properties as well as the low toxicity of PFPEs make them good candidates for use in cosmetics and biomedical applications, for example PFPEs have been used to produce barrier creams and dental and ocular implants.<sup>5,6</sup> These characteristics, good chemical and thermal resistance, low surface tension and viscosity and low toxicity, as well as their potential for use in soft-lithography

make them an excellent candidates for the preparation of alignment layers for use in liquid crystal displays (LCDs).

PFPEs exhibit all of the advantages associated with polyimide alignment layers, with the added benefit of being compatible with soft-lithography.<sup>7</sup> This characteristic allows one to generate a thin film of PFPE on a conductive substrate that may subsequently be embossed with a pattern of parallel grooves, inducing a preferential direction of liquid crystal (LC) director orientation without the hazards of mechanical rubbing. Also, the extremely low surface energies of PFPEs may allow for faster switching times. In this work, LC alignment layers were prepared using thin and embossed films of PFPE under various preparation conditions. These alignment layers were used to fabricate optical cells in which spontaneous homeotropic and/or planar alignment were examined by transmitted polarized light microscopy. The dependency of LC alignment on the dielectric anisotropy of the LCs and pre-treatment of the PFPE layer were also examined. The surface energies and surface anchoring energies of these alignment layers were probed by contact angle and voltage-dependent birefringence measurements.

## **4.2 Experimental Details**

### **4.2.1 Materials**

Poly(tetrafluoroethylene oxide-*co*-difluoromethylene oxide) $\alpha,\omega$  diol (ZDOL, 95%, Aldrich, 457302), 2-isocyanatoethyl methacrylate (EIM, 99%, Aldrich, 477060), 2,2-dimethoxy-2-phenyl acetophenone (DMPA, 99%, Aldrich, 196118), dibutyltin diacetate (DBTDA, 99%, Aldrich, 290890) and 1,1,2-trichlorotrifluoroethane (Freon 113, 99%, Aldrich, 48411) were used as received for perfluoropolyether synthesis. 1,1,1,3,3-pentafluorobutane (Solkane 365mfc, Solvay Fluorides, UN1993), 1,3-bis(trifluoromethyl)

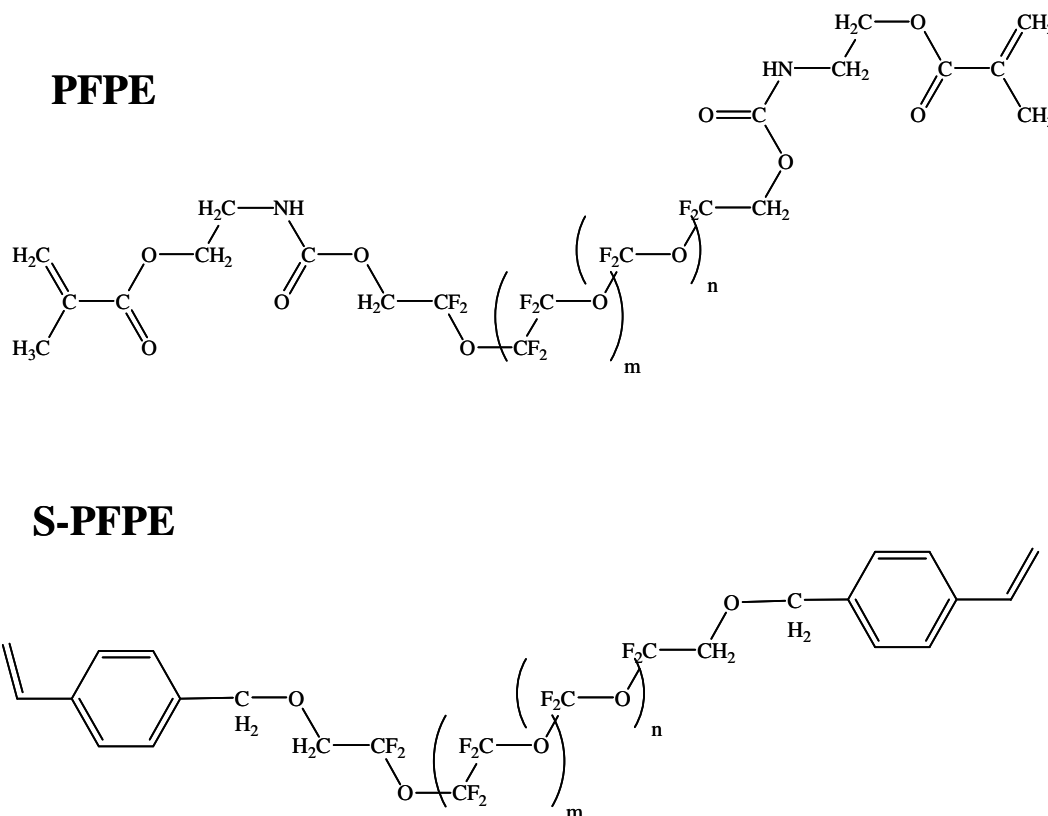
benzene (99%, Aldrich, 251186), ethanol (95%, Aaper, 05D04WB), and glacial acetic acid (Fisher Scientific, UN2789) were used as received. Ethylene glycol (Fisher Scientific, S-80005) was used as is for contact angle measurements. Trichloro(1H,1H,2H,2H-perfluorooctyl) silane (97%, Aldrich, 448931), 3-(trimethoxysilyl) propyl methacrylate (98%, Aldrich, 440159) and Teflon-AF (Dupont). Nematic liquid crystals 4-cyano-4'-pentyl 1,1'-biphenyl (K-15, EM Industries, IS-1143,  $\Delta\epsilon = +13.2$ ), MLC-6608 (Merck,  $\Delta\epsilon = -4.2$ ), MLC 6609 (Merck,  $\Delta\epsilon = -3.7$ ), MLC-6610 (Merck,  $\Delta\epsilon = -3.1$ ), ZLI-2293 (Merck,  $\Delta\epsilon = +10$ ) and ZLI-4792 (Merck,  $\Delta\epsilon = +5.2$ ) were used as received. Liquid crystal optical cells were fabricated using indium tin oxide (ITO)-coated glass (Delta Technologies, Ltd., CG-811N-S115).

#### **4.2.2 Instrumentation**

Thin polymer films were prepared using a Laurell Technologies Corporation spin caster (WS-400A-6NPP/LITE). Perfluoropolyether was cured under nitrogen purge in an ELC-500 UV chamber (120V AC, 60Hz, 15A, 4 x 9W lamps,  $\lambda = 365$  nm, Electro-Lite Corporation). An apparatus for mechanical rubbing of polymer films was built in-house. A sample mount and manipulator were fabricated with Teflon. As described in Chapter two, a felt roller was attached to an electric drill and firmly suspended above the sample mount such that sliding the sample mount to the right would mechanically rub the substrate at a controlled speed. Birefringence texture measurements were made using a Nikon Microphot FX polarizing microscope equipped with a Sony CCD-IRIS camera. Images were obtained using video generation software by Roxio. Contact angle measurements were made using a CAM200, Optical Contact Angle Meter (KSV Instruments, Ltd.) and KSV software. Surface anchoring energy measurements were made using a OptiPro polarizing microscope (Shintech) equipped with shield and AC voltage supply.

### 4.2.3 Perfluoropolyether Synthesis

The synthesis and photocuring of perfluoropolyethers was previously described in detail by J.P. Rolland *et al* and based on earlier work done by R. Bongiovanni *et al*.<sup>7-9</sup> Briefly, the reaction involved the methacrylate functionalization of poly(tetrafluoroethylene oxide-*co*-difluoromethylene oxide) $\alpha,\omega$  diol (ZDOL,  $M_n = 3800$  g/mol) with 2-isocyanatoethyl methacrylate. Purification by chromatography and evaporation of solvent yielded a clear, colorless, and viscous oil, which was further purified by passage through a  $0.22\ \mu\text{m}$  polyether-sulfone filter. Photocuring of the material was accomplished through blending the precursor polymer with 1 wt % of 2,2-dimethoxy-2-phenyl acetophenone and exposure to UV radiation. Chemical structures of the perfluoropolyethers used in this study are shown in Figure 4.2.



**Figure 4.2** Chemical structures of perfluoropolyether precursor polymers used in this research. PFPE has urethane linkages for polymerization while S-PFPE has styrene linkages.

#### **4.2.4 Deposition of Thin Perfluoropolyether Films**

Thin films of perfluoropolyether were prepared on either clean float glass or clean ITO-coated glass coated with 3-(trimethoxysilyl) propyl methacrylate by the following method: a 2 wt % solution of 3-(trimethoxysilyl) propyl methacrylate in 95% ethanol was prepared (with 2 drops of glacial acetic acid) under constant stirring. The substrate was dipped into the solution for 2 minutes, rinsed with 95% ethanol and cured at 120 °C for 10 minutes.

Perfluoropolyether pre-polymer was deposited by spin-coating at 1000 for 1 minute. The thin films were transferred to the UV chamber, which was then purged with nitrogen for 10 minutes. Under continuous nitrogen flow, the films were exposed to UV radiation ( $\lambda = 365$  nm) for 20 minutes. For rubbed films, the UV cured thin films were mechanically rubbed using the apparatus built in-house (see Figure 2.3).

#### **4.2.5 Preparation of Embossed Perfluoropolyether Films**

Perfluoropolyether films having an embossed pattern were prepared. First, a clean ITO-coated glass substrate was coated with a layer of 3-(trimethoxysilyl) propyl methacrylate by the following method: a 2 wt % solution of 3-(trimethoxysilyl) propyl methacrylate in 95% ethanol was prepared (with 2 drops of glacial acetic acid) under constant stirring. The substrate was dipped into the solution for 2 minutes, rinsed with 95% ethanol and cured at 120 °C for 10 minutes.

Diffraction gratings, having a sinusoidal cross-section, were cleaned and coated with perfluoropolyether pre-polymer. A clean and methacrylate-treated ITO-coated substrate was then placed ITO side down on the pre-polymer layer and the UV chamber was purged with

nitrogen for 10 minutes. Under continuous nitrogen flow, the film was cured by exposure to UV radiation ( $\lambda = 365$  nm) for 20 minutes. The diffraction grating was carefully removed. Replication of the diffraction grating pattern was confirmed by AFM.

#### **4.2.6 Fabrication of Liquid Crystal Optical Cells**

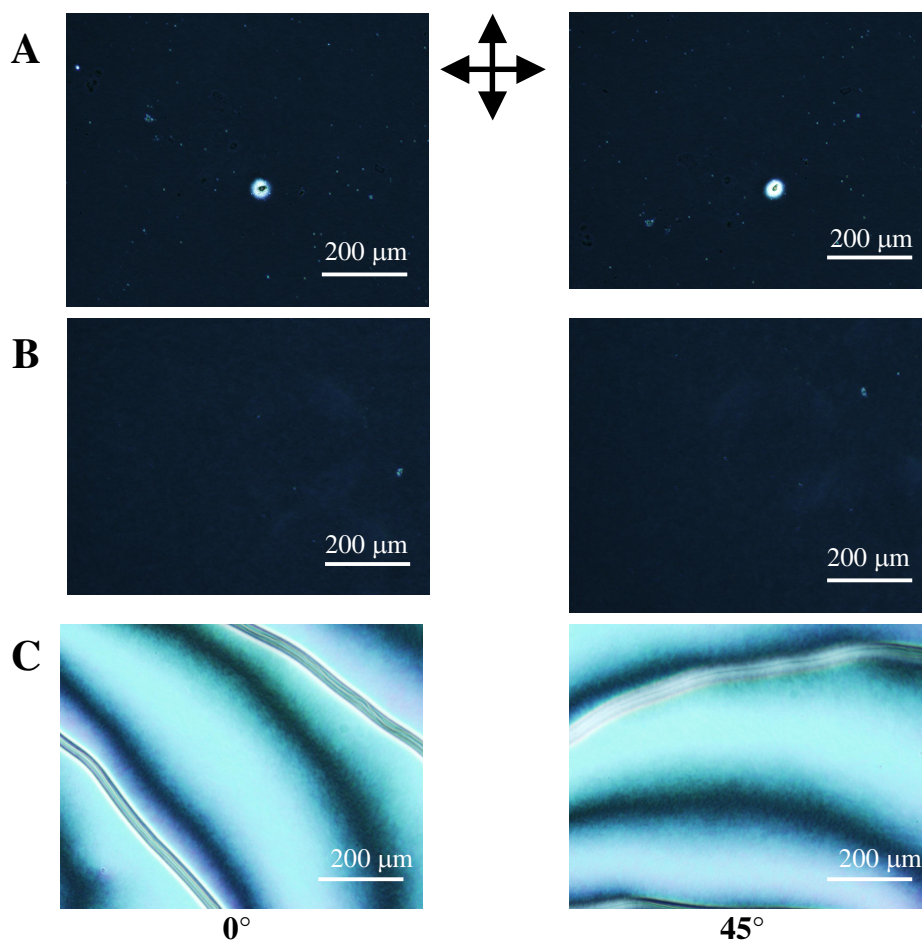
Liquid crystal optical cells, used for the observation of birefringent textures, were fabricated as follows: Two substrates were sandwiched together with the alignment layers facing each other at predetermined orientations separated by a spacer (6 or 40  $\mu\text{m}$ ) and sealed together using epoxy. The optical cells were filled with nematic liquid crystal (in the isotropic or nematic state for comparison) by capillary action and examined for light intensity changes.

### **4.3 Results and Discussion**

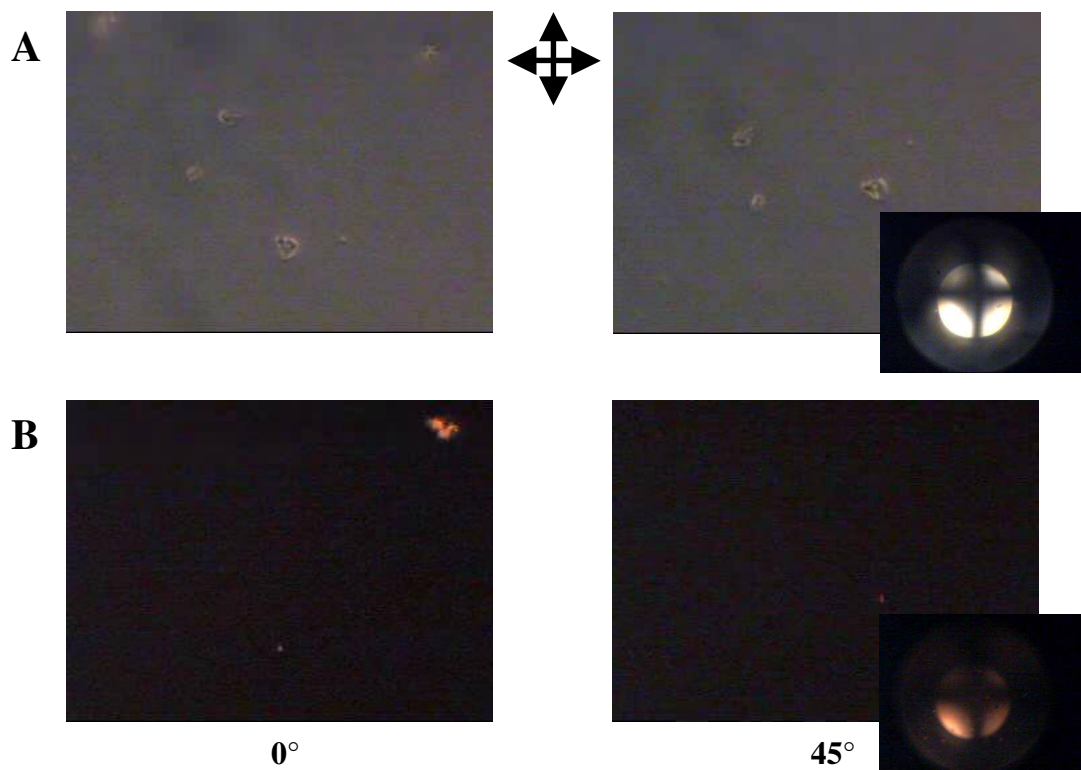
#### **4.3.1 Birefringent Textures of Thin Perfluoropolyether Films**

The LC alignment behavior of thin PFPE films of varying thickness was examined. Liquid crystal (LC) optical cells were fabricated with PFPE alignment layers prepared at concentrations of 100, 50 and 20% PFPE pre-polymer in 1,3-bis(trifluoromethyl) benzene by the spin-coating method. Presumably, as the concentration of PFPE in the spin-coating solution decreases, the thickness of the PFPE film deposited decreases (under similar spin-coating conditions). Figure 4.3 shows the birefringent textures observed for the alignment of K-15 on thin PFPE films. Figure 4.3 A and B show spontaneous homeotropic alignment of the positive dielectric LC K-15 on 100 and 50% PFPE films, respectively. These observations were verified by conoscopic measurements. This spontaneous homeotropic alignment was maintained over large distances (on the order of cm) and was attributed to the low surface energy of the fluoropolymer. Figure 4.3 C shows planar alignment (with a high

pretilt angle) of K-15 on the 20% PFPE films. It is possible that a discontinuous film is deposited at the lower concentration, exposing the high surface energy ITO-coated glass and thus inducing planar alignment. LC alignment layers prepared by depositing 100% S-PFPE on ITO-coated glass by spin-coating showed similar birefringent textures to those prepared with 100% PFPE on ITO-coated glass (Figure 4.4). Again, the low surface energy of the fluorinated material is deemed responsible for the spontaneous homeotropic LC alignment of the positive and negative dielectric LCs.



**Figure 4.3** Birefringent textures observed for alignment of K-15 on thin PFPE films of variable thickness. The alignment of K-15 on thin films prepared with PFPE solution of (A) 100%, (B) 50% and (C) 20% was examined. The orientation of the crossed polarizers is given by the black arrows.

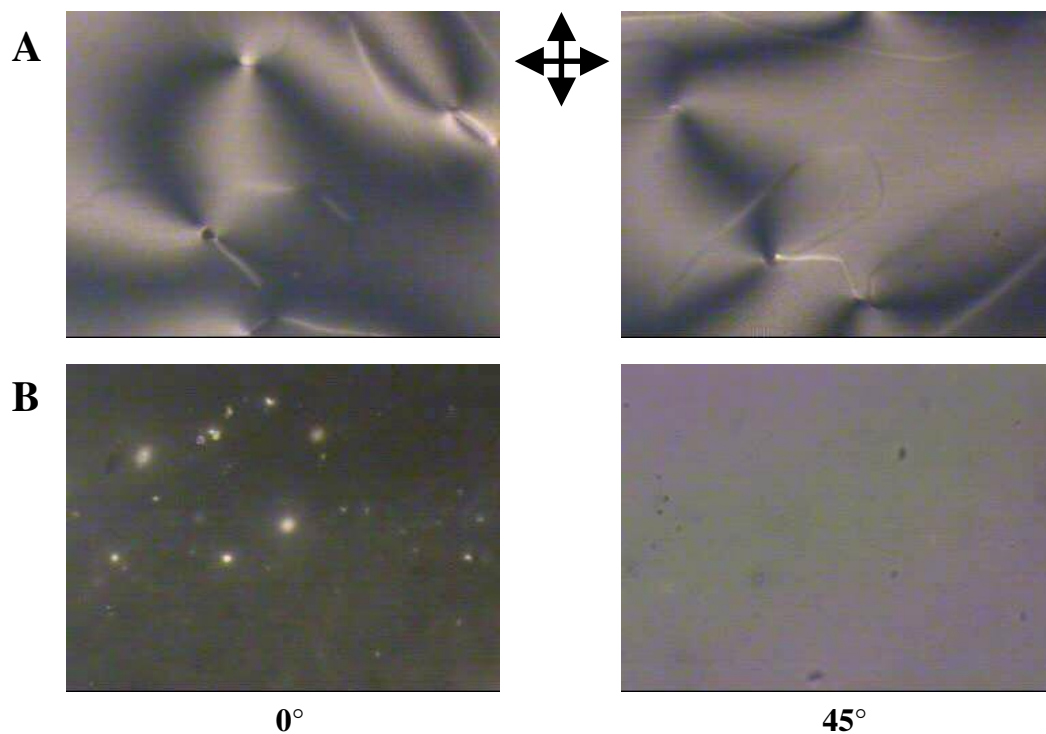


**Figure 4.4** Birefringent textures observed for alignment of (A) K-15 and (B) MLC-6608 on thin films of S-PFPE. The orientation of the crossed polarizers is given by the black arrows.

Thin films of 100% PFPE (all thin films of PFPE from this point on are made with 100% PFPE unless otherwise stated) were also deposited on bare float glass for comparison. Planar alignment of both positive and negative dielectric LCs resulted as shown in Figure 4.5. This change in alignment behavior with a change in the solid substrate is observed for other polymeric alignment layers such as polyimide. Because ITO-coated glass is conductive, an electric field is assumed to be generated between the charges on the substrate surface and image ions in the glass. The impurity ions in the LC may then interact with the small electric field present at the alignment layer surface. Bare float glass on the other hand is an insulator, thus no electric field is produced between the surface and image ions. It is



believed that LC alignment on bare float glass is dominated by intermolecular packing of the LC molecules or as defined in this work, steric interactions between between the LC molecules themselves and the LC molecules and the alignment layer.

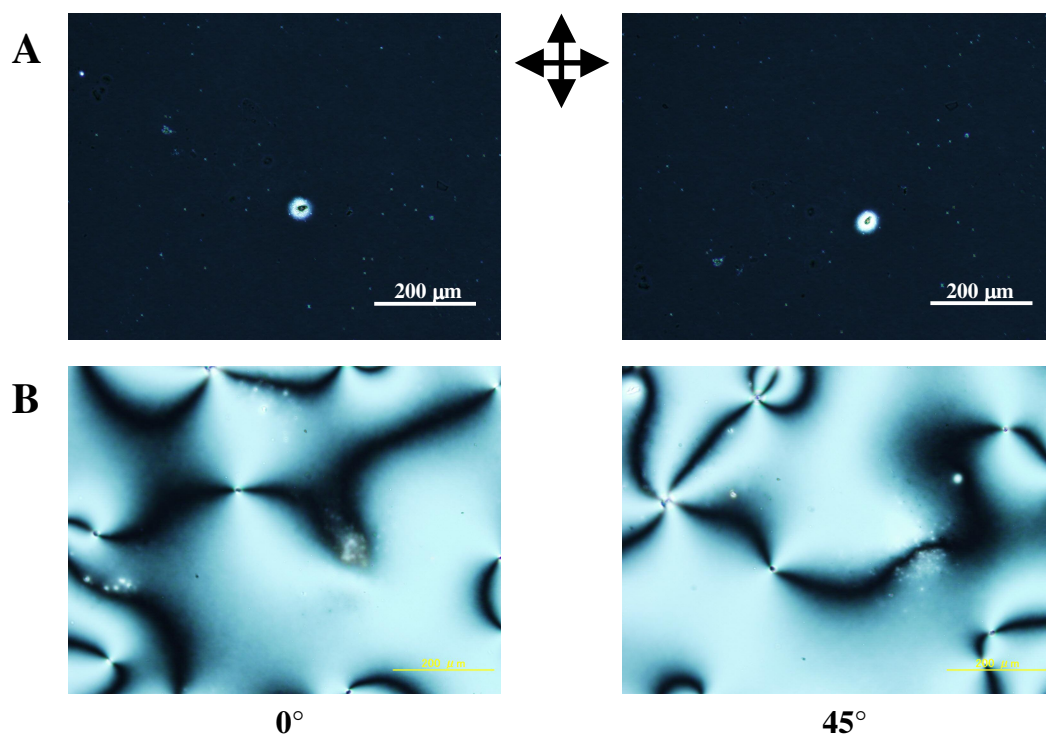


**Figure 4.5** Birefringent textures observed for alignment of (A) K-15 and (B) MLC-6608 on thin films of PFPE deposited on bare float glass. The orientation of the crossed polarizers is given by the black arrows.

### 4.3.2 Comparison of Alignment of Positive and Negative Dielectric Liquid Crystals on Fluorinated Alignment Layers

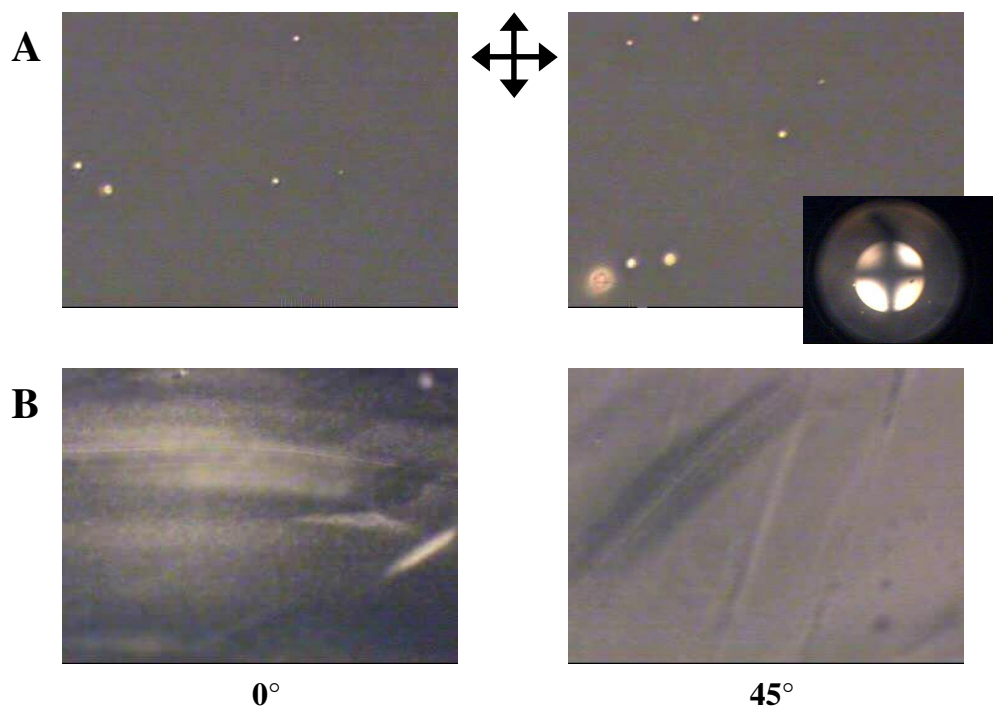
A comparison of the alignment of positive and negative dielectric LCs on thin PFPE films was conducted. Figure 4.6 shows the birefringent textures observed for the alignment of K-15 ( $\Delta\epsilon = +13.2$ ) and MLC-6608 ( $\Delta\epsilon = -4.2$ ) on thin PFPE films. Figure 4.6 A shows spontaneous homeotropic alignment of K-15 while Figure 4.6 B shows spontaneous planar alignment of MLC-6608. Both K-15 and MLC-6608 are calamitic or rod-like in structure and would have similar steric interactions, but K-15 is functionalized with a cyano group while MLC-6608 contains fluorine. This peculiar alignment behavior was compared with that of other fluorinated alignment layers as well as more traditional alignment layers such as dimethyloctadecyl[3-(trimethoxysilyl)propyl] ammonium chloride (DMOAP) and cetyl-trimethyl ammonium bromide (CTAB).

The birefringent textures observed for the alignment of both K-15 and MLC-6608 on Teflon-AF (a transparent fluoropolymer with properties similar to Teflon and PFPE) are shown in Figure 4.7. Figure 4.7 A and B shows that thin films of Teflon-AF behave in the same manner as thin PFPE films, exhibiting homeotropic alignment of the positive dielectric LC and planar alignment of the negative dielectric LC. It has been previously observed that polyimide films exhibit planar alignment of both positive and negative dielectric LCs, making the alignment behavior of these fluorinated films unique. Monolayers of fluorinated birefringent textures observed for the alignment of K-15 and MLC-6608 on trichloro(1H,1H,2H,2H-perfluoro-octyl) silane (a fluorinated monolayer deposited by evaporation) are shown in Figure 4.8. Figure 4.8 A and B shows homeotropic alignment of

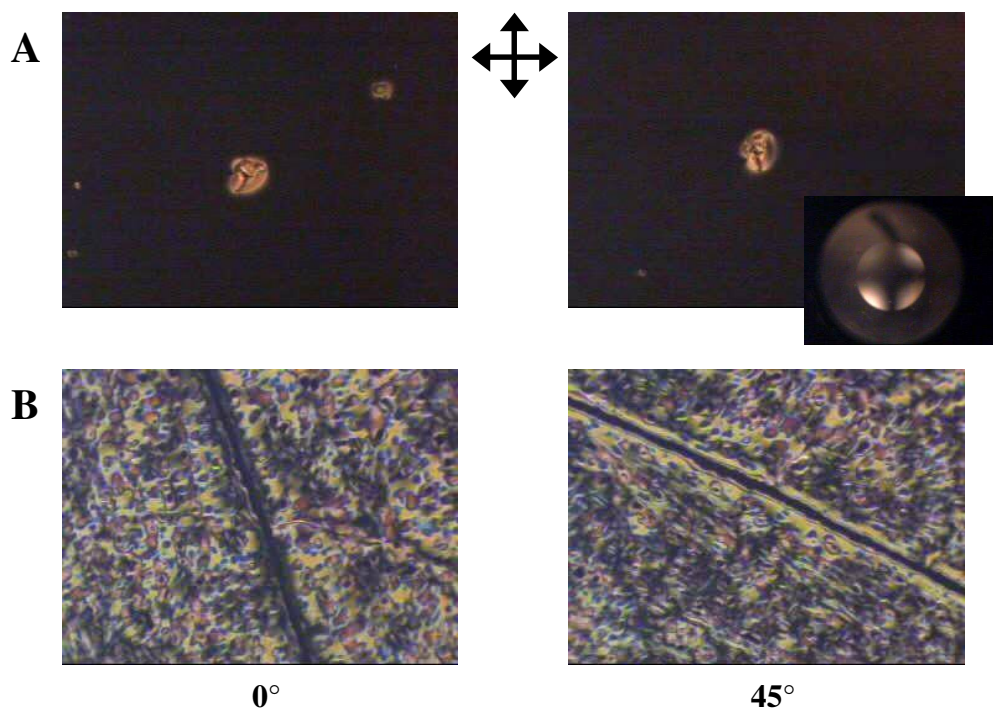


**Figure 4.6** Birefringent textures observed for alignment of (A) K-15 and (B) MLC-6608 on thin films of PFPE. The orientation of the crossed polarizers is given by the black arrows.

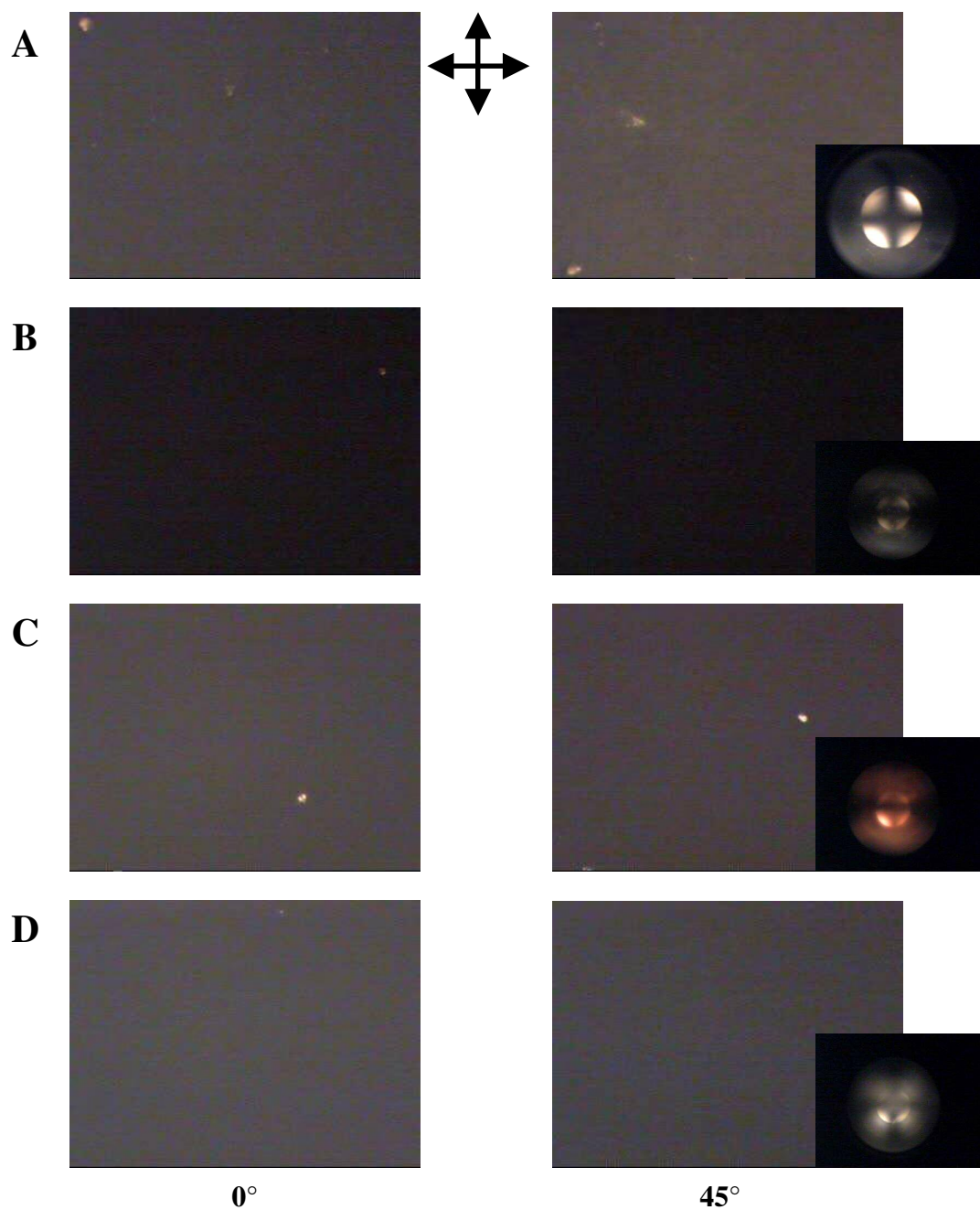
silanes were also compared with monolayers of hydrocarbon silanes. The the positive dielectric and planar alignment of the negative dielectric. These results were compared with the birefringent textures observed for the alignment of K-15 and MLC-6608 on DMOAP (Figure 4.9 A and B) and CTAB (Figure 4.9 C and D). Figure 4.9 shows that spontaneous homeotropic alignment is observed for both LCs on DMOAP and CTAB. Based on these observations, it appears that fluorinated alignment layers exhibit unique alignment behavior with regard to the dielectric constant of the LC. It is possible that the negative dielectric LC with fluorinated functionalities in the ring structure experiences dipole-dipole interactions with the fluorinated alignment layer.



**Figure 4.7** Birefringent textures observed for alignment of (A) K-15 and (B) MLC-6608 on thin films of Teflon-AF. The orientation of the crossed polarizers is given by the black arrows.



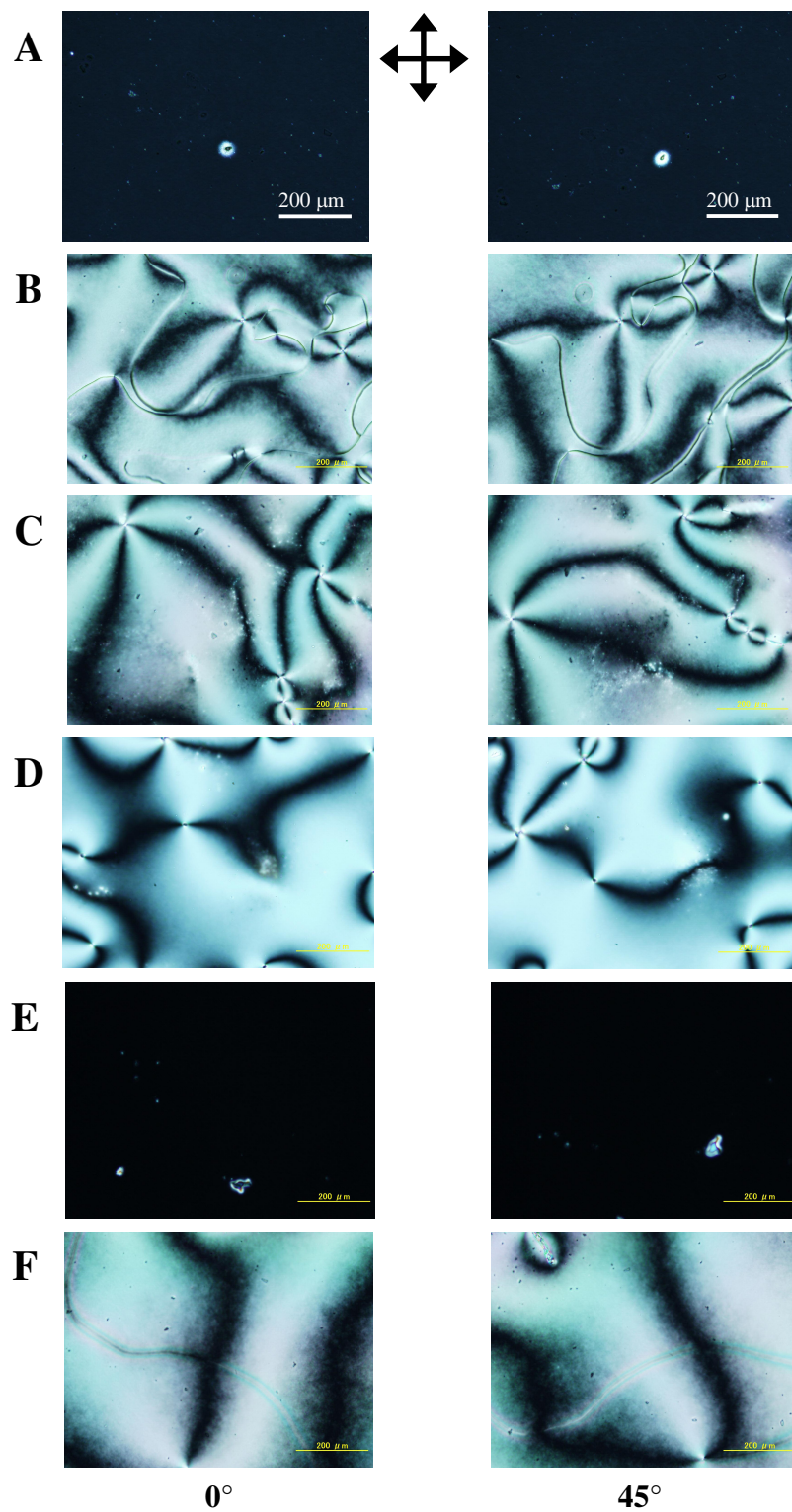
**Figure 4.8** Birefringent textures observed for alignment of (A) K-15 and (B) MLC-6608 on thin films of trichloro(1H,1H,2H,2H-perfluoro-octyl) silane. The orientation of the crossed polarizers is given by the black arrows.



**Figure 4.9** Birefringent textures observed for the alignment of K-15 and MLC-6608 on DMOAP and CTAB. Homeotropic alignment of both (A) K-15 and (B) MLC-6608 on DMOAP was observed as well as homeotropic alignment of (C) K-15 and (D) MLC-6608 on CTAB. The orientation of the crossed polarizers is given by the black arrows.

The alignment of several additional LCs on thin PFPE films was examined to better understand the alignment mechanisms associated with this material. Figure 4.10 shows the birefringent textures observed for the alignment of several LCs, including K-15 ( $\Delta\epsilon = +13.2$ ), ZLI-2293 ( $\Delta\epsilon = +10$ ), ZLI-4792 ( $\Delta\epsilon = +5.2$ ), MLC-6608 ( $\Delta\epsilon = -4.2$ ), MLC-6609 ( $\Delta\epsilon = -3.7$ ), and MLC-6610 ( $\Delta\epsilon = -3.1$ ). Figure 4.10 A shows the spontaneous homeotropic alignment observed of K-15, as previously discussed. Figure 4.10 B shows planar alignment of ZLI-2293, a liquid crystal having a cyano functionality like that of K-15. This result is somewhat surprising. Figure 4.10 C shows spontaneous planar alignment of ZLI-4792, a positive dielectric LC having fluorine functionalities oriented parallel to the long molecular axis. Figure 4.10 D through F shows planar alignment of MLC-6608 and MLC-6610, respectively while Figure 4.10 E shows a mixture of homeotropic and planar alignment for MLC-6609. MLC-6608, MLC-6609 and MLC-6610 all have fluorine functionalities, most likely oriented perpendicular to the long molecular axis. Only the chemical structure of K-15 is known (due to commercial interests), however all LCs are presumed to be calamitic or rod-like (based on catalog information), thus steric interactions should be similar for all LCs examined. These results confirm the possibility of dipole-dipole interactions between the C-F bonds in the LC molecules and the PFPE film (assuming that the C-F bonds in the PFPE film are approximately parallel to the substrate). This theory is discussed in more detail in sections 4.3.7 and 4.3.11.





**Figure 4.10** Birefringent textures for the alignment of (A) K-15, (B) ZLI-2293, (C) ZLI-4792, (D) MLC-6608, (E) MLC-6609, and (F) MLC-6610 on thin films of PFPE. The orientation of the crossed polarizers is given by the black arrows.

### **4.3.3 Time-Dependent Stability of Liquid Crystal Alignment on Thin**

#### **Perfluoropolyether Films**

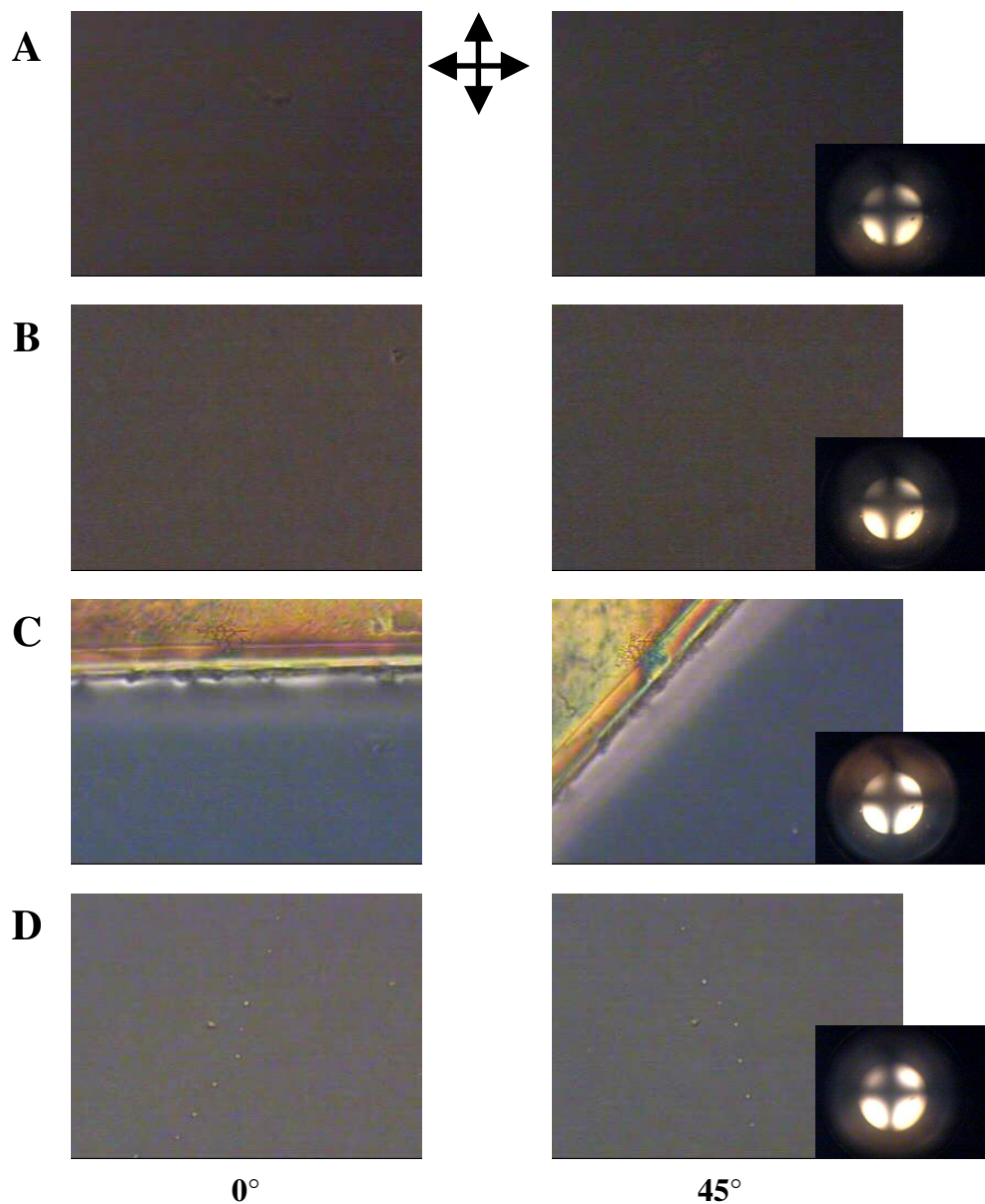
Experiments were conducted in which the alignment of both positive and negative LCs was examined at 24-hour intervals over a 144-hour period. Figure 4.11 shows that the spontaneous homeotropic alignment of the positive dielectric K-15 on thin PFPE films was stable over relatively long periods of time (144 hours). However, the planar alignment of the negative dielectric MLC-6608 was not as stable, forming a region of homeotropic alignment at 48 hours (Figure 4.12). This result may explain the domains of homeotropic and planar alignment exhibited by MLC-6609. Other time-dependence experiments showed that the alignment of both positive and negative dielectric LCs on thin S-PFPE films was stable over relatively long periods of time (96 to 144 hours).

### **4.3.4 Surface Energy Measurements on Thin Perfluoropolyether Films**

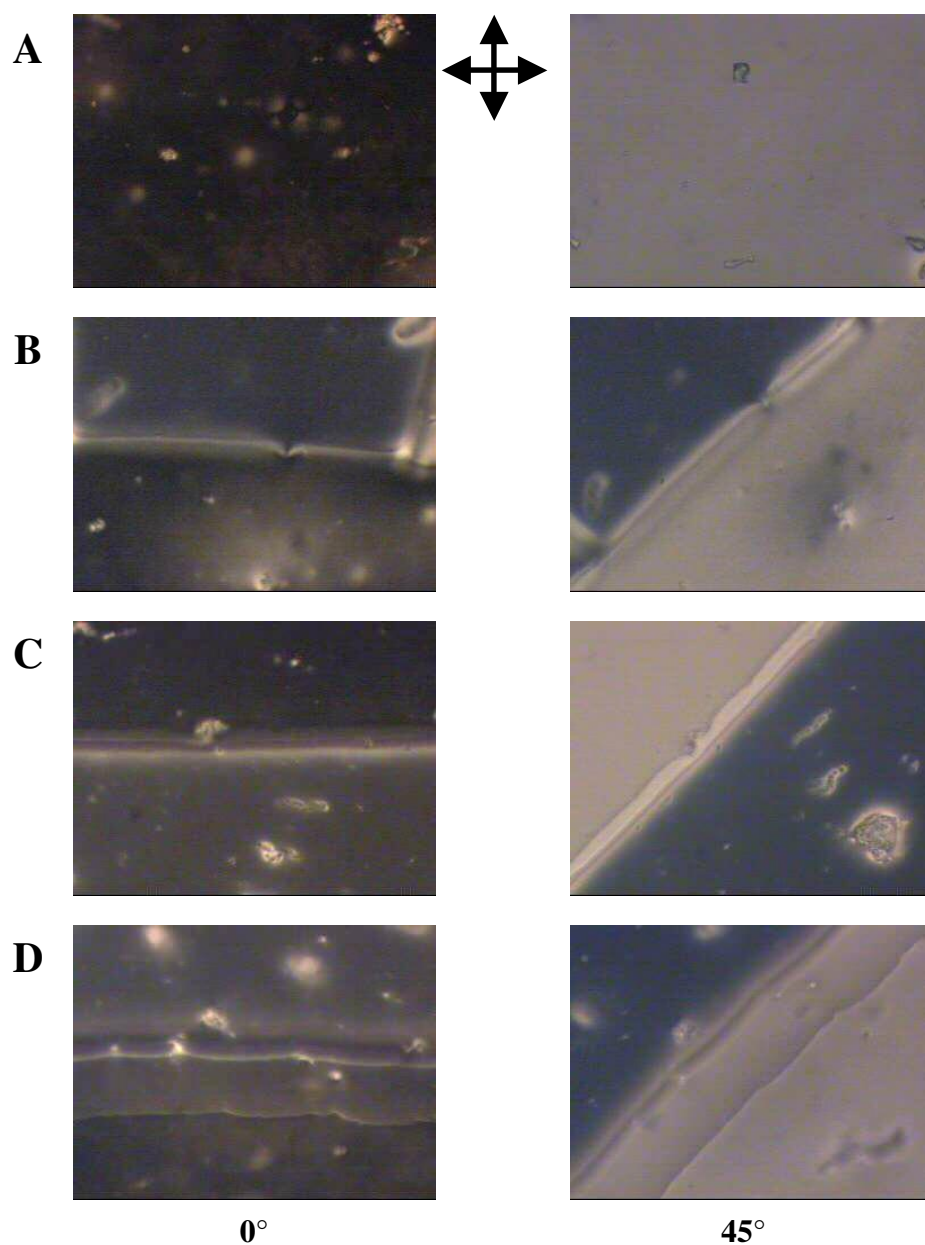
A comparison of the surface energies of fluorinated and traditional alignment layers was performed. The contact angles of both water and ethylene glycol were measured for each of the following alignment layers: thin PFPE film, thin Teflon-AF film, thin polyimide film as well as monolayers of trichloro(1H,1H,2H,2H-perfluoro-octyl) silane, DMOAP and CTAB. From this data, the surface energy of each alignment layer was calculated using the the Girifalco-Good-Fowlers-Young equation (2.1).<sup>10,11</sup> The surface energies of the fluorinated materials are very low when compared with the traditional alignment layers (Figure 4.13). Thin films of PFPE exhibited the lowest surface energy, approximately 9 mN/m while Teflon-AF and trichloro(1H,1H,2H,2H-perfluoro-octyl) silane followed closely with approximately 12 and 18 mN/m, respectively. DMOAP and CTAB exhibited surface energies similar both to one another (~29 mN/m for DMOAP and ~26 nM/m for CTAB) and



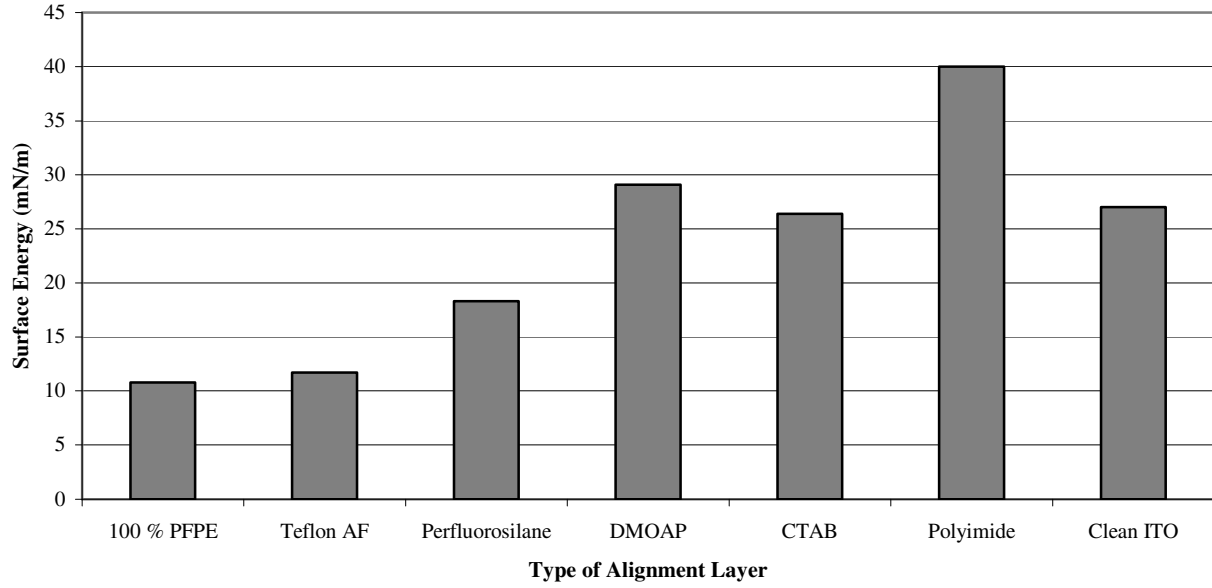
to that calculated for clean ITO-coated glass ( $\sim 27$  mN/m). Thin films of polyimide exhibited the highest surface energy, approximately 40 mN/m. The extremely low surface energies of fluorinated alignment layers may, in part, explain the spontaneous homeotropic alignment of K-15.



**Figure 4.11** Time-dependent stability of alignment of K-15 on PFPE. Birefringent textures were observed for alignment of K-15 on thin films of PFPE at (A) 0, (B) 24, (C) 48 and (D) 144 hours. The orientation of the crossed polarizers is given by the black arrows.



**Figure 4.12** Time-dependent stability of alignment of MLC-6608 on PFPE. Birefringent textures were observed for alignment of MLC-6608 on thin films of PFPE at (A) 0, (B) 24, (C) 48 and (D) 144 hours. The orientation of the crossed polarizers is given by the black arrows.



**Figure 4.13** Comparison of surface energies of fluorinated materials and traditional alignment materials.

#### 4.3.5 Surface Anchoring Energy Measurements on Thin Perfluoropolyether Films

Macroscopically, the surface effects of an alignment layer are manifested by the bulk properties of the LC director. The director orientation is determined by one of two cases: first, the strong anchoring case, in which the LC director maintains a fixed orientation (termed the easy direction by de Gennes<sup>12</sup>) and second, the weak anchoring case, in which the surfaces forces are such that a well-defined LC director orientation cannot be imposed. The weak anchoring case is the situation for the majority of alignment layers.<sup>13,14</sup> To describe the surface effects on the LC director, Rapini and Papoular (RP) developed a simple expression for the interfacial surface anchoring energy per unit area<sup>15</sup>:

$$g_s = - (A/2) (\mathbf{n} \cdot \mathbf{e})^2 \quad (4.1)$$

where  $\mathbf{n}$  is the LC director at the surface,  $\mathbf{e}$  is the easy direction and  $A$  is the anchoring strength or energy coefficient. The RP model has been used by many authors to describe the

anisotropic interaction between the LC director and the substrate, however large discrepancies exist for values reported, even when the same conditions have been used.<sup>16</sup>

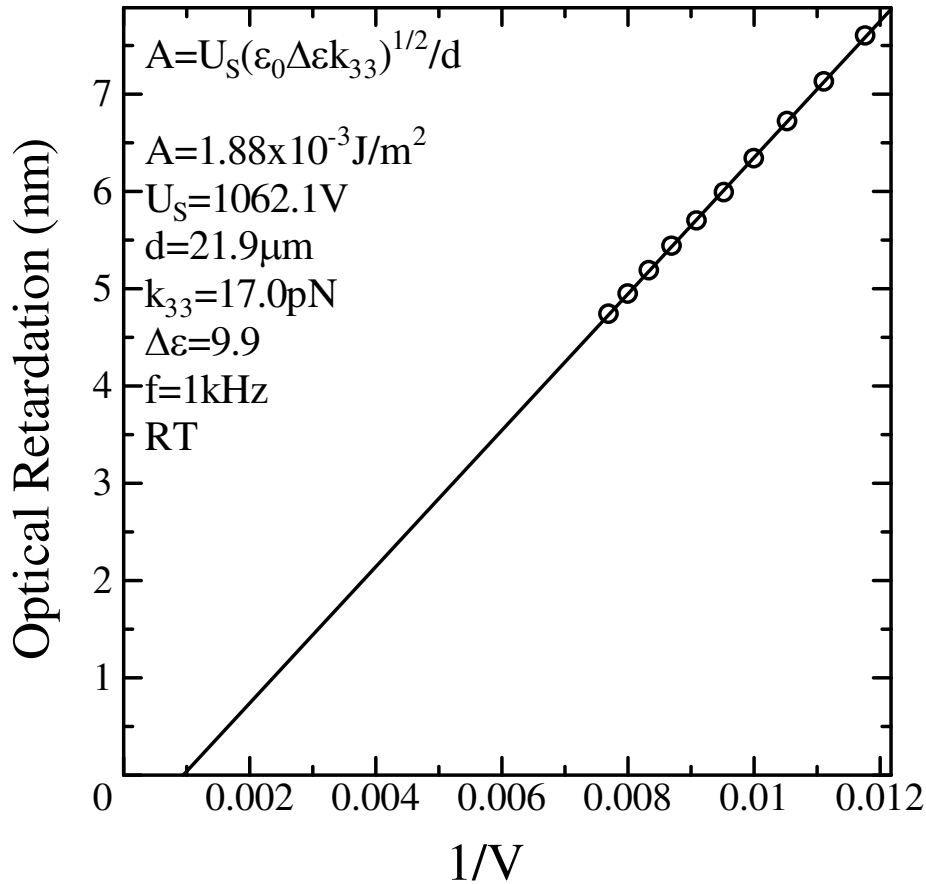
On the basis of the RP model, Sugimura and colleagues have proposed a unified surface anchoring energy with which to study the LC director deformation.<sup>17,18</sup> The unified surface anchoring energy model gives a relationship between the anchoring strength  $A$  and the deviation angle of the LC director from the easy direction by surface effects. A saturation voltage method is used to measure the unified surface anchoring energy. At the saturation transition, the LC director becomes completely homeotropic, meaning that all LC molecules are oriented parallel to the electric field at the saturation voltage for a parallel substrate LCD design. The anchoring strength is related to the saturation voltage by the following equation (4.2):

$$A = V_S(\epsilon_0 \Delta \epsilon K_3)^{1/2} / d \quad (4.2)$$

where  $V_S$  is the saturation voltage,  $\epsilon_0$  is the dielectric permittivity of vacuum,  $\Delta \epsilon$  is the dielectric anisotropy,  $K_3$  is the bend elastic constant and  $d$  is the cell thickness.<sup>18</sup> This unified surface anchoring energy model was used to probe the surface anchoring energy of thin PFPE films.

LC optical cells were fabricated with thin PFPE films (prepared as previously described) and filled with ZLI-2293. The saturation voltage method requires that a positive dielectric liquid crystal exhibit an initial planar alignment mode, thus the use of ZLI-2293. Measurements of the optical retardation were made with respect to the voltage applied across the cell. Typically, as the voltage increases the optical retardation decreases because the LC molecules are being reoriented to achieve homeotropic alignment. A plot of the optical retardation versus inverse voltage is shown in Figure 4.14. Because the optical retardation is

inversely proportional to the applied voltage in the high voltage regimes, the x-intercept of the extrapolated line gives the saturation voltage.<sup>19,20</sup> From this extrapolated voltage (1062.0 V), the surface anchoring energy was calculated to be  $1.88 \times 10^{-3} \text{ J/m}^2$ , a value typical of surfaces with weak anchoring. Surfaces with weak anchoring energies generally have faster switching times, a characteristic necessary for high-quality displays.



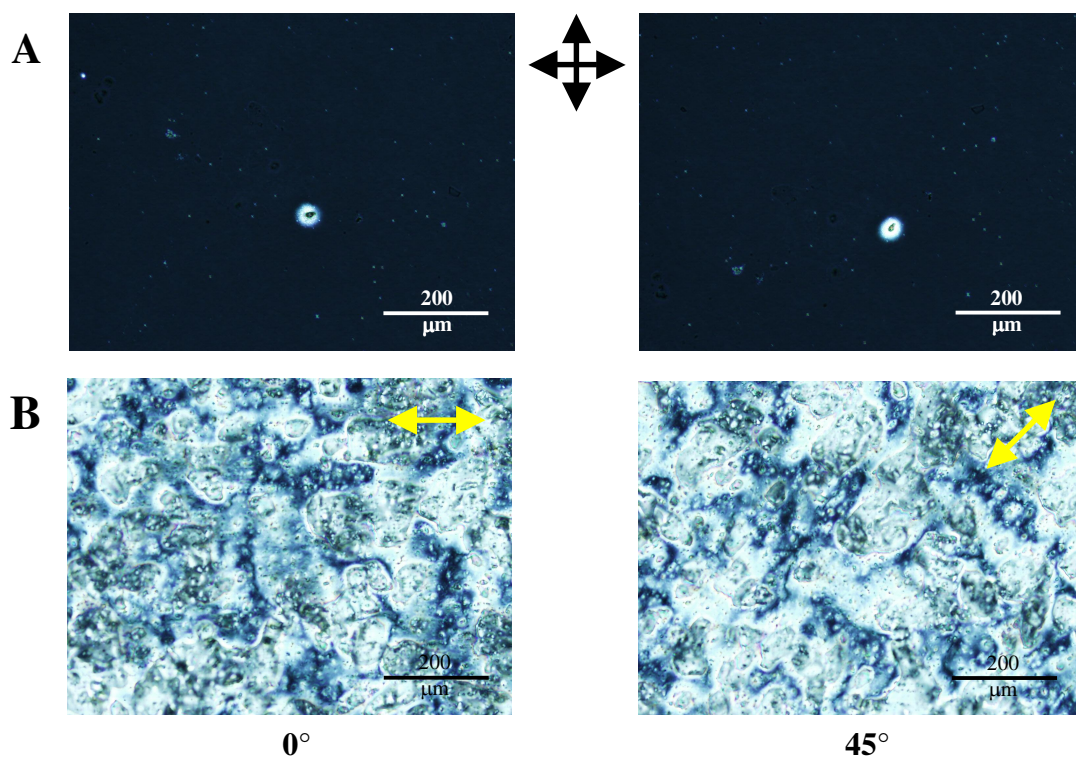
**Figure 4.14** Plot of the optical retardation versus inverse voltage for the alignment of ZLI-2293 on thin PFPE film. The calculated surface anchoring energy is shown.

#### 4.3.6 Birefringent Textures of Rubbed Perfluoropolyether Films

The LC alignment behavior of rubbed PFPE films of varying thickness was examined. Liquid crystal (LC) optical cells were fabricated with PFPE alignment layers prepared at concentrations of 100, 50 and 20% PFPE pre-polymer in 1,3-bis(trifluoromethyl) benzene by the spin-coating method and mechanically rubbed following UV polymerization. Examination of the LC optical cells under crossed polarizers showed a shift from homeotropic alignment to planar alignment with a high pretilt angle for 100% films (Figure 4.15), while 20% PFPE films merely maintained planar alignment. In some cases 50% PFPE films maintained homeotropic alignment and in others a trend similar to that of 100% PFPE was observed.

The correlation between pretilt angle of K-15 and presence of fluorine functionalities in polymer films have been previously examined.<sup>11,21,22</sup> J.-K. Park and colleagues showed that the pretilt angle of K-15 increases as the fluorine content (F:C ratio) increases in polyimide films, containing trifluoromethyl moieties, prepared by photo-induced alignment.<sup>21</sup> D.-S. Seo and S. Kobayashi examined the effects of rubbing strength (or pressure with which rubbing is applied) on similar films. These studies used polyimide alignment layers that contained trifluoromethyl moieties, were thermally cured and were rubbed at various rubbing strengths. They observed that the fluorine concentration (F:C ratio) and thus, the pretilt angle decreases with increasing rubbing strength.<sup>22</sup> From these studies, it is apparent that the decrease in pretilt angle from 90° (homeotropic) to something between 0° and 90° resulted from a decrease in the fluorine concentration in the PFPE film caused by mechanical rubbing. It is presumed that the 50% PFPE films that maintained

hometropic alignment after rubbing were prepared at a decreased rubbing strength, however this presumption cannot be confirmed since measurement of the rubbing strength is impossible with the apparatus built in-house.



**Figure 4.15** Birefringent textures observed for alignment of K-15 on (A) thin PFPE film and (B) rubbed PFPE film. The orientation of the crossed polarizers is given by the black arrows while the rubbing direction is denoted by the double-headed yellow arrow.

#### **4.3.7 Birefringent Textures of Pretreated Thin Perfluoropolyether Films**

The environmental stability of thin PFPE films was examined by means of a film pretreatment method. Fully cured PFPE films were immersed in toluene, water or some serial combination of the two solvents for 24 hours before being dried either by a stream of nitrogen gas or under vacuum and examined by transmitted polarized light microscopy for alignment of K-15 and MLC-6608. The birefringent textures observed for the alignment of K-15 on pretreated thin PFPE films are shown in Figure 4.16. Figure 4.16 A shows the homeotropic alignment of K-15 observed for a thin PFPE film, having no pretreatment. This homeotropic alignment is maintained after treatment with toluene (Figure 4.16 B). However, pretreatment with water seems to have a disruptive effect on the LC director orientation as manifested by the appearance of random domains of planar alignment with a high pretilt angle (Figure 4.16 C). The birefringent textures observed for the alignment of MLC-6608 on pretreated thin PFPE films are shown in Figure 4.17. Figure 4.17 A shows the random domains of planar alignment induced by the thin PFPE film, having no pretreatment. An interesting phenomenon occurs when the film is treated with toluene, leading to homeotropic alignment (Figure 4.17 B) just as that seen with the positive dielectric LC. Pretreatment with water also has the same effect on MLC-6608 as that seen with K-15 (Figure 4.17 C). These observations may be explained by the enhancement or suppression of one or more of the three surface effects contributing to LC alignment: electric field effects due to impurity ions in the liquid crystal, dipole-dipole interactions and steric interactions.

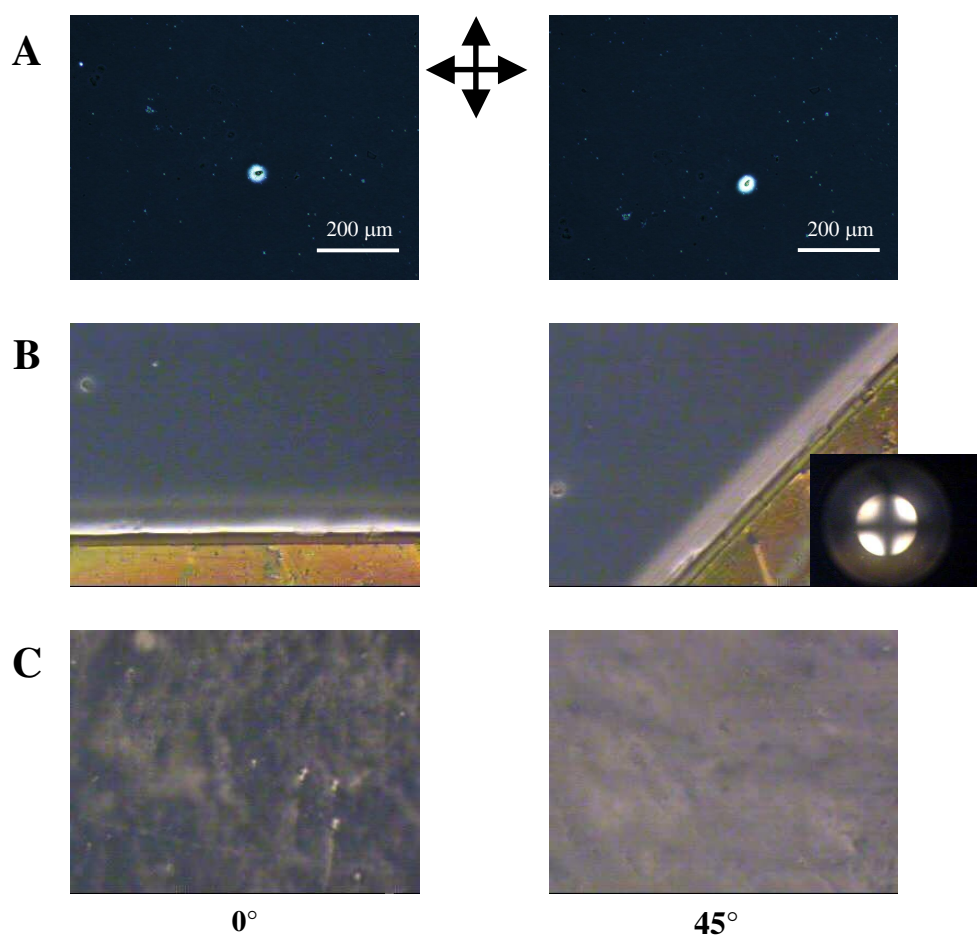
As previously discussed, ITO-coated glass is a conductive material, making it possible that a small electric field is induced between image ions in the substrate and



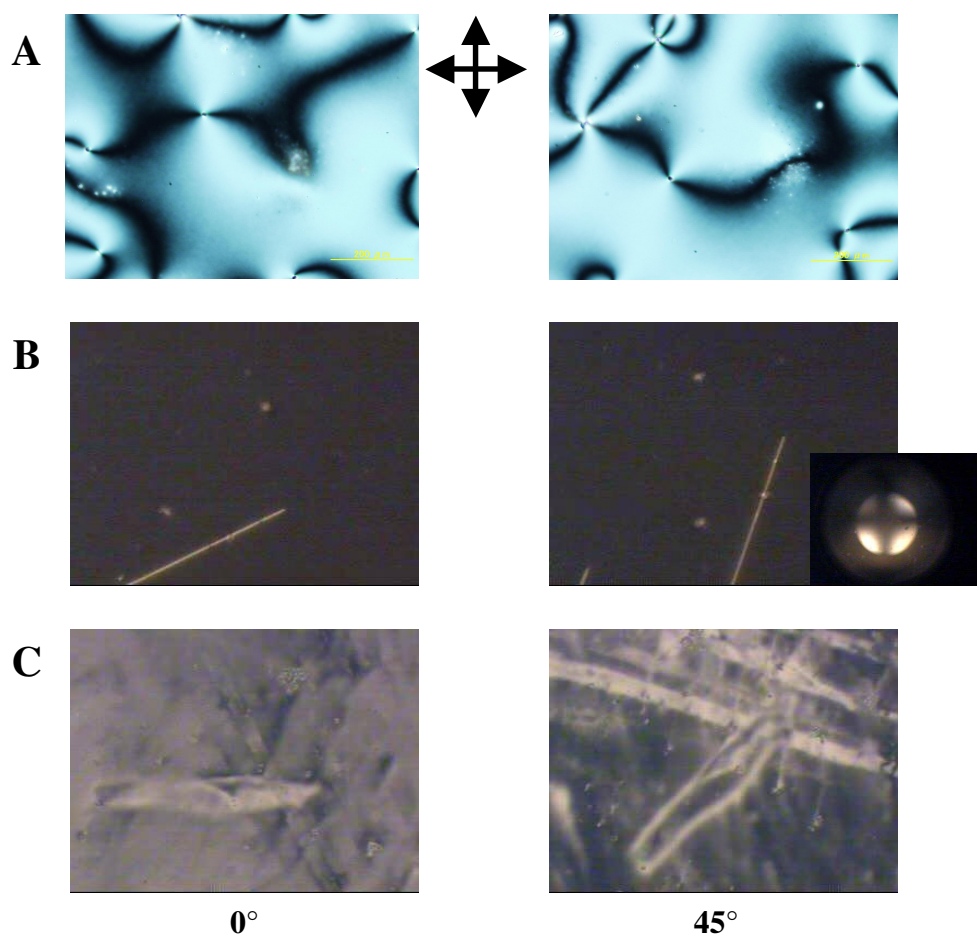
impurity ions in the LC. By nature of the synthetic method, solutions of K-15 contain many impurity ions while solutions of MLC-6608 contain very few. Due to the dielectric anisotropy of the two LCs, K-15 molecules would orient with their long axes parallel to the electric field, while MLC-6608 molecules would orient perpendicular to the electric field. However, this orientation is only temporary for MLC-6608 molecules. Because solutions of MLC-6608 have very few impurity ions, the effects of the electric field diminish over time as the impurity ions dissolve into the bulk LC layer. Thus, electric field effects dominate in the case of the untreated thin PFPE films and K-15, while both electric field effects and dipole-dipole interactions must be considered for MLC-6608. Dipole-dipole interactions between the C-F bonds in the PFPE film and the C-F and C-CN bonds in the LCs also contribute to the LC director orientation. Assuming that the C-F bonds in the PFPE film are in the plane of the film (rather than oriented perpendicular to the film), MLC-6608 molecules would orient with their long axes perpendicular to the substrate surface while K-15 molecules would orient parallel. There are also steric effects to consider. The LC molecules themselves are rod-like and prefer to pack parallel to one another. A desire to minimize energy costs and possibly small van der Waals forces at the substrate surface drive the LC molecules to orient parallel to the substrate surface.

Treating the PFPE films with water suppresses the electric field effects because adsorbed ions from the water counteract the effects of the image ions. Thus, the observation of planar alignment with a high pretilt angle is merely a balance between the diminished electric effects and the dipole-dipole interactions. On the other hand, treating the PFPE films with toluene seems to enhance the electric field effects. Thus, K-15 maintains homeotropic alignment after pretreatment. This enhancement does not however seem to affect the MLC-

6608 molecules, whose preferential homeotropic orientation remains dominated by dipole-dipole interactions.



**Figure 4.16** Birefringent textures observed for the alignment of K-15 on pretreated thin PFPE films. Homeotropic alignment of K-15 was observed for both (A) untreated PFPE films and (B) PFPE films treated with toluene. Planar alignment with a high pretilt angle was observed for (C) PFPE films treated with water. The orientation of the crossed polarizers is given by the black arrows.

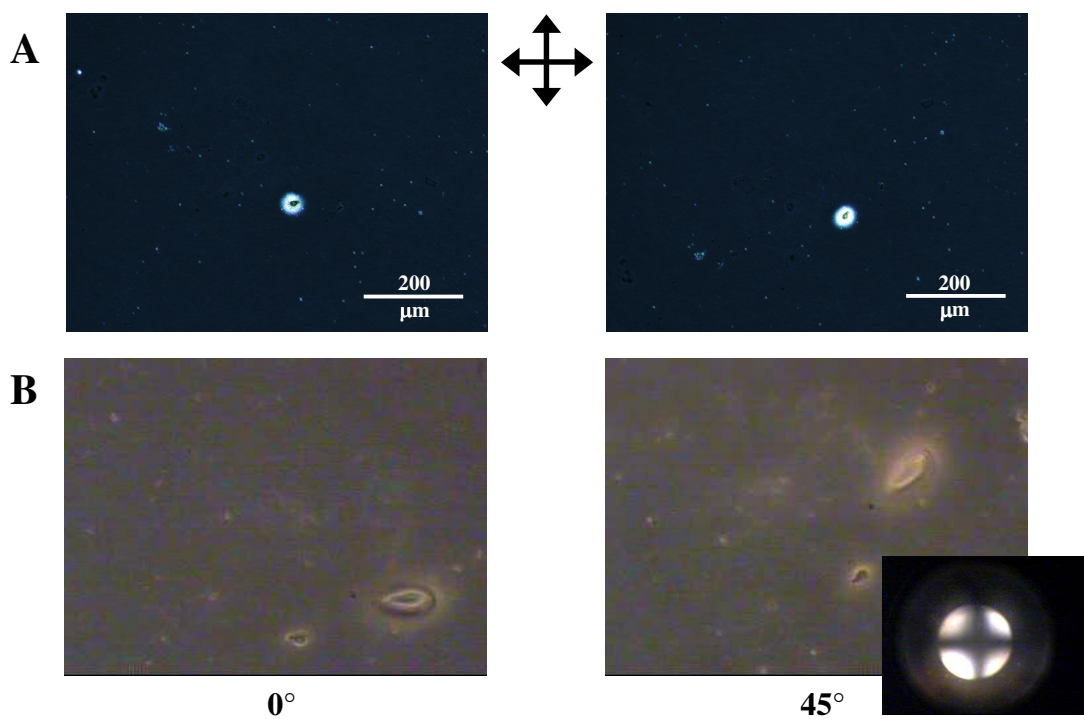


**Figure 4.17** Birefringent textures observed for the alignment of MLC-6608 on pretreated thin PFPE films. Planar alignment of MLC-6608 was observed for (A) untreated PFPE films while homeotropic alignment was observed for (B) PFPE films treated with toluene. Planar alignment with a high pretilt angle was observed for (C) PFPE films treated with water. The orientation of the crossed polarizers is given by the black arrows.

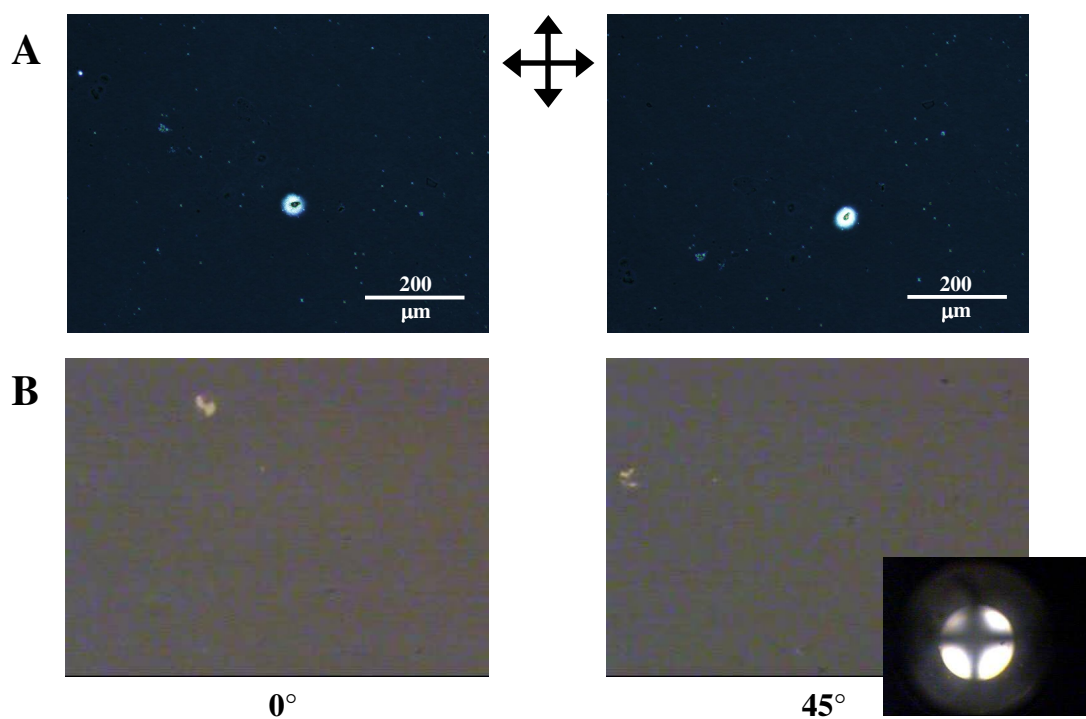
The reversibility of the pretreatment effects was examined by sequential pretreatment of the thin PFPE films. Thin PFPE films were immersed in toluene for 24 hours, dried either by nitrogen gas or under vacuum (two methods yield same results), and immersed in water 24 hours and dried by the same method. These films were then used to fabricate LC optical cells that were filled with K-15 and examined by transmitted polarized light microscopy. The birefringent textures observed for the alignment of K-15 on pretreated thin PFPE films are shown in Figure 4.18. It appears that the enhancement of the electric field effects induced by toluene is not easily counteracted by exposure to water (Figure 4.18 B). Thin PFPE films were also prepared by immersion in water for 24 hours and drying either by nitrogen gas or under vacuum followed by immersion in toluene for 24 hours and drying by the same method. When examined by transmitted polarized light microscopy for the alignment of K-15, these films also showed homeotropic alignment (Figure 4.19). It appears from these results that effects of pretreatment with toluene on the LC director orientation dominate over the effects of pretreatment with water.

The environmental stability of thin S-PFPE films was also examined by means of the film pretreatment method. Fully cured S-PFPE films were immersed in either water or toluene for 24 hours before being dried either by nitrogen gas or under vacuum and examined by transmitted polarized light microscopy for alignment of K-15. The birefringent textures observed for the alignment of K-15 on pretreated thin S-PFPE films are shown in Figure 4.20. Figure 4.20 A and B shows the homeotropic alignment of K-15 by untreated and toluene treated thin S-PFPE films, respectively. Figure 4.20 C shows homeotropic alignment of K-15 for thin S-PFPE films treated with water, an observation unique to S-PFPE. There is some perturbation of the LC director as evidenced by bright spots in the otherwise dark

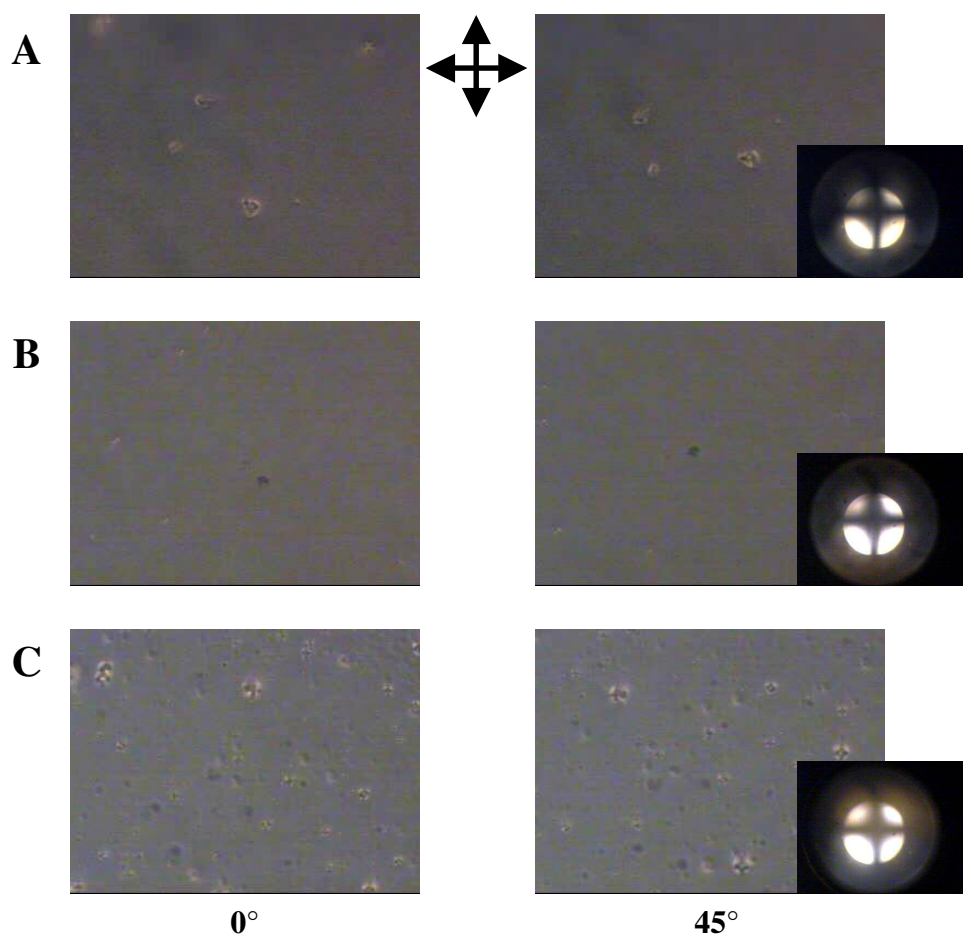
image, but conoscopic measurements confirm that the average orientation of the LC molecules is very close to  $90^\circ$ . It appears that electric field effects dominate in all cases for thin films of S-PFPE.



**Figure 4.18** Birefringent textures observed for the alignment of K-15 on pretreated thin PFPE films. Homeotropic alignment was observed for both (A) untreated PFPE films and (B) PFPE films treated sequentially with toluene and water. The orientation of the crossed polarizers is given by the black arrows.



**Figure 4.19** Birefringent textures observed for the alignment of K-15 on pretreated thin PFPE films. Homeotropic alignment was observed for both (A) untreated PFPE films and (B) PFPE films treated sequentially with water and toluene. The orientation of the crossed polarizers is given by the black arrows.



**Figure 4.20** Birefringent textures observed for the alignment of K-15 on pretreated thin S-PFPE films. Homeotropic alignment was observed for (A) untreated PFPE films, (B) PFPE films treated with toluene and (C) PFPE films treated with water. The orientation of the crossed polarizers is given by the black arrows.

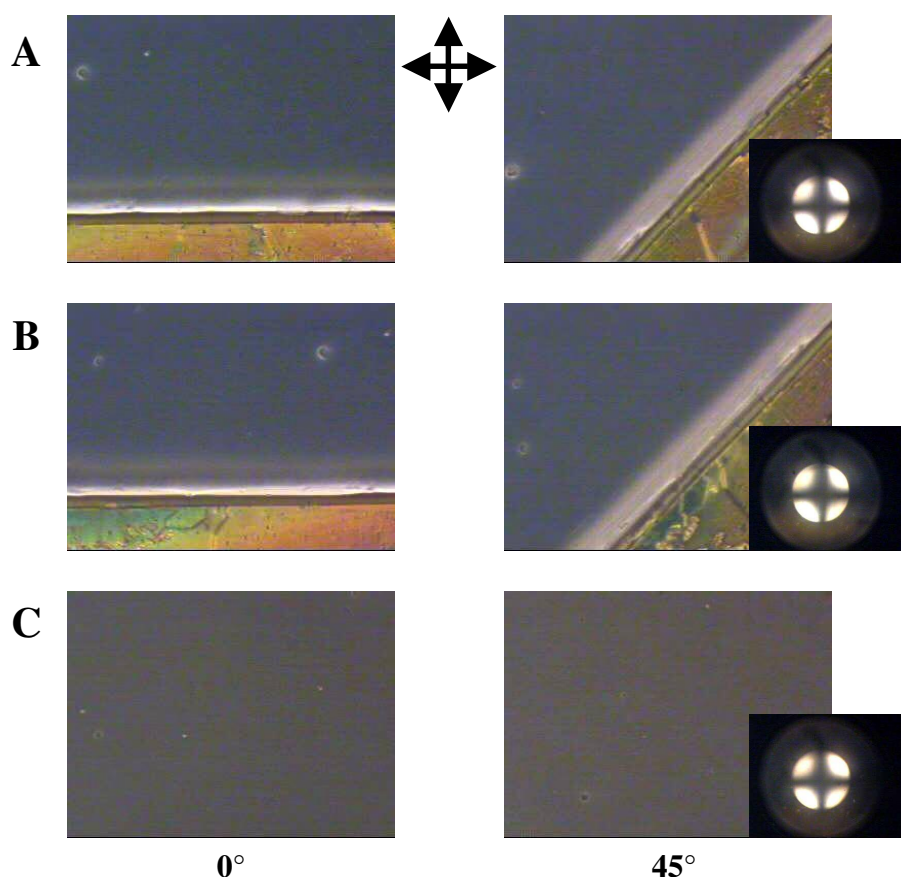
#### 4.3.8 Time-Dependent Stability of Liquid Crystal Alignment on Pretreated Thin Perfluoropolyether Films

Experiments were conducted in which the alignments of both positive and negative LCs on pretreated thin PFPE and S-PFPE films were examined at 24-hour intervals over a 96-hour period. Figure 4.21 shows that the spontaneous homeotropic alignment of K-15 on thin PFPE films pretreated with toluene was stable over relatively long periods of time (96



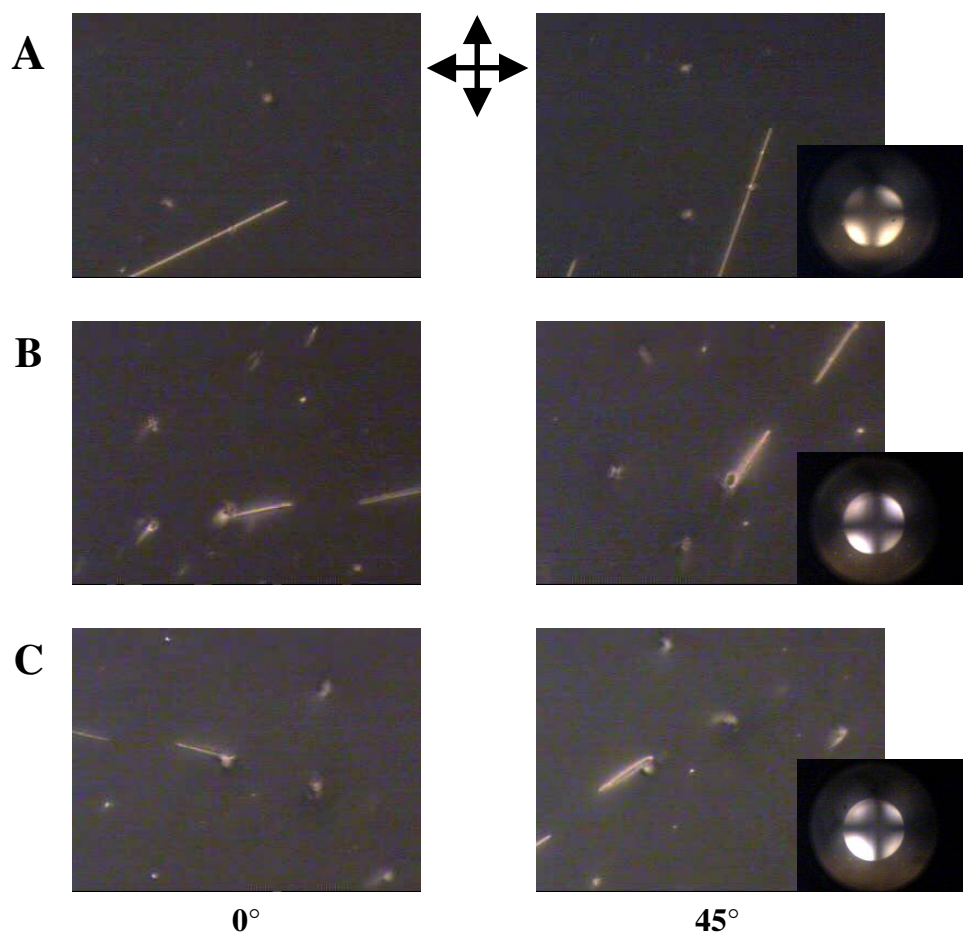
hours). Similar results were obtained for the homeotropic alignment of MLC-6608 on thin PFPE films pretreated with toluene (Figure 4.22). The planar alignment of K-15 on PFPE films pretreated with water was slightly less stable than the alignment achieved by toluene treated films. The pretilt angle of the LC director increased over time as evidenced by the decreasing contrast between the dark and bright states (Figure 4.23). This observation was also noted for the alignment of MLC-6608 on water treated films.

Time-dependence experiments were also conducted for pretreated S-PFPE films. The homeotropic alignment of K-15 on thin S-PFPE films pretreated with either toluene or water was stable over relatively long periods of time (96 hours).

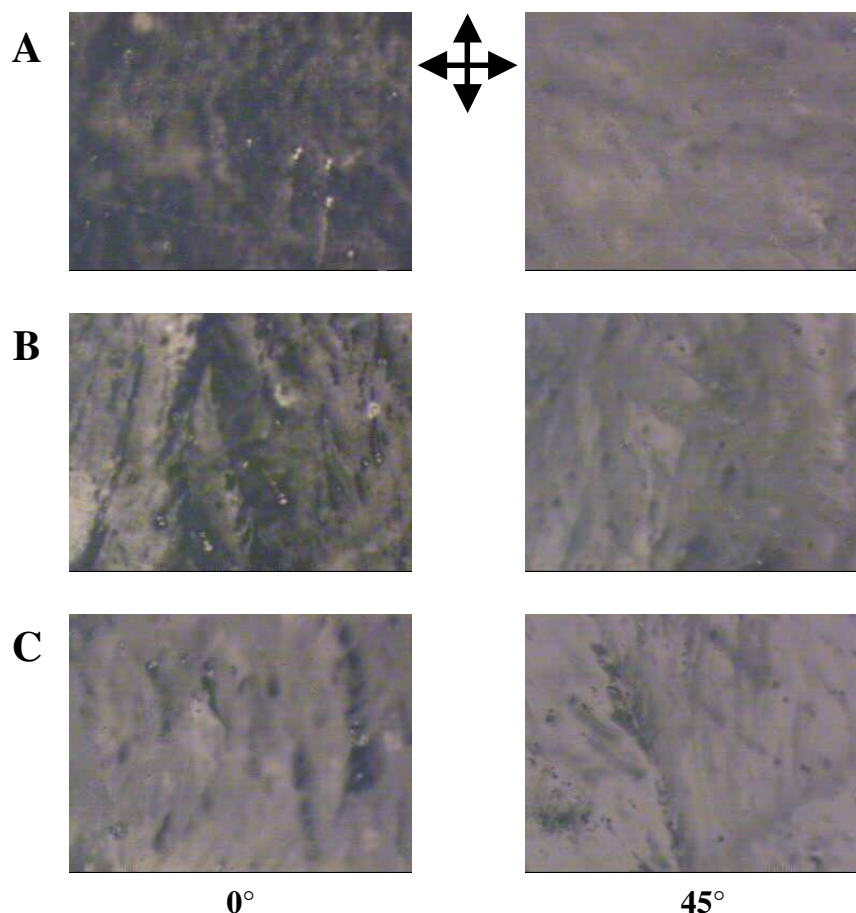


**Figure 4.21** Time-dependent stability of alignment of K-15 on PFPE treated with toluene. Birefringent textures were observed for alignment of K-15 on thin films of toluene treated PFPE at (A) 0, (B) 24, and (C) 96 hours. The orientation of the crossed polarizers is given by the black arrows.





**Figure 4.22** Time-dependent stability of alignment of MLC-6608 on PFPE treated with toluene. Birefringent textures were observed for alignment of MLC-6608 on thin films of toluene treated PFPE at (A) 0, (B) 24, and (C) 96 hours. The orientation of the crossed polarizers is given by the black arrows.

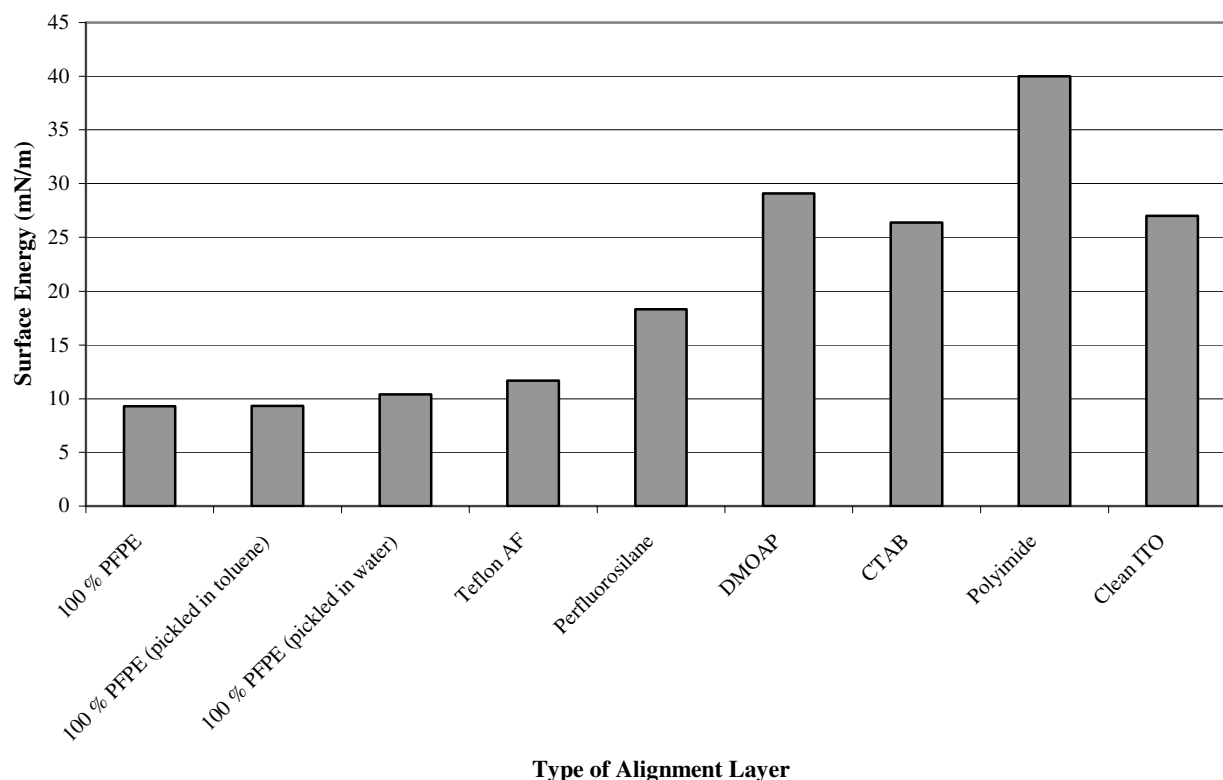


**Figure 4.23** Time-dependent stability of alignment of K-15 on PFPE treated with water. Birefringent textures were observed for alignment of K-15 on thin films of water treated PFPE at (A) 0, (B) 24, and (C) 96 hours. The orientation of the crossed polarizers is given by the black arrows.

#### 4.3.9 Surface Energy Measurements on Pretreated Thin Perfluoropolyether Films

A comparison of the surface energies of pretreated thin PFPE films with untreated thin PFPE films as well as with traditional alignment layers was performed. The contact angles of both water and ethylene glycol were measured for each of the following alignment layers: untreated thin PFPE film, toluene treated thin PFPE film, water treated thin PFPE film, polyimide film and monolayers of DMOAP and CTAB. From this data, the surface energy of each alignment layer was calculated using the Girifalco-Good-Fowlers-Young

equation (2.1)<sup>10,11</sup> As previously observed, the surface energies of the thin PFPE films were very low when compared with the traditional alignment layers (Figure 4.24). The surface energies did not seem to be affected much by the pretreatments. Untreated thin PFPE films exhibited a surface energy of approximately 9mN/m while toluene and water treated PFPE films exhibited surface energies of approximately 9 and 10 mN/m, respectively.



**Figure 4.24** Comparison of surface energies of pretreated thin PFPE films with other fluorinated materials and traditional alignment layers.

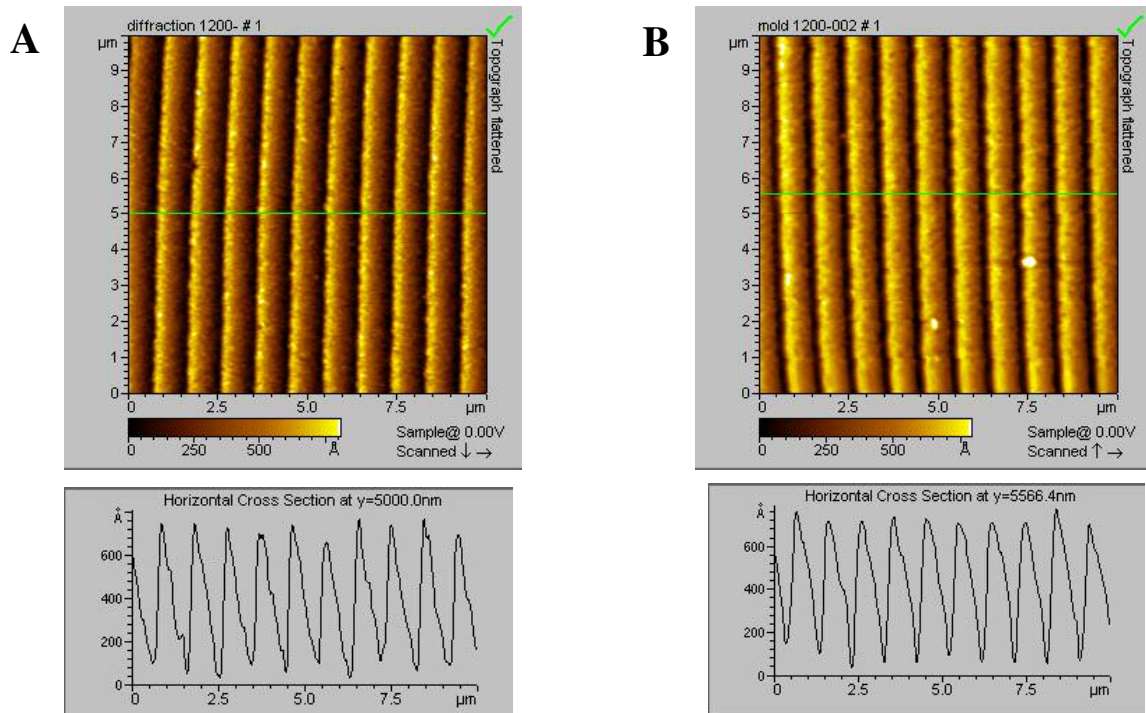
#### 4.3.10 Birefringent Textures of Embossed Perfluoropolyether Films

With a good understanding of the LC alignment characteristics of PFPE films, it is desirable to prepare embossed films that mimic traditional polyimide alignment layers. As discussed in Chapter one, the planar alignment observed for rubbed polyimide alignment layers is due in large part to the elastic energy costs associated with the LC director conforming to the surface. The energy costs associated with orienting the director parallel to the grooves are much lower, thus explaining planar alignment of the LC parallel to the rubbing direction.<sup>23</sup> PFPE films embossed with parallel grooves, having an almost sinusoidal cross-section and controlled spacing, were prepared and examined by transmitted polarized light microscopy.

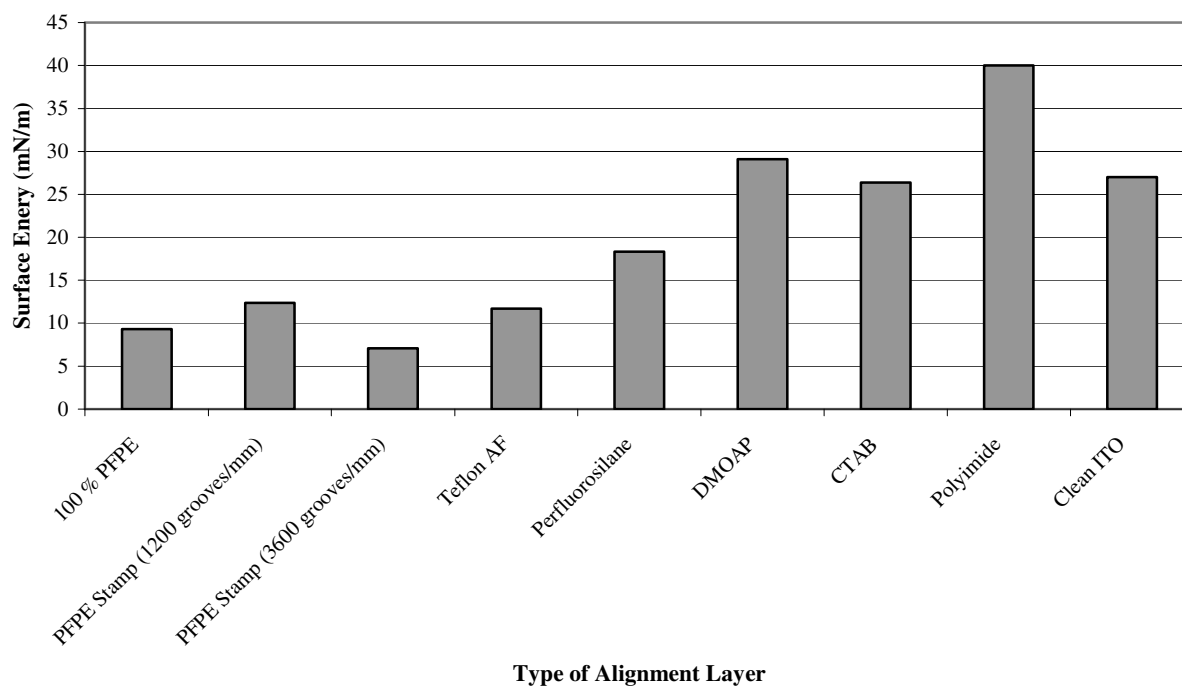
Diffraction gratings, having a sinusoidal cross-section and a spacing of either 1200 or 3600 grooves per mm, were used as the masters for embossing the PFPE films using a soft-lithography method. Atomic force microscopy (AFM) images of both the masters and the PFPE replicas were obtained. As shown in Figure 4.25, the PFPE exactly replicated the pattern of the hard master. The surface roughness (~600 nm) for the diffraction grating having 1200 grooves per mm was almost identical to that of its replica. However, the surface roughness for the replica of the 3600 grooves per mm diffraction grating decreased considerably when compared with its master. This decrease in surface roughness for the 3600 grooves per mm diffraction grating may be due to the difficulty of replicating such small features (~0.280  $\mu\text{m}$  peak to peak).

The surface energies of the PFPE replicas were calculated from the contact angles of both water and ethylene glycol, using the Girifalco-Good-Fowkes-Young equation (2.1)<sup>10,11</sup> The surface energies of the embossed PFPE films were very low and comparable to thin

PFPE films (Figure 4.26). The PFPE film embossed with a pattern having 1200 grooves per mm exhibited a surface energy slightly higher than that of the thin PFPE film ( $\sim 12$  mN/m), while the PFPE film embossed with a pattern having 3600 grooves per mm exhibited a lower surface energy of approximately 7 mN/m. This lower surface energy for the embossed films may be related to the superhydrophobicity effect observed with the lotus plant leaves and in other synthetic structure made from PFPE.<sup>24,25</sup>



**Figure 4.25** AFM images of embossed PFPE films. Images were obtained for both the (A) diffraction grating used for embossing and (B) the embossed film for comparison. The horizontal cross section (surface roughness) is shown below each image.



**Figure 4.26** Surface energies of embossed PFPE films.

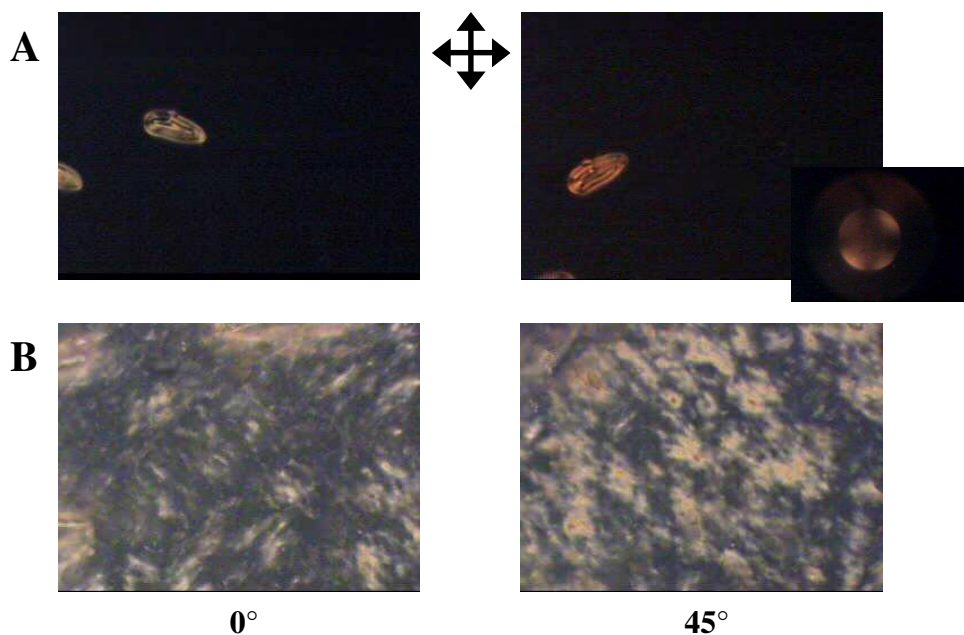
Two types of LC optical cells were fabricated to examine the alignment characteristics of embossed PFPE films. The first type of LC optical cell was fabricated with two alignment layers, both of which were embossed PFPE films. The second type of LC optical cell was fabricated with two alignment layers, one being an embossed PFPE film and the other being a thin PFPE film. LC optical cells fabricated using two films embossed with a pattern of parallel grooves (1200 grooves per mm) as alignment layers exhibited homeotropic alignment of the positive dielectric LC K-15 and random domains of planar alignment for the negative dielectric LC MLC-6608 (Figure 4.27). LC optical cells were also fabricated using two films embossed with parallel grooves of a smaller spacing (3600 grooves per mm) as alignment layers (Figure 4.28). Domains of homeotropic alignment

interspersed with domains of planar alignment were observed for the positive dielectric LC K-15, while relatively uniform planar alignment was observed for the negative dielectric LC MLC-6608.

As previously described, thin films of PFPE exhibited spontaneous homeotropic alignment of K-15. The introduction of a pattern of parallel grooves, with a spacing of 1200 grooves per mm, on the film surface had little effect on the alignment behavior. However, decreasing the groove spacing to 3600 grooves per mm disrupted the LC director orientation as shown in Figure 4.28 A. It is possible that as the groove spacing decreases, steric effects become more significant in determining the average LC director orientation. Thin films of PFPE exhibited random domains of planar alignment for the negative dielectric LC MLC-6608. Introducing a pattern of parallel grooves on the film surface generated a preferred direction of alignment. The decrease in groove spacing appeared to improve the uniformity of alignment.

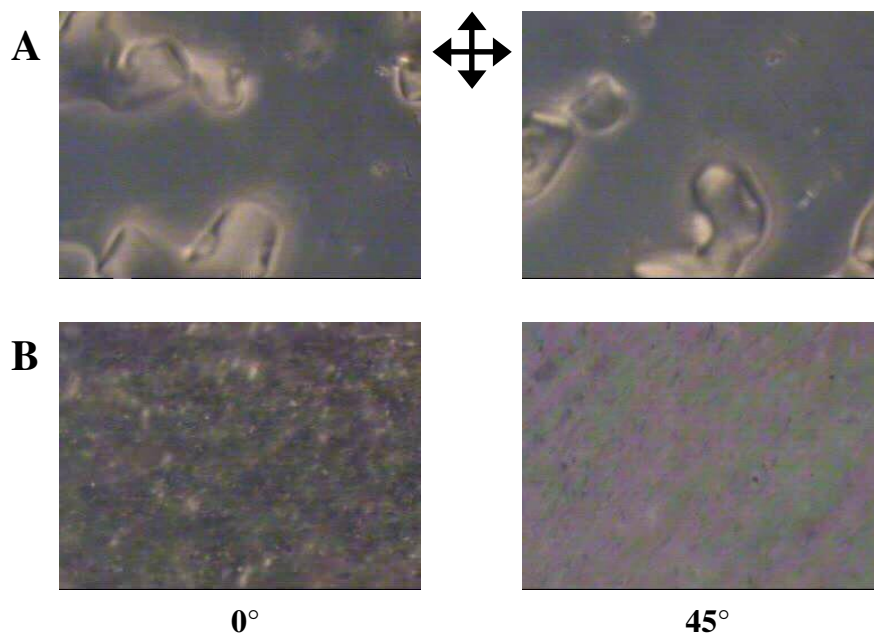
In an effort to better understand the alignment variations seen with the LC optical cells fabricated with two embossed PFPE alignment layers, cells were constructed having one embossed PFPE film and one thin PFPE film. LC optical cells fabricated using one film embossed with either 1200 or 3600 grooves per mm and one thin PFPE film as alignment layers showed homeotropic alignment of the positive dielectric LC and uniform planar alignment of the negative dielectric LC. Figure 4.29 shows the birefringent textures observed for the alignment of (A) K-15 and (B) MLC-6608 when sandwiched between one PFPE film embossed with 1200 grooves per mm and one thin PFPE film. Figure 4.30 shows the birefringent textures observed for the alignment of (A) K-15 and (B) MLC-6608 when sandwiched between one PFPE film embossed with 3600 grooves per mm and one thin PFPE

film. In both cases, homeotropic alignment of K-15 and planar alignment of MLC-6608 were achieved. The contrast between the dark and bright states in LC optical cells exhibiting planar alignment improved somewhat as the groove spacing decreased (i.e. the number of grooves per mm increased). It is possible that the cells that exhibited homeotropic alignment of K-15 may be used to fabricate LCD pixel prototypes in which an electric field is applied parallel to the LC optical cell to reorient the LC molecules and obtain uniform planar alignment. The direction of alignment would be determined by the embossed grooves and the applied electric field.

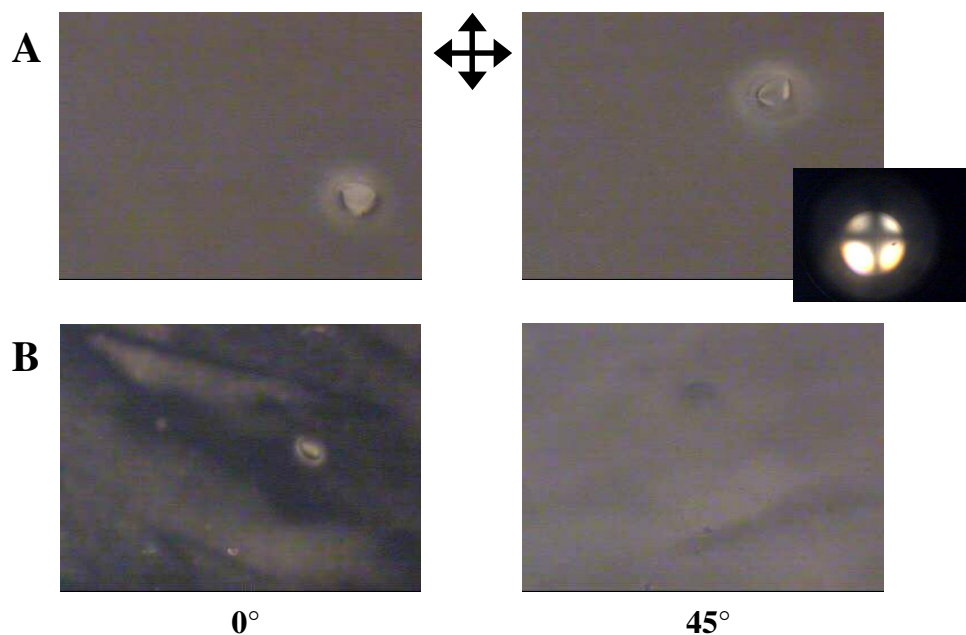


**Figure 4.27** Birefringent textures observed for the alignment of (A) K-15 and (B) MLC-6608 on embossed PFPE films. The LC optical cell was fabricated with two alignment layers, both embossed with a grooved pattern having 1200 grooves per mm. The orientation of the crossed polarizers is given by the black arrows.

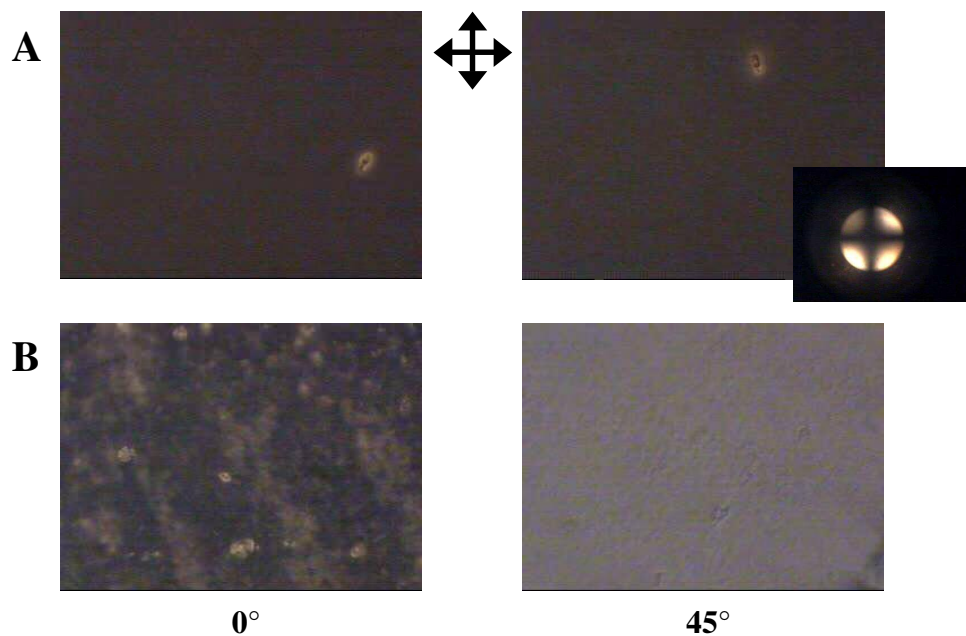




**Figure 4.28** Birefringent textures observed for the alignment of (A) K-15 and (B) MLC-6608 on embossed PFPE films. The LC optical cell was fabricated with two alignment layers, both embossed with a grooved pattern having 3600 grooves per mm. The orientation of the crossed polarizers is given by the black arrows.



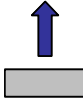
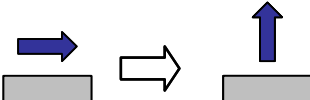
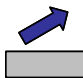
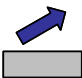
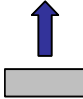
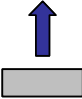
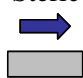
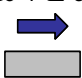
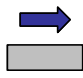
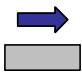
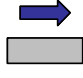
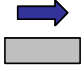
**Figure 4.29** Birefringent textures observed for the alignment of (A) K-15 and (B) MLC-6608 on embossed PFPE films. The LC optical cell was fabricated with two alignment layers, one embossed with a grooved pattern having 1200 grooves per mm and the other a thin film of PFPE. The orientation of the crossed polarizers is given by the black arrows.



**Figure 4.30** Birefringent textures observed for the alignment of (A) K-15 and (B) MLC-6608 on embossed PFPE films. The LC optical cell was fabricated with two alignment layers, one embossed with a grooved pattern having 3600 grooves per mm and the other a thin film of PFPE. The orientation of the crossed polarizers is given by the black arrows.

#### 4.3.11 Mechanisms of Liquid Crystal Alignment on Perfluoropolyether Films

While many factors may contribute to the orientation of the LC director on a surface, three types of surface interactions seem to stand out: electric field effects due to impurities in the liquid crystal, dipole-dipole interactions and steric interactions. These contributions and their individual effects on the LC director orientation have been previously discussed. A summary of the LC alignment experiments conducted in this work as well as the dominating surface effects for each experiment is summarized in tabular form in Figure 4.31. This study has attempted to assess the utility and control the properties of PFPE as an LC alignment layer. This understanding allows for greater freedom of design and improved properties in LCD displays.

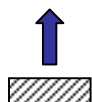
	Substrate Surface		K-15 ( $\Delta\epsilon > 0$ )	MLC-6608 ( $\Delta\epsilon < 0$ )
PFPE	ITO	Untreated	E effect 	E effect to DD 
		Pretreated	water E effect + Steric 	E effect + DD 
			toluene E effect 	DD 
	Glass	Untreated	Steric 	Steric + E effect 
		Pretreated	water Steric 	Steric + E effect 
			toluene Steric 	Steric + E effect 



Planar



Planar w/ high



Homeotropic

**Figure 4.31** Summary of alignment mechanisms associated with experimental results. The three possible contributions to alignment, electric field effects (E effect), dipole-dipole interactions (DD) and steric interactions are denoted by schematic representations that show the LC director orientation on the substrate surface. The white arrows represent a shift from one type of alignment to another.

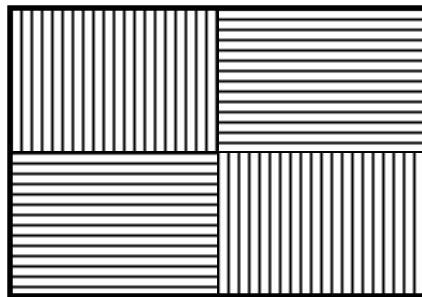
#### 4.4 Conclusions

Thin films of PFPE, having extremely low surface energies when compared with traditional alignment layer materials, exhibited spontaneous homeotropic alignment of the positive dielectric LC K-15 and planar alignment of the negative dielectric LC MLC-6608. The balance of several surface contributions, including electric field effects, dipole-dipole interactions and steric interactions, determined the orientation of the LC director. These surface contributions can be influenced by mechanical rubbing, pretreatment with polar and non-polar solvents and embossing of the PFPE film.

The alignment of positive and negative dielectric LCs on embossed PFPE films was dependent upon the composition of the LC optical cell. LC optical cells fabricated with two embossed films exhibited homeotropic alignment of the positive dielectric LC K-15, with the uniformity of alignment depending upon the groove spacing, and planar alignment of the negative dielectric LC MLC-6608. Similarly, LC optical cells fabricated with one embossed film and one thin film exhibited homeotropic alignment of positive dielectric LCs and planar alignment of negative dielectric LCs. The contrast between the dark and bright states observed for the planar-aligned cells varied slightly with groove spacing. It is desirable to generate films of variable groove spacing, possibly 1000 to 5000 grooves per mm, to examine the variation in alignment and to determine the ideal spacing for LC alignment. Also, the preparation of PFPE films embossed with a pattern having several domains of parallel grooves in which the direction of the grooves changes, such as that shown in Figure 4.32, would provide controllable and novel alignment layers. Finally, prototypes of each LC optical cell, in which an alternating current (AC) electric field is applied parallel to the cell to

reorient the LC molecules, should be fabricated. The response time of each should be measured.

Because PFPEs exhibit all of the advantages associated with polyimide alignment layers as well as compatibility with soft-lithography, alignment layers having a pattern of parallel grooves that induce a preferential LC director orientation may be produced without the hazards of mechanical rubbing. PFPE films also exhibit weak anchoring energies, which may allow for faster switching times. This material is truly a novel alignment layer and could more than double the display yield, resulting in more good displays and less electronic waste, thus having a major impact on the LCD industry.



**Figure 4.32** Schematic representation of a multi-domain embossed PFPE film.

## 4.5 References

- (1) Scheirs, J. *Modern Fluoropolymers*; John Wiley and Sons, Inc.: New York, 1997; pp 435-485.
- (2) Olah, G.A.; Chambers, R.D.; Prakash, G.K.S. *Synthetic Fluorine Chemistry*; John Wiley and Sons, Inc.: New York, 1992; pp 97-126.
- (3) Banks, R.E.; Smart, B.E.; Tatlow, J.C. *Organofluorine Chemistry: Principles and Commercial Applications*; Plenum Press: New York, 1994; pp 57-88; 431-467.
- (4) Drobny, J.G. *Technology of Fluoropolymers*; CRC Press: Boca Raton, 2001; pp 1-47; 131-154.
- (5) Ameduri, B.; Boutevin, B. *Well-Architected Fluoropolymers: Synthesis, Properties and Applications*; Elsevier: Amsterdam, 2004; pp 101-164.
- (6) Rolland, J.P.; Functional Perfluoropolyethers for Novel Applications. Ph.D. Dissertation, University of North Carolina, Chapel Hill, NC, 2005.
- (7) Rolland, J.P.; Van Dam, R.M.; Schorzman, D.A.; Quake, S.R.; DeSimone, J.M. *J. Am. Chem. Soc.* **2004**, *126*, 2322-2323.
- (8) Priola, A.; Bongiovanni, R.; Malucelli, G.; Pollicino, A.; Tonelli, C.; Simeone, G. *Macromol. Chem. Phys.* **1997**, *198*, 1893-1907.
- (9) Bunyard, W.C.; Romack, T.J.; DeSimone, J.M. *Macromolecules* **1999**, *32*, 8224-8226.
- (10) Sauer, B.B.; Dipaolo, N.V. *J. Coll. Interface Sci.* **1991**, *144*, 527-537.
- (11) Yu, T.; Peng, Z.; Ruan, S.; Xuan, L. *Thin Solid Films* **2004**, *466*, 326-330.
- (12) De Gennes, P.G. *The Physics of Liquid Crystals*; Clarendon Press: Oxford, 1974; pp1-22.
- (13) Dunmur, D.; Fukuda, A.; Luckhurst, G. *Physical Properties of Liquid Crystals: Nematics*; INSPEC: London, 2001; pp 493-502.
- (14) Sugimura, A.; Matsumoto, K.; Zhong-can, O.; Y.; Iwamoto, M. *Phys. Rev. E* **1996**, *54*, 5217-5220.
- (15) Rapini, A.; Papoular, M. *J.Phys.Colloq. (France)* **1969**, *30*, C4-C54.
- (16) Jerome, B. *Rep. Prog. Phys.* **1991**, *54*, 391-451.

- (17) Sugimura, A.; Luckhurst, G.R.; Ou-Yang, Z. *Phys. Rev. E* **1995**, 52, 681-689.
- (18) Sugimura, A.; Miyamoto, T.; Tsuji, M.; Kuze, M. *Appl. Phys. Lett.* **1998**, 72, 329-331.
- (19) Yokoyama, H.; van Sprang, H.A. *J. Appl. Phys.* **1985**, 57, 4520-4526.
- (20) Schadt, M.; Seiberle, H.; Schuster, A. *Nature* **1996**, 381, 212-215.
- (21) Sung, S.-J.; Lee, J.-W.; Kim, H.-T.; Park, J.-K. *Liquid Crystals* **2002**, 29, 243-250.
- (22) Seo, D.-S.; Kobayashi, S.; Nishikawa, M. *Appl. Phys. Lett.* **1992**, 61, 2392-2394.
- (23) Berreman, D. W. *Phys.Rev. Lett.* **1972**, 28, 1683-1686.
- (24) Callies, M.; Quere, D. *Soft Matter* **2005**, 1, 55-61.
- (25) Zhang, Lei; Fabrication of Novel Nanomaterials for Polymer Electrolyte Membrane Fuel Cells and Self-Cleaning Applications. Ph.D. Dissertation, University of North Carolina, Chapel Hill, NC, 2006.

## **CHAPTER 5**

### **ALIGNMENT OF NEMATIC LIQUID CRYSTALS USING PERFLUOROPOLYETHER LANGMUIR-BLODGETT FILMS**

#### **5.1 Langmuir-Blodgett Films**

Observations of the oil-on-water phenomenon began very early with the Babylonians and Greeks, but was first studied using the scientific method by Benjamin Franklin when he showed that a very thin layer of oil had a calming effect on the water in the Clapham Common pond.<sup>1-3</sup> In 1891, Agnes Pockels prepared the first monolayer at the water-air interface, which was followed by research by Rayleigh who proposed single molecule thickness of the films prepared by Pockels, Devaux who noted that the films were capable of both solid and fluid behavior, and Hardy who observed that oils without polar functional groups did not spread as readily as animal and vegetable oils.<sup>4-7</sup> These reports on the behavior of monolayers prompted Irving Langmuir, in 1917, to perform the first systematic study of monolayers of amphiphilic molecules at the water-air interface.<sup>8</sup> This experiment was closely followed by Katherine Blodgett's study of the deposition of multilayers of long-chain carboxylic acids onto solid substrates.<sup>9,10</sup> The experimental and theoretical concepts developed by Langmuir and Blodgett underlie the modern understanding of monolayers, thus today monolayers and multilayers transferred from the liquid-gas interface onto a solid substrate are known as Langmuir-Blodgett (LB) films.

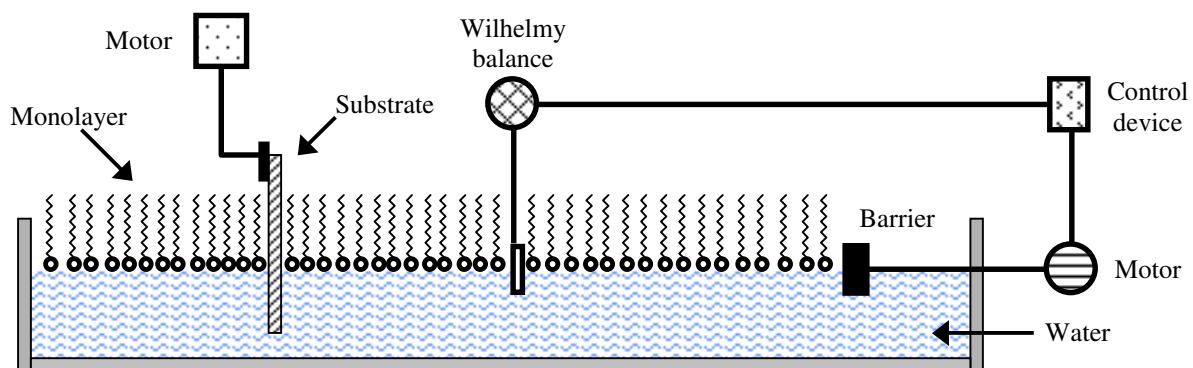


Langmuir-Blodgett film preparation was the first technique to provide a practical method for the construction of ordered molecular assemblies and is still studied extensively. The trough used in the preparation of LB films was first designed by Agnes Pockels and consisted of a rectangular trough of water filled to the brim with barriers placed across the edges of the trough.<sup>4</sup> Since that first design, the trough has been dramatically changed and is now fully computerized. A schematic representation of a modern LB trough is shown in Figure 5.1. Figure 5.1 shows a trough, generally made of Teflon, with a moving barrier that allows for controlled compression of the monolayer. This compression is driven by a motor, which is controlled by a computer capable of sensing pressure changes. The hanging Wilhelmy plate measures the surface pressure. A second motor lowers and raises the substrate at a controlled rate. The first step in the preparation of a LB film is the formation of a single layer of molecules (monolayer) on the water surface. The amphiphilic nature of the molecules used provides a specific interaction between the polar head group and water such that the molecule orients with its long aliphatic chain perpendicular to the water surface. Upon adding a dilute and known concentration of amphiphiles to the water surface, the initial monolayer is loosely packed, creating holes in the film, but reducing the surface area by sweeping the barriers forces the molecules together. The uniform layer can then be deposited onto the solid substrate.<sup>1,11-13</sup>

Research conducted by Kuhn and colleagues in the early 1970s was fueled by the desire to develop functional LB films, possibly for use in the newly developed microelectronics industry.<sup>11, 14-17</sup> Today LB films can be used in conjunction with conventional microfabrication techniques to enhance the capabilities of microelectronics devices, as anchoring films in chemical biosensors and transducers, and for optical

applications such as switches and modulators.<sup>11</sup> These films have also been examined as possible alignment layers in liquid crystal displays. Kakimoto and colleagues successfully produced polyimide LB films capable of planar liquid crystal (LC) alignment.<sup>18</sup> Alignment layers prepared by way of the LB technique offer several advantages. First, it is a system that does not require mechanical rubbing and therefore does not pose a threat to the electronic components of the displays. Second, a variety of systems with variations on the molecular level may be constructed to investigate the mechanisms associated with LC alignment. Finally, by changing the composition of the LB film, both planar and homeotropic alignment can be achieved.<sup>19</sup>

As discussed in Chapter four, thin films of perfluoropolyether (PFPE) exhibit spontaneous homeotropic alignment of positive dielectric LCs. However, understanding the LC alignment mechanisms at times requires planar alignment of the LC such as for studies of surface anchoring energy. LB films were examined as a potential means for achieving planar alignment of positive dielectric LCs on PFPE. In this work, LB films of PFPE were prepared and used as LC alignment layers. These alignment layers were used to fabricate LC optical cells in which spontaneous homeotropic and/or planar alignment were examined by transmitted polarized light microscopy. The dependency of LC alignment on the dielectric anisotropy of the LCs and pretreatment of the PFPE LB film were also examined. The surface energies and surface anchoring energies of these alignment layers were probed by contact angle and voltage-dependent birefringence measurements.



**Figure 5.1** Schematic representation of a Langmuir-Blodgett trough.

## 5.2 Experimental Details

### 5.2.1 Materials

Poly(tetrafluoroethylene oxide-*co*-difluoromethylene oxide) $\alpha,\omega$  diol (ZDOL, 95%, Aldrich, 457302), 2-isocyanatoethyl methacrylate (EIM, 99%, Aldrich, 477060), 2,2-dimethoxy-2-phenyl acetophenone (DMPA, 99%, Aldrich, 196118), dibutyltin diacetate (DBTDA, 99%, Aldrich, 290890) and 1,1,2-trichlorotrifluoroethane (Freon 113, 99%, Aldrich, 48411) were used as received for perfluoropolyether synthesis. 1,1,1,3,3-pentafluorobutane (Solkane 365mfc, Solvay Fluorides, UN1993), 1,3-bis(trifluoromethyl) benzene (99%, Aldrich, 251186), *n*-butyl acetate (99%, Acros, 1077500), ethanol (95%, Aaper, 05D04WB), and glacial acetic acid (Fisher Scientific, UN2789) were used as received. Ethylene glycol (Fisher Scientific, S-80005) was used as is for contact angle measurements. Nematic liquid crystals 4-cyano-4'-pentyl 1,1'-biphenyl (K-15, EM Industries, IS-1143,  $\Delta\epsilon = +13.2$ ) and MLC-6608 (Merck,  $\Delta\epsilon = -4.2$ ) were used as received. Liquid crystal optical cells were fabricated using indium tin oxide (ITO)-coated glass (Delta Technologies, Ltd., CG-811N-S115).

### 5.2.2 Instrumentation

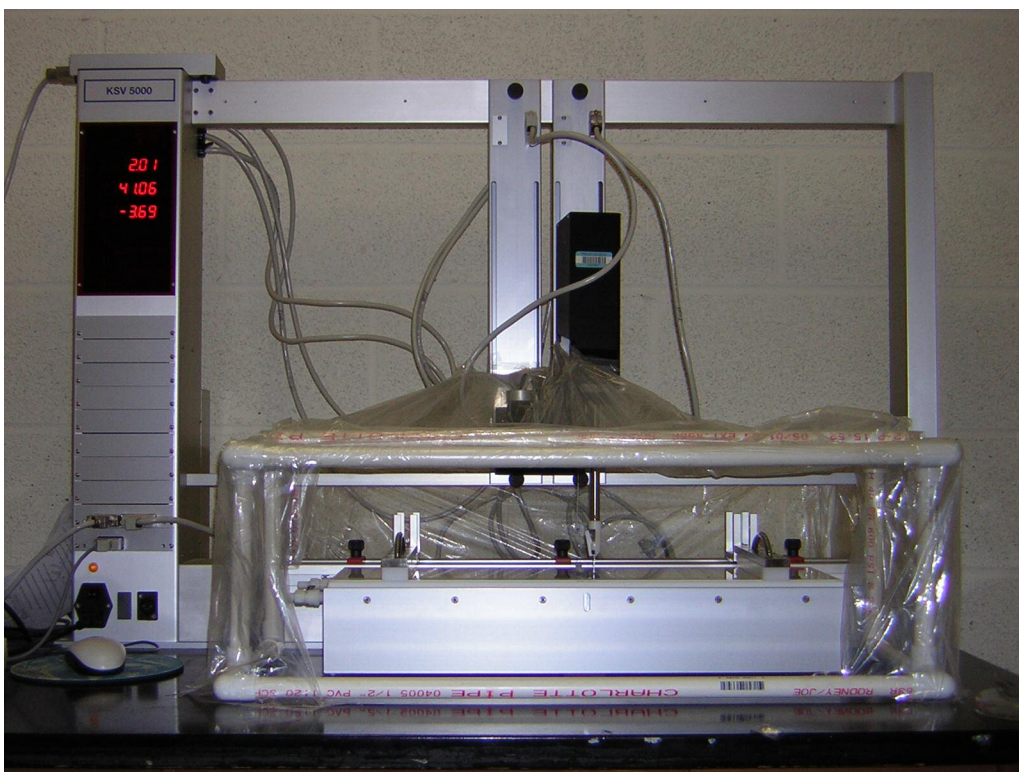
Langmuir-Blodgett films were prepared using a KSV 500 trough (standard size, KSV Instruments, Ltd), as depicted in Figure 5.2, and KSV software. Perfluoropolyether was cured under nitrogen purge in an ELC-500 UV chamber (120V AC, 60Hz, 15A, 4 x 9W lamps,  $\lambda = 365$ , Electro-Lite Corporation). Birefringence texture measurements were made using a Nikon Microphot FX polarizing microscope equipped with a Sony CCD-IRIS camera. Images were obtained using video generation software by Roxio. Contact angle measurements were made using a CAM200, Optical Contact Angle Meter (KSV Instruments, Ltd.) and KSV software. Atomic force microscopy (AFM) images were obtained in tapping mode using a Multimode IIIa Atomic Force Microscope (Veeco Metrology Group). Surface anchoring energy measurements were made using a OptiPro polarizing microscope (Shintech) equipped with shield and AC voltage supply.

### 5.2.3 Perfluoropolyether Synthesis

The synthesis and photocuring of perfluoropolyethers was previously described in detail by J.P. Rolland *et al* and based on earlier work done by R. Bongiovanni *et al.*<sup>20-22</sup> It was also described briefly in Section 4.2.3 of this work.

### 5.2.4 Preparation of Perfluoropolyether Langmuir-Blodgett Films

Langmuir-Blodgett films of perfluoropolyether were prepared on clean ITO-coated glass pre-treated with 3-(trimethoxysilyl) propyl methacrylate by the following method: a 2 wt % solution of 3-(trimethoxysilyl) propyl methacrylate in 95% ethanol was prepared (with 2 drops of glacial acetic acid) under constant stirring. The substrate was dipped into the solution for 2 minutes, rinsed with 95% ethanol and cured at 120 °C for 10 minutes.



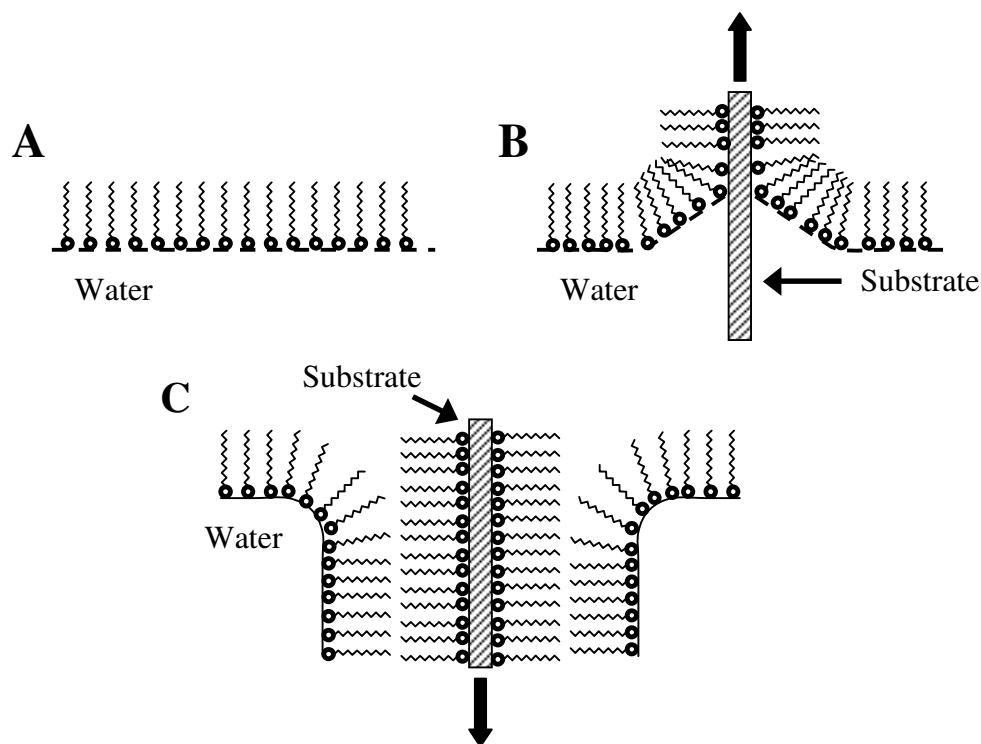
**Figure 5.2** Photograph of KSV 500 Langmuir-Blodgett trough.

The Langmuir-Blodgett trough was cleaned with n-butyl acetate, rinsed, and subsequently filled with water before calibration. A 0.5 % solution of perfluoropolyether in Solkane was prepared and used for film deposition. Approximately 25 to 50  $\mu\text{L}$  of the solution were deposited on the water layer one drop at a time. The monolayer was then compressed to a pressure of 2 mN/m at a compression rate of 10.0 mm/min. The monolayer was transferred to the substrate by vertical dipping at a rate of either 1.0 or 2.0 mm/min. The Langmuir-Blodgett films were transferred to the UV chamber, which was then purged with nitrogen for 10 minutes. Under continuous nitrogen flow, the films were exposed to UV radiation ( $\lambda = 365 \text{ nm}$ ) for 20 minutes.

A schematic representation of the preparation of Langmuir-Blodgett films is given in Figure 5.3.

### 5.2.5 Fabrication of Liquid Crystal Optical Cells

Liquid crystal optical cells, used for the observation of birefringent textures, were fabricated as follows: Two substrates were sandwiched together with the alignment layers facing each other at predetermined orientations separated by a spacer (6 or 40  $\mu\text{m}$ ) and sealed together using epoxy. The optical cells were filled with either K-15 or MLC-6608 (in the isotropic or nematic state for comparison) by capillary action and examined for light intensity changes.



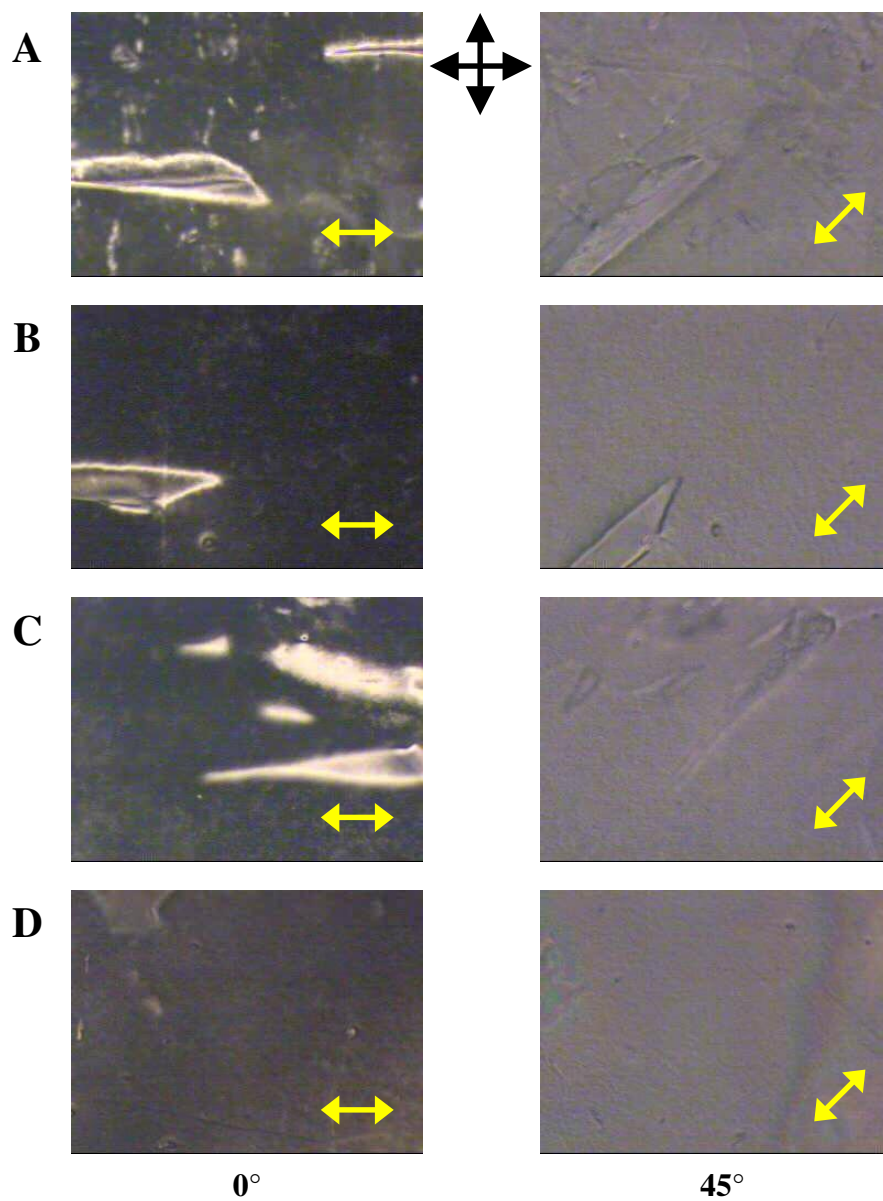
**Figure 5.3** Schematic representation of the deposition of a Langmuir-Blodgett film. The amphiphilic molecules orient such that their polar head groups interact with the water layer, while their aliphatic tails orient perpendicular to the water surface (A). As the substrate is pulled out of the water the monolayer is transferred to the substrate (B). Subsequent dips deposit additional monolayers on top of the first with like groups interacting with one another (C).

## 5.3 Results and Discussion

### 5.3.1 Birefringent Textures of Perfluoropolyether Langmuir-Blodgett Films

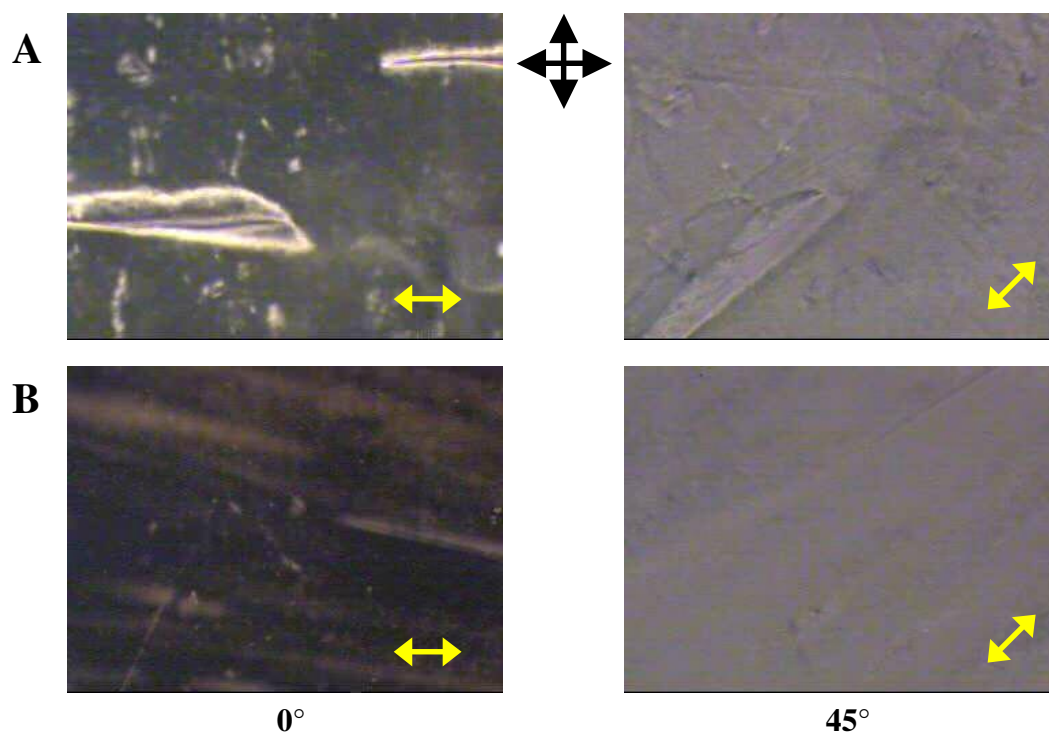
The LC alignment behavior of PFPE LB films was examined as a function of film thickness (number of monolayers). LB films, having 1, 5, 10 or 20 monolayers of PFPE were prepared as previously discussed and used as alignment layers in LC optical cells. The birefringent textures observed for the alignment of K-15 on multilayer PFPE LB films is shown in Figure 5.4. All PFPE LB films showed planar alignment of K-15 as confirmed by the presence of dark and bright states at 45° interval rotations of the sample. In each case, the director was oriented parallel to the dipping direction. The optimal thickness for LC alignment was found to be 5 monolayers of PFPE (Figure 5.4 B) as judged by the maximum contrast between the dark and bright states at this thickness.

A comparison of the alignment of positive and negative dielectric LCs on LB PFPE films was conducted. Figure 5.5 shows the birefringent textures observed for the alignment of K-15 ( $\Delta\epsilon = +13.2$ ) and MLC-6608 ( $\Delta\epsilon = -4.2$ ) on LB PFPE films of 1 monolayer thickness. In both cases the LC director was aligned planar to the substrate surface and parallel to the dipping direction, with comparable efficiency. Figures 5.6 and 5.7 show the birefringent textures observed for the alignment of K-15 and MLC-6608 on LB PFPE films of 5 and 10 monolayer thicknesses, respectively. Figure 5.6 shows a decrease in contrast between the dark and bright states when the LC is changed from K-15 to MLC-6608 for LB PFPE films having 5 monolayers. The birefringent textures observed in Figure 5.6 B are evidence of planar alignment of MLC-6608, with a high pretilt angle. Also, random domains of planar alignment are present in Figure 5.6 B as opposed to the fairly uniform planar alignment observed in Figure 5.6 A. Figure 5.7 shows the same result for LB PFPE films



**Figure 5.4** Birefringent textures for alignment of K-15 on multilayer LB films of PFPE. Planar alignment of K-15 on PFPE LB films having (A) 1, (B) 5, (C) 10 or (D) 20 monolayers is shown. The orientation of the crossed polars is indicated by the crossed black arrows, while the dipping direction is given by the double-headed yellow arrow.

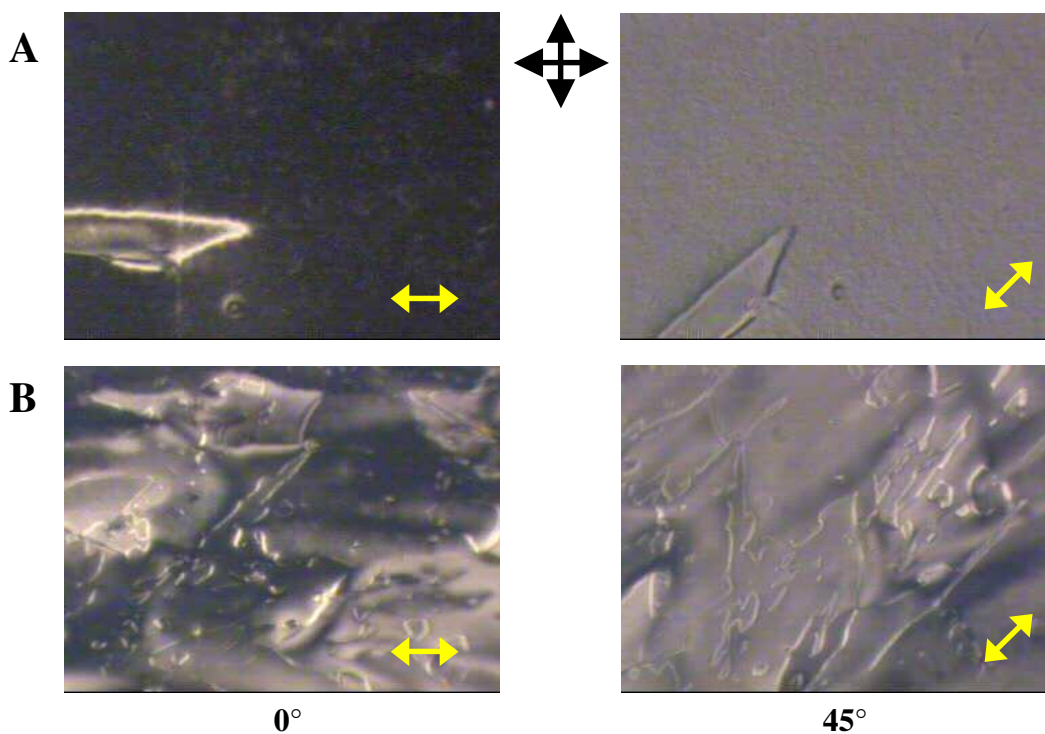




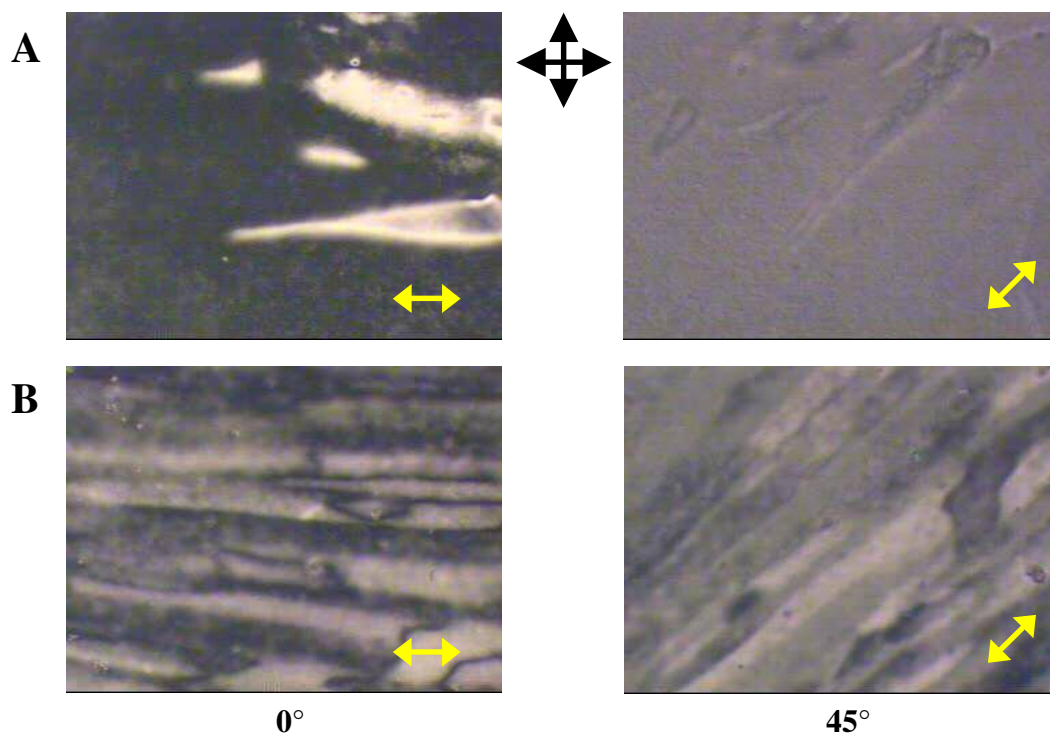
**Figure 5.5** Comparison of alignment of positive and negative dielectric LCs on PFPE LB films of 1 monolayer thickness. Birefringent textures for the alignment of (A) K-15 and (B) MLC-6608 are shown. The orientation of the crossed polars is indicated by the crossed black arrows, while the dipping direction is given by the double-headed yellow arrow.

having 10 monolayers. These results were surprising given that MLC-6608 spontaneously oriented planar to the substrate in the case of thin PFPE films. It appears that in the case of LB PFPE films, the electric field effects that bring about the spontaneous homeotropic alignment of K-15 on thin films of PFPE are dominated by the intermolecular packing of the LC molecules or steric interactions of these molecules with one another and the surface. It also appears that the alignment of MLC-6608 on LB PFPE films, especially those with increasing films thickness, results from a balance between the dipole-dipole interactions between the C-F bonds in the LC and PFPE and the steric interactions between the LC molecules and the LB film. The dominating influence of steric interactions is most plausible

in a rough film,<sup>23</sup> therefore the topographies of the multilayer LB PFPE films were examined using AFM as described hereafter.



**Figure 5.6** Comparison of alignment of positive and negative dielectric LCs on PFPE LB films of 5 monolayer thickness. Birefringent textures for the alignment of (A) K-15 and (B) MLC-6608 are shown. The orientation of the crossed polars is indicated by the crossed black arrows, while the dipping direction is given by the double-headed yellow arrow.

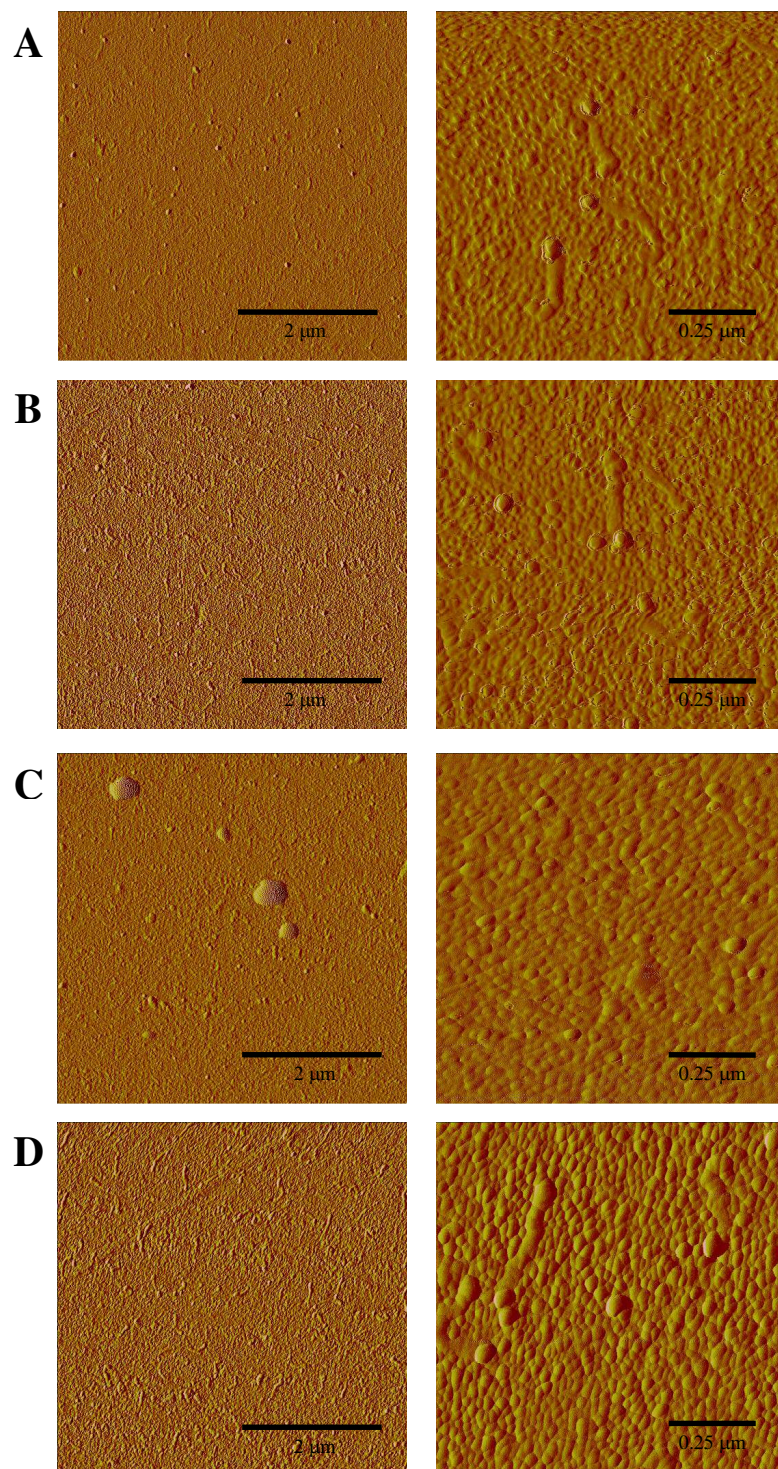


**Figure 5.7** Comparison of alignment of positive and negative dielectric LCs on PFPE LB films of 10 monolayer thickness. Birefringent textures for the alignment of (A) K-15 and (B) MLC-6608 are shown. The orientation of the crossed polars is indicated by the crossed black arrows, while the dipping direction is given by the double-headed yellow arrow.

### 5.3.2 Atomic Force Microscopy of Perfluoropolyether Langmuir-Blodgett Films

The topography of the LB PFPE film as a function of film thickness (number of monolayers) was probed by atomic force microscopy (AFM). AFM images of multilayer LB films at two magnifications are shown in Figure 5.8. It is apparent from these images that the surface roughness increases as the number of monolayers increases. The higher magnification images show striations of the polymer along the dipping direction that become more pronounced with an increasing number of monolayers. Figure 5.8 C shows that small islands of polymer begin forming at a thickness of 10 monolayers. Figure 5.9 is a comparison of LB PFPE films having 3 and 10 monolayers at a lower magnification, in

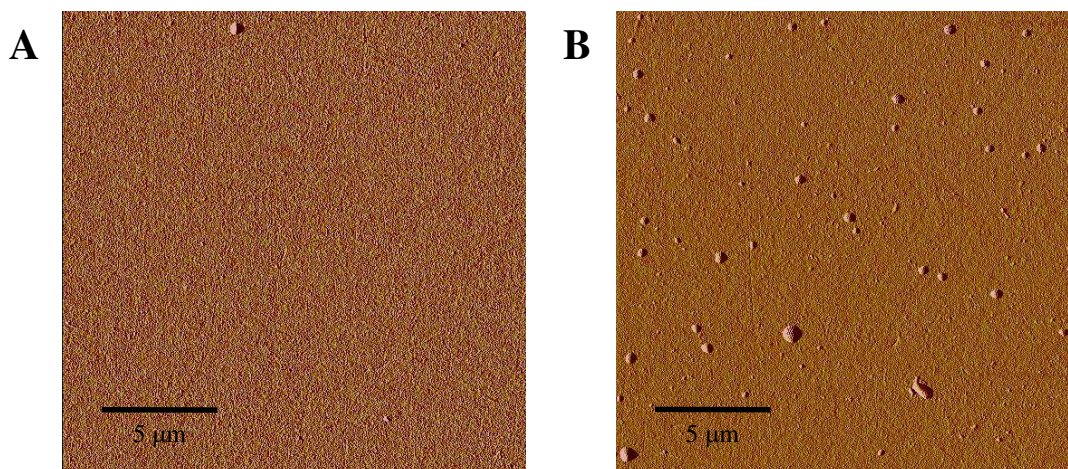




**Figure 5.8** Atomic force microscopy images of multilayer PFPE LB films. The topologies of PFPE LB films having (A) 1, (B) 5, (C) 10 and (D) 20 monolayers are shown.

which only one or two polymer islands were apparent for the 3 monolayer film while 35 or more polymer islands were apparent for the 10 monolayer film. The formation of these polymer islands is an indicator of increased surface roughness.

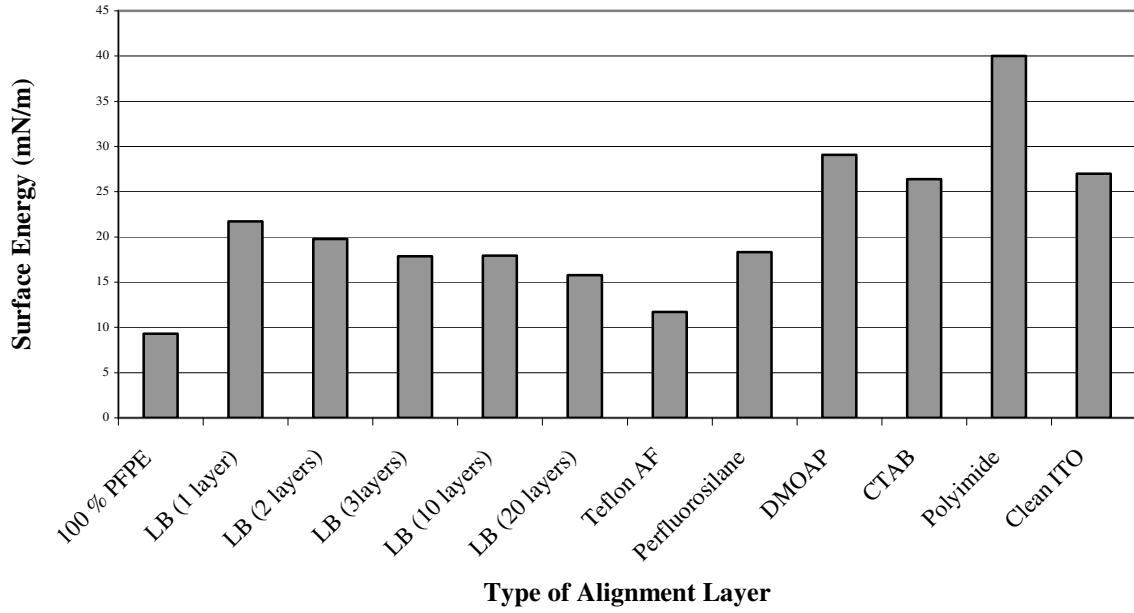
The rough surface generated with the deposition of PFPE monolayers mimics that of traditional rubbed polyimide alignment layers. The planar alignment observed for both rubbed polyimide alignment layers and LB PFPE films is due to steric interactions between the LC molecules and the surface as well as the elastic energy costs associated with the LC director conformally wetting the surface. The energy costs associated with orienting the director parallel to the grooves or striations are much lower, thus explaining planar alignment of the LC parallel to the rubbing and dipping directions.<sup>23</sup>



**Figure 5.9** AFM images of the formation of polymer islands in PFPE LB films. AFM images of PFPE LB films having (A) 3 and (B) 10 monolayers are shown.

### 5.3.3 Surface Energy Measurements on Perfluoropolyether Langmuir-Blodgett Films

A comparison of the surface energies of LB PFPE films with thin PFPE films and traditional alignment layers was performed. The contact angles of both water and ethylene glycol were measured for each of the following alignment layers: thin PFPE film, 1 monolayer LB PFPE film, 2 monolayer LB PFPE film, 3 monolayer LB PFPE films, 10 monolayer LB PFPE film and monolayers of DMOAP and CTAB. From this data, the surface energy of each alignment layer was calculated using the the Girifalco-Good-Fowlers-Young equation (2.1).<sup>24,25</sup> The surface energies of the fluorinated materials were very low when compared with the traditional alignment layers (Figure 5.10). Thin films of PFPE exhibited the lowest surface energy, approximately 9 mN/m. LB films of PFPE exhibited much higher surface energies when compared with thin PFPE films. On average, the surface energies of the LB PFPE films decreased with an increasing number of monolayers: 1 monolayer-22 mN/m, 2 monolayers-20 mN/m, 3 monolayers-18 mN/m, 10 monolayers-18 mN/m, and 20 monolayers-16 mN/m). However, the surface energies of the LB PFPE films were still lower than that of DMOAP (~29 mN/m), CTAB (~26 nM/m) and polyimide (~40 mN/m). It is possible that the surface energies measured for the LB PFPE films is a sum of the surface energy of the PFPE and ITO-coated glass (~27 mN/m). This increase in surface energy for LB PFPE films with respect to thin PFPE films would contribute to the planar of alignment of K-15 and MLC-6608 observed with these samples.



**Figure 5.10** Comparison of the surface energies of PFPE LB films with other fluorinated alignment materials.

### 5.3.4 Surface Anchoring Energy Measurements on Perfluoropolyether Langmuir-Blodgett Films

Surface anchoring energy measurements were made based on the unified surface anchoring energy model proposed by Sugimura and colleagues.<sup>26,27</sup> As discussed in Chapter four, this model gives a relationship between the anchoring strength  $A$  and the deviation angle of the LC director from the easy direction by surface effects. The saturation voltage method, in which the optical retardation is measured as a function of voltage applied across the LC optical cell, was used to measure the surface anchoring energy. The anchoring strength is related to the saturation voltage by the following equation:

$$A = V_s(\epsilon_0 \Delta\epsilon K_3)^{1/2} / d \quad (4.2)$$

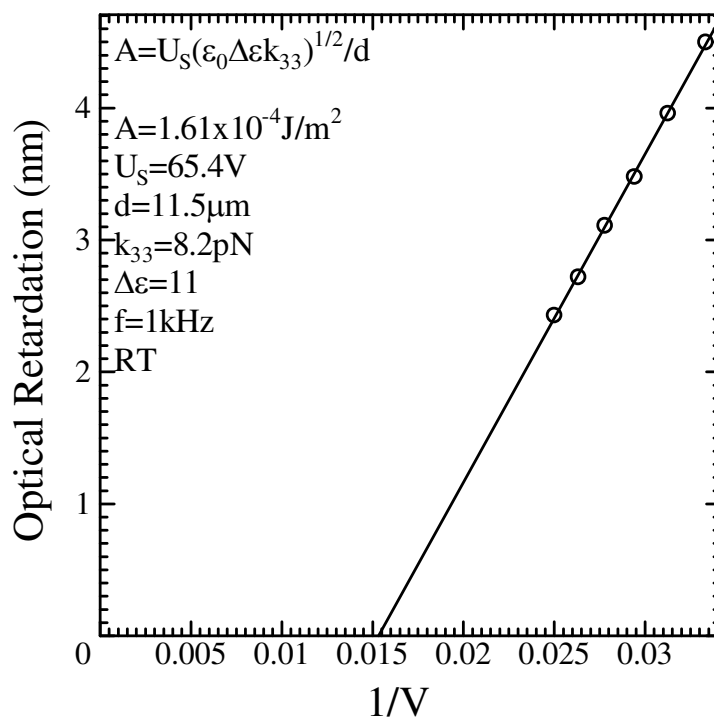
where  $V_s$  is the saturation voltage,  $\epsilon_0$  is the dielectric permittivity of vacuum,  $\Delta\epsilon$  is the dielectric anisotropy,  $K_3$  is the bend elastic constant and  $d$  is the cell thickness.<sup>26</sup> This unified



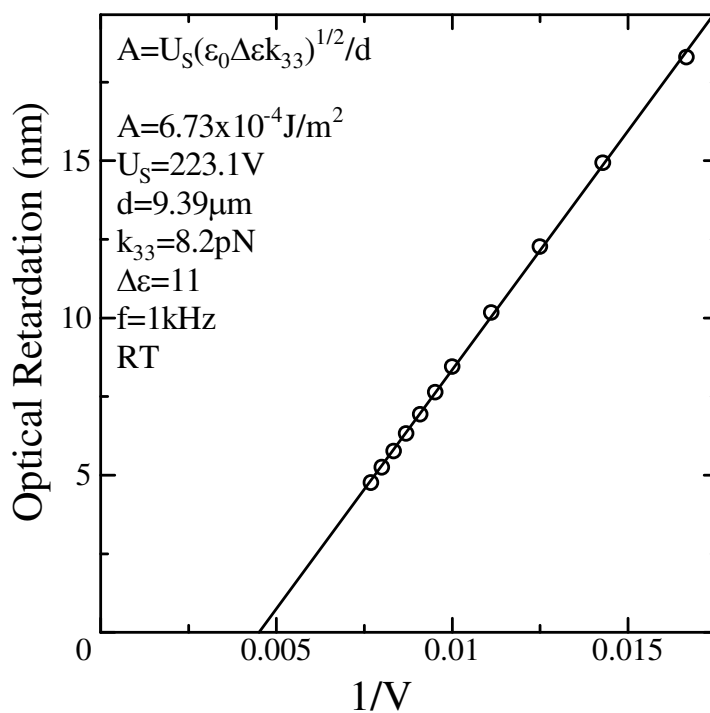
surface anchoring energy model was used to probe the surface anchoring energy of LB PFPE films as a function of film thickness (number of monolayers).

LC optical cells were fabricated with LB PFPE films, having 1, 5, and 10 monolayers of PFPE and filled with K-15. Measurements of the optical retardation were made with respect to the voltage applied across the cell. Typically, as the voltage increases the optical retardation decreases because the LC molecules are being reoriented to adopt the homeotropic alignment mode. A sample plot of the optical retardation versus inverse voltage for 1 monolayer LB PFPE films is shown in Figure 5.11. Because the optical retardation is inversely proportional to the applied voltage in the high voltage regimes, the intersection of the extrapolated line gives the saturation voltage.<sup>28,29</sup> From the extrapolated voltages of experiments conducted with 1 monolayer LB PFPE films (43.0 and 65.4 V), the surface anchoring energies were calculated to be  $1.06 \times 10^{-4} \text{ J/m}^2$  and  $1.61 \times 10^{-4} \text{ J/m}^2$ , values typical of surfaces with weak anchoring. A sample plot of the optical retardation versus inverse voltage for 5 monolayer LB films is shown in Figure 5.12. The surface anchoring energies calculated from these plots for two separate experiments were  $5.35 \times 10^{-4} \text{ J/m}^2$  and  $6.73 \times 10^{-4} \text{ J/m}^2$ , values slightly higher than that calculated for 1 monolayer LB films. A sample plot of the optical retardation versus inverse voltage for 10 monolayer LB films is shown in Figure 5.13. The surface anchoring energies calculated from the extrapolated voltages (24.2 and 87.9 V) of two separate experiments were  $7.27 \times 10^{-5} \text{ J/m}^2$  and  $2.64 \times 10^{-4} \text{ J/m}^2$ . A plot of calculated anchoring energies with respect to film thickness (number of monolayers) is shown in Figure 5.14. An unusual trend of increasing and then decreasing surface anchoring energy as the number of monolayers increases is evident.

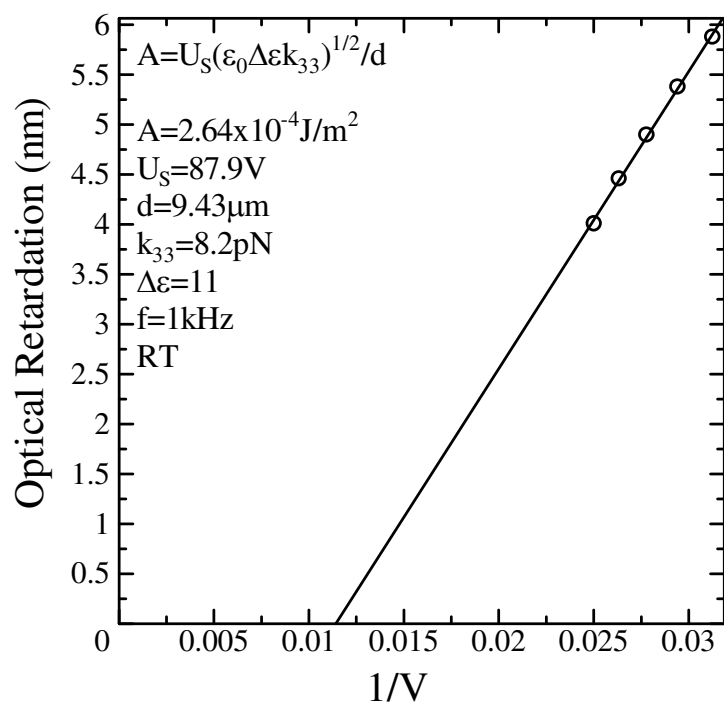




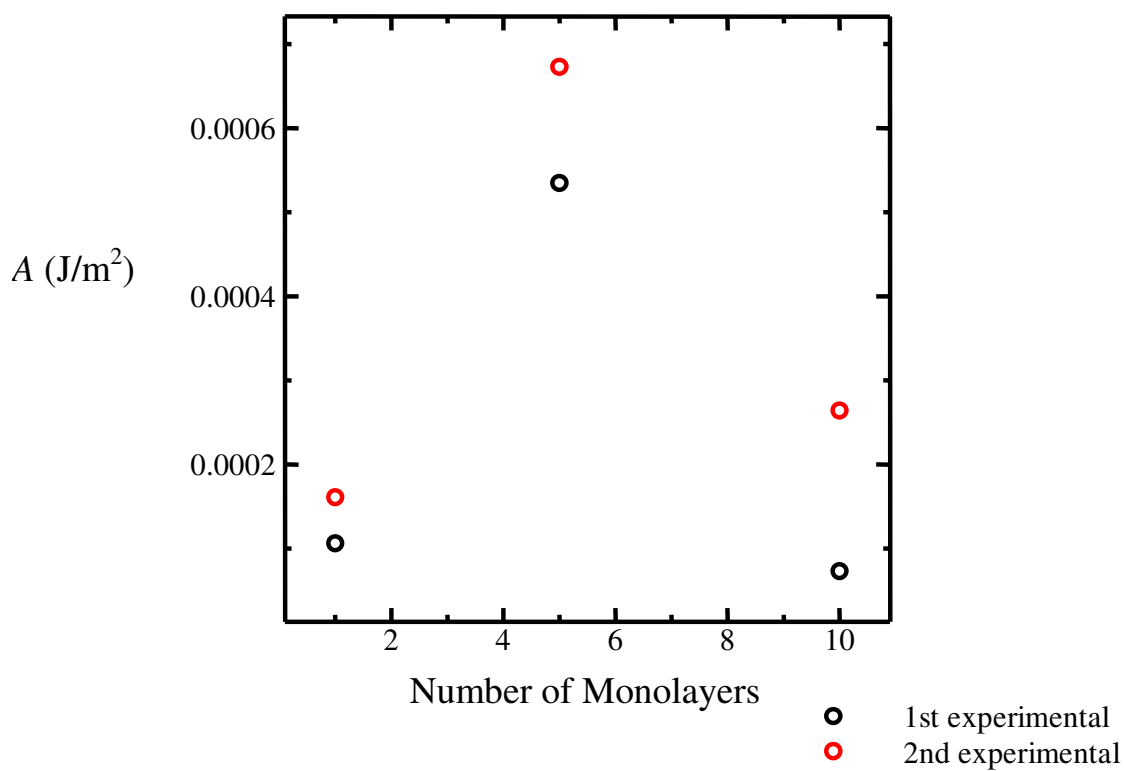
**Figure 5.11** Plot of the optical retardation versus inverse voltage for PFPE LB film of 1 monolayer thickness. The calculated surface anchoring energy is shown.



**Figure 5.12** Plot of the optical retardation versus inverse voltage for PFPE LB film of 5 monolayer thickness. The calculated surface anchoring energy is shown.



**Figure 5.13** Plot of the optical retardation versus inverse voltage for PFPE LB film of 10 monolayer thickness. The calculated surface anchoring energy is shown.



**Figure 5.14** Plot of surface anchoring energy versus thickness (number of monolayers).

Sugimura and colleagues examined the surface anchoring energy of LB films of polyimide as a function of film thickness (number of monolayers).<sup>30</sup> In this experiment, LB films having 1, 5, 9, 15 and 21 monolayers of polyimide were deposited onto  $\text{In}_2\text{O}_3$  substrates and examined using the unified surface anchoring energy model previously discussed. It was found that the surface anchoring energy increased as the number of monolayers increased, saturating at a thickness somewhere between 15 and 20 monolayers. Other reports have shown a decrease in surface anchoring energy with an increase in film thickness.<sup>31</sup> From these reports it is concluded that the surface anchoring energy is a function of the substrate, alignment layer and LC used in the experiment.

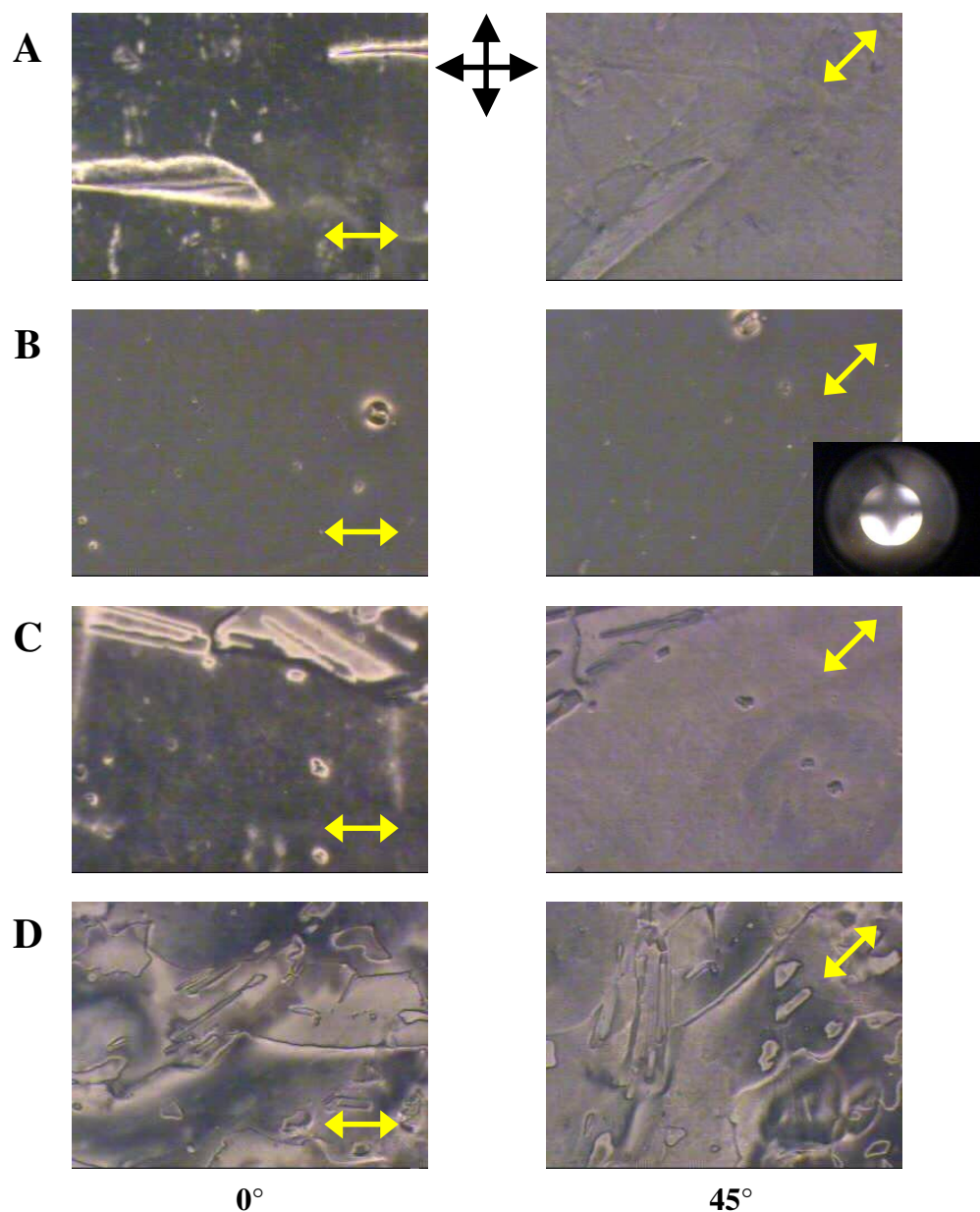
As previously discussed in Chapter four, there is a correlation between the surface energy of a material, the orientation of the LC director and the presence of fluorine functionalities.<sup>32-34</sup> It was found that the surface energy decreases and the pretilt angle of the LC director increases as the fluorine content (F:C ratio) increases in a given material. An increase in the pretilt angle of the LC director would result in a decrease in the surface anchoring energy because a lower voltage would be required to achieve homeotropic alignment. Therefore, an increase in the surface coverage of PFPE (a highly fluorinated material) would theoretically result in a decrease in surface anchoring energy. However, an increase followed by a decrease in surface anchoring energy was observed for LB films with increasing thickness from 1 to 5 to 10 monolayers. This surface anchoring energy data correlates with the birefringent textures observed for LB PFPE films of increasing thickness (Figure 5.4), in which the optimal planar alignment was achieved at a thickness of 5 monolayers. It appears from Figure 5.4 that the pretilt angle of the director is slightly lower for LB PFPE films having a thickness of 5 monolayers when compared to films having a

thickness of 1 and 10 monolayers, which would result in the 5 monolayer films having a slightly higher surface energy. The decrease in the pretilt angle of the LC director observed for an increase in film thickness from 1 monolayer to 5 monolayers may result from the increase in surface roughness and thus increase in steric interactions between these samples. As the sample thickness is increased from 5 to 10 monolayers, it is possible that the electric field effects become more prominent, resulting in a balance between the steric interactions induced by the rough surface and the electric field effects of the polymer and causing a slightly increase in the pretilt angle of the LC director and thus lower surface anchoring energy. It is evident that an examination of LB PFPE films of increasing thickness ( 15 and 20 monolayers) is necessary to fully understand the surface anchoring energy trends associated with LB PFPE films.

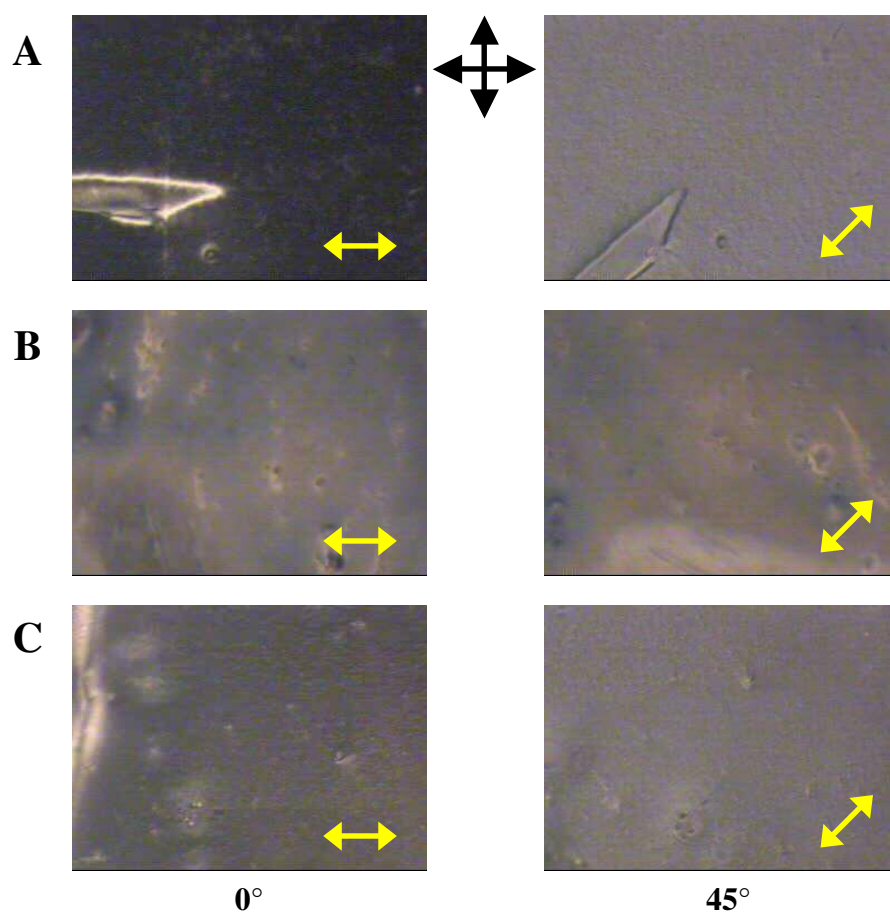
### **5.3.5 Birefringent Textures of Pretreated Perfluoropolyether Langmuir-Blodgett Films**

The environmental stability of LB PFPE films was examined by means of a film pretreatment method. Fully cured LB PFPE films were immersed in either toluene or water for 24 hours before being dried either by a stream of nitrogen gas or under vacuum and examined by transmitted polarized light microscopy for alignment of K-15. The birefringent textures observed for the alignment of K-15 on pretreated LB PFPE films having 1 monolayer of PFPE are shown in Figure 5.15. Figure 5.15 A shows the planar alignment of K-15 observed for a 1 monolayer LB PFPE film, having no pretreatment. Treating the LB film with toluene induced regions of homeotropic alignment (Figure 5.15 B) as well as regions of planar alignment with a high pretilt angle (Figure 5.15 C). Treating the film with

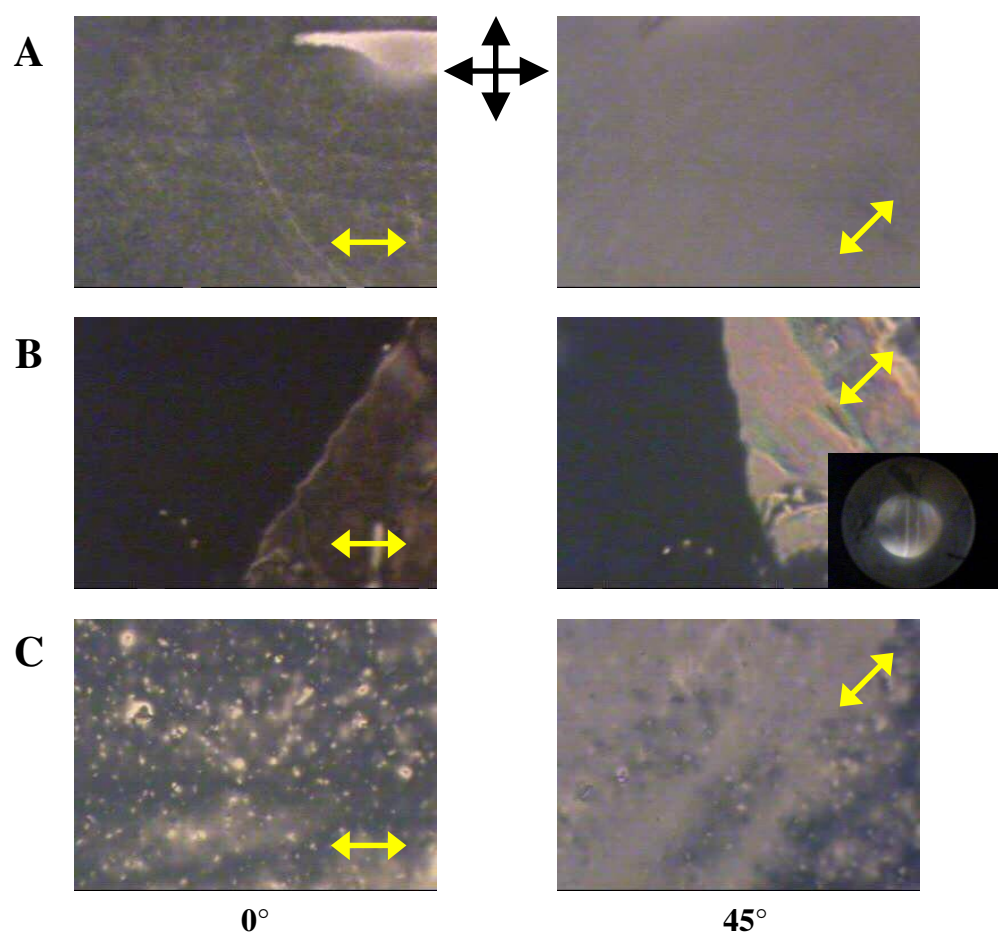
water had a disruptive effect on the LC director alignment, generating random domains of planar alignment with an even higher pretilt angle (Figure 5.15 D). The birefringent textures observed for the alignment of K-15 on pretreated LB PFPE films having 5 monolayers of PFPE were similar to those observed for 1 monolayer LB films, as shown in Figure 5.16. Figure 5.16 A shows the planar alignment of K-15 induced by LB PFPE films of 5 monolayers, having no pretreatment. When treated with toluene, these films exhibited mixed regions of planar and homeotropic alignment (Figure 5.16 B), while treating these films with water resulted in planar alignment with a high pretilt angle (Figure 5.16 C). The birefringent textures observed for LB PFPE films of 10 monolayers were similar to those observed for LB films of 1 and 5 monolayers with one exception. Like LB films of 1 and 5 monolayers of PFPE, LB films of 10 monolayers of PFPE exhibited planar alignment with no treatment (Figure 5.17 A) and mixed regions of planar and homeotropic alignment when treated with toluene (5.17 B). Unlike LB films of 1 and 5 monolayers of PFPE, mixed regions of planar and homeotropic alignment were observed when treated with water (Figure 5.17 C). The homeotropic regions became planar over a relatively short period of time. The fact that uniform homeotropic alignment was not achieved with the toluene treatments is not surprising given that the monolayers may not be complete, leaving portions of the ITO-coated glass substrate exposed. ITO-coated glass has a relatively high surface energy ( $\sim 27$  mN/m) and induces random domains of planar alignment.



**Figure 5.15** Birefringent textures of alignment of K-15 on pretreated PFPE LB films of 1 monolayer thickness. Polarizing micrographs of PFPE LB films having no pretreatment are shown (A). Polarizing micrographs of PFPE LB films treated with toluene (B and C) and water (D) are also shown. The orientation of the crossed polars is indicated by the crossed black arrows, while the dipping direction is given by the double-headed yellow arrow.



**Figure 5.16** Birefringent textures of alignment of K-15 on pretreated PFPE LB films of 5 monolayer thickness. Polarizing micrographs of PFPE LB films having no pretreatment are shown (A). Polarizing micrographs of PFPE LB films treated with toluene (B) and water (C) are also shown. The orientation of the crossed polars is indicated by the crossed black arrows, while the dipping direction is given by the double-headed yellow arrow.



**Figure 5.17** Birefringent textures of alignment of K-15 on pretreated PFPE LB films of 10 monolayer thickness. Polarizing micrographs of PFPE LB films having no pretreatment are shown (A). Polarizing micrographs of PFPE LB films treated with toluene (B) and water (C) are also shown. The orientation of the crossed polars is indicated by the crossed black arrows, while the dipping direction is given by the double-headed yellow arrow.

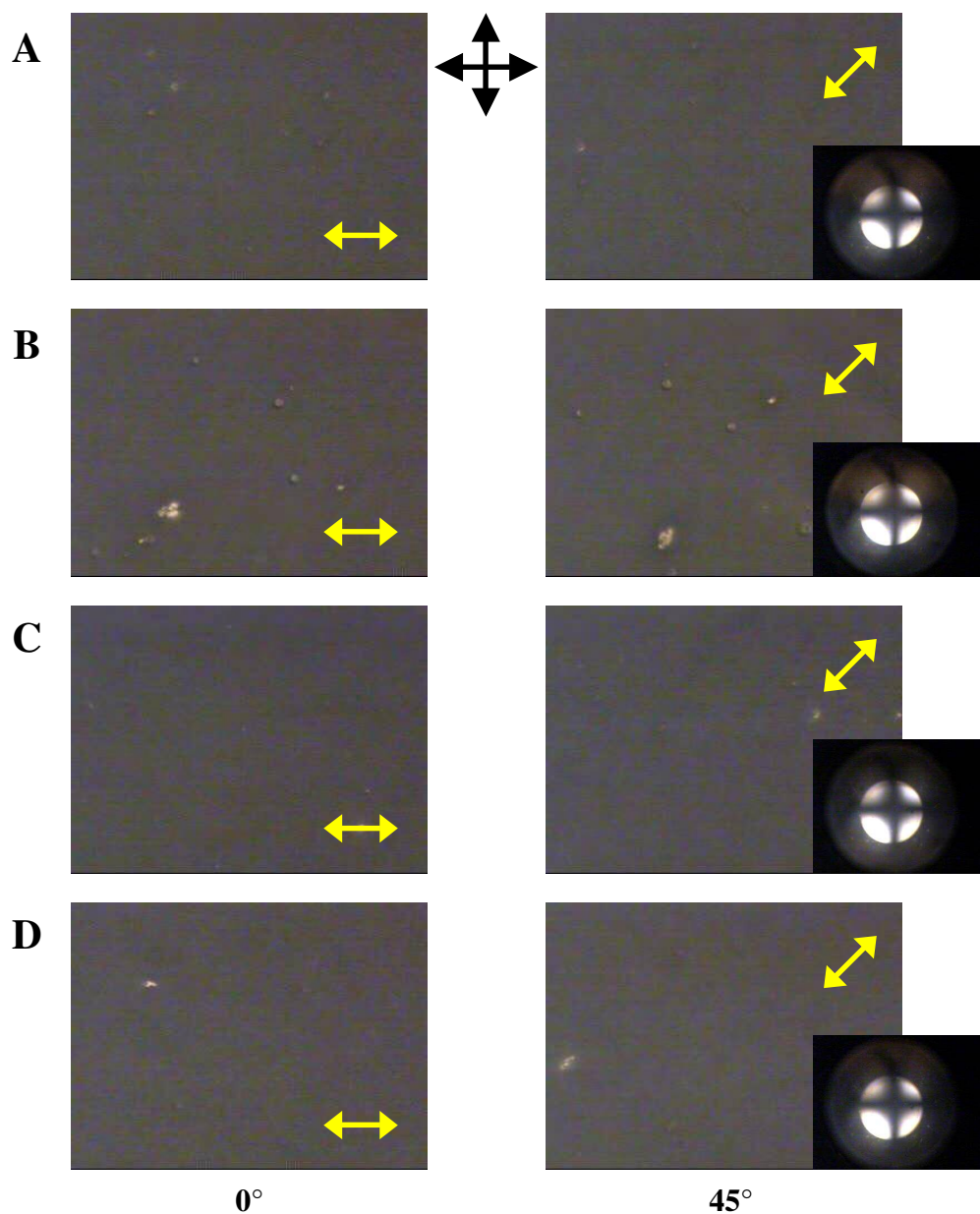


### **5.3.6 Time-Dependent Stability of Liquid Crystal Alignment on Pretreated Perfluoropolyether Langmuir-Blodgett Films**

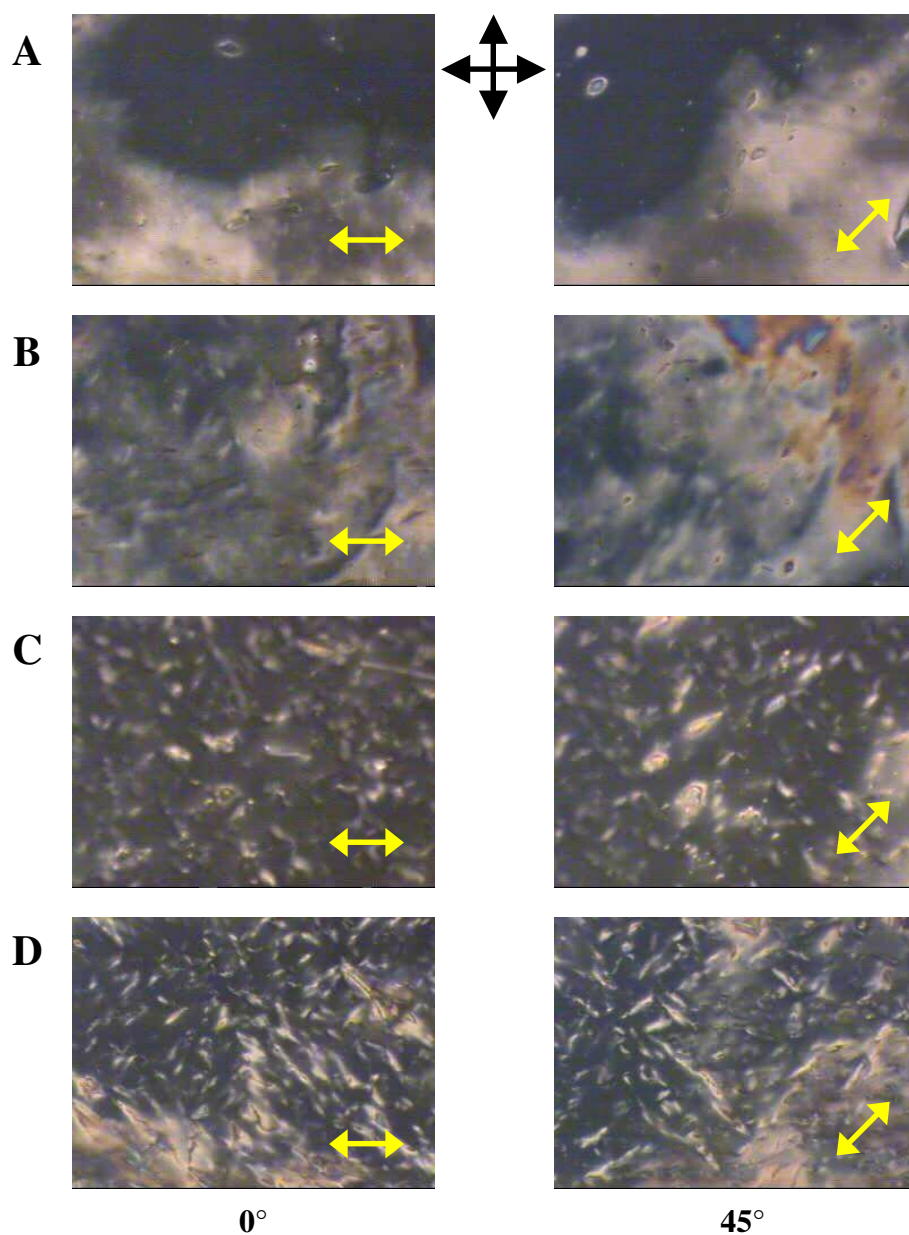
Experiments were conducted in which the alignment of both positive and negative LCs on pretreated LB PFPE films of 1 monolayer thickness was examined at 24-hour intervals over a 120- to 144-hour period. Figure 5.18 shows the birefringent textures observed for the alignment of K-15 on LB films treated with toluene. The regions of homeotropic alignment induced by this pretreatment appear to be stable for relatively long periods of time (~144 hours). Figure 5.19 shows the results of time-dependence experiments for water treated LB films. A region that initially exhibited homeotropic alignment was observed for 144 hours. At 24 hours domains of planar alignment with a high pretilt angle began to appear (Figure 5.19 B). These domains expanded as time went on, showing that surface effects induced by water pretreatment were most likely a result from the balance of electric field effects and steric interactions and were much less stable than those induced by pretreatment with toluene.

The stability of the alignment of the negative dielectric LC MLC-6608 on pretreated LB PFPE films was also examined. Figure 5.20 shows the birefringent textures observed for the alignment of MLC-6608 on LB films treated with toluene. Initially, domains of planar and homeotropic alignment were observed (Figure 5.20 A). These regions became more disordered over time. Figure 5.21 shows the birefringent textures observed for LB films treated with water. A region exhibiting homeotropic alignment was observed for approximately 120 hours. A dramatic change was noted at 24 hours, in which the region showed random domains of planar alignment, possibly mixed with domains of homeotropic alignment (Figure 5.21 A). This disorder increased over time. Again, the surface effects

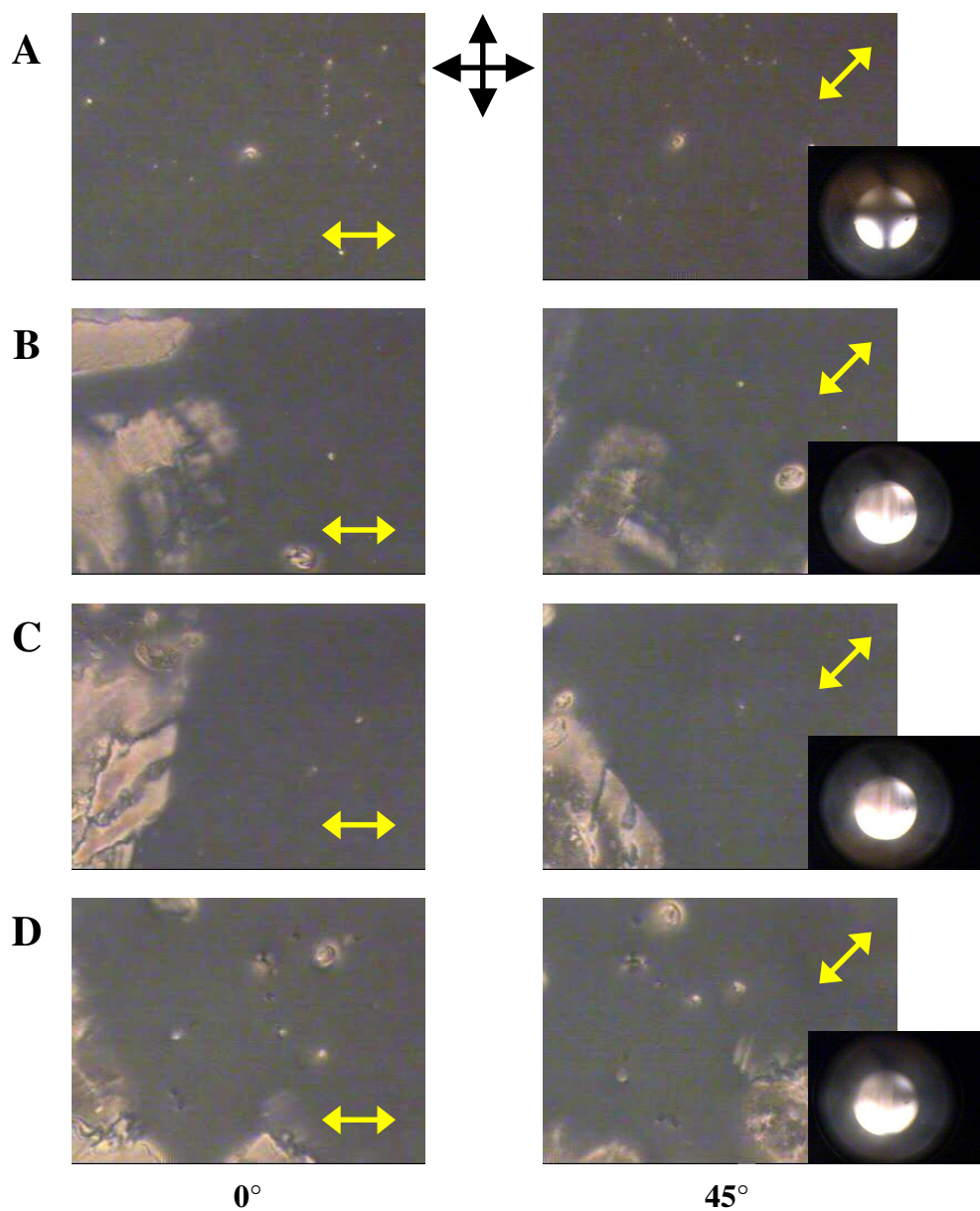
induced by pretreatment with water appear to be unstable over relatively long periods of time.



**Figure 5.18** Time-dependent alignment stability of PFPE LB films pretreated with toluene. Alignment of the positive dielectric LC K-15 was examined. The orientation of the crossed polars is indicated by the crossed black arrows, while the dipping direction is given by the double-headed yellow arrow.

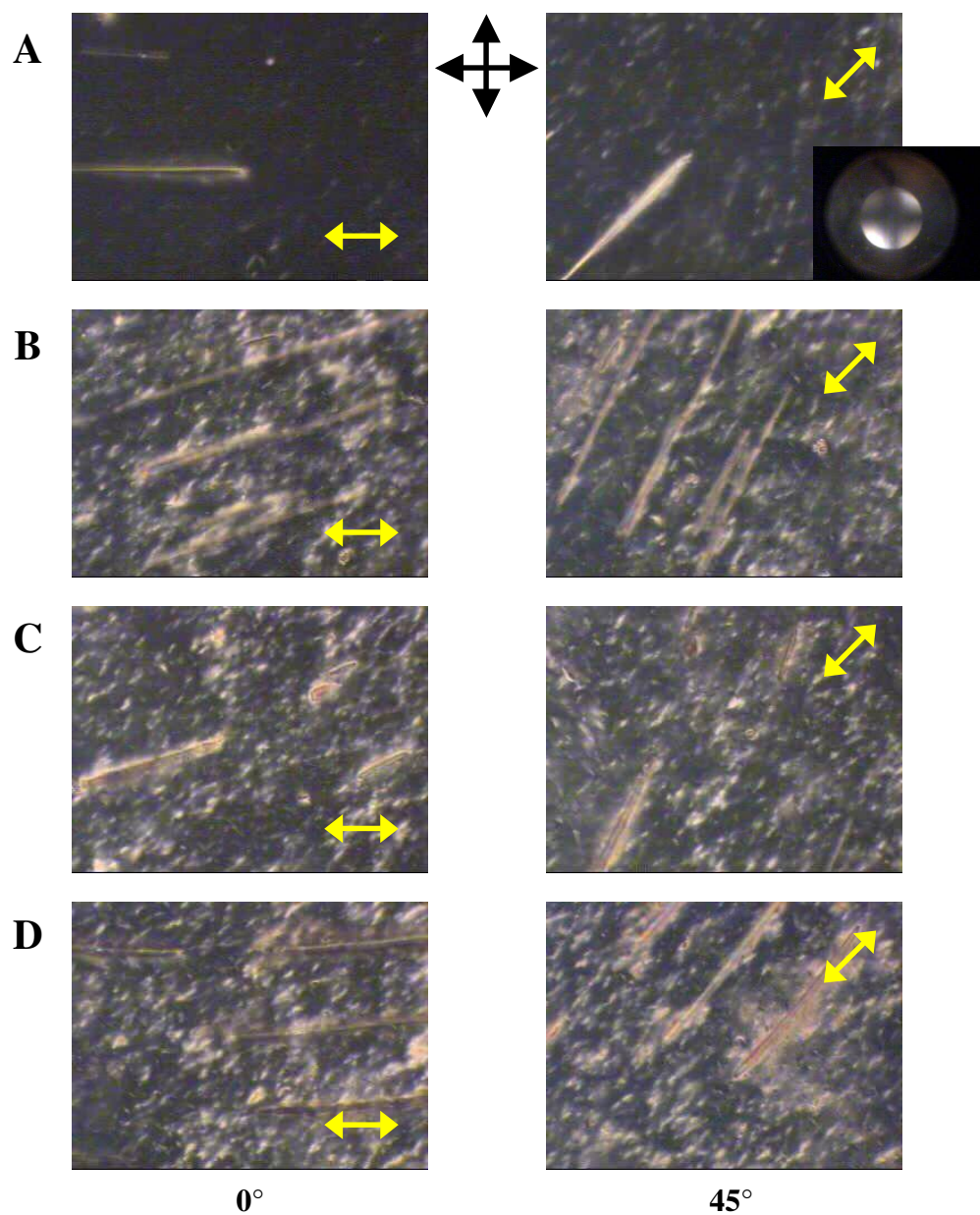


**Figure 5.19** Time-dependent alignment stability of PFPE LB films pretreated with water. Alignment of the positive dielectric LC K-15 was examined. The orientation of the crossed polars is indicated by the crossed black arrows, while the dipping direction is given by the double-headed yellow arrow.



**Figure 5.20** Time-dependent alignment stability of PFPE LB films pretreated with toluene. Alignment of the negative dielectric LC MLC-6608 was examined. The orientation of the crossed polars is indicated by the crossed black arrows, while the dipping direction is given by the double-headed yellow arrow.





**Figure 5.21** Time-dependent alignment stability of PFPE LB films pretreated with water. Alignment of the negative dielectric LC MLC-6608 was examined. The orientation of the crossed polars is indicated by the crossed black arrows, while the dipping direction is given by the double-headed yellow arrow.

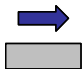
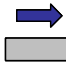

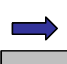


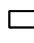
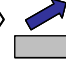
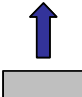



### **5.3.7 Mechanisms of Liquid Crystal Alignment on Perfluoropolyether Langmuir-Blodgett Films**

Several factors may contribute to the orientation of the LC director on a surface, however three types of surface interactions seem to stand out: electric field effects due to impurity ions in the liquid crystal, dipole-dipole interactions and steric interactions. Because ITO-coated glass is conductive, an electric field is generated between the charges on the substrate surface and image ions in the glass. The impurity ions in the LC may then interact with the small electric field on the alignment layer surface. By nature of the synthetic method, solutions of K-15 contain many impurity ions while solutions of MLC-6608 contain very few. Due to the dielectric anisotropy of the two LCs, K-15 molecules would orient with their long axis parallel to the electric field, while MLC-6608 molecules would orient perpendicular to the electric field. However, this orientation is only temporary for MLC-6608 molecules. Because solutions of MLC-6608 have very few impurity ions, the effects of the electric field diminish over time as the impurity ions dissolve into the bulk, thus the alignment mode of MLC-6608 is more likely to change over time if the dominating contribution to alignment is electric field effects.

Dipole-dipole interactions between the C-F bonds in the PFPE film and the C-F and C-CN bonds in the LCs also contribute to the LC director orientation. Due to shear forces associated with the LB method, it is assumed the C-F bonds in the PFPE film are in plane with the film. With this assumption, MLC-6608 molecules would orient with their long axes perpendicular to the substrate surface while K-15 molecules would orient parallel. The effects of dipole-dipole interactions would become more influential with increasing thickness. There are also steric effects to consider. The LC molecules themselves are rod-

like and prefer to pack parallel to one another. A desire to minimize energy costs and possibly small van der Waals forces at the substrate surface drive the LC molecules to orient parallel to the substrate surface, especially if that surface is a rough one.

In some cases, one contributor clearly dominates over another while in other cases the observed alignment appears to be a result of the balance of one or more contributors. A summary of the LC alignment experiments conducted in this work as well as the dominating surface effects for each experiment is summarized in tabular form in Figure 5.22.

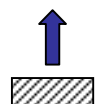
Substrate Surface				K-15 ( $\Delta\epsilon > 0$ )	MLC-6608 ( $\Delta\epsilon < 0$ )
PFPE	ITO	Untreated LB Films		Steric 	E effect + Steric or DD+ Steric  or 
		Pretreated	water	E effect and Steric  or 	DD to E effect + DD + Steric   
			toluene	E effect 	DD to E effect + DD + Steric   



Planar



Planar w/ high



Homeotropic

**Figure 5.22** Summary of alignment mechanisms associated with experimental results. The three possible contributions to alignment, electric field effects (E effect), dipole-dipole interactions (DD) and steric interactions are denoted by schematic representations that show the LC director orientation on the substrate surface. The white arrows represent a shift from one type of alignment to another.



## 5.4 Conclusions

LB films of PFPE, having surface energies lower than traditional alignment materials, exhibited spontaneous planar alignment of both the positive dielectric LC K-15 and the negative dielectric LC MLC-6608. The efficiency of this alignment was dependent upon film thickness (number of monolayers), with the 5 monolayer LB film showing the best alignment of K-15. AFM images verified that the surface roughness of the film increased with an increasing number of layers, thus making steric interactions the dominating contributor to LC alignment in this system. It would be interesting to observe the effects of changing the surface pressure of the trough during LB deposition on film topology and LC alignment. It is possible that as the surface pressure is increased and the molecules are pushed closer together that the LB film will become similar to the thin PFPE films and that LC alignment will gradually change from a planar to homeotropic.

The low surface anchoring energies exhibited by these LB films were typical of surfaces with weak anchoring, but showed an unusual trend of increasing and then decreasing with increasing film thickness. Measurements of the surface anchoring energies of PFPE LB films having 15 and 20 monolayers should be obtained to better understand this trend.

LCD pixel prototypes in which LB films of PFPE are used as the alignment layers should be fabricated and examined for optical switching with the application of an alternating current (AC) electric field across the cell. Comparison of the switching times measured for these cells to those fabricated with traditional polyimide alignment layers is also desirable. It is believed that the extremely low surface energy attributed to PFPE will generate faster switching times.

## 5.5 References

- (1) Ulman, A. *An Introduction to Ultrathin Organic Films: from Langmuir Blodgett to Self-assembly*; Academic Press: Boston, 1991; pp 101-219.
- (2) Gaines, G.L. *Insoluble Monolayers at Liquid-Gas Interfaces*; Interscience Publishers: New York, 1966; pp 1-5.
- (3) Baird, D. *J. of American History* **1990**, 77, 632.
- (4) Pockels, A. *Nature* **1891**, 43, 437.
- (5) Rayleigh, L. *Phil. Mag.* **1899**, 48, 321.
- (6) Devaux, H. *Smithsonian Inst. Ann. Rep.* **1913**, 261.
- (7) Hardy, W.B. *Proc. R. Soc. A.* **1913**, 86, 610-635.
- (8) Langmuir, I. *J. Am. Chem. Soc.* **1917**, 39, 1848-1906.
- (9) Blodgett, K.B. *J. Am. Chem. Soc.* **1935**, 57, 1007-1022.
- (10) Blodgett, K.B.; Langmuir, I. *Phys. Rev.* **1937**, 51, 964-982.
- (11) Peterson, I.R. *J. Phys. D: Appl. Phys.* **1990**, 23, 379-395.
- (12) Petty, M.C. *Langmuir-Blodgett Films: An Introduction*; Cambridge University Press: Cambridge, 1996; pp 12-83.
- (13) Butt, H.-J.; Graf, K.; Kappl, M. *Physics and Chemistry of Interfaces*; Wiley-VCH: Weinheim, 2003; pp 246-298.
- (14) Mann, B.; Kuhn, H. *J. Appl. Phys.* **1971**, 42, 4398-4405.
- (15) Kuhn, H. *Naturwiss.* **1967**, 54, 429-435.
- (16) Mobius, D. *Acc. Chem. Res.* **1981**, 14, 63-68.
- (17) Kuhn, H. *Thin Solid Films* **1983**, 99, 1-3.
- (18) Shah, D.O. *Micelles, Microemulsions, and Monolayers: Science and Technology*; Marcel Dekker, Inc.: New York, 1998; pp 543-579.
- (19) Lu, Z.; Deng, H.; Wei, Y. *Supramolec. Sci.* **1998**, 5, 649-655.

- (20) Rolland, J.P.; Van Dam, R.M.; Schorzman, D.A.; Quake, S.R.; DeSimone, J.M. *J. Am. Chem. Soc.* **2004**, *126*, 2322-2323.
- (21) Priola, A.; Bongiovanni, R.; Malucelli, G.; Pollicino, A.; Tonelli, C.; Simeone, G. *Macromol. Chem. Phys.* **1997**, *198*, 1893-1907.
- (22) Bunyard, W.C.; Romack, T.J.; DeSimone, J.M. *Macromolecules* **1999**, *32*, 8224-8226.
- (23) Berreman, D. W. *Phys.Rev. Lett.* **1972**, *28*, 1683-1686.
- (24) Sauer, B.B.; Dipaolo, N.V. *J. Coll. Interface Sci.* **1991**, *144*, 527-537.
- (25) Yu, T.; Peng, Z.; Ruan, S.; Xuan, L. *Thin Solid Films* **2004**, *466*, 326-330.
- (26) Sugimura, A.; Luckhurst, G.R.; Ou-Yang, Z. *Phys. Rev. E* **1995**, *52*, 681-689.
- (27) Sugimura, A.; Miyamoto, T.; Tsuji, M.; Kuze, M. *Appl. Phys. Lett.* **1998**, *72*, 329-331.
- (28) Yokoyama, H.; van Sprang, H.A. *J. Appl. Phys.* **1985**, *57*, 4520-4526.
- (29) Schadt, M.; Seiberle, H.; Schuster, A. *Nature* **1996**, *381*, 212-215.
- (30) Sugimura, A.; Matsumoto, K.; Young-can, O.; Y.; Iwamoto, M. *Phys. Rev. E* **1996**, *54*, 5217-5220.
- (31) Jerome, B.; Pieranski, P. *Europhys. Lett.* **1990**, *13*, 55-59.
- (32) Yu, T.; Peng, Z.; Ruan, S.; Xuan, L. *Thin Solid Films* **2004**, *466*, 326-330.
- (33) Sung, S.-J.; Lee, J.-W.; Kim, H.-T.; Park, J.-K. *Liquid Crystals* **2002**, *29*, 243-250.
- (34) Seo, D.-S.; Kobayashi, S.; Nishikawa, M. *Appl. Phys. Lett.* **1992**, *61*, 2392-2394.